

A Thesis Submitted for the Degree of PhD at the University of Warwick

Permanent WRAP URL:

<http://wrap.warwick.ac.uk/136835>

Copyright and reuse:

This thesis is made available online and is protected by original copyright.

Please scroll down to view the document itself.

Please refer to the repository record for this item for information to help you to cite it.

Our policy information is available from the repository home page.

For more information, please contact the WRAP Team at: wrap@warwick.ac.uk

THE PREPARATION AND PROPERTIES OF A GLASS-CERAMIC
WITH AN ALIGNED MICROSTRUCTURE

BY

D. I. H. ATKINSON, B.Sc.

A dissertation submitted
to the University of Warwick for
admission to the degree of
Doctor of Philosophy



0331007

MEMORANDUM

This dissertation is submitted to the University of Warwick in support of my application for admission to the degree of Doctor of Philosophy. It contains an account of my own work performed at the Department of Physics of the University of Warwick in the period October 1971 to September 1974 under the general supervision of Dr. P. W. McMillan. No part of it has been used previously in a degree thesis submitted to this or any other University. The work described in this thesis is the result of my own independent research except where specifically acknowledged in the text.

D. I. H. Atkinson.

D. I. H. Atkinson

ACKNOWLEDGEMENTS

I am extremely grateful to Dr. P. W. McMillan for his interest and advice during the course of this work, especially in the preparation of this thesis. I should also like to thank Professor A. J. Forty for making available to me the facilities of the Department of Physics. My thanks are due to the Science Research Council and G.E.C. Power Engineering, Stafford for the provision of a CAPS award.

This project could not have been completed without the aid of the technical staff, especially Mr. G. Smith for maintaining the Scanning Electron Microscope, Mr. A. Draper for introducing me to the art of glass making and Mr. E. C. Billington for his patience in machining the extrusion dies.

I am extremely grateful to Dr. D. K. Bowen of the Department of Engineering, University of Warwick, who kindly set up and let me use his X-ray diffractometer and to Mr. P. Watt who collected the data on cathodoluminescence in sections 4.4.3, 4 and 5, which proved so interesting. Furthermore I should like to thank Dr. P. Bell (University of Warwick) and Messrs. G. Partridge and S. V. Phillips (G.E.C.) for their help and valuable discussions concerning all aspects of this work.

My thanks are also due to Mrs. R. Franklin who carefully prepared the typescript and to the librarians Mr. L. Bulmer and Mr. M. Davies for their efficiency in dealing with my requests.

Finally, I would like to thank my parents for their encouragement throughout the period of this work.

ABSTRACT

The work described in this thesis was performed on glass-ceramics in which a random arrangement of crystals is grown as a dispersed phase. The physical properties of this material are isotropic.

The technique of hot extrusion has been used to produce a material with an aligned crystal microstructure in a $\text{Li}_2\text{O}-\text{SiO}_2$ glass-ceramic. The extruded material consists of a glass matrix and two crystalline phases; one of these phases is aligned morphologically and crystallographically parallel to the extrusion axis.

The microstructure of this extruded material was analysed statistically in terms of the volume fraction of crystalline phases, the mean crystal-crystal spacing and the distribution function of the number of crystals $N(\theta)$, making an angle θ with a reference direction. Control specimens of the same composition heat-treated at the same temperature and for the same time as the extruded samples were also analysed statistically.

The following physical properties were measured on the control and extruded specimens:

- (i) the coefficient of thermal expansion
- (ii) Young's modulus, rupture strength and microhardness
- (iii) Resistivity, dielectric constant and loss tangent.

In the case of the extruded samples these measurements were made in directions parallel and perpendicular to the extrusion axis; the coefficient of thermal expansion, the mechanical properties and the resistivity were found to be anisotropic for these specimens.

The physical properties were compared with the statistical description of the microstructure; different correlations were found to exist for the control and extruded specimens. A possible explanation

for this difference has been proposed based upon the different internal stresses in the two materials.

A preliminary investigation of the phenomenon of cathodoluminescence from a glass-ceramic surface was also carried out. A strong contrast exists between the intensity of visible radiation emitted from the crystalline and amorphous phases. The intensity of this radiation decays with time and is also a function of the angle the specimen makes to the incident electron beam. Possible mechanisms for this are discussed.

PUBLICATIONS

Certain parts of the work reported in this thesis have been published as follows:

- (1) "Some observations of glass-ceramic microstructures by cathodoluminescence", D. I. H. Atkinson and P. W. McMillan, J. Mat. Sci. 9, 692 (1974)
- (2) "Glass Ceramic Bodies", U. K. Patent Application No. 43700/74, P. W. McMillan and D. I. H. Atkinson.

THE PREPARATION AND PROPERTIES OF A GLASS-CERAMIC
WITH AN ALIGNED MICROSTRUCTURE

BY

D. I. H. ATKINSON, B.Sc.

A dissertation submitted
to the University of Warwick for
admission to the degree of
Doctor of Philosophy

1971

MEMORANDUM

This dissertation is submitted to the University of Warwick in support of my application for admission to the degree of Doctor of Philosophy. It contains an account of my own work performed at the Department of Physics of the University of Warwick in the period October 1971 to September 1974 under the general supervision of Dr. P. W. McMillan. No part of it has been used previously in a degree thesis submitted to this or any other University. The work described in this thesis is the result of my own independent research except where specifically acknowledged in the text.

D. I. H. Atkinson

D. I. H. Atkinson

ACKNOWLEDGEMENTS

I am extremely grateful to Dr. P. W. McMillan for his interest and advice during the course of this work, especially in the preparation of this thesis. I should also like to thank Professor A. J. Forty for making available to me the facilities of the Department of Physics. My thanks are due to the Science Research Council and G.E.C. Power Engineering, Stafford for the provision of a CAPS award.

This project could not have been completed without the aid of the technical staff, especially Mr. G. Smith for maintaining the Scanning Electron Microscope, Mr. A. Draper for introducing me to the art of glass making and Mr. E. C. Billington for his patience in machining the extrusion dies.

I am extremely grateful to Dr. D. K. Bowen of the Department of Engineering, University of Warwick, who kindly set up and let me use his X-ray diffractometer and to Mr. P. Watt who collected the data on cathodoluminescence in sections 4.4.3, 4 and 5, which proved so interesting. Furthermore I should like to thank Dr. P. Bell (University of Warwick) and Messrs. G. Partridge and S. V. Phillips (G.E.C.) for their help and valuable discussions concerning all aspects of this work.

My thanks are also due to Mrs. R. Franklin who carefully prepared the typescript and to the librarians Mr. L. Bulmer and Mr. M. Davies for their efficiency in dealing with my requests.

Finally, I would like to thank my parents for their encouragement throughout the period of this work.

ABSTRACT

The work described in this thesis was performed on glass-ceramics in which a random arrangement of crystals is grown as a dispersed phase. The physical properties of this material are isotropic.

The technique of hot extrusion has been used to produce a material with an aligned crystal microstructure in a $\text{Li}_2\text{O} - \text{SiO}_2$ glass-ceramic. The extruded material consists of a glass matrix and two crystalline phases; one of these phases is aligned morphologically and crystallographically parallel to the extrusion axis.

The microstructure of this extruded material was analysed statistically in terms of the volume fraction of crystalline phases, the mean crystal-crystal spacing and the distribution function of the number of crystals $N(\theta)$, making an angle θ with a reference direction. Control specimens of the same composition heat-treated at the same temperature and for the same time as the extruded samples were also analysed statistically.

The following physical properties were measured on the control and extruded specimens:

- (i) the coefficient of thermal expansion
- (ii) Young's modulus, rupture strength and microhardness
- (iii) Resistivity, dielectric constant and loss tangent.

In the case of the extruded samples these measurements were made in directions parallel and perpendicular to the extrusion axis; the coefficient of thermal expansion, the mechanical properties and the resistivity were found to be anisotropic for these specimens.

The physical properties were compared with the statistical description of the microstructure; different correlations were found to exist for the control and extruded specimens. A possible explanation

for this difference has been proposed based upon the different internal stresses in the two materials.

A preliminary investigation of the phenomenon of cathodoluminescence from a glass-ceramic surface was also carried out. A strong contrast exists between the intensity of visible radiation emitted from the crystalline and amorphous phases. The intensity of this radiation decays with time and is also a function of the angle the specimen makes to the incident electron beam. Possible mechanisms for this are discussed.

PUBLICATIONS

Certain parts of the work reported in this thesis have been published as follows:

- (1) "Some observations of glass-ceramic microstructures by cathodoluminescence", D. I. H. Atkinson and P. W. McMillan, J. Mat. Sci. 2, 692 (1974)
- (2) "Glass Ceramic Bodies", U. K. Patent Application No. 43700/74, P. W. McMillan and D. I. H. Atkinson.

CONTENTS

CHAPTER 1:	GENERAL INTRODUCTION	
1.1	Glass-Ceramics	1
1.1.1	Definition	1
1.1.2	History	2
1.2	Properties of Glass-Ceramic Materials	4
1.2.1	Thermal Properties	4
1.2.2	Optical Properties	4
1.2.3	Mechanical Properties	4
1.2.4	Electrical Properties	5
1.3.1	Defining the Project	6
1.3.2	Choice of Experiments	7
1.4	Plan of Thesis	8
	References	10
CHAPTER 2:	A REVIEW OF THE LITHIA-SILICA GLASS-CERAMIC SYSTEM	
2.1	Introduction	12
2.2	The Binary $\text{Li}_2\text{O} - \text{SiO}_2$ Glass System	12
2.3	The Microstructure of Lithia-Silica Glass-Ceramics	14
2.4	The Mechanical Properties of $\text{Li}_2\text{O} - \text{SiO}_2$ Glass-Ceramics	16
2.5	Viscous Deformation and Creep Resistance of Glass-Ceramics	19
2.6	Electrical Properties of Glass-Ceramics	21
2.7	Summary	23
	References	24

CHAPTER 3: EXPERIMENTAL METHODS FOR DETERMINING THE PHYSICAL
PROPERTIES OF THE GLASS-CERAMIC

3.1	Introduction	27
3.2	Glass Preparation	27
3.3	Differential Thermal Analysis	28
3.3.1	Introduction	28
3.3.2	DTA Apparatus	29
3.4	Density Measurement	31
3.5	Mechanical Properties	31
3.5.1	Introduction	31
3.5.2	Microhardness Measurements	32
3.5.3	Three-Point Bending Experiments	33
3.5.4	Miniature Three-Point Bend Experiments	35
3.6	Electrical Measurements	36
3.6.1	Introduction	36
3.6.2	Apparatus and Measurement	37
3.7	Thermal Expansion Measurements	39
3.7.1	General Introduction	39
3.7.2	Measurement of the Thermal Expansion Coefficient	40
	References	44

CHAPTER 4: TRANSMISSION AND SCANNING ELECTRON MICROSCOPY

4.1	Introduction	46
4.2	Transmission Electron Microscopy	46
4.2.1	Introduction	46
4.2.2	Fragmentation	47
4.2.3	Carbon Replication	48
4.2.4	Chemical Thinning	48
4.2.5	Other Methods of Preparing Transmission Specimens	49

4.2.6	Summary of Transmission Electron Microscope Specimen Preparation	49
4.3	Scanning Electron Microscopy (SEM)	50
4.3.1	The Microscope	50
4.3.2	Specimen Preparation for SEM	52
4.3.3	Calibration of Image Magnification and Rotation in the SEM	53
4.4	Investigation of Cathodoluminescence from Glass-Ceramic Surfaces	53
4.4.1	Introduction	53
4.4.2	Initial Observations of CL from Glass-Ceramics	54
4.4.3	Variation of CL Intensity with Time	55
4.4.4	Variation of CL Intensity with the Angle of Incidence of the Electron Beam	59
4.4.5	Determination of the Frequency of CL Emitted from $\text{Li}_2\text{O} \cdot 2\text{SiO}_2$ Crystals	62
4.4.6	Summary of CL observations in the SEM	62
4.5	X-Ray Diffraction Techniques	63
4.5.1	Preparation of Samples for X-ray Studies	63
	References	65

CHAPTER 5: METHODS OF PRODUCING AN ALIGNED MICROSTRUCTURE

5.1	Introduction	67
5.2	General Considerations	67
5.3	Electric Field Experiments	69
5.3.1	Introduction	69
5.3.2	The Effect of an Electric Field on Phase Separation and Crystallisation	70
5.4	Hot Extrusion	73

5.4.1	Introduction	73
5.5	The Extrusion Apparatus	74
5.5.1	Introduction	74
5.5.2	The Extrusion Die	75
5.5.3	Flow Behaviour During Hot Extrusion	77
5.5.4	The Hot Extrusion of a Glass-Ceramic	81
5.5.5	Experiments with Glass-Ceramic Filaments	83
	References	85

CHAPTER 6: THE STATISTICAL ANALYSIS OF THE MICROSTRUCTURE

6.1	Introduction	87
6.2	The Significance of Statistical Analysis	87
6.3	Optical Analysis of the Microstructure	88
6.3.1	Introduction	88
6.3.2	The Fraunhofer Diffraction Patterns of Ideal "Microstructures"	89
6.3.3	Fraunhofer Diffraction Images of Real Microstructures	91
6.3.4	Comments on the Optical Diffraction Technique	93
6.4	Specification and Measurement of Microstructural Anisotropy	94
6.4.1	Introduction	94
6.4.2	Determination of the Angular Distribution Function	95
6.4.3	Mathematical Derivation of the Angular Distribution Function	96
6.4.4	The Detection of Morphological Anisotropy in the Real System	99
6.4.5	Determination of the Volume Fraction and Inter-Crystal Spacing	101
	References	103

5.4.1	Introduction	73
5.5	The Extrusion Apparatus	74
5.5.1	Introduction	74
5.5.2	The Extrusion Die	75
5.5.3	Flow Behaviour During Hot Extrusion	77
5.5.4	The Hot Extrusion of a Glass-Ceramic	81
5.5.5	Experiments with Glass-Ceramic Filaments	83
	References	85

CHAPTER 6: THE STATISTICAL ANALYSIS OF THE MICROSTRUCTURE

6.1	Introduction	87
6.2	The Significance of Statistical Analysis	87
6.3	Optical Analysis of the Microstructure	88
6.3.1	Introduction	88
6.3.2	The Fraunhofer Diffraction Patterns of Ideal "Microstructures"	89
6.3.3	Fraunhofer Diffraction Images of Real Microstructures	91
6.3.4	Comments on the Optical Diffraction Technique	93
6.4	Specification and Measurement of Microstructural Anisotropy	94
6.4.1	Introduction	94
6.4.2	Determination of the Angular Distribution Function	95
6.4.3	Mathematical Derivation of the Angular Distribution Function	96
6.4.4	The Detection of Morphological Anisotropy in the Real System	99
6.4.5	Determination of the Volume Fraction and Inter-Crystal Spacing	101
	References	103

CHAPTER 7: THE MICROSTRUCTURE AND PHYSICAL PROPERTIES OF THE
GLASS-CERAMICS STUDIED

7.1	Introduction	104
7.2	The Glass Compositions Studied	104
7.3	Differential Thermal Analysis Results	106
7.4	Glass-Ceramic Microstructures	106
7.4.1	The Microstructure of the Glass-Ceramic Devitrified from Glass A	106
7.4.2	The Microstructure of the Glass-Ceramic Devitrified from Glass B	108
7.4.3	Comments on the Glass-Ceramic Microstructures	110
7.5	The Statistical Analysis of Glass-Ceramic A	111
7.5.1	Introduction	111
7.5.2	The Effect of an Etching Solution on Glass-Ceramic A	111
7.5.3	The Volume Fraction and Mean Particle Spacing of Glass-Ceramic A	112
7.6	Density of Glass-Ceramic A	113
7.7	The Coefficient of Thermal Expansion	114
7.7.1	Results	114
7.7.2	Discussion	115
7.8	Mechanical Properties	117
7.8.1	Introduction	117
7.8.2	Young's Modulus and Rupture Modulus Results	118
7.8.3	Discussion of Moduli Results	119
7.9	The Electrical Properties of Glass-Ceramic A	124
7.9.1	Introduction	124
7.9.2	The Resistivity of Glass-Ceramic A	124

7.9.3	Discussion of Resistivity Measurements	126
7.9.4	The Dielectric Constant and Loss Tangent of Glass-Ceramic A: Introduction	129
7.9.5	The Dielectric Constant of Glass-Ceramic A	129
7.9.6	Comments on the Dielectric Constant Measurements	130
7.9.7	The Loss Tangent of Glass-Ceramic A	131
7.9.8	Comments on the Loss Tangent Results	133
7.10	A Summary of the Properties of Glass-Ceramic A	134
	References	137

CHAPTER 8: THE PROPERTIES OF A HOT EXTRUDED GLASS-CERAMIC

8.1	Introduction	139
8.2	The Hot Extrusion of Glass A and Glass B	139
8.2.1	General Considerations	139
8.2.2	Extrusion of Glass-Ceramic A	139
8.2.3	Extrusion of Glass-Ceramic B	141
8.2.4	General Conclusions on the Extrusion of Glass B	143
8.3	The Microstructure of Extruded Specimens of Glass-Ceramic A	144
8.3.1	Introduction	144
8.3.2	Statistical Analysis of the Morphological Orientation	145
8.3.3	Determination of the Crystallographic Orientation	147
8.3.4	Comments on the Microstructure of the Extruded Glass-Ceramic	149
8.4	The Density of the Extruded Material	149

8.5	The Coefficient of Thermal Expansion of the Extruded Material	150
8.5.1	Results	150
8.5.2	Comments on the Expansion Coefficient Results	151
8.6	Mechanical Properties of the Extruded Material	153
8.6.1	The Young's Modulus and Rupture Modulus	153
8.6.2	Comments on the Moduli Measurements	154
8.6.3	The Knoop Microhardness	160
8.7	Electrical Properties of the Extruded Glass- Ceramic	161
8.7.1	Resistivity	161
8.7.2	The Dielectric Constant and Loss Tangent	163
8.7.3	Comments on the Electrical Properties	163
8.8	A Summary of the Properties of the Extruded Material	167
	References	170

CHAPTER 9:

CONCLUSIONS

9.1	Introduction	171
9.2	General Considerations	171
9.3	A Comparison of the Properties of the Control and Extruded Glass-Ceramics	172
9.4	Other Conclusions	174
9.5	Suggestions for Future Work	175

".... that it was only after long periods of preparation, measured in months, not days, that they came to a 'result' - one day of excitement, and afterwards another period of building, routine, long-drawn-out suspense".

The New Men

C. P. Snow

(MacMillan 1954)

CHAPTER 1: GENERAL INTRODUCTION

1.1 Glass-Ceramics

1.1.1 Definition

Glass-ceramics are polycrystalline solids prepared by the controlled crystallisation of glasses; this is accomplished by subjecting suitable glasses to a carefully regulated heat-treatment schedule which results in the nucleation and growth of crystal phases within the glass (1).

A glass-ceramic is produced by first preparing a glass which usually contains a suitable nucleating agent; the glass is moulded in its molten or plastic state to the required shape using standard glass forming techniques and then subjected to a controlled heat-treatment programme. This cycle typically comprises of heating the glass fairly slowly to a nucleation temperature, maintaining this temperature for a fixed time in order to introduce into the material a large number of nuclei around which subsequent crystal growth can occur, then raising the temperature to a second value (the crystallisation temperature) and after maintaining this temperature for a fixed period, cooling to room temperature.

Essentially a glass-ceramic is a composite material in which the dispersed crystalline phase is grown from an amorphous matrix; this distinguishes them from traditional ceramics in which the majority of the crystalline material is introduced when the ceramic composition is prepared, although some recrystallisation may occur or new crystal phases may arise from solid state reactions.

Glass-ceramics are also referred to in the technical literature as "vitrocerams", "devitrocerams", "sitalls" and "melt-formed ceramics". The term glass-ceramic is generally restricted to materials which are highly crystalline. There are several other types of glass products, such as

fluoride opals and copper ruby glasses, in which minor amounts of a crystalline phase are produced by controlled crystallisation (usually less than 10%). These are generally not considered to be glass-ceramics.

1.1.2 History

In the eighteenth century Reaumur (2) produced polycrystalline materials from glass. He showed that if glass bottles were heated in a mixture of gypsum and sand for several days they were converted into opaque porcelain-like objects. The materials produced by this process had low mechanical strengths and distortion of the articles during the heat-treatment process could occur. This was because Reaumur was unable to achieve the control of the crystallisation process which characterises a true glass-ceramic.

In the early 1900's Tammann (3) investigated crystallisation in detail and from a series of theoretical and experimental studies supplied the basis for much of the present understanding of the nucleation and crystallisation process. In the same period a flourishing industry arose in Europe based on the controlled crystallisation of molten rocks, particularly basalts. Utilizing the principles derived by Tammann (loc. cit.), rock-like ceramics in a variety of sizes and shapes were produced and used in a number of applications. Portevin (4) provides a detailed summary of the principles of melting and crystallisation of fused basalts with photographs of the production articles.

The necessity for the control of the crystallisation process was recognised by Blau (5, 6) and used to produce glasses for illumination systems with the desired opacity. Blau defined the necessary relationships that must exist between the nucleation and crystallisation rates to allow adequate control of the crystallisation process. This process may be completely controlled when there exists a separation of the temperature

regions of the Tammann curves for the formation of nuclei and the subsequent growth process.

The development of glass-ceramics in their present form was a result of research carried out at the Corning Glass Works in the United States in the 1950's on photosensitive glasses. These glasses contain small amounts of copper, silver or gold which during heat treatment of the material can be precipitated out in the form of very small crystals. The precipitation process occurs much more readily if the glasses are irradiated with ultra-violet light prior to heat-treatment. It was shown that photosensitive glasses could be opacified in the irradiated regions by the precipitation of further crystals upon the metallic crystals. However these materials are not true glass-ceramics since the crystalline content is only a minor proportion of the total material.

Stookey of the Corning Glass Works found that on heating a photosensitively opacified glass to a higher temperature than was normally used, the glass was converted to a polycrystalline ceramic material. This material had a higher mechanical strength than the original glass and other properties were markedly improved (e.g. electrical insulation). In this glass the small metallic crystals evidently acted as nucleation sites for the subsequent crystallisation of major phases from the material; the large number and even distribution of these nuclei resulted in uniform crystal growth throughout the material which can be considered as the first true glass-ceramic (7). Stookey subsequently developed a wide range of glass compositions which did not require a prior irradiation step and contained titanium dioxide as a nucleation catalyst (8); the trademark for these materials is "Pyroceram" (9-11).

The use of metallic phosphates to promote the controlled crystallisation of glasses was developed in Britain (12); later researches by workers in a

number of different countries have led to the discovery of many different types of nucleation catalyst for glass-ceramic production (13, 14).

1.2 Properties of Glass-Ceramic Materials

1.2.1 Thermal Properties

The thermal expansion coefficient can be varied over a wide range. It is possible to develop negative - expansion materials, zero-expansion materials, materials with very high expansions and materials with expansion coefficients matching those of many metals and alloys. The wide range of thermal expansion coefficients is a property which has been exploited commercially; this is particularly true for low expansion glass-ceramics (15 - 17) and for glass-ceramics with expansion coefficients matching those of metals and alloys (18).

The thermal stability of glass-ceramics is a function of the degree of crystallinity and the phases that are present. At elevated temperatures the glass matrix can cause deformation due to viscous flow or further crystal growth; the primary crystalline phases can also undergo transformation to other phases.

1.2.2 Optical Properties

The transmission of glass-ceramics in the visible can vary over wide ranges. Transparent glass-ceramics have been reported in a number of systems (19), but the majority of glass-ceramics are translucent or opaque. Some compositions have been shown to display electro-optical activity (20).

1.2.3 Mechanical Properties

Glass-ceramics like ordinary glasses and ceramics are brittle

materials at room temperature. The abraded strengths of most glass-ceramics generally fall within the range of $7 \cdot 10^7$ to $14 \cdot 10^7 \text{ N/m}^2$. Glass given the same abrasion and test conditions has strengths of $4 \cdot 10^7$ to $7 \cdot 10^7 \text{ N/m}^2$. Glass-ceramics are probably stronger for a number of reasons; they appear to have a higher abrasion resistance than glass which implies that glass-ceramics are less prone to surface damage. The fracture propagation in glass-ceramics probably requires more energy than in a glass because of the nature of the fine grained microstructure.

Kanbara and Tashiro (21) have shown that in the lithia aluminosilicate system the addition of fluorine to the original glass batch can increase the flexure strength up to $6 \cdot 10^8 \text{ N/m}^2$ through controlled heat-treatments. High flexure strengths of $7 \cdot 10^8 \text{ N/m}^2$ have been reported for glass-ceramics in the magnesium aluminosilicate system (22).

A number of techniques have been reported for increasing the strength of glass-ceramics. Duke et al. (23) applied compressive glazes to glass-ceramics and observed a fivefold increase in the rupture modulus. The technique of ion exchange has also been applied to glass-ceramic surfaces which resulted in abraded moduli of rupture of $14 \cdot 10^8 \text{ N/m}^2$ (24).

1.2.4 Electrical Properties

The majority of glass-ceramics are insulators; the conduction mechanism is primarily ionic as opposed to electronic and is much more complicated than in a glass of the same composition because of the complex microstructure. A diffusing ion may encounter several different structural environments. The resistivity decreases with increasing temperature.

The dielectric properties can be varied over wide ranges; in general the dielectric loss of a glass-ceramic is less than that of a glass of the same composition because the alkali ions are tied up more tightly in the

crystal lattice. Materials with high dielectric constants can be produced by the choice of composition (25).

Pincus (26) has reviewed the applications of glass-ceramics which vary from cooking-ware to radomes to printed circuit boards. The combination of unique properties which glass-ceramics have makes these materials suitable for many technological uses.

1.3.1 Defining the Project

In a glass-ceramic the crystalline phase is randomly oriented in a glass matrix and the physical properties of this material are isotropic. One would expect that the properties of a glass-ceramic with an aligned crystal microstructure would reflect the anisotropy in the system. An investigation of a material of this type would clearly be of great interest from a technological point of view and would also provide information upon the structural factors which control these properties.

The object of this research was to investigate means of modifying the microstructure of glass-ceramics with the aim of orientating the crystalline phase in a preferred direction.

The basic principle upon which this research was carried out was that the glass or the glass-ceramic system would have to be subjected to an anisotropic stress during the nucleation stage or during the crystal growth stage to produce an oriented microstructure. In the former case of producing a glass with "aligned" nuclei the argument is that the subsequent crystal growth on these nuclei would reflect their orientation and produce crystals in a preferential direction.

A third possibility is that the glass-ceramic could be deformed in such a way as to produce a morphological orientation of the crystalline phase. In this case the crystalline phase would have to have an aspect ratio which was not equal to one and the technique would be similar to

wire-drawing or the rolling of metal.

1.3.2. Choice of Experiments

The experiments performed in this work fall into two main sections:

- (i) preparation of a glass-ceramic with an aligned microstructure.
- (ii) the investigation of the properties of this material relative to this orientation and the interpretation of these measurements in terms of the microstructure of the material.

In the first category, some initial experiments were conducted on the effects of an electric field upon the kinetics of glass in glass phase separation and attempts were made to crystallise a glass in an electric field. These experiments were not too promising and the major emphasis of the research was placed on the hot extrusion of a glass-ceramic. The extrusion technique is essentially one of deforming a glass-crystal composite in such a way that the crystalline phase is oriented in a preferred direction. This method of alignment places certain restrictions upon the glass-ceramic which is extruded. In the glass-ceramic there should ideally be only one crystalline phase which has a needle-shaped morphology; it is purposeless trying to align spheres. Also for experimental ease the glass-ceramic should be easily deformed at temperatures less than 1000°C . Concurrent with the design of the hot-extrusion apparatus, a glass-ceramic with these properties was investigated.

The microstructure of the extruded glass-ceramic together with that of the control specimens heat-treated at the same temperature and for the same time was investigated using a scanning electron microscope.

The physical properties of the extruded and control specimens which were investigated were as follows:

- (i) Mechanical properties: Young's modulus in bending and the rupture modulus; the Knoop microhardness.

(ii) The thermal expansion coefficient.

(iii) Electrical properties: resistivity, dielectric constant and loss tangent.

In the case of the extruded material these property measurements were made in directions parallel and perpendicular to the extrusion axis. It was believed that these measurements would provide a picture of the advantages if any, of a glass-ceramic with an aligned microstructure.

In order to correlate the physical properties with the structure of the extruded and control specimens of the glass-ceramic, the microstructure was analysed statistically in terms of the volume fraction of crystalline phases present, the mean crystal size and the mean crystal-crystal spacing. In the case of the extruded material a technique was developed to evaluate the width of the angular distribution the crystals made with the preferred direction of orientation.

Using these techniques it was hoped that a clearer understanding of the factors which control the properties of a glass-ceramic with a random crystal microstructure could be achieved.

1.4 Plan of Thesis

The contents of this thesis which is divided into nine chapters are listed on the pages preceding this introductory Chapter.

Chapter 2 contains a brief review of the microstructure and properties of glass-ceramics derived from the lithia-silica system.

In the third chapter details are presented of the experimental methods used for determining the physical properties of the glass-ceramic.

The techniques of investigating the microstructure of the material are described in Chapter 4; this chapter also contains results of the observation of cathodoluminescence from glass-ceramic surfaces.

Chapter 5 deals with the methods of producing a glass-ceramic with an aligned microstructure and in the sixth chapter the techniques used to analyse statistically the structure of the material are described.

Chapters 7 and 8 contain the results of the physical property measurements and the analysis of the microstructure for the control glass-ceramic and the extruded material respectively.

In the final chapter, Chapter 9, the properties of the control and extruded specimens are compared and the major conclusions are stated; this chapter also contains suggestions for future work.

22. K. M. Henry and W. E. Smith, U.S. Patent No. 3,117,881 (1964)
23. D. A. Duke, J. E. Megles, J.F. MacDowell and H. R. Bopp, J. Am. Ceram. Soc. 51 98 (1968)
24. D. A. Duke, J. F. MacDowell and B. R. Karstetter, *ibid* 50 67 (1967)
25. M. M. Layton and A. Herczog, *ibid* 50 369 (1967)
26. A. G. Pincus, *Advances in Nucleation and Crystallization in Glasses*
Edited by L. L. Hench and S. W. Freiman (Am. Ceram. Soc. Ohio 1971)

CHAPTER 2: A REVIEW OF THE LITHIA - SILICA GLASS-CERAMIC SYSTEM

2.1. Introduction

The majority of the work in this thesis was performed using glass-ceramics crystallised from glasses based on the $\text{Li}_2\text{O} - \text{SiO}_2$ system. This chapter contains a review of the research which has been conducted on this system and the glass-ceramics devitrified from it.

2.2 The Binary $\text{Li}_2\text{O} - \text{SiO}_2$ Glass System

Kracek (1) has thoroughly studied the phase equilibria in the $\text{Li}_2\text{O} - \text{SiO}_2$ system following earlier work by Jaeger and Van Klooster (2). For glasses containing approximately 30 mol.% Li_2O it can be seen from the phase diagram (Figure 2.1) that the system contains compounds of Li_2SiO_3 , $\text{Li}_2\text{Si}_2\text{O}_5$ and Li_4SiO_4 .

Glasser (3) has studied the equilibrium crystallisation products of $\text{Li}_2\text{Si}_2\text{O}_5 - \text{SiO}_2$ glasses containing > 66.7 mol.% SiO_2 and shown them to be stoichiometric $\text{Li}_2\text{Si}_2\text{O}_5$ and SiO_2 . At temperatures between the solidus and approximately 900°C the products obtained from crystallising the $\text{Li}_2\text{Si}_2\text{O}_5 - \text{SiO}_2$ glasses were essentially the equilibrium products predicted from Kracek's phase diagram (Figure 2.1). However, at temperatures below approximately 750°C , an important crystallisation product is a lithium disilicate - silica solid solution. The existence of this anomalous solid solution which extends from $\text{Li}_2\text{Si}_2\text{O}_5$ (80.08 wt.% SiO_2) to approximately 84 wt.% SiO_2 was demonstrated both by the non-appearance of silica as a crystalline phase and by the progressive shift in X-ray d-spacings of the lithium disilicate phase. The solid solutions could be made to exsolve their excess silica by rapid dynamic heating.

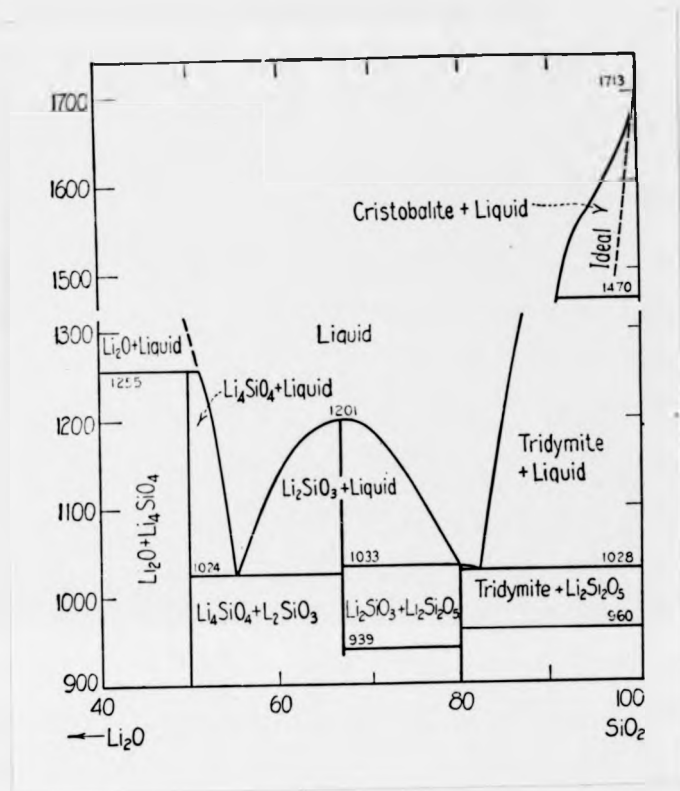


Figure 2.1 Phase diagram for the $\text{SiO}_2 - 2\text{Li}_2\text{O} \cdot \text{SiO}_2$ system, after Kracek (1).

West et al. (4) have shown that $\text{Li}_2\text{O} - \text{SiO}_2$ melts containing 25 mol.% Li_2O can be crystallised at $\sim 890^\circ\text{C}$ to give $\text{Li}_2\text{Si}_3\text{O}_7$ as the principal crystalline product. $\text{Li}_2\text{Si}_3\text{O}_7$ is thermodynamically metastable and in glasses and melts of this composition which have undergone amorphous phase separation* prior to recrystallisation, the trisilicate yield is greatly reduced. The relationship between glass in glass phase separation and crystallisation is not well understood despite extensive study; several authors (5 - 8) have observed that phase separation precedes crystallisation and modifies the kinetics of subsequent crystal nucleation and growth. Various processes have been proposed for the mechanism of crystallisation through glass in glass phase separation, however there is no experimental confirmation of these mechanisms (9 - 12).

Harper et al. (13) in a study of crystal nucleation in lithium silicate glasses have suggested that glass in glass phase separation did not promote crystal nucleation directly but could affect it indirectly by influencing the crystal growth rate. Nakagawa and Izumitani (14) after a detailed study concluded that there was no relation between glass in glass phase separation and crystallisation.

On the other hand, Doremus and Turkalo (15) comparing the data of Nakagawa et al. and the extrapolated metastable immiscibility boundary suggested the existence of a close relationship between phase separation and nucleation of a crystal. Furthermore, Tomozowa (16) has shown using an X-ray small-angle scattering technique that glass phase separation accelerates the nucleation rate. Charles (17) has studied the phase separation characteristics of various lithium - silicate glasses and shown that the shape factors and concentrations of the separated phases can be estimated from dielectric measurements.

* Glass can exhibit amorphous phase separation which consists of droplets of glass dispersed in a glass matrix of a different composition.

The electrical properties and thermal expansion coefficients of glasses selected from parts of the $\text{Li}_2\text{O} - \text{SiO}_2$ system have been studied by Dale et al. (18); an equation for the activation energy of ionic conduction in silica glasses has been developed by Anderson and Stuart (19) and compared with experimental results.

2.3 The Microstructure of Lithia - Silica Glass Ceramics

An important class of crystallised glass is based on lithium silicates and as an aid in understanding more complex systems, crystallisation in binary lithium silicates has been extensively studied (20-23).

The effects of various nucleation catalysts on the crystallisation of $\text{Li}_2\text{O} - \text{SiO}_2$ glasses has been studied as part of an overall investigation of the $\text{Li}_2\text{O} - \text{Al}_2\text{O}_3 - \text{SiO}_2$ system by McMillan (24). The binary glasses had Li_2O contents ranging from 25 to 35 mol.% and the nucleation catalysts employed were phosphorus pentoxide, titanium dioxide and metallic platinum. Two crystalline phases were produced when glasses of this type were heat-treated. The first phase was lithium disilicate and this crystallised in the temperature range $557 - 569^\circ\text{C}$. This temperature was not affected by any of the nucleation catalysts and was unchanged even when the nucleation catalysts were omitted from the composition. The second crystalline phase was quartz and in the absence of a nucleation catalyst, this phase developed at a temperature between 615°C and 690°C . When phosphorus pentoxide was included in the glass batch, the temperature at which quartz developed was lowered to between 585°C and 595°C ; titanium dioxide did not affect the crystallisation temperature significantly. Platinum had a similar but less marked effect to phosphorus pentoxide in lowering the quartz crystallisation temperature.

McMillan concluded from these experimental observations that the crystallisation of lithium disilicate from the glasses may be homogeneously

nucleated because none of the nucleation catalysts influenced the temperature at which this phase developed. Furthermore it appears that while phosphorus pentoxide catalyses the crystallisation of quartz, titanium dioxide is not an effective nucleation catalyst for this crystal; platinum acts as a nucleation catalyst for quartz but is less effective than phosphorus pentoxide.

The compositions containing phosphorus pentoxide produced microcrystalline ceramics of high strength whereas those containing titanium dioxide or no nucleation catalyst were coarsely crystalline and of low strength. The compositions containing platinum were also microcrystalline but were less strong than those containing phosphorus pentoxide.

The morphologies of lithium disilicate crystals growing in lithium silicate glasses with and without phosphorus pentoxide has been studied by Doremus and Turkalo (25) using transmission electron microscopy. The crystals grew in the matrix embedding silica rich particles that were formed by phase separation. In the glass without phosphorus the crystals nucleated on impurity particles and grew out from the particles in spherical rosettes. In the glass containing phosphorus it was found that many more particles were nucleated and they had a different morphology. Similar effects have been observed by several other authors (26, 27).

Cherneva et al. (28) have shown that when a glass having the composition $\text{Li}_2\text{O} \cdot 2\text{SiO}_2$ was crystallised the first crystalline phases to separate consisted not of the disilicate phase but of a mixture of silicates in which the lithia content was < 33.3 mol.% and of silicates in which it is above 33.3 mol.%. It was concluded that the lithium disilicate crystals were formed by a reaction in the solid phase between the crystals which separated initially; the reaction involving a series of intermediate phases. This crystallisation sequence has been confirmed by Kinser et al. (29, 30).

The kinetics of the crystallisation of lithium disilicate from glasses in the $\text{Li}_2\text{O}-\text{SiO}_2$ system have been studied by Freiman and Hench (31). Analysis of the volume percent crystallisation data showed that crystallisation occurred through the nucleation and growth of rods and the spherulitic nature of the crystals was substantiated by the petrographic examination of the partially crystalline glass. The activation energy for nucleation was shown to be a function of composition and thermal treatment by an analysis of the temperature dependence of the crystallisation rate.

Booth and Rindone (32) have studied the effect of inorganic surface treatments on the orientation of lithium disilicate crystals formed in $\text{Li}_2\text{O} \cdot 2.75\text{SiO}_2$ glass fibres. Fibres of several diameters were subjected to various surface treatments at room temperature and then heat-treated between 550°C and 800°C . It was found that metal salt solutions applied to the fibre surfaces prior to heating decreased the degree of orientation during the heat-treatment only if the metal entered the glass and formed nucleation sites within the fibres. Orientation could also be decreased by removing lithium from the glass surfaces. A comparison of the crystallisation characteristics of untreated and AgNO_3 treated fibres indicated that the crystallisation behaviour was controlled by either a growth process or a nucleation process depending on whether the temperature was below or above 625°C respectively.

2.4 The Mechanical Properties of $\text{Li}_2\text{O}-\text{SiO}_2$ Glass-Ceramics

Glass-ceramics consist of a dispersed crystalline phase embedded in a glass matrix; they can therefore be regarded as composites of a dispersion type. The properties of composite materials depend upon not only the physical properties of the individual phases but also their physical and chemical interactions.

The strength of glass-crystal composites has been studied by several investigators. Experimental data has been published for the mechanical strength of such materials, including glass-alumina (33-36), glass-zirconia (33, 36, 37) and glass-thoria (38).

Hasselman and Fulrath (34) have analysed the effects of the particle size and volume fraction of the crystalline phase on the mechanical strength of glass-crystal composites free of internal stresses. They hypothesized that the hard crystalline particles within the glass matrix will limit the size of the Griffith flaws, and hence strengthen the composite. Based upon this criterion, they derived the following expression for the mechanical strength of a glass-crystal composite:

$$\sigma = \sigma_0 (1 - \varphi)^{-\frac{1}{2}}$$

for lower volume fractions or larger particle sizes at which the flaw size is smaller than the average distance between particles and:

$$\sigma = \left[\frac{3\gamma E \varphi}{\pi R (1 - \varphi)} \right]^{\frac{1}{2}}$$

for higher volume fractions or smaller particle size at which the average flaw size is governed by the average distance between particles. In the above expressions:

σ = fracture strength of composite

σ_0 = fracture strength of glass matrix

R = radius of crystalline particle

φ = the volume fraction of dispersed phase

E = Young's modulus of glass matrix

γ = surface energy of glass matrix

Hasselman and Fulrath (loc.cit.) interpreted their experimental results for glass-alumina composites in terms of the derived expressions and obtained good agreement in the region of smaller mean distances between particles. In the region of larger mean distances, however, a deviation

from the strength dependence on the particle size was found. This was attributed in part to stress concentrations near the dispersed particles arising from differences in the elastic properties of the two phases.

Miyata and Jinno (39) have proposed a fracture theory for two phase glass-crystal composites in which they propose that the fracture mechanism in such solids consists of the processes of crack nucleation and of crack propagation round the dispersed particles. For low volume fractions of the dispersed phase, macroscopic fracture will occur due to the growth of micro-cracks originating in the vicinity of the pre-existing structural imperfections through a heterogeneous crack nucleation process; in this case the strength decreases with the volume fraction of the dispersed phase. At higher volume fractions where crack propagation is hindered by the crystalline particles, the process of crack propagation round the particles may be responsible for the macroscopic fracture of the composite; in this case the strength is an increasing function of the volume fraction. Miyata et al. have formulated expressions for the mechanical strength of a glass-crystal composite based on the nucleation theory and Griffith's criterion. The proposed theory is in good agreement with the strength behaviour of glass-alumina composites, and in particular, the dependence of the strength reduction on particle size at lower volume fractions. However the theory is only applicable to the strength behaviour of composites free of internal stresses due to differences in thermal expansion coefficients of the two phases.

It has been suggested (40) that the mechanical strength of a glass-ceramic, σ , is dependent upon the mean grain diameter, d , according to:

$$\sigma = k d^{-\frac{1}{2}}$$

where k is a constant. The crack length, c , in the Griffith equation:

$$\sigma = \left(\frac{2 E \gamma}{\pi c} \right)^{\frac{1}{2}}$$

would thus be proportional to, or equal to, the grain diameter. This suggests that the critical flaws are present within the crystalline grains and do not extend into the glass phase or that they exist at the glass-crystal interface and are therefore proportional to the circumference of the grains.

Freiman and Hench (41) have investigated the mechanical strengths of a series of glass-ceramics derived by heat-treating a glass of the molecular percentage composition $33\text{Li}_2\text{O}\cdot 67\text{SiO}_2$. After a nucleation heat-treatment at 475°C for times ranging between 3 and 48 hours, the glass was heated at 575°C to develop a lithium disilicate crystalline phase. The volume fraction of the crystalline phase was between 0.05 and 0.95 and the crystal sizes ranged between $4.2\ \mu\text{m}$ and $61\ \mu\text{m}$; the mean crystal-crystal spacing was from $2.8\ \mu\text{m}$ to $178\ \mu\text{m}$. Inserting the appropriate values into the Griffith equation Freiman et al. calculated a critical flaw size of $85\ \mu\text{m}$ and concluded that in the early stages of crystallisation when the strengthening effect was greatest, fracture is controlled by the initiation of flaws in the glass phase rather than in the lithium disilicate spherulites. They also showed that an increase in the mechanical strength was associated with an increase in the square root of the mean crystal-crystal spacing, thus lending support to the theory of Hasselmann and Fulrath (loc.cit.). This dependence has also been confirmed by Hing and McMillan (42).

2.5 Viscous Deformation and Creep Resistance of Glass-Ceramics

In a glass-ceramic the glass phase is capable of viscous deformation and this will affect the creep resistance of the material. Many substances exhibit curves of deformation against time that can be divided into three sections (after McMillan (43)):

- (i) Primary creep which occurs from the instant of loading and decays with time.

(ii) Secondary creep where a steady creep rate is maintained for a significant period.

(iii) Tertiary creep, where the creep rate rises rapidly leading to failure of the specimen.

The secondary creep rate is usually assumed to be a separable function of three variables, the temperature T , stress, σ , and a structure factor, s . The latter factor is assumed to include the effects of grain size and other structural variables which effect creep (e.g. porosity and dislocation density). The creep rate $\dot{\epsilon}$, can then be represented by:

$$\dot{\epsilon} \propto f(T) g(\sigma) \cdot h(s)$$

The dependence of the creep rate on the applied stress is not linear and is generally of the form:

$$\dot{\epsilon} \propto \sigma^n$$

where the value of the stress exponent, n , is characteristic of the deformation process. When n has values close to unity the deformation mechanism is associated with viscous flow; values of approximately 3-4 are generally accepted as evidence of a non-viscous process.

Creep is a thermally activated process and the dependence $f(T)$, on the temperature T , is a function of the form:

$$f(T) \propto \exp \left(-\frac{\Delta H}{RT} \right)$$

where ΔH is the activation energy for creep.

Morrell (44) has studied the tensile and compressive creep behaviour of a glass-ceramic of the $\text{Li}_2\text{O}-\text{ZnO}-\text{SiO}_2$ type. The material contained crystalline phases of lithium disilicate, lithium zinc silicate and quartz together with a glass phase which constituted approximately 20 vol.%. It was deduced that the weight percentage composition of the residual glass phase was 88 SiO_2 .12 K_2O by assuming that all of the lithium and zinc ions in the original glass were incorporated in known stoichiometric crystal phases. This glass-ceramic should behave as a Newtonian fluid if this

glass phase were the rate controlling phase allowing relative sliding of the crystal phases. In this case the material would demonstrate infinite extensibility, a stress exponent of unity and an activation energy for creep characteristic of the glass phase.

The three characteristic creep regions were observed by Morrell and he deduced that the primary creep was caused by a delayed build up of elastic strain in the crystalline material; this was controlled by the viscoelastic behaviour of the glass phase. For secondary creep the activation energy was found to be the same for specimens in tension and compression and it had approximately the same value as that observed for primary creep (130 - 160 kcal/mole). Tertiary creep was caused in tension by "tearing" or crack generation from the surface and in compression by void formation and shear failure.

It was concluded that in this glass-ceramic the creep properties are controlled by the structural morphology and rate controlled by the glass phase. Viscous flow behaviour with a stress exponent, n , of approximately unity was only observed at low stresses. At higher stresses the stress exponent had values equal to or greater than six. It was suggested that under high stresses the existence of high negative hydrostatic pressures within the residual glass phase caused the nucleation and growth of voids so that the deformation was no longer at constant volume.

In the specimens tested Morrell observed evidence in the etch pattern that some grain re-orientation had occurred, compared to an as-crystallised control sample, but no preferred orientation was evident in X-ray texture patterns and no change in the volume fractions of the phases by area analysis was detected.

2.6 Electrical Properties of Glass-Ceramics

McMillan (45) has studied the electrical properties of specimens of a glass of molecular composition $30 \text{ Li}_2\text{O} \cdot 70 \text{ SiO}_2$ heat treated at 450°C -

600°C for periods of one hour. Activation energies for electrical conduction of 15.4 - 16.0 kcal/mole were measured for samples heat-treated at temperatures up to 525°C; these values were close to those of the untreated glass. After a heat-treatment at 550°C the activation energy rose to 22.8 kcal/mole; at 575°C it fell to 21 kcal/mole and to 16.7 kcal/mole after a heat treatment at 600°C. The increase in the activation energy after the heat-treatment at 525°C was interpreted in terms of a reduction of the lithia content of the glass matrix as a result of the development of lithium silicate crystals. The reduction of the activation energy resulting from the heat treatment at higher temperatures was accounted for in terms of the lithia content of the residual glass phase increasing.

Ito et al. (46) have shown that marked changes of the electrical properties of a $\text{Li}_2\text{O} \cdot 2\text{SiO}_2$ glass occurred as the material was progressively crystallised. Heat-treatment at 450°C led to no change in the activation energy but a heat-treatment at 480°C resulted first in an increase from 14 kcal/mole to 24 kcal/mole after 40 hours heat-treatment followed by a gradual decrease. This behaviour can be understood in terms of the initial formation of a residual glass phase of relatively low lithia content as a result of the crystallisation of lithium metasilicate. The gradual decomposition of this phase to lithium disilicate accompanied by the release of lithium and oxygen ions into the glass phase would account for the gradual reduction of the activation energy for conduction.

Harper et al. (13) have used loss tangent measurements to investigate crystallisation in a $\text{Li}_2\text{O} - \text{SiO}_2$ glass. Samples of the glass were heat-treated for periods of one hour at temperatures in the range 450°C - 800°C. Measurements of the loss tangent on these specimens at 20°C and 1 MHz showed that this was changed very little by heat-treatments up to 550°C.

In the heat-treatment range $600^{\circ}\text{C} - 650^{\circ}\text{C}$ however, a marked reduction of loss tangent was measured; higher temperature heat-treatments resulted in only small further changes of the loss tangent. Harper et al. attributed the reduction in loss tangent to the formation of lithium disilicate crystals which depleted the glass phase of lithium ions.

Harper and McMillan (47) have related changes in the loss tangent to changes in the volume fraction of crystals in glass-ceramics subjected to isothermal heat-treatments at 600°C .

2.7 Summary

Glass-ceramics crystallised from glasses in the $\text{Li}_2\text{O} - \text{SiO}_2$ system have been reviewed in terms of the resulting microstructure, mechanical and electrical properties. Even for this simple binary system the properties of the glass-ceramic are poorly understood. A glass-ceramic can be considered to be a two phase composite consisting of a glass matrix and dispersed crystalline phases. Interpretation of the properties of the glass-ceramic in terms of this model is not easy because the properties of the individual phases and their interactions are difficult to determine.

References

1. F.C. Kracek, J. Phys. Chem. 34 2641 (1930)
2. F. M. Jaeger and H. S. van Klooster, Proc. Amst. Acad. Sci. 16 857 (1914)
3. F. P. Glasser, Phys. Chem. Glasses 8 224 (1967)
4. A. R. West and F. P. Glasser, Mater. Res. Bull. 5 837 (1970)
5. S. M. Ohlberg, H. R. Golob and D. W. Strickler, Symposium on Nucleation and Crystallisation in Glasses and Melts. Edited by M. K. Reser (Am. Ceram. Soc. Ohio 1962)
6. W. Vogel and K. Gerth, *ibid*
7. R. D. Maurer, J. Appl. Phys. 33, 2132 (1962)
8. I. I. Kitaigorodkii and P. Ya. Khodakavskaya, The Structure of Glass Vol. 3: Catalyzed Crystallisation of Glass. Edited by E.A. Porai-Koshits (Consultants Bureau, New York 1964)
9. R. Roy, Symposium on Nucleation and Crystallisation in Glasses and Melts. Edited by M. K. Reser (Am. Ceram. Soc. Ohio 1962)
10. W. B. Hillig, *ibid*
11. J. W. Cahn, J. Am. Ceram. Soc. 52 118 (1969)
12. M. Tashiro, Proceedings of the Eighth International Congress on Glass (The Society of Glass Technology Sheffield 1968)
13. H. Harper, P. F. James and P. W. McMillan, Discuss. Faraday Soc. 50 206 (1970)
14. K. Nakagawa and T. Izumitani, Phys. Chem. Glasses 10 179 (1969)
15. R. H. Doremus and A. M. Turkalo, Presented at the Seventy-Third annual meeting of the American Ceramic Society Paper 22 - GS - 71.
16. M. Tomozowa, Phys. Chem. Glasses 13 161 (1972)
17. R. J. Charles, J. Am. Ceram. Soc. 46 235 (1963)
18. A. E. Dale, E. F. Pegy and J. E. Stanworth, J. Soc. Glass Technol. 35 T136 (1951)
19. O. L. Anderson and D. A. Stuart, J. Am. Ceram. Soc. 32 573 (1954)

20. E. A. Porai Koshits, Editor: Catalysed Crystallisation of Glass
(Consultants Bureau, New York 1964)
21. E. A. Porai Koshits and N. A. Toropov, Structural Transformation in Glasses
at High Temperatures (Consultants Bureau, New York 1965)
22. S. V. Phillips and P. W. McMillan, Glass Technol. 6 46 (1965)
23. J. G. Morley, *ibid* 6 77 (1965)
24. P. W. McMillan, Glass-Ceramics (Academic Press, London and New York 1964)
25. R. H. Doremus and A. M. Turkalo, Phys. Chem. Glasses 13 14 (1972)
26. P. Hing and P. W. McMillan, J. Mater. Sci. 8 340 (1973)
27. M. A. Matveev and V. V. Velya, Steklo i Keram 16 14 (1959)
28. E. F. Cherneva and V. A. Florinskaya, Russ. J. of Phys. Chem. 39 269 (1965)
29. D. L. Kinser and L. L. Hench, J. Mater. Sci. 5 369 (1970)
30. D. L. Kinser and L. L. Hench, J. Am. Ceram. Soc. 51 445 (1968)
31. S. W. Freiman and L. L. Hench, *ibid* 51 382 (1968)
32. C. L. Booth and G. E. Rindone, *ibid* 47 25 (1964)
33. D. B. Binns, Science of Ceramics Vol. 1 edited by G. H. Stewart
(Academic Press, London 1962)
34. D. P. H. Hasselman and R. M. Fulrath, J. Am. Ceram. Soc. 49 68 (1966)
35. D. P. H. Hasselman and R. M. Fulrath, Ceramic Microstructures: edited by
R. M. Fulrath and J. A. Pask (John Wiley & Sons, New York 1968)
36. W. J. Frey and J. D. Mackenzie, J. Mater. Sci. 2 124 (1967)
37. R. R. Tummala and A. L. Friedberg, J. Am. Ceram. Soc. 52 228 (1969)
38. R. W. Davidge and T. J. Green, J. Mater. Sci. 3 629 (1968)
39. N. Miyata and H. Jinno, *ibid* 7 973 (1972)
40. Y. Usumi and S. Sakka, J. Am. Ceram. Soc. 53 286 (1970)
41. S. W. Freiman and L. L. Hench, *ibid* 55 86 (1972)
42. P. Hing and P. W. McMillan, J. Mater. Sci. 8 1041 (1973)
43. P. W. McMillan, Glass Technol. 15 5 (1974)

44. R. Morrell, Ph.D. Thesis, University of Bristol (1970)
45. P. W. McMillan in *Advances in Nucleation and Crystallization in Glasses*.
Edited by L. L. Hench & S. W. Freiman (Am. Ceram. Soc. Ohio 1971)
46. M. Ito, T. Sakano and T. Moriya, *Bull. Tokyo Inst. Tech.* 88 151 (1968)
47. H. Harper and P. W. McMillan, *Phys. Chem. Glasses* 13 97 (1972)

CHAPTER 3: EXPERIMENTAL METHODS FOR DETERMINING THE PHYSICAL PROPERTIES OF THE GLASS-CERAMIC

3.1 Introduction

In this chapter details are presented of the experimental apparatus and techniques used in the measurement of the physical properties of the glass-ceramics studied.

The preparation of the initial glass and subsequent devitrification into a glass-ceramic is described. The construction and use of a differential thermal analysis apparatus is presented. The apparatus and experimental techniques used in measuring the density, certain mechanical and electrical properties and the coefficient of thermal expansion are described.

3.2 Glass Preparation

The compositions of the glass studied are given in Table 3.1; these compositions were selected because of the shape of the crystalline phases present and the low melting point of the glass-ceramic (Chapter 7 contains details of the crystalline phases).

The glasses were prepared from Brazilian quartz, ground to pass through a 60 mesh sieve, high purity lithium carbonate and A.R. lithium orthophosphate, potassium carbonate, aluminium oxide and boric oxide. The materials were thoroughly dried, weighed and mixed by milling in a rotary ball mill for two hours. The glasses were melted and refined in a platinum crucible at 1400°C until bubble-free, quenched into a melting mixture of ice, and then crushed and dried. This process was repeated twice with the object of achieving good homogeneity. The glasses were remelted for two hours and cast into moulds coated with a graphite suspension to prevent the glass sticking.

	SiO ₂	Li ₂ O	K ₂ O	Al ₂ O ₃	P ₂ O ₅	B ₂ O ₃
Glass A	61.0	30.5	15	10	10	5.0
Glass B	67.5	24.0	15	10	10	5.0

Table 3.1 Glass compositions in mol. %.

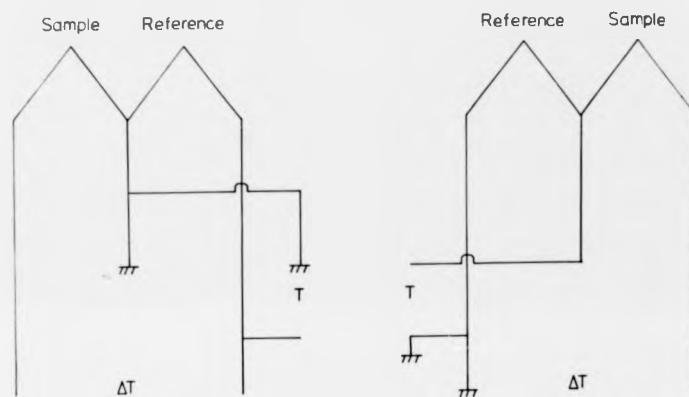


Figure 3.1 Thermocouple circuitry for DTA;

T is the temperature of the reference material and
 ΔT is the temperature difference between the sample
 and the reference material.

The glasses were heat-treated by placing samples on a platinum sheet in a muffle furnace. Thermocouples of Pt. and Pt.-13% Rh. were used to control and monitor the temperature unless otherwise stated. The range of temperature over which the glass devitrified was determined by a heat-treatment schedule and by differential thermal analysis.

3.3 Differential Thermal Analysis

3.3.1 Introduction

When a material passes from one state to another, energy in the form of heat is either absorbed or evolved. Differential thermal analysis (DTA) is a technique for measuring the magnitude of the heat effect and the temperature at which it occurs. In the case of a glass-ceramic, DTA can be used to determine the transformation temperature T_g , the temperature at which crystallisation of the glass starts and the temperature at which the first melting of the material occurs.

In a DTA apparatus, thermocouples are placed in close contact with two finely powdered and compressed samples, one of which is the substance under investigation and the other, an inert material or a substance with known thermal properties (the reference material). The thermocouples are connected so that their e.m.f.s. are opposed; the net e.m.f. therefore represents the temperature difference between the sample and the reference material (Figure 3.1).

The two materials, usually contained in small crucibles, are heated together at a constant rate. In the steady state, the differential e.m.f. which is a function of the temperature difference will be a constant. Whenever the temperature passes through some point of exothermic (endothermic) transition the extra amount of heat released (absorbed) tends to increase (retard) the rate of temperature rise of the specimen.

After the required amount of heat has been released (absorbed), the differential e.m.f. gradually returns to a constant. If the differential temperature is plotted as the ordinate against the temperature of the reference material as abscissa, then endothermic effects are indicated as dips in the curve and exothermic effects as perks (1-3).

3.3.2 DTA Apparatus

An apparatus was designed and constructed to measure the differential e.m.f. between the sample and the reference material and the temperature of the latter. The two samples were contained in small platinum crucibles 0.6 cm in diameter and 0.7 cm in height; each crucible contained approximately 0.5 grams of material. The temperature and the differential temperature were measured with Pt. - Pt. - 1% Rh. thermocouples embedded in the material. Aluminium oxide was used as the reference material. To ensure that the temperature and rate of rise of temperature were identical for both crucibles, they were positioned close together in a block of firebrick. This specimen holder was placed inside a tube furnace which could be rolled away from the specimen holder to quench the samples.

Preliminary experiments to check the performance of the system were carried out using lithium sulphate as a sample. Lithium sulphate has a liquidus temperature of 865°C , at which temperature a cubic modification of the salt crystallises from the melt; on further cooling a polymorphic inversion to a hexagonal modification occurs at 575°C (4). These two transition temperatures were used as test parameters in an evaluation of the sensitivity of the DTA apparatus.

Initially a differential DC amplifier was used to increase the differential e.m.f. signal (5); this method of amplification did not prove to be very satisfactory because of noise and drift problems associated with

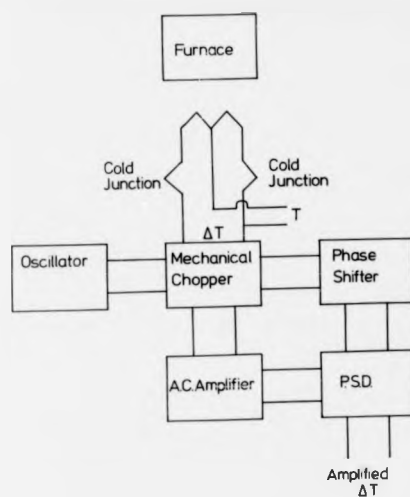


Figure 3.2(a) Block diagram of the DTA apparatus.



Figure 3.2(b) Photograph of the DTA apparatus.

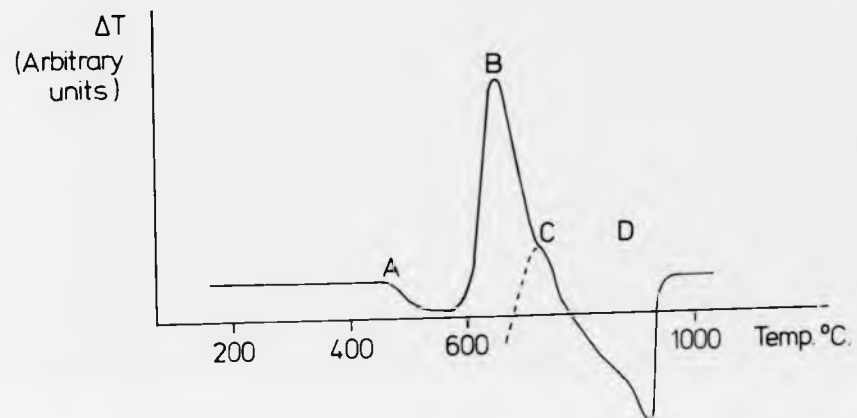


Figure 3.3 DTA thermogram of Glass A.

the amplifier. To overcome these difficulties, the differential e.m.f. was mechanically chopped and amplified with a low noise AC amplifier. This signal was then detected and rectified with a phase sensitive detector. The mechanical chopper operated at 79 c.p.s. and was positioned in the circuit so that the A.C. amplifier was never open circuited. All electrical wiring outside the furnace was shielded in earthed conduits from electrical interference. Specimens were prepared for DTA by powdering the quenched glass (< 300 mesh) and lightly tamping the powder in the crucible around the thermocouple. The rate of rise of temperature in all the DTA experiments was 20°C/min. Figure 3.2(a) shows a block diagram of the apparatus and Figure 3.2(b) is the apparatus in use.

A typical DTA curve of glass A is shown in Figure 3.3. As the temperature is increased a dip A, can be seen in the DTA curve due to a slight absorption of heat which occurs when the glass transformation temperature is reached. With a further increase of temperature a sharp exothermic peak B, can be seen, corresponding with the appearance of a crystal phase. A second exothermic peak at C may also occur. At a higher temperature still, an endothermic effect D, associated with the first melting of the glass or crystalline phases occurs.

The results obtained with the apparatus described were compared with those obtained with a Dupont 900 Differential Thermal Analysis Apparatus with a specimen of the same preparation and composition. The endothermic and exothermic peak positions and widths obtained for the two apparatus corresponded almost exactly.

The transition temperature of a phase change, observed by DTA can be defined in two ways. The onset transition temperature is the temperature at which the thermogram starts to depart from the baseline; the extrapolated onset is the temperature corresponding to the intersection of extrapolations of the baseline and the longest straight line of the

low temperature side of the endotherm or exotherm. Extrapolated onset transition temperatures were measured from the thermograms in this work.

The DTA curve can provide information which is of assistance in devising heat-treatment schedules for glass-ceramics. The thermogram indicates the temperature ranges in which crystallisation occurs and the maximum temperature to which the glass-ceramic can be heated without encountering deformation due to the melting of the phases. It must be stressed however, that care must be taken in interpreting the data obtained from the DTA curve. The position and width of the exotherm or endotherm is not only a function of the phase transition occurring^r but also of the rate of rise of temperature and the specimen preparation[^] technique. The transition temperatures are not the same when measured with a solid sample compared with a powdered sample (1,2). The DTA of glass-ceramics can only be used as a guide for subsequent heat-treatment temperatures.

3.4 Density Measurement

Archimedes method was used to measure the density of the glass-ceramics studied. Distilled water was used in most cases as the standard density; for small specimens a suitably dense liquid, namely ethylene dibromide was used to increase the accuracy of the results.

3.5 Mechanical Properties

3.5.1 Introduction

The mechanical strength of a material is one of its most important properties because it is often the major factor in determining the suitability of the material for a particular application. At room temperature glass-ceramics, like ordinary glass and ceramics, are brittle materials. They exhibit no region of ductility or plasticity and show

perfectly elastic behaviour up to the load which causes failure. Like other brittle solids, glass-ceramics have relatively high elasticities and are capable of developing forked fractures.

In this present work, microhardness measurements and three-point bend experiments were made on the glass-ceramics studied.

3.5.2 Microhardness Measurements

Indentation hardness has been widely applied in the metallurgical field and this method has also been used to study glasses and similar materials. Under suitable conditions, the point of a diamond pyramid will penetrate a glass surface leaving a permanent indentation.

The mechanism by which the indentation is formed is complex. The fact that glass flows during indentation, resulting in a permanent impression has been attributed by several authors to plastic flow analogous to that which occurs in metals (6-8). Ernsberger (9) however, believes that yielding results from localized densification of the glass around the indenter. Douglas (10) has shown by theoretical considerations that the indentation hardness is a function of the fictive temperature and viscosity of the glass.

The flow mechanism which occurs when a surface is indented will be impeded by the closely spaced second phase particles which exist in a glass-ceramic. This will lead to an increase in hardness; the dependence of the microhardness on the morphology of the crystalline phases present in a glass-ceramic has been reported by several authors (11-13).

In this present work values of the Vickers Hardness and the Knoop hardness were measured for glass-ceramic specimens. The Vickers Hardness Number H_v , is a number related to the applied load and the surface area of the permanent impression made by a square-based pyramidal diamond indenter having included face angles of 136 degrees. The hardness

H_v is defined as (14):

$$H_v = \frac{2P \sin \alpha / 2}{D^2} = \frac{1854 P}{D^2} \text{ kg/mm}^2$$

where P = indenting load in grams
 D = mean value of the impression diagonal in microns
 α = 136° angle between opposite indenter faces.

The Knoop indenter (15) gives an indentation in the form of an elongated pyramidal impression, its length being seven times the width and thirty times the depth. The variation in the hardness of a material as a function of orientation can be measured using the long axis of the Knoop indenter as a reference. The Knoop hardness H_k is defined as:

$$H_k = \frac{14230 P}{L^2} \text{ kg/mm}^2$$

where P = indenting load in grams
 L = length of the long diagonal of the indent in microns.

The diamond indenter was contained in a modified McCrone microhardness apparatus mounted on an inverted optical microscope. Indentations were made on glass-ceramic surfaces polished to a one micron diamond paste finish. A 200 gram load was used for both types of indenter. A minimum of ten indentations were made for each value of the hardness evaluated and the loading cycle was standardized with a period of 10 seconds at full load. The diagonal lengths of the impression were measured with a calibrated eyepiece graticule.

3.5.3 Three-Point Bending Experiments

The modulus of rupture and Young's modulus in bending of glass-ceramic specimens were determined by a three-point bend technique. In this method a beam of rectangular cross-section is placed across two parallel knife edges. A third knife edge is positioned between and parallel to these two knife edges and loads the specimen at a constant rate.

The modulus of rupture σ_F , of a rectangular bar for centre loading is determined from the expression:

$$\sigma_F = \frac{3P_F L}{2bd^2} \quad \text{Equation 3.1}$$

where P_F = the load to fracture
 L = distance between outer knife edges
 b = width of the beam
 d = thickness of the beam

The Young's modulus in bending E_b , is determined from the force-deflection curve using the expression:

$$E_b = \frac{PL^3}{4bd^3y} \quad \text{Equation 3.2}$$

where y = the deflection corresponding to a load P (16).

Initially a three-point bending jig with a 3.8 cm span between the outer knife edges was used; an Instron Universal Testing Machine operating at a cross-head speed of 0.02 cm/min. was used to load the specimen. On average ten specimens were used for each strength determination, all of which were made at room temperature.

The effect of the condition of the surface upon the mechanical strength of glass-ceramics has been investigated by Watanabe et al. (17). Their investigations showed that a glass-ceramic which had been heat-treated to achieve maximum strength was weakened by a standard abrasion treatment (18). In the present work the specimens for mechanical strength measurements were given a standard surface abrasion to reduce the scatter in the results. All the three-point bend specimens were abraded in a rotary mill for 60 minutes with silicon carbide (\leq 100 mesh).

The glass-ceramic with a preferred crystal orientation was produced as rods 0.25 inch in diameter. Three-point bend tests were carried out on this material parallel and perpendicular to the orientation. A miniature jig was constructed for this purpose.

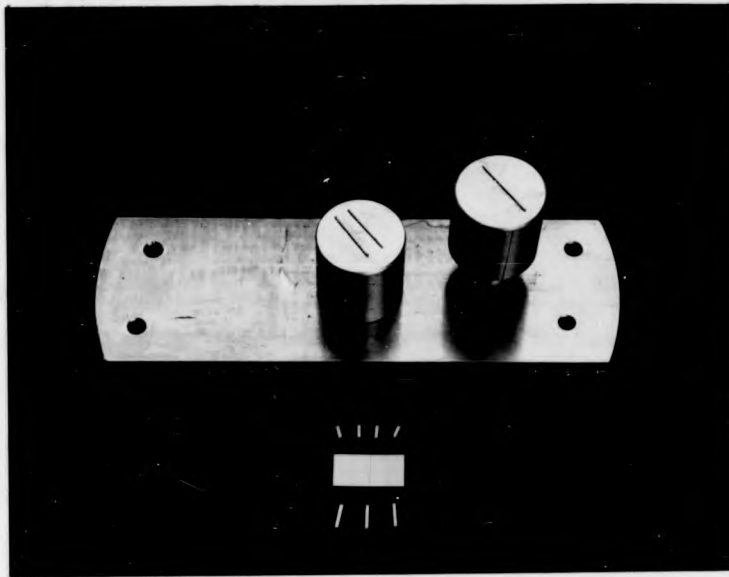


Figure 3.4 Miniature 3-point bend apparatus.

3.5.4 Miniature Three-Point Bending Experiments

The miniature three-point bending jig which was constructed consisted of stainless steel knife edges made from pins. These knife edges were glued into position on two stainless steel blocks. One of these blocks was fitted to a load cell and the other was attached to the cross-head of an Instron machine. The span between the outer two knife edges was 0.41 cm and the dimensions of the specimen were typically 0.1 cm x 0.1 cm x 0.6 cm. The speed of the cross-head was 0.002 cm/min and the specimens were fractured at room temperature. The dimensions of the specimen and apparatus were scaled down by the same factor relative to the large three-point bending apparatus. It was found that the rate of loading of the miniature specimen had also to be scaled down so that the bending characteristics of the sample could be measured. Figure 3.4 shows the miniature apparatus and specimens before and after testing.

The load was applied at a constant rate by the cross-head and was monitored against time on a chart recorder; a graph of the load against the displacement of the cross-head could therefore be drawn. A load cell rated at 50 kg maximum load and having 'soft' loading characteristics was used. The measured displacement of the cross-head, for a given load on the cell corresponded to the sum of the deflection of the specimen and the downward movement of the load cell. To take this effect into account the load-displacement curve of the apparatus without a specimen was measured after testing each batch of specimens. The measured load-displacement curve of each specimen was then corrected to give the load-specimen deflection curve; the gradient of this curve was used to evaluate the Young's modulus of the specimen from Equation 3.2.

Berg et al. (19) have numerically studied the deformation of a short beam specimen in three-point bending and conclude that areas of

high stress concentration exist in the specimen in the vicinity of the knife edges. This stress concentration results in a plastic zone under the contact load and then Equations 3.1 and 3.2 are no longer valid for the system.

To test these conclusions glass-ceramic beams were broken on the large span jig and small beams were then prepared from the fractured halves of each specimen. These specimens were tested on the miniature jig. The results calculated from Equations 3.1 and 3.2 for the large and miniature span tests showed very good agreement. It was concluded that the scaling down of the three-point bending apparatus did not produce any points of stress concentration in the specimen and Equations 3.1 and 3.2 were still valid (20).

The size of a poly-phase specimen in miniature bend tests has to be chosen with care; the thickness of the sample must represent the bulk material. In the limit of very thin glass-ceramic specimens the results obtained would relate to single crystals and not the bulk material. The specimens used in this work contained a minimum of 300 crystals across the shortest dimension of the beam. The technique of using small specimens has the advantage of using a small volume of material and variations in heat-treatment between specimens are negligible.

3.6 Electrical Measurements

3.6.1 Introduction

The resultant electrical properties of a multiphase material depend on the electrical properties of the individual phases and the boundaries between them, and also on their size, shape and connectivity. In practice the information which can be obtained from electrical measurements on such a material may be rather limited. However, the technique of electrical

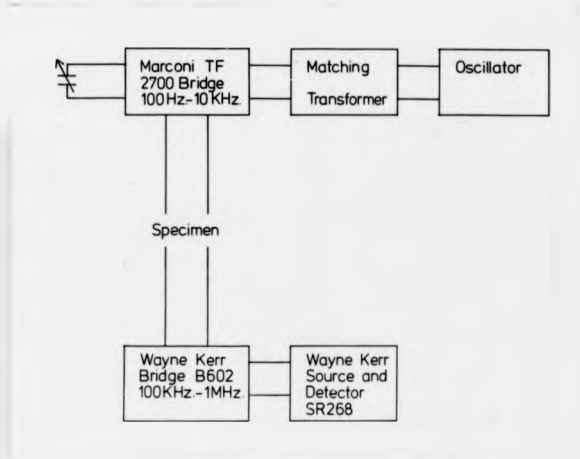


Figure 3.5(a) The circuit for the electrical property measurements.

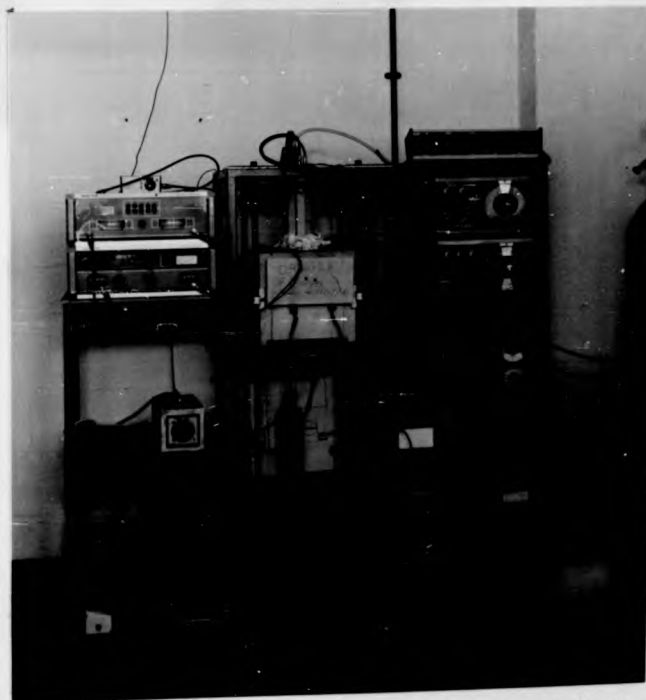


Figure 3.5(b) Photograph of the Electrical Measurement Apparatus

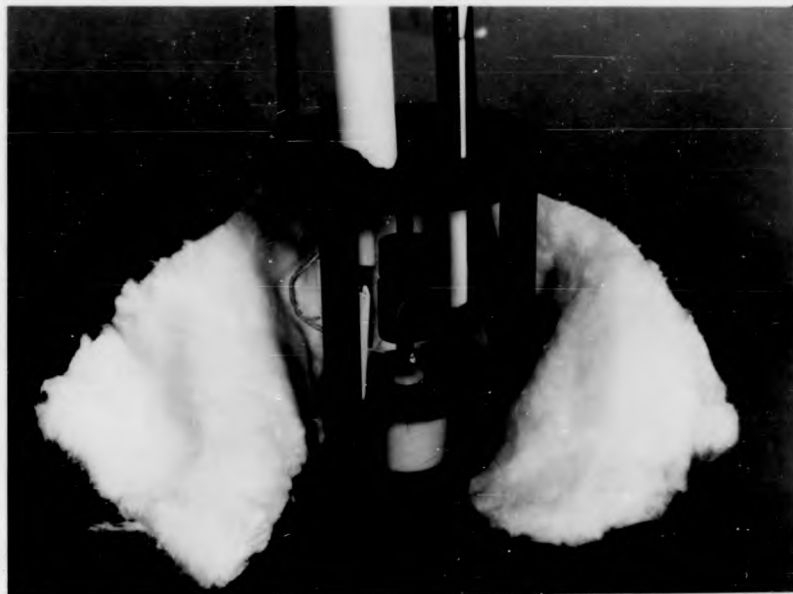


Figure 3.6 The specimen holder for the electrical property measurements.

measurement is particularly relevant to studies of the microstructure and formation of glass-ceramics, since those most commonly produced are ionic conductors.

An apparatus was constructed to measure the real and complex parts of the impedance of a glass-ceramic between 100 Hz and 1 MHz.

3.6.2 Apparatus and Measurement

Impedance measurements in the range 100 Hz to 10 KHz were made with a Marconi TF 2700 Universal Bridge. This bridge is basically an AC Wheatstone Bridge and was used to measure the resistance of the specimen; the shunt capacitance of the specimen was balanced out with a variable capacitance in the circuit. Resistances less than $10^7 \Omega$ could be measured with an accuracy of the order $\pm 2\%$. From 100 KHz to 1 MHz a Wayne-Kerr bridge type B602 was used; the accuracy of this bridge depends upon the relative magnitudes of the real and complex components of the impedance which is being measured. In practice it was found that measurements of the resistivity and dielectric constant were usually made to an accuracy of a few per cent. Figure 3.5 shows the measuring circuit and the apparatus.

A specimen holder was constructed similar to the one described by Owen (21). It was made entirely of stainless steel and refractory tubing (Figure 3.6); the specimens were clamped between plane electrodes in the holder. The temperature of the specimen was measured with a chromel-alumel thermocouple and the holder was bandaged with a refractory wool to minimise convection currents. The holder was electrically shielded in a stainless steel tube which fitted into a Super Kanthal furnace, arranged to heat the specimen holder. Electrical measurements could be made from room temperature to approximately 750°C ; with the specimen in a dry nitrogen atmosphere the maximum rate of rise of temperature at the specimen was approximately $4^\circ/\text{minute}$.

Specimens were prepared by cutting parallel sided slices (~ 0.1 cm thick) of the glass-ceramic and polishing both sides to a 6 micron diamond paste finish. Silver electrodes of unequal size were evaporated onto the specimen. One side of the specimen was completely coated with silver to form one electrode and to the other side a smaller circular electrode of diameter 0.31 cm was applied. The electrodes were painted with a silver "Dag" suspension for strength. The specimens were dried at 120°C for 30 minutes before making measurements to eliminate the possibility of surface conduction by water through small cracks which the heat-treatment might have produced. A guard ring was found to be unnecessary and a series of different electrode materials (Au, Ag, Pt, Au/Ir) were found to give equivalent results.

The electrical measurements were interpreted in terms of the volume resistivity, the dielectric constant and the loss tangent ($\tan \delta$) of the specimen.

The volume resistivity ρ is related to the measured resistance of the specimen, R , by:

$$\rho = \frac{AR}{\ell}$$

where A = the area of the smaller circular electrode

ℓ = the thickness of the specimen.

Corrections due to the expansion of the holder and specimen were negligible.

The dielectric constant of the specimen, K' , is the ratio of the capacitance, C_x , for a given configuration of electrodes with the specimen as dielectric, to the capacitance, C_v , of the same electrode configuration with a vacuum (or to a good approximation, air) as the dielectric:

$$K' = \frac{C_x}{C_v}$$

The capacitance of the specimen, C_x , was measured and C_v , for the electrode configuration used is given by (22)

$$C_v = \frac{0.06954d^2}{\ell} \text{ pF}$$

where d = diameter of smaller electrode (cm)

ℓ = thickness of specimen (cm)

The vacuum capacitance can be corrected for fringing and stray capacitance caused by not using a guard ring but this was considered to be unnecessary (22). The capacitance of the electrical connections between the specimen and measurement bridges was found to be less than 5% of the specimen capacitance and was not taken into account.

The loss tangent, $\tan \delta$, was evaluated from the measured capacitance, C_x and the resistance, R , of the specimen by (23):

$$\tan \delta = \frac{1}{\omega RC_x}$$

where ω is the angular frequency at which R and C_x were measured.

Experimentally it was found that the resistance of the specimen was too high to be measured below 300°C and that the calculated electrical properties were independent of the sample dimensions. Measurements of the resistance and capacitance of the specimen were made from a temperature of approximately 300°C and at temperatures increasing by intervals of approximately 40°C. At each temperature these two parameters were measured at 100 Hz and frequencies increasing by a factor of 10 to 1 MHz. The resistivity, dielectric constant and power factor were then evaluated as a function of frequency and temperature.

3.7 Thermal Expansion Measurements

3.7.1 General Considerations

The change in dimensions which occur with change of temperature of

a glass-ceramic are important for a number of reasons. For a material with a high thermal shock resistance, the coefficient of thermal expansion should be as low as possible to minimise strains resulting from temperature gradients within the material. Also if the glass-ceramic is to be sealed to another material, close matching of the thermal expansion coefficients is necessary to prevent the generation of high stresses when the composite article is heated or cooled.

Glass-ceramics are remarkable for the very wide range of thermal expansion coefficients which can be obtained. At one extreme, materials with a negative coefficient of thermal expansion can be prepared, while for other compositions very high positive coefficients are available. Between these two extremes there exist glass-ceramics having thermal expansion coefficients practically equal to zero and others whose expansion coefficients are similar to those of ordinary glass, ceramics, metals or alloys.

The thermal expansion coefficients of glass-ceramics are generally markedly different from those of the parent glass. Devitrification of the glass may result in raising or lowering of the expansion coefficient depending upon the types of crystal which are formed.

3.7.2 Measurement of the Thermal Expansion Coefficient

The coefficient of thermal expansion of the glass-ceramics studied was measured with a silica dilatometer. The apparatus used consisted of a fused silica specimen holder and a linear variable differential transformer (LVDT). The LVDT produced an electrical signal proportional to the linear displacement of its core. The specimen holder was positioned in a furnace and the expansion of the specimen was transmitted via a vertical silica push rod to the core of the LVDT. The top of this push rod and the LVDT were kept at a constant temperature. The LVDT had a sensitivity of 4.32 mV per micron displacement of the push rod and the

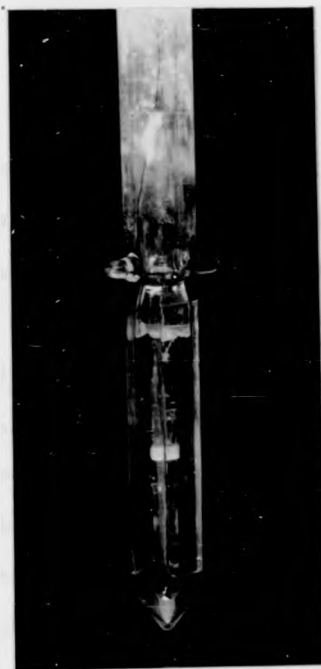


Figure 3.7 The Dilatometer specimen holder.

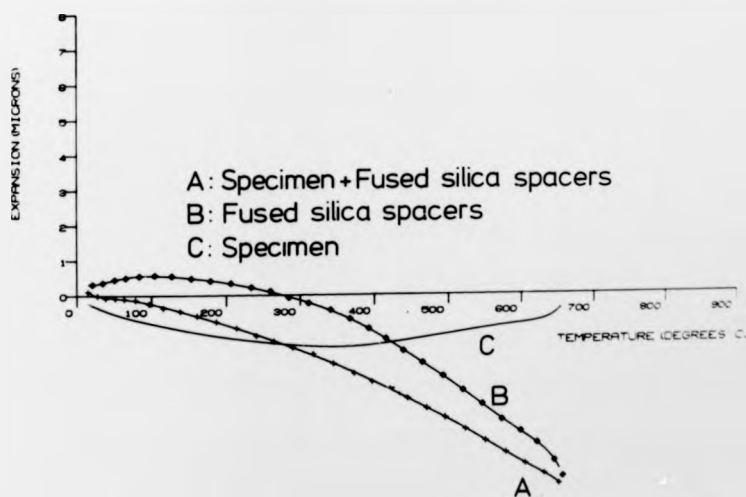


Figure 3.8 The expansion curve of a silica specimen.

specimen holder could be heated to approximately 1000°C . The rate of rise of temperature was 2.5°C per minute and the temperature at the specimen was measured with a chromel-alumel thermocouple.

The apparatus was designed to measure the expansion of specimens approximately 6 cm in length. In this present work the average size of the specimens was 0.3 cm; to accommodate these small specimens, fused silica spacers were used in the specimen holder. Figure 3.7 shows the specimen holder; the bottom of the silica push rod and the spacers can be seen with a specimen in position (white, centre). The output from the LVDT and the thermocouple e.m.f. of the specimen temperature were recorded against time on a two pen chart recorder.

If l_0 is the length of the specimen at temperature T_0 and l is the specimen length at temperature T , then the coefficient of thermal expansion, α , is given by:

$$l = l_0 [1 + \alpha (T - T_0)]$$

In an ideal silica dilatometer, if the 'specimen' was made of silica, the expansion measured by the LVDT would be independent of temperature; the expansions of the specimen holder and specimen would nullify each other. The coefficient of thermal expansion of a specimen would then be measured relative to that of vitreous silica. In the apparatus used the expansion of the silica spacers was measured and was found to be a function of the temperature of the specimen holder. This characteristic expansion of the specimen holder was taken into account when evaluating the expansion of a specimen. The expansion of a specimen was measured as a function of temperature and the characteristic expansion of the specimen holder was subtracted from this curve. This difference expansion curve for the specimen should then be a measure of the specimen's expansion relative to that of silica.

The expansion of a 0.3 cm thick silica specimen (the typical size of the glass-ceramic specimens) together with the silica spacers used to calibrate the specimen holder was measured. Figure 3.8 is a graph of the expansion of the silica spacers and the expansion of the silica spacers plus the silica specimen against temperature. The difference between these two expansion curves is approximately a straight line and the coefficient of expansion of the silica specimen measured from this difference curve gives a value of $\alpha = 9.8 \cdot 10^{-7}$ per C. degree in the temperature range 400°C to 600°C. The coefficient of expansion of fused silica is $5.4 \cdot 10^{-7}$ per C. degree. The cause of this effect is not understood but it is thought to be a consequence of temperature gradients along the silica push rod and the increased length of the push rod with a silica specimen in position.

The expansion curve of each glass-ceramic specimen was measured as a function of increasing and decreasing temperature. The temperature cycle was repeated five times and the characteristic expansion of the specimen holder was subtracted from each curve. Then values of the coefficient of expansion for each specimen were evaluated from these difference curves. If no systematic variation in the expansion with temperature cycling was noted the mean thermal coefficient of expansion and the standard deviation were evaluated from the gradients of the ten difference curves. The standard deviation of the mean coefficient of expansion of the glass-ceramic specimens measured by this technique was approximately equal to the expansion coefficient of fused silica.

The coefficient of expansion was measured using large specimens (approximately 6 cm in length) for selected glass-ceramics. The results obtained from these specimens were in very good agreement with the values calculated from the difference curves of similar small specimens.

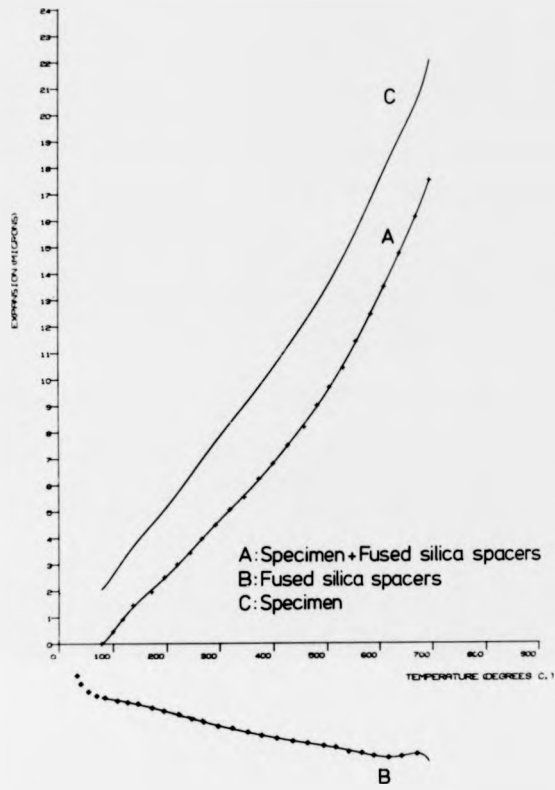


Figure 3.9 Typical computer output of thermal expansion curves.

A computer programme was developed to evaluate the difference expansion curves. The programme fitted a polynomial function by a generalised least squares method to the specimen expansion - temperature curve and to the characteristic expansion of the specimen holder. Data for these two curves were measured at approximately 20 C. degree intervals from the chart recorder output. The specimen holder expansion polynomial was subtracted from the polynomial fitted to the specimen expansion curve and this difference curve and the input data were plotted by the programme. Figure 3.9 shows the typical computer output. The coefficient of thermal expansion was measured from the gradient of the difference curve.

References

1. W. J. Smothers & Chiang Yao, Differential Thermal Analysis: Theory and Practice (Chem. Pub. Co. Ltd. 1958)
2. W. J. Smothers & Chiang Yao, Handbook of Differential Thermal Analysis (Chem. Pub. Co. Ltd. 1964)
3. R. C. Mackenzie (editor) Differential Thermal Analysis (Acad. Press, London 1970)
4. American Institute of Physics Handbook (McGraw-Hill, New York 1963)
5. see for example: S. W. Amos, Principles of Transistor Circuits (Illiffe Books Ltd., London 1969)
6. E. W. Taylor, Nature 163 323 (1949)
7. L. Ainsworth, J. Soc. Glass Technol. 38 479 T (1954)
8. W. C. Lonvengood, J. Am. Ceram. Soc. 52 403 (1969)
9. F. M. Ernsberger, *ibid*, 51 545 (1968)
10. R. W. Douglas, J. Soc. Glass Technol. 42 145 T (1958)
11. I. W. Donald & R. A. McCurrie, J. Am. Ceram. Soc. 55 289 (1972)
12. N. A. Toropov & N. A. Sirazhiddinov, Neorganicheskie Materialy 2 738 (1966)
13. M. Tashiro & S. Sakka, Kyoto Univ. Inst. for Chem. Res. Bull. 42 351 (1964)
14. American Society for Testing and Materials ASTM Designation: E92 - 67
15. F. Knoop, C. G. Peters & W. B. Emerson, J. Res. Nat. Bur. Standards, 23 39 (1946)
16. see for example: J. Marin, Mechanical Behaviour of Engineering Materials (Prentice-Hall International, London 1962)
17. M. Watanabe, R. V. Caporali & R. E. Mould, Symposium on Nucleation and Crystallization of Glasses (American Ceramic Society 1962)
18. R. E. Mould & R. D. Southwick, J. Am. Ceram. Soc. 42 582 (1954)
19. C. A. Berg, J. Tirosh & M. Israeli, Composite Materials: Testing and Designing (2nd Conference) ASTM STP 497 (American Society for Testing and Materials 1972)

20. R. E. Mould, J. Appl. Phys 29 1263 (1958)
21. A. E. Owen, Phys. Chem. Glasses 2 87 (1961)
22. ASTM Designation: D150 - 65 T
23. see for example: B. I. Bleaney & B. Bleaney, Electricity and Magnetism (Oxford University Press, London 1962)

CHAPTER 4: TRANSMISSION AND SCANNING ELECTRON MICROSCOPY

4.1 Introduction

This chapter contains details of the techniques used to investigate the microstructure of glass-ceramic materials. Methods of specimen preparation for transmission electron microscopy, scanning electron microscopy and X-ray diffraction experiments are described.

Results of the observation of cathodoluminescence from glass-ceramics are presented and the potential of using this technique for the examination of low atomic number materials is discussed.

The data in sections 4.4.3, 4 and 5 was collected by Mr. P. Watt.

4.2 Transmission Electron Microscopy

4.2.1 Introduction

The main difficulty in investigating glass-ceramic microstructures by transmission electron microscopy is the preparation of sections thin enough to transmit the electron beam. Several methods have been investigated. A JEM 7 electron microscope operating at 100 kV was used in this work. Thin specimens were mounted in a $+30^\circ$ tilting stage.

4.2.2 Fragmentation

The fragmentation technique for producing thin areas was found to be useful for the study of brittle materials in this work (1,2). A sample of the material to be studied was crushed to a powder initially using a percussion mortar and then an agate mortar and pestle. The powdered material was then tapped onto a glass microscope slide. A 100 mesh copper grid which had been previously coated in a solution of 'sellotape' adhesive dissolved in chloroform, was pressed into the finest

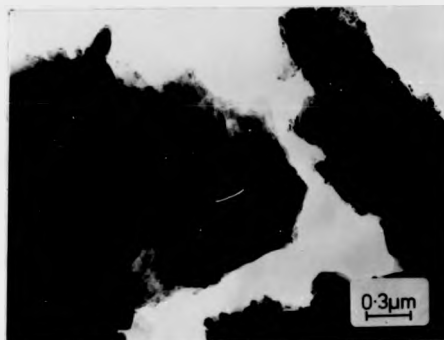


Figure 4.1 A thin area of a glass-ceramic produced by the fragmentation technique.

fragments. The grid was then inverted and gently tapped to release any loose particles and placed in the microscope specimen holder. The grid squares were then systematically examined, and the position of those containing thin areas noted for subsequent investigation. Figure 4.1 shows a typical micrograph of a thin area prepared by this technique.

This procedure of specimen preparation was found to give only small areas thin enough to transmit the electron beam in glass-ceramic specimens. Specimen charging was also found to be a problem. This could be diminished by coating the specimen and grid with a thin layer ($< 250 \text{ \AA}$) of evaporated carbon or using a copper grid pre-coated with a carbon support film before dusting the powdered specimen onto it. The advantage of this method is that it permits selected area diffraction and dark field image micrographs to be recorded.

4.2.3 Carbon Replication

The preparation of replicas or casts of specimens which are opaque to electrons enables their surface structure to be studied in the electron microscope. Replicas consist of thin films of electron transparent material corresponding exactly to the surface topography of the specimen.

The use of carbon replicas pre-shadowed with platinum was investigated(3). The surface of the specimen to be replicated ($\sim 1 \text{ cm}^2$) was polished flat with 6 \mu m followed by 1 \mu m diamond paste and etched in a 5% solution of hydrofluoric acid. A five second etch with gentle agitation was found to give the best results. The etching solution attacked the glass phase of the glass-ceramic faster than the crystalline phases and hence produced a surface topography.

To increase the contrast in the microscope, the specimen was pre-shadowed with platinum in vacuo ($< 10^{-3} \text{ mm Hg}$) from an angle of 60° to the normal; carbon was then evaporated onto the surface at normal incidence.

To remove the replica from the specimen, areas approximately 4 mm square were scratched onto the surface and the specimen was slowly immersed at an angle into a 5% solution of hydrofluoric acid. After several repeated immersions the carbon film remained on the liquid surface as the specimen was lowered into the liquid. Each 4 mm square was then floated onto a copper grid and refloated onto distilled water, this process was repeated several times to remove the acid solution. The replicas can be easily seen floating on the liquid surface by the observation of reflected light. The replica was finally floated onto a copper grid and carefully dried in front of a lamp. Figure 4.2 shows a typical pre-shadowed replica of a glass-ceramic surface.

This technique for preparing specimens was found to be reasonably simple and efficient, however the selected area diffraction and dark field image modes of the microscope no longer contain information about the replicated material. The observed microstructures can also depend on the precise etching treatment applied and hence care must be used in the interpretation of the micrographs.

4.2.4 Chemical Thinning

This method enables thin sections to be obtained where the bulk material contains a single phase or a small volume fraction of a second phase (4).

Thin slices approximately 250 μm thick were cut, using a diamond saw, from the specimen. The surfaces of the slice were polished flat with 6 micron, followed by 1 micron diamond paste. Each specimen was held near the rim with a pair of fine tweezers and the rim was covered with a thin coating of material inert to chemical attack (Lacomit varnish was found suitable). The slice was then immersed in a thinning solution of volume composition $5\text{HF} - 2\text{HCl} - 93\text{H}_2\text{O}$ (5). The specimen was frequently

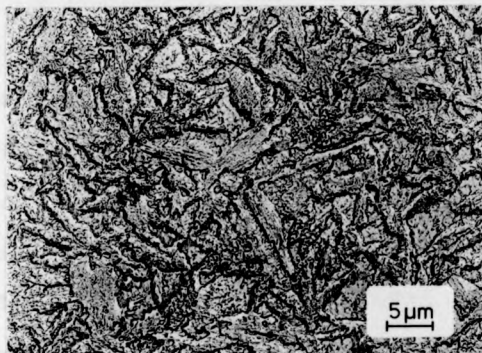


Figure 4.2 Typical pre-shadowed replica of a glass-ceramic surface.



Figure 4.3 Typical chemically thinned area of a phase separated glass.

agitated in the solution until perforation of the slice occurred. The slice was then carefully washed in distilled water and methanol and a small piece of the specimen was broken off from the edge of the hole and mounted in a double copper grid for examination in the microscope. Figure 4.3 shows a typical thinned area of a phase separated glass.

Chemical thinning is a very powerful method of preparing electron microscope specimens from single phase materials or multi phase materials in which the different phases present are all etched at approximately the same rates. In the glass-ceramics studied in this work, the glass phase was found to be etched faster than the crystalline phases and this thinning technique could not be used.

4.2.5 Other Methods of Preparing Transmission Specimens

Two other methods of preparing thin sections for transmission electron microscopy are mentioned here for completeness but have not been used in this work.

Several authors (6-7) have reported techniques of thinning a bulk specimen to an electron transparent thickness by mechanical thinning. The technique essentially consists of grinding the specimen and then polishing it with successively finer grade diamond pastes.

The second method is that of ion beam machining (8-9) in which a beam of ions ^{is} ~~are~~ accelerated towards the specimen and the surface is slowly eroded away. The technique is very slow and Doremus and Turkalo (9) report surface artifacts produced by the ion thinning process (10) which are subsequently removed on etching.

4.2.6 Summary of Transmission Electron Microscope Specimen Preparation

In order to correlate any ordering of the crystalline phases in a glass-ceramic with the alignment technique used, the orientation of the

thin section relative to the bulk specimen has to be known.

In the techniques described above for the preparation of thin foils for transmission electron microscopy the relative orientation of the specimen to the bulk material is not obvious; in the fragmentation method, the orientation of the transmission specimen relative to the initial bulk material is unknown. The chemical thinning of specimens was used in studying the effect of the electric field on phase separation, but the technique was found to be unsatisfactory for glass-crystal systems.

Carbon replication of specimen surfaces could be used to detect crystal alignment in glass-ceramics if the replicated areas were of a shape which indicated a direction (e.g. a rhomboid shape where the long axis points in a reference direction). In low magnification work (< 2500 X), there are no obvious differences between viewing a carbon replica in transmission and the scanning electron microscopy of the surface of a specimen; for insulating materials where the scanning microscope specimens are coated with a conducting 'replica' the two techniques are very similar. The preparation of specimens for scanning electron microscopy was found to be considerably easier than replication techniques and in this instrument the position of an area viewed at high magnification is easily related to a reference direction in the bulk material. This instrument also has a large depth of focus compared with light microscopes and for the above reasons was used to study the microstructure of the glass-ceramics prepared.

4.3 Scanning Electron Microscopy (SEM)

4.3.1 The Microscope

Although the technical details of the scanning electron microscope system are outside the scope of this present work, a brief resumé is

necessary since the results presented in the latter part of this chapter have been obtained by the exclusive use of this instrument.

An electron beam is focussed by a series of lenses to interact with the specimen to give among other effects, secondary electron emission, a reflected electron current, X-ray emission and cathodoluminescence. Each of these signals can be detected and used to control the brightness of a cathode ray tube (CRT). Incorporated in the final lens assembly of the electron beam focussing system are two sets of magnetic scanning coils which when energized by a suitable scan generator, cause the beam to be deflected in a raster-like pattern over the specimen surface. The spot position on the CRT is determined by the scan generator which affixes the position of the electron beam on the specimen surface. In this way, for example, the secondary electron signal from a given surface element is used to control the brightness of a corresponding point on a CRT so that a 'map' of the secondary electron current can be obtained (11).

Electrons emitted from the surface are arbitrarily divided into two main classes. Secondary electrons are those emitted from the surface with energies ≤ 50 eV; electrons with greater energies are regarded as back-scattered (or reflected) electrons. The backscattered electron intensity increases with the average atomic number of the area being irradiated (12) and these electrons can therefore be used to obtain an atomic number picture of the specimen.

The system used to detect the electron emission usually consists of a metal cup with a metal gauze over the opening which is held at, say, 200 volts positive, relative to earth (the specimen is at earth potential). Backscattered and secondary electrons are attracted towards this collector. Some of these electrons penetrate through the gauze and are accelerated towards a scintillator crystal on top of which is a thin aluminium film maintained at 10 - 12 kV. The energy acquired by the electron is converted

into light by the processes of impact ionization followed by radiative recombination. A large fraction of this light is guided by a light pipe into a photomultiplier tube, the output of which is displayed on the CRT. The backscattered electrons alone can be detected by applying a small negative potential ($\sim -250V$) to the gauze on the collector which prevents the low energy secondaries reaching the scintillator crystal.

Several different methods of detecting cathodoluminescence (CL) have been described in the literature (13-16). In the present work the system used to detect the CL consisted of an EMI type 6255B photomultiplier tube and a 1 inch diameter lens of focal length equal to 1 inch, to give a solid collection angle in excess of 0.75 steradians.

A Cambridge Scientific Instruments Ltd. Mk IIA Stereoscan was used.

4.3.2 Specimen Preparation for SEM

The specimens which were studied using the SEM were insulators and to prevent the build up of surface charge the surfaces were coated with a thin film of a gold-palladium alloy ($<1000 \text{ \AA}$ thick).

Specimens were polished to a $1 \mu\text{m}$ diamond paste finish and topographical contrast was produced by etching the polished surface. The specimens which were usually 3mm thick, were attached to SEM stubs with a conducting paint (colloidal silver Dag was used). A conducting path was painted from the stub to the specimen surface to maintain the latter at earth potential. Gold-palladium was evaporated onto the surface of the specimen using standard vacuum evaporation techniques. Six specimens were coated at the same time; to ensure an even coating the specimens were simultaneously rotated in one plane and rocked through 120° in a perpendicular plane during evaporation (17).

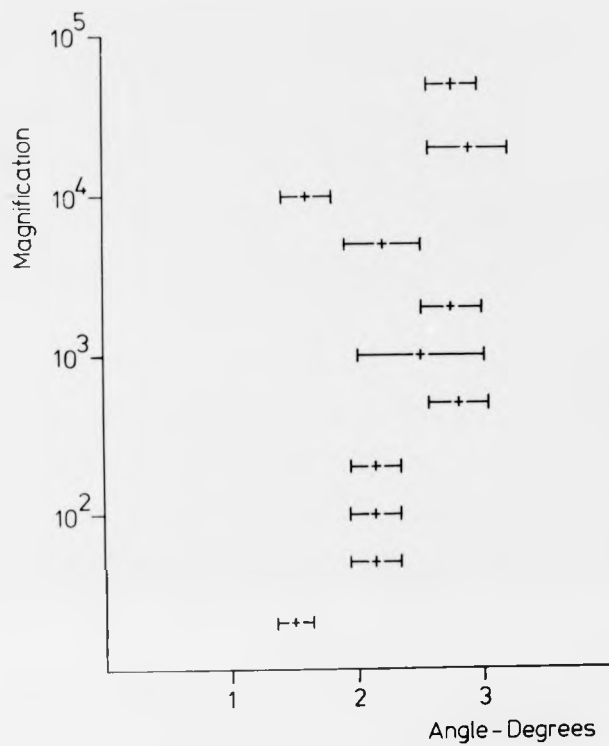


Figure 4.4 Image rotation in the SEM as a function of magnification.

4.3.3 Calibration of Image Magnification and Rotation in the SEM

The operating magnification of the SEM was calibrated using a transmission electron microscope grid onto which a replica of a diffraction grating (30,000 lines/inch) had been placed. The spacing of the grid bars was used as a reference at low magnifications and the grating replica at higher magnifications.

It was important to know whether any image rotation occurred as the magnification was increased because high magnification micrographs were to be related to a reference direction in the bulk specimen. The specimen used in the magnification calibration was used for this. A maximum rotation of $+1^\circ$ was observed between magnifications of 20X and 20000X (Fig. 4.4); this rotation was probably caused by slight non-linearities in the scan coils.

4.4 Investigation of Cathodoluminescence from Glass-Ceramic Surfaces

4.4.1 Introduction

Cathodoluminescence (CL) or photon emission induced by electron bombardment has been observed from the surfaces of many different materials (13, 18-21).

The physical processes which lead to CL can be divided into three parts (after P.R. Thornton (11)):

- (i) The incident electron beam is used to excite the lattice by creating electron-hole pairs by impact ionization of either the atoms of the host lattice or of impurity atoms.
- (ii) In the general case, the electron and hole pairs need not be created at the same point at which they recombine. They can move either by drift in an electric field or by diffusion from the point of formation to some other position in the crystal where they can be converted to a photon.

4.3.3 Calibration of Image Magnification and Rotation in the SEM

The operating magnification of the SEM was calibrated using a transmission electron microscope grid onto which a replica of a diffraction grating (30,000 lines/inch) had been placed. The spacing of the grid bars was used as a reference at low magnifications and the grating replica at higher magnifications.

It was important to know whether any image rotation occurred as the magnification was increased because high magnification micrographs were to be related to a reference direction in the bulk specimen. The specimen used in the magnification calibration was used for this. A maximum rotation of $\pm 1^\circ$ was observed between magnifications of 20X and 20000X (Fig. 4.4); this rotation was probably caused by slight non-linearities in the scan coils.

4.4 Investigation of Cathodoluminescence from Glass-Ceramic Surfaces

4.4.1 Introduction

Cathodoluminescence (CL) or photon emission induced by electron bombardment has been observed from the surfaces of many different materials (13, 18-21).

The physical processes which lead to CL can be divided into three parts (after P.R. Thornton (11)):

- (i) The incident electron beam is used to excite the lattice by creating electron-hole pairs by impact ionization of either the atoms of the host lattice or of impurity atoms.
- (ii) In the general case, the electron and hole pairs need not be created at the same point at which they recombine. They can move either by drift in an electric field or by diffusion from the point of formation to some other position in the crystal where they can be converted to a photon.

	SiO ₂	Li ₂ O	K ₂ O	Al ₂ O ₃	P ₂ O ₅	B ₂ O ₃
Glass A	610	305	15	10	10	50
Glass B	675	240	15	10	10	50

Table 4.1 Glass compositions in mol.%.
5



Figure 4.5 Secondary/reflected emission from a polished sample of glass A.

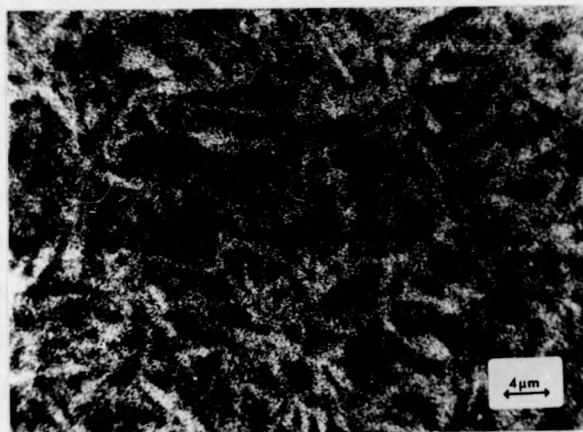


Figure 4.6 CL from the same area as Figure 4.5.



Figure 4.7 Secondary/reflected emission from an etched sample of glass A;
A is the silica crystalline phase.

(iii) The recombination of an electron-hole pair in the crystal can be equivalent to the creation of a photon at that point. To detect this photon it must be emitted from the surface. This emission can be prevented by total internal reflection at a boundary or absorption between the point of creation and the point of emission.

4.4.2 Initial Observations of CL from Glass-Ceramics (21)

Two glasses were prepared of compositions shown in Table 4.1. (Chapter 3 contains an account of glass preparation and heat-treatment processes); glass A was heat-treated for 2 hours at 800°C and glass B was extruded at 825°C. Both glass-ceramics contained needle shaped crystals of lithium disilicate as their major crystalline phase and a crystalline form of silica as a minor crystalline phase together with a residual glassy phase.

Polished surfaces of both specimens were examined in the SEM by the secondary emission mode and the CL mode. The accelerating potential was 30 kV, the beam current approximately 150 μ A and the specimen was positioned normal to the incident electron beam.

Figures 4.5 and 4.6 show a comparison of the same area of glass A observed in the two modes; Fig. 4.7 shows a sample of the same specimen etched for 30 seconds in a 7% HF solution and observed in the secondary/reflected mode. There is obviously a marked contrast mechanism in the CL mode which enables the lithium disilicate crystalline phase to be easily distinguished from the glass matrix; the CL micrograph has a speckled appearance because of noise associated with the photomultiplier tube.

Figures 4.8 and 4.9 show a similar comparison in glass B. A weak contrast mechanism can be observed in the secondary/reflected emission

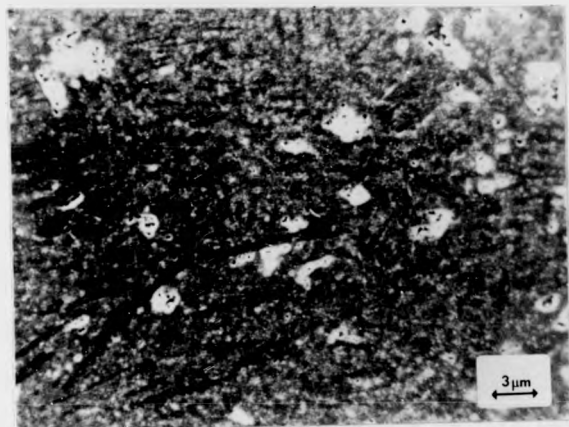


Figure 4.8 Secondary/reflected emission from a polished sample of glass B.



Figure 4.9 CL from the same area as Figure 4.8.



Figure 4.10 Secondary/reflected emission from an etched sample of glass B:
A is the silica crystalline phase and B is the disilicate phase.

micrograph which is caused by the back-scattered electrons; the disilicate crystals are of a lower average atomic number than the glassy matrix (12). The darker crystalline regions in Figure 4.8 show little electron emission but a strong photon emission in Fig. 4.9. Prior etching of the glass-ceramic enabled the micrograph in Fig. 4.10 to be obtained by the secondary/reflected mode.

CL has been observed in quartz (22) but in this work no CL was observed from the silica crystalline phase; one of the emission bands in quartz (23) is positioned outside the range of the photomultiplier tube used and the strong emission from the disilicate phase together with the small volume fraction of the silica crystals makes detection of the CL from the latter difficult.

The CL emission from the sample contains information about the material itself. The specimen is coated with a uniform layer of conducting film which if it luminesces would not show the contrast observed from the polished surfaces. This contrast can be related to the back-scattered electron image (Figs. 4.8 and 4.9) and from this comparison it can be seen that it is the crystalline phase which is strongly emitting the photon radiation.

4.4.3 Variation of CL Intensity with Time

The intensity of the CL emission was qualitatively noted to decrease with time if the same area of the specimen was continuously scanned with the electron beam; this phenomena was investigated in a quantitative fashion.

A polished sample of glass B was prepared for SEM and a suitable area ($\sim 100 \mu\text{m}^2$) was selected (this glass-ceramic was used because it emitted the strongest CL signal of the two studied). The selected area was scanned continuously with the electron beam; an accelerating potential of 30 kV and a beam current of approximately 150 μA were used.

The recorded intensity of the CL emission was maintained at a constant value in time by increasing the voltage across the photomultiplier dynode chain (PM voltage). Increasing the PM voltage increased the gain of the photomultiplier tube. Hence if the PM voltage had to be increased the CL intensity was decreasing. The criteria of constant intensity was gauged by displaying the CL intensity from a single line of the scanning raster on an oscilloscope. Figure 4.11 is an example of a CL micrograph with the intensity along a line superposed. The characteristic features of this line scan were sketched on the perspex screen of the oscilloscope and it was then possible to maintain the CL signal at a constant value by altering the PM voltage. A series of PM voltages against time of scanning the surface were recorded. The manufacturer's specification of PM voltage versus sensitivity for the photomultiplier tube was used to convert each PM voltage to a quantity proportional to the intensity of CL incident upon the tube. The constant of proportionality relating the PM voltage to the incident CL intensity is not easily evaluated and is a function of the characteristics of the photomultiplier tube and related amplifiers. This constant of proportionality is not necessary for the interpretation of the data in terms of relative values.

An alternative method of recording the intensity would be to maintain the PM voltage at a constant value and monitor the variation in output current with time from the photomultiplier tube. This technique was tried but difficulties were experienced in selecting a single PM voltage such that the variation of output current over the time scale of the experiment (~ 60 mins) could be monitored. A more sophisticated electronic system would enable this to be carried out resulting in greater accuracy and experimental ease.

A number proportional to the intensity of the CL emitted was

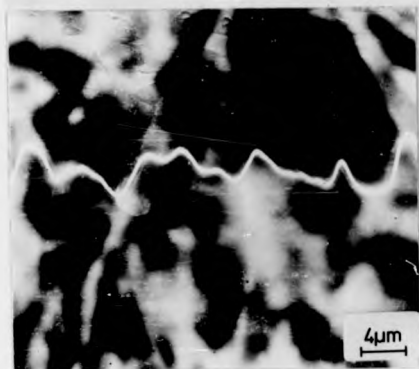


Figure 4.11 CL micrograph of a glass-ceramic surface with the intensity along a line superposed.

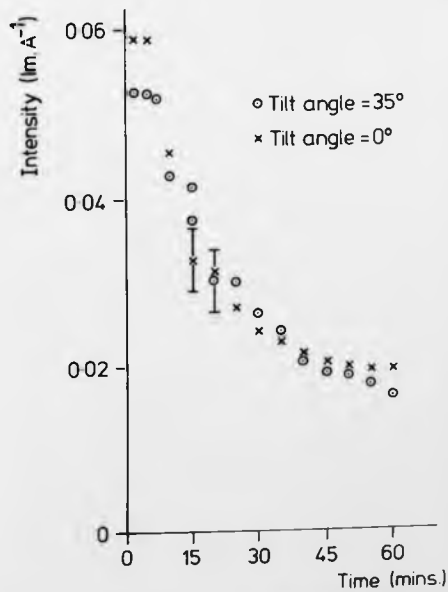


Figure 4.12 The decay in CL intensity from a glass-ceramic surface with time.

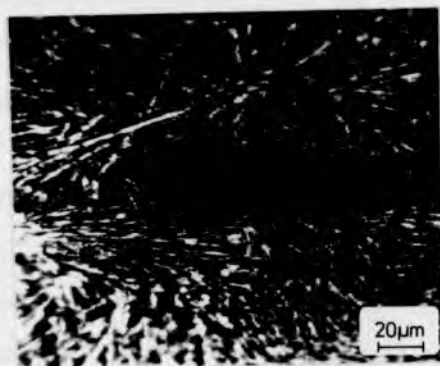


Figure 4.13 CL micrograph indicating the decreased emission from a glass-ceramic surface.

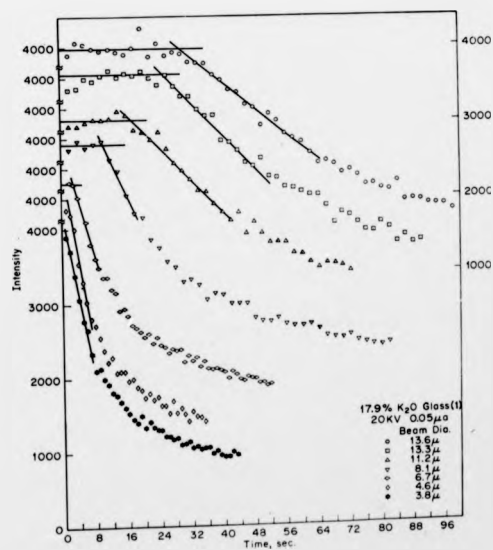


Figure 4.14 X-ray intensity-time flux curves for a K₂O-SiO₂ glass.
After Vassamillet and Caldwell (30).

evaluated as a function of time for two different angles of incidence of the electron beam, with the incident beam normal to the polished surface and making an angle of 35° with the surface normal (Fig. 4.12). The CL intensity decreased by approximately a factor of three after irradiation by the electron beam for 1 hour; the intensity appears to be asymptotically approaching a minimum value. Figure 4.13 shows a CL micrograph which illustrates the decreased emission; the darker area in the centre shows a region which was scanned continuously for a period of 1 hour.

The loss of CL intensity was a permanent feature, the damaged area could be easily found a week after irradiation. The conducting film on the surface of the specimen did not appear to be damaged as shown by the electron emission image, indicating no localised charge buildup. The electron emission intensity from the specimen remained constant throughout the period the CL intensity was noted to decay.

Radiation damage caused by an electron probe has been observed in polymers and glasses (24 - 26, 27 - 30). Vassamillet and Caldwell (30) describe results of the decay in X-ray intensity with time on irradiating a K_2O-SiO_2 glass at room temperature with an electron beam. Their X-ray intensity - time - flux curves (Fig. 4.14) have the same shape as the CL intensity - time curves described in this work. It must be noted however that their work was with X-ray emission and a glass specimen. The electron irradiation time scale is also different. The decay in the X-ray intensity for glass specimens has been attributed to the electron beam damaging the specimen. Two different mechanisms have been proposed (27, 29) which both rely on part of the incident electron energy being dissipated as heat with subsequent ionic diffusion.

Almasi et al. (31) have analysed the heat flow problem in electron beam microprobe analysis. They have deduced approximate solutions for evaluating

the temperature in a sample irradiated with an electron beam. The solutions proposed contain an integral which has to be evaluated numerically; Friskney and Haworth (32) have developed an approximate algebraic solution based on the work of Almasi et al. (31).

If $T(m)$ is the maximum temperature on the surface of the specimen at the centre of the electron beam of diameter d then

$$T(m) = \frac{9I_s (1 + 2 \ln 2R/d)}{4\pi [13ak + 3K_1d(1 + 2 \ln 2R/d)/2]} \quad \text{Equation 4.1}$$

where I_s = strength of heat source, i.e. incident power dissipated as heat.

a = thickness of conducting film.

R = thickness of specimen.

K = thermal conductivity of conducting film.

K_1 = thermal conductivity of specimen.

Equation 4.1 is after Friskney and Haworth (32).

If the following assumptions are made:

thickness of conducting layer $a = 1000 \text{ \AA}$

beam diameter $d = 1000 \text{ \AA}$

thermal conductivity of conducting layer $K = 2 \text{ W/cm-C}^\circ$

thermal conductivity of specimen $K_1 = 0.02 \text{ W/cm-C}^\circ$

thickness of specimen $R = 0.5 \text{ cm}$

then using Equation 4.1 the temperature at the centre of the beam is

$$T(m) \approx 7.10^4 I_s \text{ }^\circ\text{C} \quad \text{Equation 4.2}$$

Assuming 0.1% of the incident electron energy is absorbed as heat then for a beam current of $150 \text{ }\mu\text{A}$ and an accelerating potential of 30 kV , from Equation 4.2

$$T(m) \approx 300^\circ\text{C}.$$

The calculation is estimated to be accurate to within a factor of five.

Differential thermal analysis results (see Chapter 7) indicate that the glass-ceramic formed from glass B undergoes an endothermic transformation at approximately 920°C ; calculations based on Equation 4.1 show that it is possible that the temperature in the centre of the electron beam at the surface could reach this value.

A model of the decay in CL intensity with time is proposed in which the electron beam destroys the periodic structure of the crystal lattice. As the crystals in the specimen emitting the CL become more 'amorphised' the CL intensity will decrease asymptotically reaching a minimum value where the electron beam is penetrating only amorphous material. Associated with this melting process will be ionic diffusion in the temperature gradients and electric fields produced by the incident electron beam. This model of CL intensity decay would produce permanent damage in the material. A complete theoretical analysis of the electron beam - specimen interaction is very complicated and is outside the scope of this present work.

4.4.4 Variation of the CL Intensity with the Angle of Incidence of the Electron Beam

The variation of the CL emission intensity with the angle of incidence of the electron beam was investigated (in the following, the angle between the incident electron beam and the normal to the surface of the specimen is referred to as the incident angle).

A sample of glass B which had been extruded at 825°C was cut using a diamond saw to produce a section in which the lithium disilicate crystals were orientated with their c - crystallographic axes parallel to the plane of the surface. Furthermore in this plane the c - crystallographic directions of these crystals pointed in a preferred direction; the half width of the distribution curve of number of crystals versus angle was 70° for this

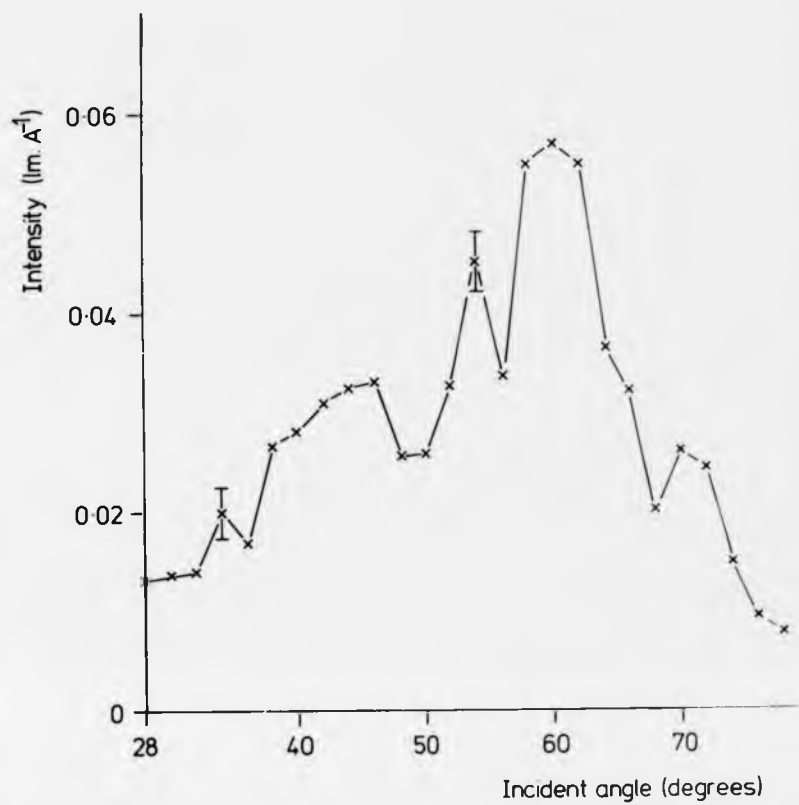


Figure 4.15 Variation of the corrected CL emission intensity with the incident angle of the electron beam.

specimen (see Chapter 6 for details of the distribution curve analysis). This surface was polished to a $1\ \mu\text{m}$ diamond paste finish and coated with a conducting layer of gold/palladium alloy in the manner described in section 4.3.2.

In order to vary the incident angle the specimen was tilted about an axis parallel to the plane of the specimen surface and perpendicular to the direction of preferred orientation in the surface.

Measurements of the CL emission intensity were taken as a function of incident angle as described in section 4.4.3. The intensity measurements were taken with the value of the incident angle decreasing; this procedure ensured that no 'fresh' specimen was irradiated in time with the incident angle decreasing. The same region of the specimen was scanned continuously as the incident angle was decreased, by adjusting the x and y controls of the specimen stage so that a salient feature of the electron emission image remained in the field of view. The CL emission intensity data were normalised to unit area and zero time; as the incident angle θ decreases the area scanned decreases by a factor of $1/\cos\theta$. The normalisation to zero time was calculated with the aid of Figure 4.12; from this graph the CL intensity decay appears to have no dependence on the incident angle.

Figure 4.15 is a graph of the corrected CL emission intensity versus the incident angle. The electron emission from the specimen surface showed little variation with the incident angle (33). The CL emitted intensity shows maxima and minima as the incident angle is varied.

The specimen was essentially an array of crystals all in the same approximate orientation with respect to their c-crystallographic axis. As a first approximation, therefore, the specimen can be considered to be a 'single' crystal. On rotating this 'single' crystal about an axis

perpendicular to the incident beam the electrons will be incident upon different crystallographic planes. It is qualitatively postulated that the CL intensity observed from a crystal is a function of the angle which the incident electron beam makes with the crystal lattice. Different directions in a crystal lattice contain different numbers of atoms per unit plane and different inter-planar spacings (lithium disilicate crystals belong to the orthorhombic system). Hence the probability of an impact ionization of atoms in the lattice is a function of the direction of the incident electron beam relative to the crystal lattice.

Jones and Gopinath (20) quote an equation which relates the luminescence intensity to various crystal parameters. The intensity predicted by this equation (the Roosbroeck - Shockley equation (34)) varies with parameters relating to the photon emission from the crystal (e.g. the absorption coefficient). In the measurement of the CL intensity variation with incident angle described in this work the CL intensity was detected over a large solid angle (~ 0.75 steradians) and any angular dependence on the intensity for a given incident angle would not have been resolved. The Roosbroeck - Shockley equation does not predict the intensity of the luminescence as a function of the direction of the incident electron beam relative to the crystal lattice.

The hypothesis that the CL intensity varies with the direction of the incident beam implies that this technique could prove to be a very powerful one in determining the lattice spacings of crystals which exhibit CL in the SEM. In this present work no simple relationship could be found between the angular position of the peaks in the CL intensity (Figure 4.15) and the crystallographic d-spacings of the crystal upon which the electron beam was incident. It must be noted however, that the present experimental evidence is not very substantial and that a theoretical analysis of this system has to be performed before the technique can be placed on a sound footing.

4.4.5 Determination of the Frequency of CL Emitted from Lithium Disilicate Crystals

In an attempt to determine the frequency band of the CL radiation emitted by the lithium disilicate crystals in the glass-ceramic an elementary experiment was performed.

A series of optical filters was placed between the window of the photomultiplier tube and the specimen chamber window. The CL intensity was measured for each filter and by comparing these results it was determined that the radiation emitted covered approximately the range 3500Å to 5000Å and was emitting most strongly in the blue-violet region of the visible spectrum.

A more sophisticated experiment would be to use a spectrometer to determine the wavelength emitted from the specimen.

4.4.6 Summary of CL Observations in the SEM

The emission of CL from a glass-ceramic when irradiated with an electron beam has been investigated. The main results of this work are summarised as follows:

- (i) CL was observed from a polished surface of a glass-ceramic. A strong contrast mechanism existed which permitted the lithium disilicate crystalline phase to be easily distinguished from the glassy matrix.
- (ii) The intensity of the CL emission decreases with time of irradiation; a similar phenomenon has been reported in the literature when detecting the X-ray emission from a glass specimen irradiated with an electron beam. A mechanism has been proposed for this effect, relating the decreasing CL intensity with the 'amorphisation' of the crystalline phase present in the glass-ceramic.
- (iii) The CL intensity varies with the angle the incident electron beam makes with an orientated specimen. A mechanism has been proposed which relates this variation with the direction of the

incident beam in the crystal lattice.

(iv) The wavelength of the CL intensity emitted from lithium disilicate crystals lies between 3500\AA and 5000\AA with a peak intensity in the blue-violet region of the spectrum.

It is clear from the present work that the observation of CL can provide an additional and valuable technique for the investigation of glass-ceramic microstructures. In this study the CL observed was confined to lithium disilicate crystals; however this had the advantage of enabling these crystals to be readily distinguished from the crystalline silica phase which was also present. CL enables micrographs showing good contrast to be obtained without the necessity of etching the glass-ceramic surface. The latter could cause modifications to the microstructure which are clearly undesirable. With an improved system for the detection and analysis of the radiation emitted, it may be possible to extend the technique to selectively reveal the morphology of the silica crystals in the system studied, and of other crystal types in different glass-ceramic compositions. The variation of the CL intensity with the angle of incidence of the electron beam may contain information about the lattice of the crystal emitting the radiation. A more sophisticated experiment would enable this phenomenon to be studied in greater detail with different glass-ceramic compositions; this would help to determine the potential of the technique.

4.5 X-ray Diffraction Techniques

4.5.1 Preparation of samples for X-ray studies

Debye Scherrer powder X-ray photographs were recorded to determine the crystalline phases present in the glass-ceramics studied. Crystallographic orientation in the aligned glass-ceramics was studied

using an X-ray diffractometer and back reflection photographs.

For Debye Scherrer samples, a finely powdered specimen contained in an amorphous capillary tube (supplied by Pye Unicam Ltd.) was rotated in a beam of copper $K\alpha$ X-rays. The apparatus used was a Philips X-ray generator, with matching Debye Scherrer camera. Typical operating conditions were 40 kV/15 mA with an exposure time for the Ilford G film of 4 hours. The position of the lines on the powder pattern was measured from an Automatic Recording Densitometer (Joyce-Loebl Model Mk IIIc) trace of the film blackening along the film. Crystalline phases were identified from the calculated d-spacings and the ASTM X-ray Powder Data File (35).

The detection of crystallographic orientation in the aligned glass-ceramic was carried out using back reflection photographs and an X-ray diffractometer. In both cases the samples consisted of a polished glass-ceramic surface which had been etched for ten seconds in a 5% hydrofluoric acid solution to remove any surface damage. Back reflection photographs were taken with a Laue camera and copper $K\alpha$ radiation. The diffractometer used was a standard 2 circle diffractometer with a Cobalt $K\alpha$ source. The reflected X-rays were detected with a scintillation counter and a Philips HV Supply - Ratemeter - Channel Analyser. The latter allowed the background white radiation to be removed from the signal. Typical scanning speeds used were $1/4^\circ$ per minute and $1/16^\circ$ per minute.

References

1. A.M. Turkalo, J. Am. Ceram. Soc. 51 470 (1968)
2. A.F. Prebus & J.W. Michener, Ind. Eng. Chem. 46 147 (1954)
3. D. E. Bradley, Techniques for Electron Microscopy, ed. D.H. Kay (Blackwell Scientific Publications, Oxford 1965)
4. P. F. James & P.W. McMillan, Phil. Mag. 18 863 (1968)
5. I.M. Stewart & L. Green, J. Sci. Instr. 44 216 (1967)
6. P.E. Doherty & R.R. Leonbruno, J. Am. Ceram. Soc. 47 368 (1964)
7. T.P. Seward, D.R. Uhlmann, D. Turnbull & G.R. Pierce, *ibid*, 50 25 (1967)
8. P. Hing and P.W. McMillan, J. Mat. Sci. 8 340 (1973)
9. R.H. Doremus & A.M. Turkalo, Phys. Chem. Glasses 13 14 (1972)
10. P. Sigmund, J. Mat. Sci. 8 1545 (1973)
11. P.R. Thornton, Scanning Electron Microscopy (Chapman & Hall Ltd., London 1968)
12. H.E. Bishop, Ph.D. Dissertation, Cambridge (1966)
13. J.P. Davey, X-ray Optics and Microanalysis (Hermann, Oxford 1966)
14. M.D. Muir, F.R. Grant, G. Hubbard & J. Mundell, Proc. 4th Ann. SEM Symp. (IIT Research Institute, Chicago 1971)
15. E.M. H⁸rl & E. M⁸gsl, Proc. 5th Eur. Cong. on Electron Microscopy (Institute of Physics, London 1972)
16. L. Carlsson & C.G. van Essen, J. Phys. E: Sci. Instr. 7 98 (1974)
17. G. Smith & I.D. Ward, Unpublished work.
18. D.B. Whittry & D.F. Kyser, J. Appl. Phys. 36 1387 (1965)
19. G. R^emond, S. Kimoto & H. Okuzumi, JEOL News 8 32 (1970)
20. G.A.C. Jones & A. Gopinath, Scanning Electron Microscopy: Systems & Applications (Institute of Physics, London 1973)
21. D.I.H. Atkinson & P.W. McMillan, J. Mat. Sci. 2 692 (1974)
22. D.H. Krinsley & P.J.W. Hyde, Proc. 4th Ann. SEM Symp. (IIT Research Institute, Chicago 1971)

23. R.F. Sippel & A.B. Spencer, Proc. Apollo 11 Lunar Science Cong. 3 2413 (1970)
24. D.T. Grubb, A. Keller & G.W. Groves, J. Mat. Sci. 7 131 (1972)
25. D.T. Grubb & A. Keller, *ibid.*, 7 822 (1972)
26. W. Wu, A.S. Argon & P.L. Turner, *ibid.*, 8 1670 (1973)
27. J.L. Lineweaver, J. Appl. Phys. 34 1786 (1963)
28. A.K. Varshneya, A.R. Cooper & M. Cable, *ibid.*, 37 2199 (1966)
29. M.P. Borom & F.E. Hanneman, *ibid.*, 38 2406 (1967)
30. L.F. Vassamillet & V.E. Caldwell, *ibid.*, 40 1637 (1969)
31. G.S. Almasi, J. Blair, R.E. Ogilvie & R.T. Schwartz, *ibid.*, 36 1848 (1965)
32. C.A. Friskney & C.W. Haworth, *ibid.*, 38 3797 (1967)
33. E. Weinryp & J. Philibert, Compt. Rend., 258 4535 (1964)
34. W. van Roosbroeck & W. Shockley, Phys. Rev. 94 1558 (1954)
35. ASTM X-ray Powder Data File, Special Technical Publications No.48-J (1960)

CHAPTER 5: METHODS OF PRODUCING AN ALIGNED MICROSTRUCTURE

5.1 Introduction

The methods used to obtain a glass-ceramic with an aligned microstructure are described in this chapter. Initial experiments investigating the effect of an electric field on phase separation are described. Details are presented of the apparatus and technique of hot extruding a glass-ceramic which resulted in an aligned microstructure. Hot-extrusion was the principle technique used in this research.

5.2 General Considerations

When a glass is devitrified under conditions where no external constraints are applied to it, the crystalline phase in the bulk material is randomly oriented in a glassy matrix (1). Surface crystallisation can produce an ordered microstructure within the boundary layers of the glass-ceramic (2,3). This preferred crystal orientation at the surface of the material results from the anisotropy of the crystal growth rates; although the crystals at the nucleating surface may be randomly oriented, the crystals oriented with the fast growth direction perpendicular to the surface take precedence.

In a glass-ceramic the crystalline phase may be aligned with respect to the crystal planes or the morphology of the crystals or both. The morphological orientation of the crystals requires that the crystalline phase is asymmetric in shape; no such orientation could be detected in spherical crystals.

A basic concept of the techniques proposed to align the crystals in a glass-ceramic is that an asymmetric stress is introduced into the system. Under the influence of this asymmetry the crystals in the glassy matrix will be induced to re-distribute or grow in a preferred direction which minimises

the free energy of the system. This asymmetrical stress can be applied to the glass/glass-ceramic by a mechanical, electrical or magnetic technique.

Mechanical methods of producing an aligned crystalline phase in the glass-ceramic depend on the re-orientation or growth of the crystals in a stress field in the matrix. In metallography, the extrusion or drawing of wires is a technique which results in the metal having an asymmetric microstructure. This feature in the metal is a consequence of the deformation of the crystals and crystal-crystal interactions (4-7).

Hoffmann et al. (8-9) have studied the influence of an electric field on the growth of metal whiskers. The whiskers showed a strong tendency to grow along the lines of force of the electric field. The effect of a D.C. electric field on a lithia-silica glass whilst it is devitrifying has been investigated by Phillips (10). The glass-ceramic contained a greater number density of smaller crystals than the control specimen; no orientation of the crystalline phase was detected however.

Ceramic composites containing a second phase arranged with a regular aligned microstructure can be obtained by the technique of unidirectional solidification of eutectic mixtures (11). Carpay and Cense (12) have shown that regular composite structures can be grown by the directional decomposition of quenched-in liquids, independent of whether the starting composition is near a eutectic composition or not.

Charles (13, 14) has reported the effect of a thermal gradient on a borosilicate glass. On heat-treating the glass in a temperature gradient a minor phase underwent a secondary decomposition into another glass phase and a crystalline phase. A strong preferred orientation of the crystalline phase in the minor glass phase residue was evident. Charles concludes that the orientation is not a result of epitaxial effects and attributes it either directly or indirectly to the thermal gradients in processing.

In this present work investigations have been limited to the mechanical deformation of a glass-ceramic; some preliminary studies have also been performed on the effect of applying an electric field to a glass whilst it is being heat-treated.

5.3 Electric Field Experiments

5.3.1 Introduction

A number of glass compositions exist which form homogeneous liquids in their molten state but on cooling, separation into two liquid or glass phases occurs. In many cases, one of these glass phases forms droplets; this phase will be the one possessing the higher surface tension. The theory of the coarsening of these droplets, or 'Ostwald ripening' by diffusion processes has been developed rigorously by Lifshitz and Slyozov (15) and Wagner (16) following earlier treatment by Greenwood (17).

The influence of an electric field on nucleation and growth kinetics has been analysed by Kashchiev (18). A parent phase situated in an externally applied uniform electric field E is considered and the amount of work required for the formation of a cluster of atoms is evaluated. If E_c and E_m are the dielectric permeabilities of the new and parent phase, then when $E_c < E_m$ the electric field will stimulate the formation of the new phase and when $E_c > E_m$ the field will inhibit its formation. At $E_c = E_m$, the electric field has no effect regardless of the field strength. Tomlinson (19) has performed a similar analysis and concluded that the formation of a periodic array of low-resistance, precipitated material will be enhanced in the direction of an applied field provided that the polarization of the material is a function of the local glass composition.

The effect of an electric field on the phase separation of glass has been investigated for glasses in the $\text{CaO} - \text{Al}_2\text{O}_3 - \text{SiO}_2 - \text{M}_2\text{O}$ system (20).

	Glass A	Glass B	Glass C	
SiO ₂	675	675	CaO	45
Li ₂ O	315	240	SiO ₂	489
K ₂ O		15	Al ₂ O ₃	222
Al ₂ O ₃		10	MgO	134
P ₂ O ₅	10	10	TiO ₂	110
B ₂ O ₃		50		

Table 5.1 Glass compositions in mol.% used in the electric field experiments.

The application of an A.C. or D.C. electric field to the glass produced well formed nuclei of moderate size whereas a control specimen heat-treated for the same time and temperature showed no nucleation. An enhanced growth rate of the nuclei was noted but no significant increase in the number density of nuclei was detected.

In this present work the effect of an electric field on the phase separation and crystallisation of glasses in the $\text{Li}_2\text{O}-\text{SiO}_2$ system has been investigated.

5.3.2 The Effect of an Electric Field on Phase Separation and Crystallisation

The compositions of the glasses studied in these experiments are given in Table 5.1. A quantitative study of the phase separation of glass A has been made by James and McMillan (21); glass C is one of the compositions studied by De Vekey and Majumdar (20).

Samples of glass A and glass C approximately 0.3 cm thick and 1.5 cm square were prepared with diamond ground flat and parallel faces. Thick platinum electrodes 1 cm square were vacuum evaporated onto these faces and the specimen was etched with a 1% solution of hydrofluoric acid to prevent electrical tracking. A D.C. high voltage supply and an induction coil driven by a sine wave generator were used as high voltage sources. The specimen electrodes were connected by pressure contacts held in position with fused silica tubes to the voltage sources. In all experiments two similar specimens were positioned in close proximity in a horizontal muffle furnace; both of these specimens were prepared with platinum electrodes and one was used as a control. A maximum electric field of 15 kV either A.C. (frequency between 50 Hz and 15 kHz) or D.C. was applied to the specimen throughout the heating period; the temperature near the specimens was measured with a chromel-alumel thermocouple. Thin foils

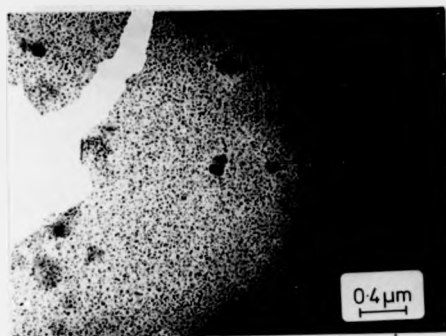


Figure 5.1(a) Transmission electron micrograph of a chemically thinned specimen of glass A heat-treated for 1 hour at 550°C.



Figure 5.1(b) Transmission electron micrograph of a chemically thinned specimen of glass A heat-treated for 1 hour at 550°C with an applied electric field gradient of 150V/cm (A.C. 10 kHz).

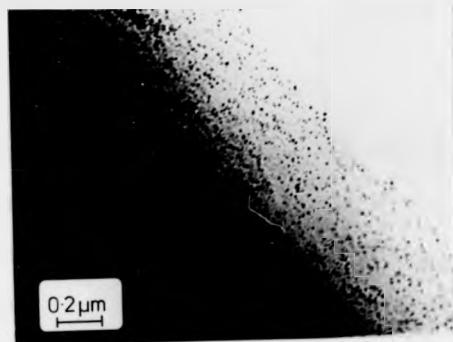


Figure 5.2(a) Transmission electron micrograph of a chemically thinned specimen of glass C heat-treated for 22 hours at 700°C.

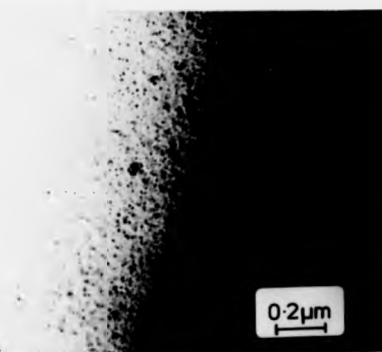


Figure 5.2(b) Transmission electron micrograph of a chemically thinned specimen of glass C heat-treated for 22 hours at 700°C with an applied electric field gradient of 34 kV/cm (A.C. 50 Hz.)

of each specimen were prepared for transmission electron microscopy by the chemical thinning technique (Chapter 4); sections perpendicular and parallel to the electric field were prepared from the specimen which had been heat-treated in the field.

An electrically conducting path caused by ionic conduction and localised Joule heating prevented field gradients greater than approximately 200V/cm at 550°C being applied across specimens of glass A. The specimens of glass A heat-treated in a D.C. or A.C. electric field did not contain a greater number density or different size distribution of phase separated droplets compared with the control specimens; no elongation of the droplets was observed in the field specimens. Figure 5.1 shows typical micrographs of phase separation in the two specimens of glass A; an electric field gradient of 150 V/cm (A.C. 10 kHz) was applied to one specimen for 1 hour at 550°C.

De Vekey and Majumdar (20) clearly show in their paper that an electric field enhances the phase separation in a glass of the $\text{CaO} - \text{Al}_2\text{O}_3 - \text{SiO}_2 - \text{MgO}$ system. A specimen of glass C was used to repeat one of the experiments performed on this system. An A.C. electric field gradient of 34 kV/cm was applied to this specimen at a temperature of 700°C for 22 hours. Figure 5.2 shows typical phase separated regions of this specimen and the control specimen. No statistically significant difference in the number density of phase separated droplets was observed between the two specimens. In the experiments of De Vekey and Majumdar (loc.cit.) on the composition of glass C an electric field gradient of 4 kV/cm (A.C. 50 Hz) applied for 74 hours at 690°C produced a phase separated glass whereas the control specimen contained very little phase separation. The electrodes on the electric field specimen in this case were made of a gold - palladium alloy.

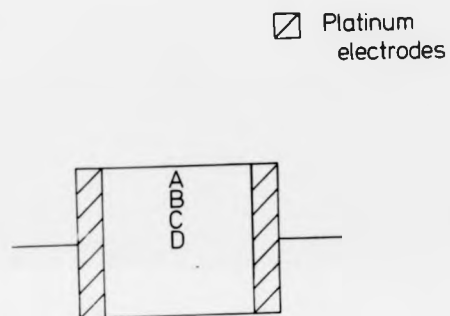


Figure 5.3 Schematic diagram of the electrode configuration used in the crystallisation experiments.

No definite conclusions can be made about the negative results obtained from the experiments described above. The inability to repeat the results of De Vekey and Majumdar (*loc.cit.*) cannot be simply explained. It is unclear in the published work whether or not the control specimen was coated with electrodes; the diffusion coefficients in the glass of the gold-palladium alloy electrodes is probably different to that of the platinum electrodes used in this work. It is possible also that the rate of phase separation of glass C is very sensitive to the applied field gradient and heat-treatment schedule. The control specimen in this experiment heat-treated for 22 hours at 700°C showed heavy phase separation, whereas the control specimen of De Vekey, heat-treated for 74 hours at 690°C showed little or no phase separation. The results obtained indicated that the electric field produced no orientation effects in the phase separated droplets; for this reason these experiments were not continued.

To investigate the effect of an asymmetric electric field on the devitrification of a glass a technique was used which is similar to the principle of operation of a Nernst filament.

A sample of glass B approximately 2 cm x 1 cm x 0.5 cm was prepared and platinum electrodes were vacuum evaporated onto opposite ends of the specimen so that the two electrodes sandwiched a volume of glass between them (Figure 5.3). A voltage of 50 volts (A.C. 50 Hz) was placed across the electrodes and the specimen was gently heated. When the temperature of the specimen had reached approximately 670°C the current through the specimen was 1.1 amperes and the external heat source was removed. The temperature of the specimen remained approximately constant, the heat losses by convection, thermal conduction and radiation being balanced by Joule heating in the specimen. The current through the specimen was maintained at approximately 1.0 ampere for thirty minutes and the specimen temperature

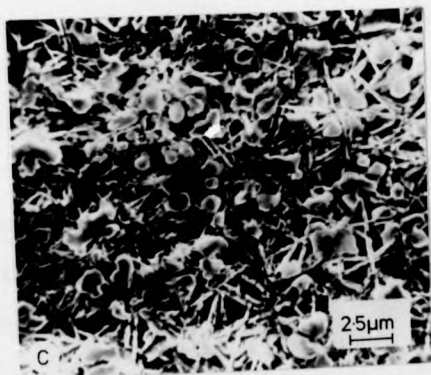
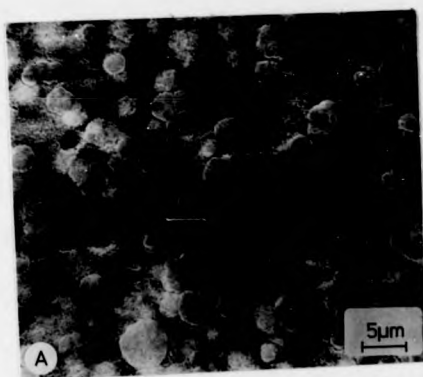


Figure 5.4 Representative SEM micrographs of the areas shown schematically in Figure 5.3.

remained at approximately 650°C. During this period the original transparent glass specimen had become milky white colour in appearance indicating that devitrification had occurred.

Specimens were prepared for scanning electron microscopy from sections cut perpendicular and parallel to the electrodes. Four different regions were found to exist in the specimen; these regions are lettered A to D in Figure 5.3. In each of these areas the morphology of the crystalline phase was different; X-ray powder diffraction of these areas showed that they contained a mixture of lithium disilicate and tridymite crystals. Figure 5.4 is a series of representative micrographs for each area; no crystal alignment was detected in these specimens.

The different crystal morphologies observed in the specimen are due to temperature variations in the specimen. When part of the specimen devitrifies, the resistivity will increase and the localised current density will decrease; the current density in the specimen is also a function of the electrode configuration. The Joule heating at any point in the specimen will be a function of the resistivity at that point and consequently localised temperature variations will occur.

The elementary experiments performed with this technique indicated that the system is very complicated; no morphological or crystallographic orientation was detected using this method and these experiments were not continued.

5.4 Hot Extrusion

5.4.1 Introduction

Extrusion is a well documented process in the technology of metals and plastics for the manufacture of rods, tubes or other profiles (4, 5, 23). In composite materials in which a second phase is mixed with the matrix, an

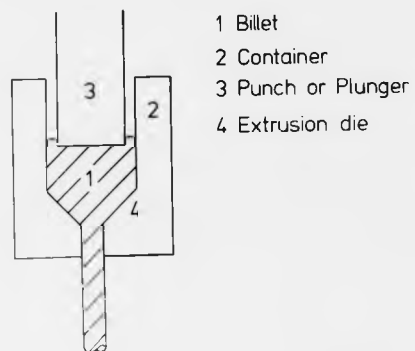


Figure 5.5(a) Direct Extrusion

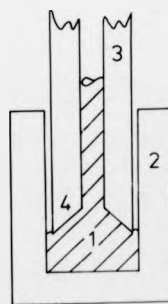


Figure 5.5(b) Inverted Extrusion

extrusion technique is used to align this phase (24). Roeder has investigated the flow behaviour of glasses when they are hot extruded (25, 26).

There are two distinct methods of extrusion: direct and inverted extrusion. In direct extrusion a billet of material, contained in a cylinder, is compressed by a plunger or punch, which forces the material through a die aperture (Figure 5.5a). The cross-sectional area of the die aperture is less than that of the initial billet and the cross-section of the extruded product is determined by the shape of this aperture. During the direct extrusion process the punch and the extruded rod move in the same direction.

In the inverted extrusion process (Figure 5.5b) a hollow punch supporting the die in front is pressed against the billet; the extruded rod inside the punch moves in the opposite direction to the plunger. In this method, there are no frictional forces between the billet and the cylinder wall, since there is no relative motion between the two. This technique therefore, requires less compressive force, but owing to some technical difficulties mainly arising from the hollow punch, inverted extrusion is only applied in special cases. In both methods the billets are usually heated during extrusion to increase their plasticity.

In this present work the direct extrusion method was used to produce a glass-ceramic with an aligned microstructure.

5.5 The Extrusion Apparatus

5.5.1 Introduction

The equipment which was developed to extrude a glass-ceramic does not differ significantly from that used for extruding metals or plastics. The apparatus which is shown in Figure 5.6a and b, consists of a stainless steel plunger with a water jacket which is attached to the cross-head of an Instron Universal Testing Machine. The plunger descends into a die which

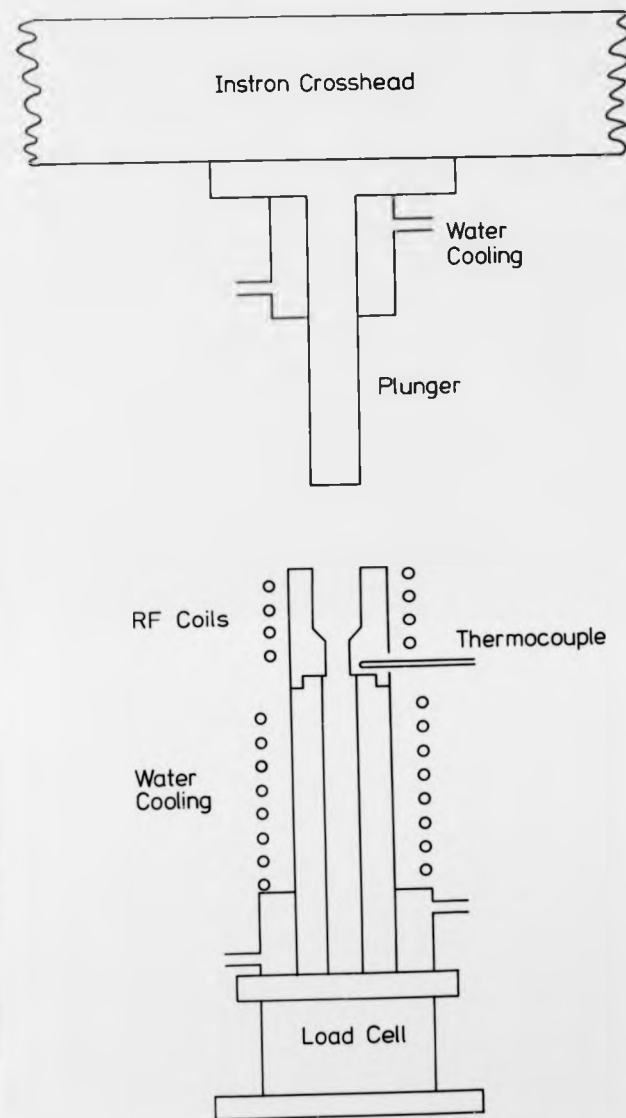


Figure 5.6(a) Schematic Diagram of the Extrusion Apparatus.

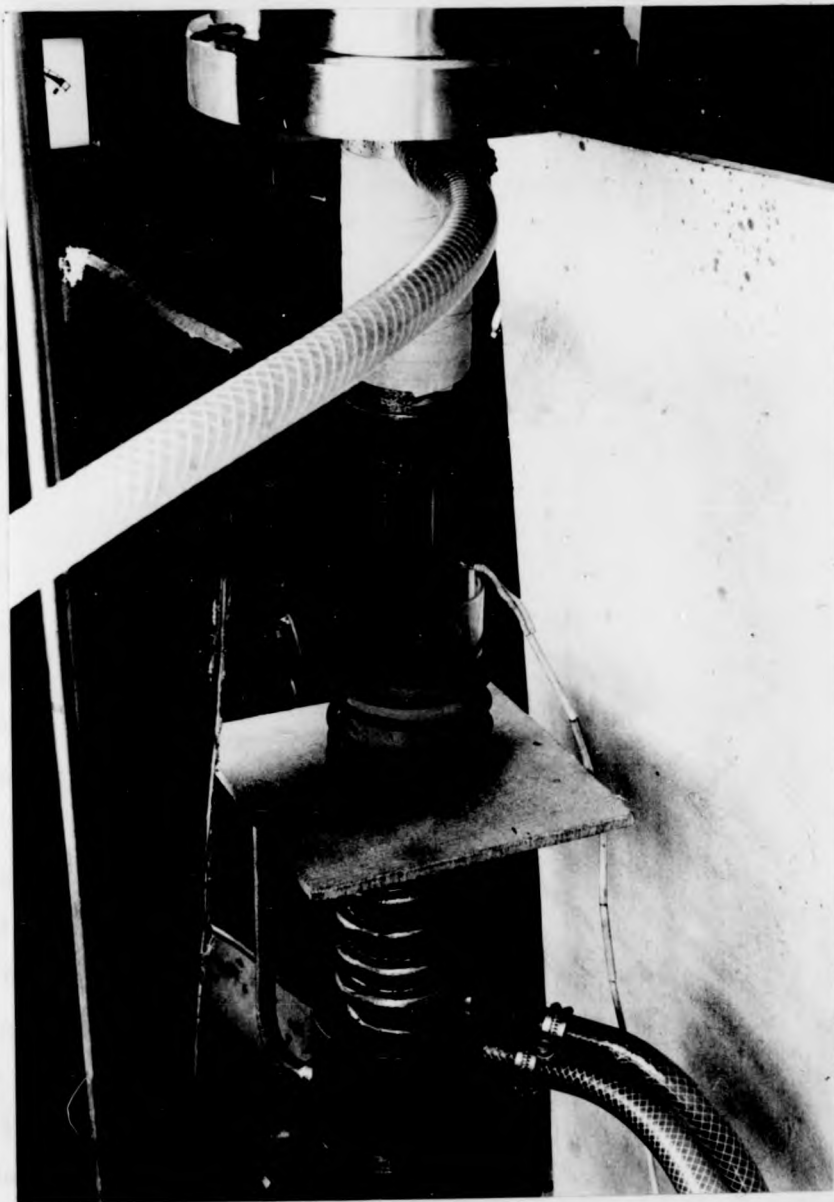


Figure 5.6(b) Photograph of the Extrusion Apparatus

is heated by high frequency induction and stands on the load cell of the Instron Machine. The temperature of the die can be monitored by optical pyrometry or by a thermocouple which is situated in the die near the aperture. The induction coil is electrically insulated from the die by a fused silica tube. When the extruded material is clear of the die it enters a water cooled collection zone; the die is a loose fit on the stand at room temperature and can be lifted off to collect the extruded material.

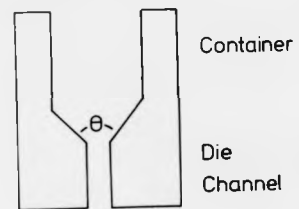
5.5.2 The Extrusion Die

The design of the extrusion die and container was evolved by a trial and error method; the analysis of the stress distribution in the die is mathematically complex and was not attempted. High frequency induction heating was used because of space limitations on the Instron Machine; this method of heating limited the choice of die material to a high strength heat resistant alloy or graphite. The latter material was not used because of the requirements of an inert atmosphere.

Figure 5.7 shows schematically the die; the die channel is the exit tube from the container after the material has been compressed by a cone joining the two. The aperture angle of the die is defined as twice the angle of this cone.

The velocity of extrusion of a material through the die depends upon the following parameters:

- (i) the applied punch pressure.
- (ii) the diameter of the die channel.
- (iii) the length of the die channel.
- (iv) the viscosity of the extruding material.
- (v) the frictional forces between the die walls and the extruding material.
- (vi) the aperture angle of the die.



θ = Angle of the die aperture

Figure 5.7 Schematic diagram of the extrusion die



Figure 5.8 Initial extrusion die

For a given extrusion velocity the applied punch pressure is a function of the frictional forces between the die walls and the billet and the ratio of the cross-sectional areas of the container and the die channel. The aperture angle of the die will determine the flow pattern of the material in the die; an aperture angle of 180° will produce areas of stagnant flow in the corners of the die. The dependence of these parameters on the rate of extrusion of a glass-ceramic and the degree of crystal orientation produced was not investigated in this present work. The dies used for all the extrusion experiments had the following parameters:

diameter of die channel	= 0.25 inches
length of die channel	= 0.75 inches
aperture angle of die	= 90°
ratio of the cross-sectional areas of the container and die channel	= 16 : 1

The die channel and the container were of circular cross-section so that the temperature distribution inside the die possessed circular symmetry. If this is not the case the extruded material will leave the die channel obliquely.

The extrusion dies were constructed from a high strength, heat resisting nickel-base alloy (Inconel alloy 600*). The initial die designs consisted of a thick walled tube (the container) which was threaded onto the die (Figure 5.8). The dimensions of the tube were determined from Laue's formula (27) which relates the wall thickness to the internal pressure and the allowable tensile stress of the container material. When these two-

* Inconel alloy 600 composition (wt. %): 0.15C; 1.0Mn; 6.0 - 10.0 Fe;
0.015 S; 0.5 Si; 0.5 Cu; 14.7 - 17.0 Cr; balance Ni + Co;

piece dies were used to extrude a glass-ceramic it was found that the extruded material flowed into the screw thread joining the container to the die and forced the two apart.

To eliminate this problem, the die and container were machined in one piece from a solid cylinder of Inconel 600, three inches long and two inches in diameter. It was estimated that the die was capable of withstanding a maximum pressure of 10^7 N/m² at temperatures up to approximately 950°C.

5.5.3 Flow Behaviour During Hot Extrusion

At high temperatures a glass forming liquid behaves as an ideal viscous (Newtonian) fluid, for which the rate of shear, $\dot{\gamma}$ is directly proportional to the applied shear stress τ :

$$\tau = \eta \dot{\gamma}$$

where η is the coefficient of dynamic viscosity. The rheological model for this fluid is represented by a dash pot. At temperatures beneath the glass transformation temperature T_g ($\eta = 10^{13.4}$ poise), a glass shows ideal elastic (Hookean) behaviour, for which the shear γ is directly proportional to the imposed shear stress τ :

$$\tau = G\gamma$$

where G is the modulus of rigidity. The corresponding rheological model for this behaviour is a helical spring. Within their working range ($\eta = 10^3$ until $\eta \approx 10^7$ poise), glasses can be regarded as pure Newtonian liquids (28).

A glass-ceramic is essentially a two phase composite consisting of a glass matrix and a dispersed phase of discrete particles. At high temperature it is expected that a glass-ceramic will respond to an applied stress in a manner similar to that of a solid-liquid mixture. The crystalline phase will be rigid compared with the non-crystalline material which will be fluid, since it must have a finite temperature coefficient of viscosity.

Shear alignment or changes in shape or distribution of suspended particles in a multi-phase material can cause a decrease in the viscosity of the material. This phenomenon is known as thixotropy and such systems possess an effective yield stress and properties similar to those to a Bingham plastic solid. These materials show little or no flow up to a critical shear stress and relatively easy flow at higher stresses. This flow is characterised by a coefficient of dynamic viscosity η given by:

$$\eta = \frac{\dot{\gamma}}{\tau - \tau_y}$$

where $\dot{\gamma}$ = rate of shear

τ = applied shear stress

τ_y = yield stress

A dilatant solid-liquid system shows Newtonian flow at low rates of strain, but on increasing the shear rate, the material requires a disproportionate amount of stress to maintain a given shear rate.

Ashbee and Morrell (29, 30) have studied the transient creep produced during cyclic loading in compression of a lithium zinc silicate glass-ceramic. The deformation process for this material is viscoelastic and linear with stress, the viscous glass phase controls the rate. They conclude that all stages of the creep of this particular glass-ceramic composition, the deformation behaviour is controlled by the residual glass phase, and that crystalline deformation of any type is insignificant.

Roeder (25) has studied the flow of glass during extrusion through circular die apertures and has shown that under certain conditions this flow obeys the Hagen - Poiseuille law, which describes the flow of viscous liquids through capillaries.

The Hagen - Poiseuille law states that for an incompressible Newtonian fluid, the isothermal laminar volumetric flow rate V , is given

$$\text{by: } V = \frac{\pi \Delta p r^4}{8 \eta \ell} \quad \text{Equation 5.1}$$

where Δp is the pressure difference between the entrance and exit of the tube, and r and ℓ are its radius and length respectively; η is the viscosity of the liquid. Frictional forces at the walls of the die produce an inhomogeneous distribution of flow velocity v across the die aperture. If it is assumed that a completely stagnant layer exists at the die walls, the velocity profile becomes parabolic:

$$v = \frac{\Delta p}{4 \eta \ell} (r^2 - x^2) \quad \text{Equation 5.2}$$

where x is a radial component. The maximum velocity is at the axis of the tube ($x=0$) and the velocity is zero at the walls ($x=r$). The assumption that a stagnant layer exists at the walls is not valid for all die materials, e.g. graphite.

The pressure at the die exit may be assumed to be atmospheric pressure. Since this value is generally small compared with the pressure at the die entrance p , the pressure difference over the die length Δp , can be substituted by the pressure p .

The viscosity in Equations 5.1 and 5.2 may be a function of the pressure in the material and no longer a true constant. Investigations on the boric oxide glass system (31, 32), which has an abnormally high compressibility, have shown that for this glass a viscosity-pressure relationship exists of the form:

$$\eta_p = \eta_0 \exp(\alpha p)$$

where η_p is the viscosity at pressure p , η_0 is the viscosity at normal pressure and α is a coefficient which is inversely proportional to temperature.

This dependence was not investigated for the glass-ceramics which were extruded. The values of the viscosity of the glass-ceramics

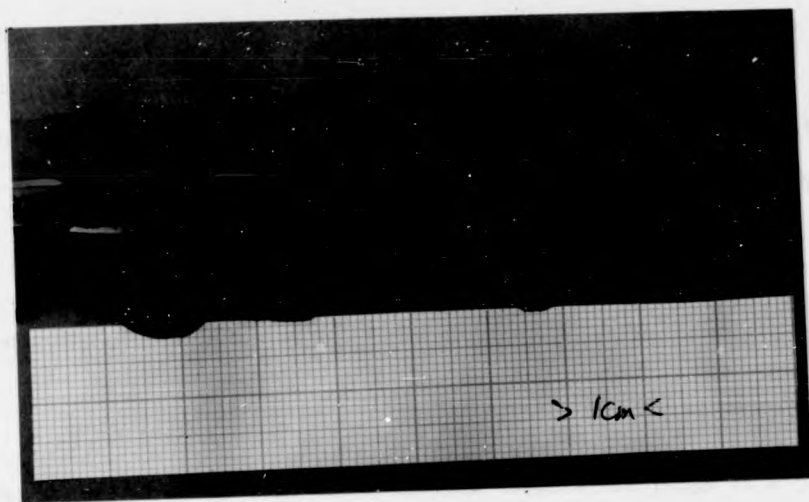


Figure 5.9 Flow pattern during extrusion of a glass-ceramic/cupric oxide billet.

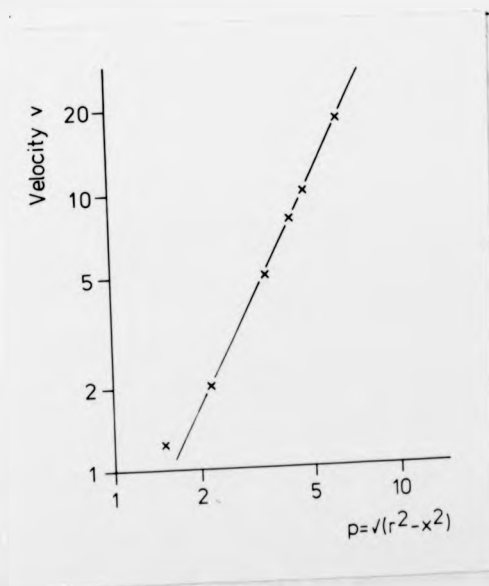


Figure 5.10 Dependence of the extrusion velocity v , on the radial direction.

derived from Equations 5.1 and 5.2 have been calculated on the basis that no viscosity-pressure relationship exists.

The viscosity-temperature function for a glass is of the form (33):

$$\eta = A \exp(B/RT) \quad \text{Equation 5.3}$$

where η = viscosity

T = temperature

A and B = constants, B is a measure of the activation energy for viscous flow

R = the gas constant.

This equation holds only for a limited temperature range in a glass. An improved formula proposed by Fulcher (34) has the form:

$$\eta = A' \exp\left(\frac{B'}{T - T_0}\right)$$

where T_0 is a third adjustable constant.

In the present work the viscosity-temperature dependence of glass-ceramics was taken to be that of Equation 5.3, which is a simple Arrhenius law.

An experiment was carried out to determine the flow of the material through the die. A billet consisting of alternate layers of glass-ceramic and cupric oxide was extruded at approximately 830°C with an applied punch pressure of approximately 8.10⁷N/m². The resulting section cut parallel to the extrusion axis of the rod is shown in Fig. 5.9.

At any moment during the extrusion process the distortion of the dark interface (cupric oxide) reveals the course of the glass-ceramic flow. It can be seen that the material flows much faster in the inner zone than at the edge. If the flow pattern is parabolic in form then the velocity distribution is in accordance with the Hagen-Poiseuille theory of flow (Equation 5.2). Figure 5.10 is a plot of $\ln(v)$ versus $\ln(p)$ for

data obtained from this flow experiment where:

$$p^2 = r^2 - x^2$$

This graph is a good straight line with a gradient of approximately 2 (an arbitrary origin was chosen for the $\ln(v)$ axis). The flow of alternate layers of a glass-ceramic and cupric oxide therefore follows the Hagen-Poiseuille law and behaves like a Newtonian liquid.

The rate of formation of the extruded rods can be calculated from displacement measurements of the punch. The velocity of the punch v_p is related to the velocity of the extruded rod \bar{v} , by the extrusion ratio $R = A_0/A$, where A_0 and A are the cross-sectional areas of the container chamber and the die respectively:

$$\bar{v} = Rv_p$$

5.5.4 The Hot Extrusion of a Glass-Ceramic

The extrusion apparatus can be operated in two modes:

- (i) Extrusion can be achieved by maintaining a constant pressure on the sample in the die. This is performed by varying the rate of descent of the plunger.
- (ii) The rate of descent of the plunger can be maintained at a constant value and the applied pressure allowed to vary accordingly.

When the plunger is applying a load to the glass-ceramic which is to be extruded, the stress is relieved by material flowing through the aperture of the die. A certain amount of material is extruded in the reverse direction between the wall of the container and the plunger. This "back-extruded" material helps to lubricate the plunger in the container and prevent the apparatus seizing (Figure 5.11).

To extrude a glass-ceramic, a glass billet was placed in the die and heat-treated in situ for a predetermined period of time at a set

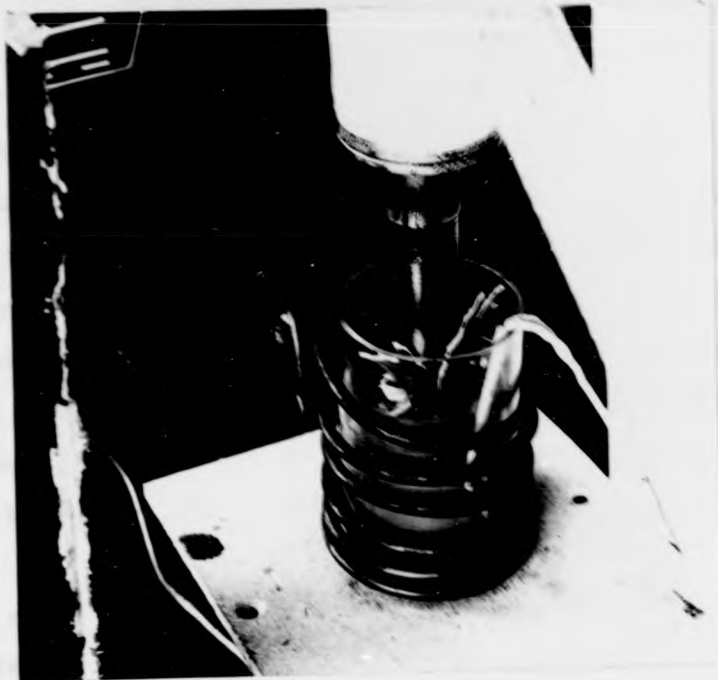


Figure 5.11 Back Extrusion



Figure 5.12 The original glass billet, the extruded rod and the back extruded material.

temperature to produce a glass-ceramic. When the specimen had been heat-treated the plunger was lowered into the die and the extrusion process carried out in one of the two modes described above. The temperature of the die was maintained at the constant value of the heat-treatment throughout the extrusion process. The constant pressure method of operation was found to be the easiest to perform experimentally and subsequently analyse. The constant pressure was maintained on the specimen by a feed-back loop which regulated the rate of descent of the plunger; the pressure was held to within $\pm 2\%$ of its value.

The rate of descent of the plunger was recorded and the temperature of the die was measured with a chromel-alumel thermocouple situated in the die near the aperture. Temperature measurements with an optical pyrometer showed that a temperature gradient of $100^{\circ}/\text{cm}$. existed in the die between the top of the container and the bottom of the die (approximately 8 cm in length) in the range of temperature at which extrusion was performed.

Two different compositions in the $\text{Li}_2\text{O}-\text{SiO}_2$ glass system were extruded between 800°C and 900°C with pressures varying between $5 \cdot 10^7 \text{N/m}^2$ and 10^6N/m^2 (see Chapter 8 for details). The viscosity of the material in this range was between 10^{10} poise and 10^7 poise. The maximum value of Reynold's number was found to be seventeen orders of magnitude below the critical lower limit for turbulent flow; hence the flow was concluded to be of a lamina nature. A typical extrusion experiment lasting 150 minutes produced a rod 8 cm in length. Figure 5.12 shows the original glass billet, the extruded rod and the back extruded material.

After each extrusion experiment the plunger was removed from the die and cleaned by a process of heating and rapid quenching in a melting mixture of ice. It was found that the die could be cleaned faster if a small quantity of potassium iodide was placed in it; this chemical

when molten ($\sim 700^{\circ}\text{C}$) prevents the glass-ceramic wetting the walls of the container and on subsequent quenching the glass-ceramic is easily removed (35).

In all the extruded rods produced, an alignment of the asymmetric crystalline phase parallel to the extrusion axis was observed. The mechanism which causes this orientation is not easy to analyse; shear alignment and crystal-crystal interactions are involved in the process. Several authors have considered the alignment of rigid cylinders immersed in a sheared viscous fluid (36 - 38). A particle which is not lying with its major axis parallel to the flow direction experiences an angular velocity about its centre of mass and a translational velocity parallel to the flow direction. The angular velocity causes the particle to rotate towards an orientation parallel to the direction of flow. For a system of non-interacting particles a preferred orientation of particles parallel to the axis of flow can be shown to exist.

In the present work, the glass-ceramics which were extruded had a volume fraction of crystalline phases of approximately 80% and crystal-crystal interactions in this system must occur.

McMillan (39) has likened the extrusion of a glass ceramic and the subsequent alignment to the flow of logs down a river; the logs flow with their major axis pointing down river and log-log interactions do occur but a preferred orientation of logs is maintained.

5.5.5 Experiments with Glass-Ceramic Filaments.

When a fibre is pulled from a bulk material the flow of the material is similar to that observed when the material is extruded. Some preliminary experiments on pulling glass-ceramic fibres from a glass-ceramic specimen at a high temperature were carried out.

In this work a specimen of a glass-ceramic produced from glass B (see Table 5.1) was maintained at approximately 900°C ; at this temperature

the glass phase of the material was above its softening point and an asymmetric crystalline phase of lithium disilicate was present. A stiff platinum wire with a loop on the end was pushed into the material and quickly drawn away; this produced a fibre of glass-ceramic material approximately 250 microns in diameter. X-ray fibre texture photographs produced inconclusive results and great difficulty was found in preparing samples parallel to the fibre axis for scanning electron microscopy.

This experimental technique was not continued because of the difficulties associated with making physical property measurements perpendicular to the fibre axis.

References

1. P. W. McMillan, Glass Ceramics (Academic Press, London, 1964)
2. C. L. Booth & G. E. Rindone, J. Am. Ceram. Soc. 47 25 (1964)
3. G. E. Rindone in Symposium on Nucleation and Crystallisation in Glasses and Melts. Edited by M. K. Reser, G. Smith & H. Insley (Am. Cer. Soc. Inc., Columbus Ohio, 1962)
4. R. Chadwick, Met. Rev. 4 189 (1959)
5. C. E. Pearson and R. N. Farkins, The Extrusion of Metals (Chapman and Hall, 1960)
6. A. Kelly and G. J. Davies, Met. Rev. 10, 1 (1965)
7. N. Cratchley, *ibid.* 10 79 (1965)
8. T. Hoffmann, J. Mazur, J. Nikliborc and J. Rafalowicz, Brit. J. Appl. Phys. 12 342 (1961)
9. T. Hoffmann, J. Mazur, J. Nikliborc and J. Rafalowicz, *ibid.* 12 635 (1961)
10. S. V. Phillips, private communication
11. W. H. Sutton in Proceedings of the Third International Materials Symposium, Berkeley, Calif.: Ceramic Microstructures edited by R. M. Fulrath and J. A. Pask (John Wiley & Sons, Inc., New York 1968)
12. F. M. A. Carpay and W. A. Cense, Scripta Metall. (U.S.A.) 8 11 (1974)
13. R. J. Charles, Am. Ceram. Soc. Bull. 52 673 (1973)
14. R. J. Charles and A. M. Turkalo in The Glassy State. The Fifth All-Union Conference, Leningrad, U.S.S.R. 1969, Published by Acad. Nauk. 1971.
15. I. N. Lifshitz and V. V. Slyozov, J. Phys. Chem. Solids 19 35 (1961)
16. C. Wagner, Z. Elektrochem 65 581 (1961)
17. G. W. Greenwood, Acta Metall. 4 243 (1956)
18. D. Kashchiev, Phil. Mag. 25 459 (1972)
19. J. L. Tomlinson, J. Electron Mater. 1 357 (1972)
20. R. C. De Vekey and A. J. Majumdar, Nature 225 172 (1970)

References

1. P. W. McMillan, Glass Ceramics (Academic Press, London, 1964)
2. C. L. Booth & G. E. Rindone, J. Am. Ceram. Soc. 47 25 (1964)
3. G. E. Rindone in Symposium on Nucleation and Crystallisation in Glasses and Melts. Edited by M. K. Reser, G. Smith & H. Insley (Am. Cer. Soc. Inc., Columbus Ohio, 1962)
4. R. Chadwick, Met. Rev. 4 189 (1959)
5. C. E. Pearson and R. N. Parkins, The Extrusion of Metals (Chapman and Hall, 1960)
6. A. Kelly and G. J. Davies, Met. Rev. 10, 1 (1965)
7. N. Cratchley, *ibid.* 10 79 (1965)
8. T. Hoffmann, J. Mazur, J. Nikliborc and J. Rafalowicz, Brit. J. Appl. Phys. 12 342 (1961)
9. T. Hoffmann, J. Mazur, J. Nikliborc and J. Rafalowicz, *ibid.* 12 635 (1961)
10. S. V. Phillips, private communication
11. W. H. Sutton in Proceedings of the Third International Materials Symposium, Berkeley, Calif.: Ceramic Microstructures edited by R. M. Fulrath and J. A. Pask (John Wiley & Sons, Inc., New York 1968)
12. F. M. A. Carpay and W. A. Cense, Scripta Metall. (U.S.A.) 8 11 (1974)
13. R. J. Charles, Am. Ceram. Soc. Bull. 52 673 (1973)
14. R. J. Charles and A. M. Turkalo in The Glassy State. The Fifth All-Union Conference, Leningrad, U.S.S.R. 1969, Published by Acad. Nauk. 1971.
15. I. M. Lifshitz and V. V. Slyozov, J. Phys. Chem. Solids 19 35 (1961)
16. C. Wagner, Z. Elektrochem 65 581 (1961)
17. G. W. Greenwood, Acta Metall. 4 243 (1956)
18. D. Kashchiev, Phil. Mag. 25 459 (1972)
19. J. L. Tomlinson, J. Electron Mater. 1 357 (1972)
20. R. C. De Vekey and A. J. Majumdar, Nature 225 172 (1970)

21. P. F. James and P. W. McMillan, *Phys. Chem. Glasses* 11 64 (1970)
22. P. F. James and P. W. McMillan, *ibid.* 11 59 (1970)
23. E. C. Bernhardt, *Processing of Thermoplastic Materials* (Reinhold, New York; Chapman & Hall, London 1959)
24. R. W. Jech, E. P. Weber and A. D. Schwope in *Reactive Metals* editor, W. R. Clough (Interscience Pub., 1959)
25. E. Roeder, *J. Non-Crystalline Solids* 2 377 (1971)
26. E. Roeder, *ibid.* 2 203 (1971)
27. *Machinery Handbook* (Industrial Press New York, 1942)
28. G. Meerlender, *Glass-Inst. Tech.* 2 490,553 (1965)
29. R. Morrell and K. H. G. Ashbee, *J. Mat. Sci.* 8 1253 (1973)
30. R. Morrell and K. H. G. Ashbee, *ibid* 8 1271 (1973)
31. E. B. Jr. Done and F. Birch, *J. Appl. Phys.* 2 669 (1938)
32. L. L. Sperry and J. D. Mackenzie, *Phys. Chem. Glasses* 2 91 (1968)
33. J. E. Stanworth, *Physical Properties of Glass* (Oxford, London 1950)
34. G. S. Fulcher, *J. Am. Ceram. Soc.* 8 339,789 (1925)
35. P. S. Bell, private communication.
36. G. B. Jeffery, *Proc. Roy. Soc. Lond.* A102 161 (1923)
37. S. G. Mason and R. St. J. Manley, *ibid* A238 117 (1956)
38. E. Anczurowski and S. G. Mason, *Trans. Soc. Rheol.* 12 209 (1968)
39. P. W. McMillan, private communication.

CHAPTER 6: THE STATISTICAL ANALYSIS OF THE MICROSTRUCTURE

6.1 Introduction

This chapter contains details of the techniques used to analyse statistically the microstructure of the glass-ceramics studied. Methods for determining the "degree of orientation" in an anisotropic specimen are described. Results of an optical method for determining the various parameters describing an ideal microstructure are described and the usefulness of this method is discussed.

A theoretical analysis, relating the number of intersections of objects or features per unit length of test line, to a distribution curve of the number of features, $N(\theta)$ making an angle θ to a reference direction is presented. The experimental method of using this analysis is described. Details of evaluating the volume fraction of the crystalline phases and the mean inter-crystal spacing are presented.

6.2 The Significance of Statistical Analysis

The properties of glass-ceramics (and all materials) are a consequence of their internal structures. Although some properties are directly related to the atomic and crystal structures present, others are related to the microstructure. The purpose of this chapter is to develop the techniques required to quantify the parameters of random and oriented microstructures which, will permit physical property measurements to be related to the structure.

The basic structural information required about a poly-phase material is the volume fraction of each phase present, the mean particle size if the phases are discrete, and the mean inter-particle spacing. If the system is oriented a "degree of orientation" can be defined as the ratio

of the maximum to minimum values of a vector which describes a measurable parameter of the microstructure. For an isotropic system this degree of orientation will be unity, for an anisotropic system its value will be greater than unity.

The statistical analysis of the microstructure of a material usually involves relating measurements made on a two dimensional polished or lightly etched section of the specimen to three dimensions (1,2). The procedure for evaluating, for example the mean particle spacing, is very tedious and time consuming; for this reason the possibility of determining the various parameters describing the microstructure by another method was investigated.

6.3 Optical Analysis of the Microstructure

6.3.1 Introduction

The Fraunhofer diffraction pattern of an array of apertures in a plane screen contains all the information about this system in terms of the phase and amplitude of the waves in the diffraction pattern. Essentially the original set of apertures are being viewed in a Fourier transform space (3). The optical transform of transmission electron micrographs has been used quite extensively to detect periodicity in these micrographs (4-6).

The Fourier transform of a set of rectangular apertures with given distributions of position and orientation on a screen is outside the scope of this present work. An empirical approach to the problem of how to deduce the various parameters describing this "microstructure" from its Fraunhofer diffraction pattern was performed. In the following the angular distribution function is taken to mean the probability $P(\theta)$ of finding a crystal making an angle θ with a reference direction.

6.3.2 The Fraunhofer Diffraction Patterns of Ideal "Microstructures"

The glass-ceramic systems studied in this work consisted of needle shaped crystals with an aspect ratio greater than one (the ratio of the maximum to minimum crystal dimensions) and a second crystalline phase with an aspect ratio of approximately one. These two crystalline phases were positioned randomly in a glassy matrix; the angular distribution of these crystals could be varied between random and aligned (in this sense aligned is taken to mean non-random). This system was approximated to an ideal two dimensional microstructure consisting of a set of rectangular apertures (the crystals) randomly positioned on a plane (the glassy matrix). The angular distribution function of these "crystals" could then be predetermined together with the other parameters describing the system.

A computer programme was developed to draw "micrographs" of this idealised system. The programme allowed the aspect ratio and the angular distribution function of the particles to be varied. In all the cases studied the particles were positioned randomly over the plane and the aspect ratio was a constant or varied as a square distribution function. The angular distribution function could be square shaped in which the probability $P(\theta)$, of finding a particle making an angle θ with a reference direction was defined as:

$$P(\theta) = 1 \text{ if } a \leq \theta \leq b$$

and

$$P(\theta) = 0 \text{ if } a > \theta > b$$

where $(b - a)$ is the width of the distribution function. An angular distribution function of Gaussian shape could also be chosen; in this case:

$$P(\theta) = \frac{1}{\sqrt{(2\pi\sigma^2)}} \exp \left[-\frac{\theta^2}{2\sigma^2} \right]$$

where 2σ is the width of the distribution function measured at:

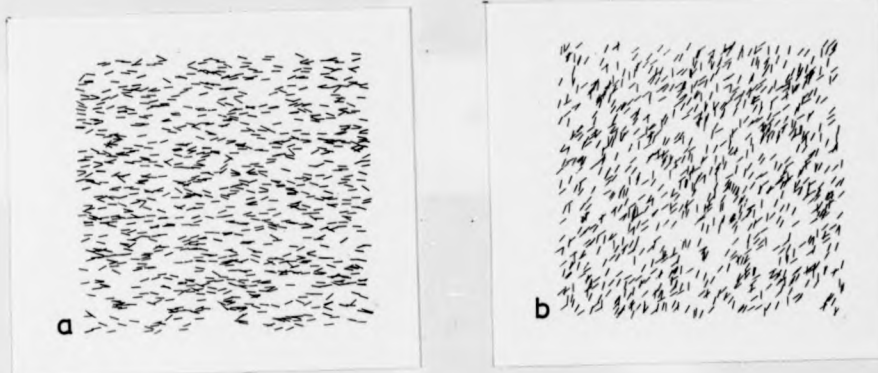


Figure 6.1 The Fraunhofer diffraction masks: (a) Gaussian angular distribution function; (b) square function.

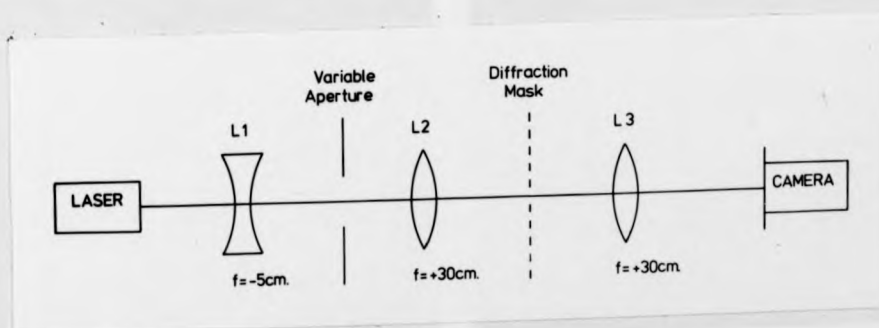


Figure 6.2 The optical bench for the Fraunhofer diffraction experiments.



$\sigma = 16$



$\sigma = 10$



$\sigma = 2$



(a)

Figure 6.3 Fraunhofer diffraction patterns of masks with Gaussian angular distribution functions of decreasing widths (σ).



(f) Aligned



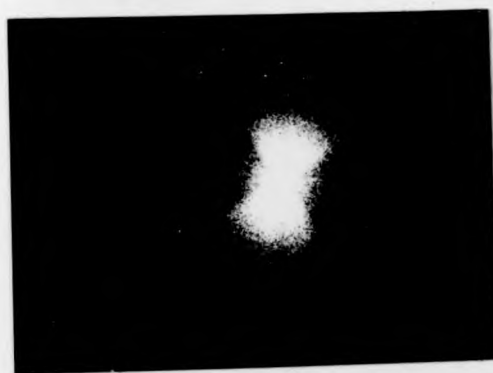
(e) $\sigma = 12$



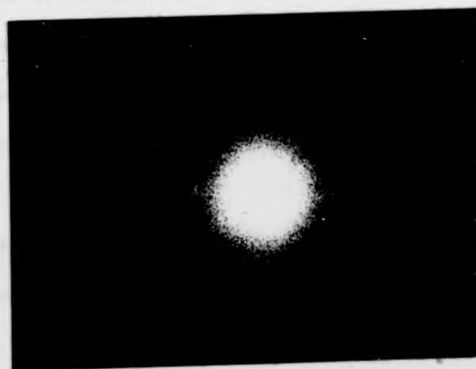
(d) $\sigma = 20$



(c) $\sigma = 50$



(b) $\sigma = 75$



(a) Random

Figure 6.4 Fraunhofer diffraction patterns of masks with square angular distribution functions of decreasing width (σ).

$$P(\theta) = \frac{1}{\sqrt{e}} P(\theta_{\max})$$

The pictures, which were 15 cm x 15 cm as drawn and contained 500 particles were photographed, and reduced by a factor of 20 on reproduction as positive prints on glass slides; these "micrographs" were then used as diffraction masks. Figure 6.1 shows an example of a mask with each type of angular distribution function.

An optical bench was constructed so that the Fraunhofer diffraction pattern of the masks could be recorded (Figure 6.2). The apparatus consisted of a He/Ne laser (6328 Å); the light beam from the laser was broadened by lenses L1 and L2. The diffraction mask was placed between lenses L2 and L3 where the light beam was parallel and the diffracted image was recorded in the focal plane of lens L3 with a camera.

Figure 6.3 is a series of Fraunhofer diffraction images of the masks with a Gaussian angular distribution function of decreasing width. The speckled appearance of these images is caused by the laser beam interacting with airborne particles and is random. These diffracted images show higher order maxima in the intensity as the width of the distribution curve decreases; this is to be expected (3). When the array of N apertures are all parallel the diffraction intensity is N times the light intensity diffracted by a single aperture. Figure 6.4 is a series of Fraunhofer diffraction patterns of masks containing apertures with square angular distribution functions. A diffraction pattern of a random distribution of angles is shown in Figure 6.4(a); the width of the angular distribution curve decreases throughout the series a to f. These patterns show similar features to those produced by Gaussian angular distribution function; the contrast at the edge of the central maxima is sharper because of the shape of the distribution function.

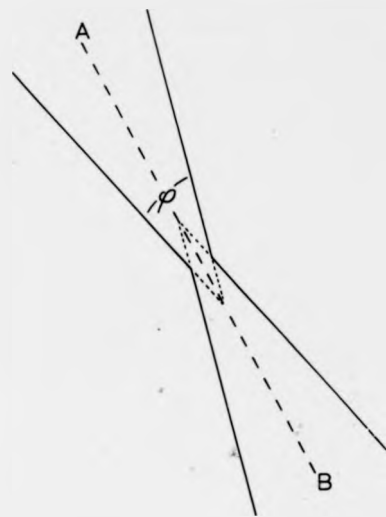


Figure 6.5 Schematic diagram of the central band of maximum intensity (cf Figure 6.3(b)). AB is the symmetry axis; φ is a measure of the width of the angular distribution function.

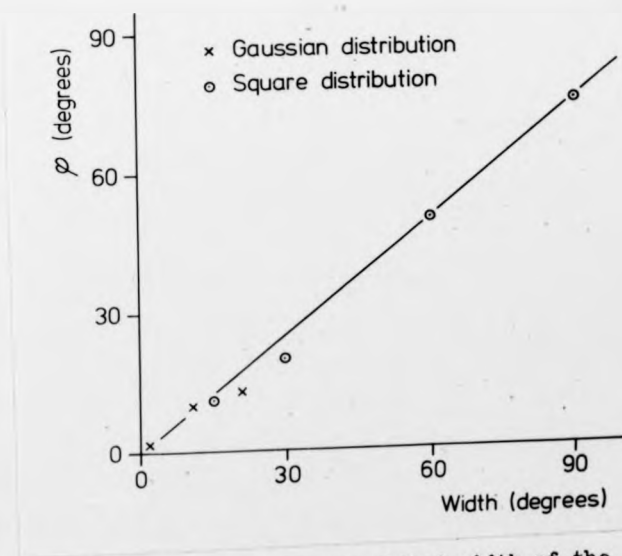


Figure 6.6 A comparison of φ and the calculated width of the angular distribution function.



Figure 6.7 A densitometer trace along the line of symmetry
AB of Figure 6.3(a).

The central band of maximum intensity in the diffraction pattern is equivalent to two isosceles triangles intersecting along a symmetry axis AB (see Figure 6.5). If φ is the angle each triangle subtends at the intersection, then φ increases as the width of the angular distribution function increases. Figure 6.6 shows a comparison of φ and the calculated width of the distribution function.

The intensity of the diffracted light measured along the symmetry axis AB appears to contain information about the aspect ratio of the apertures. Figure 6.7 is a densitometer trace along the line of symmetry AB of Fig. 6.3a; the intensity variation appears to be composed of two superimposed Gaussian functions of different widths. The ratio of the widths of these two Gaussians is related to the aspect ratio.

The Fraunhofer diffraction produced by an "ideal" microstructure contains all the information in the diffraction mask presented in a different form. The results indicate that empirically it is possible to obtain information about the width of the angular distribution function and the aspect ratio of the particles in the microstructure. A mathematical analysis of the system to find the diffracted intensity at a point $P(\alpha, \beta)$, where α and β are direction cosines, involves summing the amplitude and phase of the diffracted waves from each aperture which contribute to the intensity at P. This can be solved for a random and perfectly aligned set of apertures (3); intermediate angular distributions require a numerical solution.

6.3.3 Fraunhofer Diffraction Images of Real Microstructures

To determine whether this technique could be applied to a real system, scanning electron microscope (SEM) micrographs of etched specimens of a glass-ceramic were prepared as optical diffraction masks. Two types of



Figure 6.8(a) Fraunhofer diffraction pattern of an SEM micrograph:
random microstructure.

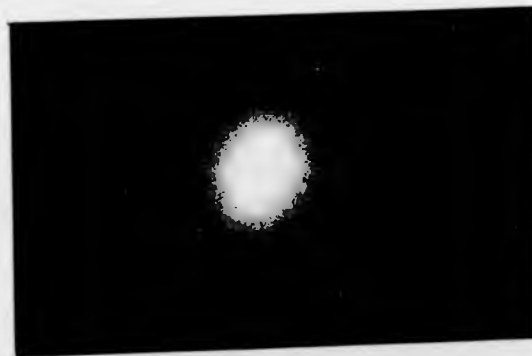


Figure 6.8(b): some crystal alignment.

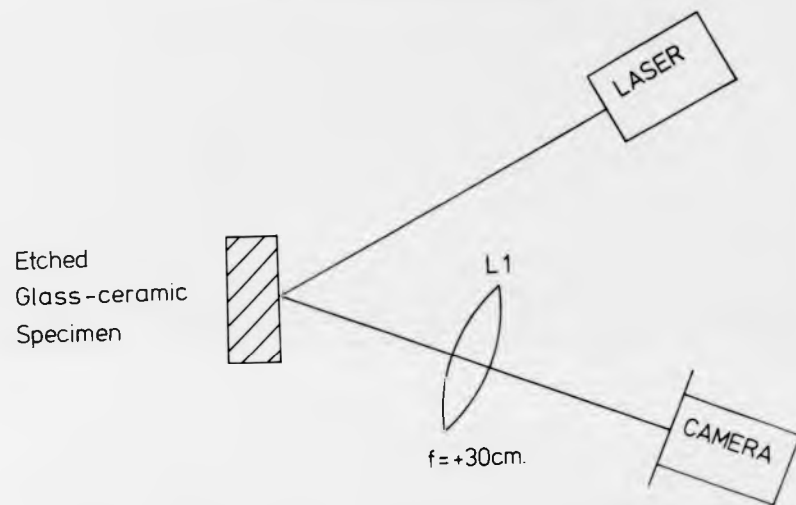


Figure 6.9 The optical bench for the reflection/diffraction experiments.



Figure 6.10(a) Reflection/diffraction image from a randomly oriented glass-ceramic surface.



Figure 6.10(b): from a glass-ceramic surface with some crystal orientation.

specimen were used, micrographs in which the microstructure was randomly oriented and micrographs in which preferred crystal orientation was apparent. Figure 6.8 shows the result of using these images as Fraunhofer diffraction masks. The diffraction pattern of the random microstructure is approximately circular (Figure 6.8(a)), whilst, that of the specimen with some crystal alignment is elliptical in shape. These images indicate that there is a difference between the two micrographs in terms of crystal orientation. The ellipse shaped diffraction image from the aligned micrograph was a real effect; the major axis of the ellipse rotated as the mask was rotated and was independent of the orientation of the micrograph image on the glass slide.

It is difficult to directly relate the diffraction pattern of the aligned micrograph with the 'ideal' micrographs studied above. There are superficial similarities between the patterns but ascribing a number to the width of the angular distribution function of the real aligned microstructure is impossible based on the arguments presented above. One of the reasons for this difficulty is believed to be the poor contrast between the crystals and glass matrix in the SEM micrographs resulting in a low diffraction efficiency.

In an attempt to overcome this problem an etched specimen was used as a reflection/diffraction grating. A He/Ne laser was used to illuminate the etched glass-ceramic surface with a beam of coherent light; the diffracted/reflected image was brought to a focus with a lens L1 in the focal plane of which was a camera (Figure 6.9). Figure 6.10 shows the image of a random and an aligned surface using this technique; the random surface (Fig. 6.10(a)) shows an approximately circular pattern and the aligned surface an ellipse shaped pattern (Fig. 6.10(b)). The major axis of this ellipse rotated as the specimen was rotated in a plane

perpendicular to the incident beam, indicating that the ellipse was a real effect associated with the etched microstructure. There are marked similarities between these diffraction images and the images produced by SEM micrographs in the transmission diffraction mode. The problem still remains however, of how to analyse the diffraction images to produce numbers describing parameters in the real images.

6.3.4 Comments on the Optical Diffraction Technique

The preliminary experiments described in the previous sections indicate that the optical diffraction technique could be used to analyse micrographs of the microstructure of multi-phase materials. Without a theoretical analysis of the system, the difficulties remain of which physical parameters in the real image to ascribe to measurable quantities in the diffracted image.

The differences in the diffraction patterns produced by the real and ideal microstructures have been attributed partly to the poor contrast in the SEM micrographs. Real images with greater contrast could have been produced by photographic techniques or by using the cathodoluminescence mode of the SEM (see Chapter 4).

It should also be noted that the ideal microstructure is only an approximation to the real structure and comparisons between the two should be made with care.

The technique of using optical transform methods for the analysis of electron microscope micrographs is becoming an accepted one. Tovey (7) describes the experimental analysis of the structure of clay particles in soil using a convolution square camera. The optical correlation analysis of two-phase micrographs has been extensively studied by Bieringer and his co-workers (8-11).

In the present work not enough is known about the analysis of the diffraction images produced by the system used; for this reason the glass-ceramic microstructures were analysed by statistical counting methods.

6.4 Specification and Measurement of Microstructural Anisotropy

6.4.1 Introduction

To detect any anisotropy in the morphological orientation of the crystals in a glass-ceramic, a technique of counting the number of features intercepted by a test line of given orientation was used (1,2). This method consisted of rotating an array of parallel lines about a reference point on a SEM micrograph of an etched glass-ceramic surface. The number of crystal boundaries intercepted by unit length of this test array for a given orientation of the array relative to a reference direction was evaluated.

The number of interceptions per unit length of the test array $N(\theta)$, for a given angle θ , of the array to a reference direction, is a measure of any structure anisotropy in the micrograph. If the crystal shape is isometric (i.e. the aspect ratio is unity), then no preferred orientation will be apparent and $N(\theta)$ will be a constant; $N(\theta)$ will also be a constant for crystals with an aspect ratio greater than one, if the crystals are randomly oriented in the test plane. $N(\theta)$ will be a function of θ if the crystals are aligned with respect to their shape in a preferred direction. A maximum number of intersections $N(\theta_{max})$, will occur in a direction perpendicular to the orientation and a minimum, $N(\theta_{min})$, parallel to it. Saltykov (12) has defined a degree of orientation ω , based on the values of $N(\theta_{max})$ and $N(\theta_{min})$:

$$\omega = \frac{100 [N(\theta_{max}) - N(\theta_{min})]}{N(\theta_{max}) + 0.571 N(\theta_{min})} \text{ per cent}$$

This definition of the degree of orientation present in the micrograph analysed is difficult to directly relate to the anisotropy present. Ideally a measure of the width of the distribution curve describing the number of crystals pointing in a given direction (the angular distribution function) is required.

6.4.2 Determination of the Angular Distribution Function

Hilliard (13) has provided a mathematical framework for the quantitative description of anisotropic microstructures. The treatment of the problem is a completely general one; two systems of lines are superimposed on one another and their probabilities of intersection are considered. One system of lines is arbitrarily designated as the test array and the general equation is set up relating the line length of the other system of lines to the number of intersections with the test array. Methods are then deduced for obtaining the specific line length as a function of direction. Similar procedures are followed for systems of surfaces.

Hilliard (13) deduces an equation which relates the expected number of intersections per unit length of test array with the microstructure, $N(\theta)$, to a function $L_A(\omega)$. $L_A(\omega)d\omega$ is the total line length per unit area having tangents with angles in the range $\omega \pm (d\omega/2)$, where ω is measured from an arbitrary reference direction. The function $L_A(\omega)$ as defined is not the function which relates the probability $p(\omega)d\omega$ of finding a crystal making an angle $\omega \pm (d\omega/2)$ with an arbitrary reference direction.

In order to determine the function $p(\omega)$, from the number of intersections per unit length of test line $N(\theta)$, an analysis of the system was performed.

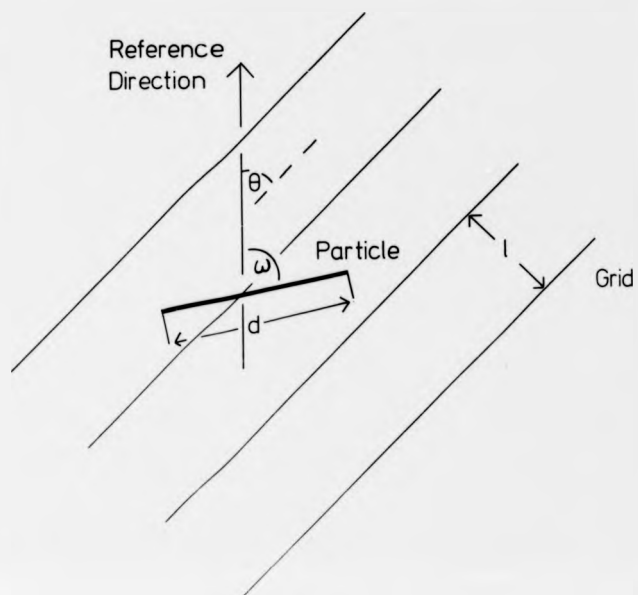


Figure 6.11 Notation for the mathematical derivation of the angular distribution function.

6.4.3 Mathematical Derivation of the Angular Distribution Function (14)

Consider a system of N particles with a distribution function $p(\omega)$ lying at random on a grid. Let the grid be composed of parallel lines separated by a distance ℓ and let the length distribution of the particles be described by a function d (for mathematical convenience d is assumed to be a constant). Let $N(\theta)$ be the number of particles intercepted by this grid when it is making an angle θ with an arbitrary reference direction. The probability distribution $p(\omega)d\omega$ is assumed to be a continuous probability distribution so that a grid line which is a tangent to a particle has measure zero.

The resolved component τ , of the length of one of the particles perpendicular to the grid is (Figure 6.11):

$$\tau = |d \sin(\omega - \theta)|$$

The position of the particles in the plane is random so that the expectation number of intersections for one particle with the grid is:

$$\frac{\tau}{\ell} = \frac{|d \sin(\omega - \theta)|}{\ell}$$

$$\text{Thus } N(\theta) = \int_{-\pi}^{\pi} p(\omega) \frac{\tau}{\ell} d\omega$$

$$\text{hence } N(\theta) = \frac{Nd}{\ell} \int_{-\pi}^{\pi} p(\omega) |\sin(\omega - \theta)| d\omega \quad \text{Equation 6.1}$$

$p(\omega)$ and $N(\theta)$ must be periodic in π , therefore if $p(\omega)$ is expanded as a Fourier series:

$$p(\omega) = \sum_{n=0}^{\infty} (a_n \cos 2n\omega + b_n \sin 2n\omega) \quad \text{Equation 6.2}$$

and substituted into Equation 6.1 then $N(\theta)$ can be expanded as a Fourier series:

$$N(\theta) = \sum_{n=0}^{\infty} (\alpha_n \cos 2n\theta + \beta_n \sin 2n\theta) \quad \text{Equation 6.3}$$

$$\text{where } \alpha_n = \frac{-4Nd a_n}{(4n^2 - 1)\ell}$$

$$\text{and } \beta_n = \frac{-4Nd b_n}{(4n^2 - 1)\ell}$$

Equation 6.4

This result is essentially the same as that of Hilliard (13); the difference is that the Fourier coefficients are a function of the spacing of the test grid (ℓ) and the size of the particles being analysed (d).

It can be seen from Equations 6.2 and 6.3 that if a Fourier series is fitted to the number of interceptions versus angle data ($N(\theta)$), then the angular distribution function of these particles ($p(\omega)$), can be easily derived from the new Fourier coefficients (Equation 6.4).

The computation involved in estimating the Fourier coefficients of $N(\theta)$ is relatively simple if a computer is employed. The Fourier analysis of $N(\theta)$ has the advantage of automatically smoothing the data compared with a second differences approach to the problem. In addition, the first few coefficients provide a convenient means of characterising the function $p(\omega)$ without resorting to a histogram. The number of Fourier coefficients which can be estimated depends on the increments of θ at which $N(\theta)$ is measured. The optimum size of the increment will be determined by the standard deviation of the measurements.

To test the validity of Equations 6.2-6.4 and develop the necessary computer programmes the pictures drawn by the computer for the Fraunhofer diffraction experiments (see section 6.2.2) were analysed. A programme was developed to count the number of intersections made by the particles in these pictures with a parallel array of lines. This test grid could be rotated about a fixed point in the centre of the picture, relative to a reference direction. The programme analysed the angular distribution of the particles into a histogram of the number of particles making an

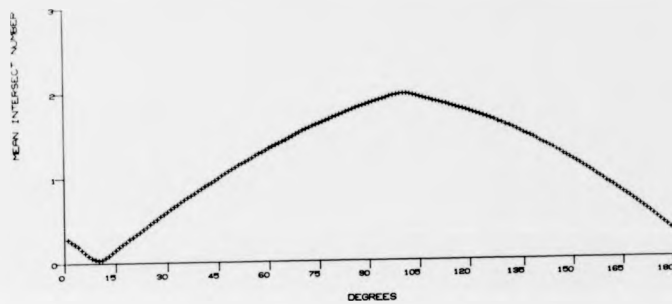


Figure 6.12(a) The number of intersections per unit length of test array versus the angle the array makes with a reference direction.

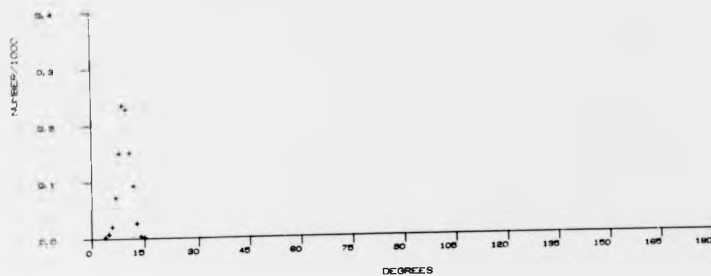


Figure 6.12(b) Histogram of the number of particles versus angle.

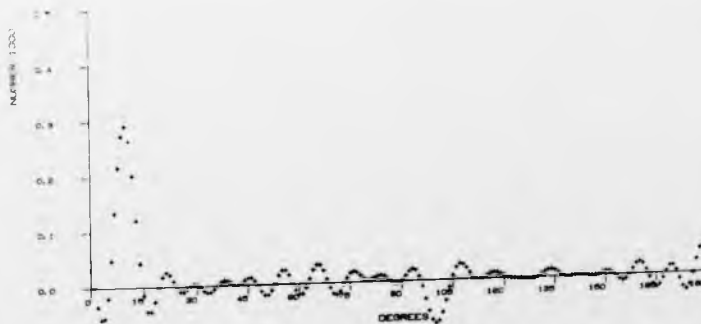


Figure 6.12(c) The result of analysing the intercept data in Figure 6.12(a) according to Equations 6.2 to 6.4.

angle θ with the reference direction. The number of intersections of particles with the grid was counted at one degree intervals between zero degrees and 180 degrees relative to the reference direction. This data was transformed according to Equations 6.2 - 6.4 using a procedure to fit a Fourier series to the intercept data. The angular distribution function was calculated from the Fourier coefficients and the results were displayed using the digital plotter of the computer. Figure 6.12 shows the typical graphs produced by this programme for a Fourier series containing 39 Fourier coefficients. Figure 6.12(a) is a graph of the number of interceptions per unit length of test array versus the angle the array makes with a reference direction. The orientation in the picture analysed is reflected in the maximum and minimum values of $N(\theta)$. The maximum and minimum values of $N(\theta)$ are 90 degrees apart. A random picture would result in a constant value for $N(\theta)$. The intercept curve bears no obvious relationship with the histogram of the number of particles versus angle (Figure 6.12(b)); the minimum value of $N(\theta)$ indicates the angle relative to the reference direction of the preferred orientation. Figure 6.12(c) shows the result of analysing the intercept data according to Equations 6.2 to 6.4; a comparison of this graph with the histogram of the picture (Figure 6.12(b)) reveals the power of this technique. The small amplitude oscillations in the calculated distribution function are a result of termination errors in fitting the intercept data to a Fourier series; the negative values plotted are physically meaningless. The termination errors could have been reduced by supplying the programme with dummy data produced from the fact that the number of intersections has a period of 180 degrees. This could not be done in the case of the computer generated pictures because of a shortage of core space in the computer.

This technique of determining the angular distribution function of the crystals in the glass matrix in a glass-ceramic was used to detect any morphological anisotropy.

6.4.4 The Detection of Morphological Anisotropy in the Real System

Glass-ceramic specimens in which preferred orientation of the crystals was expected were prepared for scanning electron microscopy (SEM). The area of the surface to be examined was approximately 7mm x 7mm and the section was generally rectangular in shape.

The coordinates of the corners of the specimen in the SEM were recorded so that a map of the surface could be drawn. Onto this map a rectangular grid was drawn so that the interceptions of the grid lines could be used as positions on the specimen. The size of the grid was such that 15 positions were mapped. SEM micrographs of the glass-ceramic microstructure were recorded at these 15 positions. This procedure of pre-determining the areas viewed at higher magnifications prevented only "presentable" micrographs being recorded and a statistical bias being introduced into the results.

The 15 micrographs formed a 5 x 3 array of representative areas of the specimen; the central column and row of this array comprising of 7 micrographs were analysed for morphological anisotropy. The remaining 8 micrographs were recorded in case the errors in the results from the 7 micrographs analysed were unacceptable and more data was required. All the surfaces sampled in this fashion were of extruded glass-ceramic specimens. The large quantity of statistical analysis which the above procedure produced was necessary to show that any preferred crystal orientation developed by the extrusion technique existed throughout the length and diameter of the extruded rod.

The area of each micrograph which was analysed for preferred crystal orientation contained approximately 300 crystals. The test grid used consisted of four parallel and equally spaced chords of a circle. This array was rotated about the centre of the circle and the number of intersections with crystal boundaries on the micrograph was counted at 12 orientations at 15 degree increments.

For each increment of angle a new test array drawn with a water soluble ink on a thin transparent polyester sheet was used. This sheet was placed on top of a positive print of the micrograph on a light box. Each intersection of a crystal boundary with the test line was drawn onto the grid. The order of the angles the test grids made with a reference line drawn on the micrograph was selected by a table of random numbers to prevent any statistical bias. In this way the crystal boundary - array line intercepts were all marked onto different transparent sheets for each angle of the test array. The number of intercepts on each line for a given angle was then counted. Each picture took approximately one hour to analyse by this technique.

The data of the number of intercepts per line of the test grid for a given angle was then analysed to find the mean number of intersections per micron and the standard deviation of the mean for each orientation of the grid. A Fourier series of order two was fitted to this data plus "dummy data" which extended the angular range from (0 deg. to 180 deg.) to (-75 deg. to 255 deg.). The "dummy data" was evaluated from the fact that the number of intersections $N(\theta)$ was periodic in 180 degrees; this additional data minimised any spurious oscillations caused by data termination errors in fitting the Fourier series. The number of intersections versus angle data was transformed to an angular distribution curve as described in section 6.3.3.

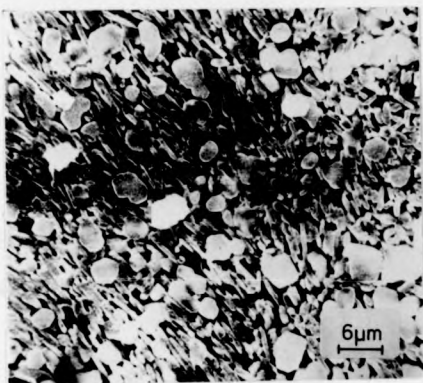


Figure 6.13(a) Part of an SEM micrograph of an extruded glass-ceramic specimen.

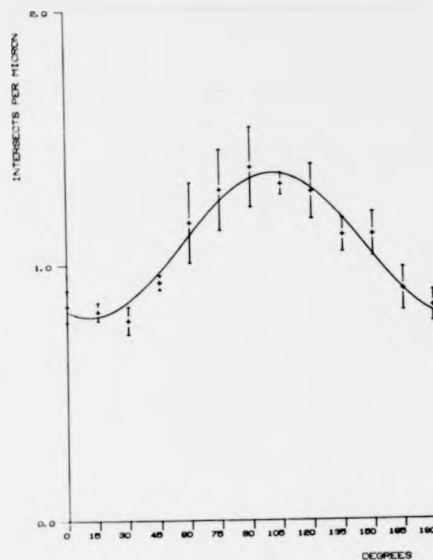


Figure 6.13(b) The number of intersections versus angle curve associated with Figure 6.13(a).

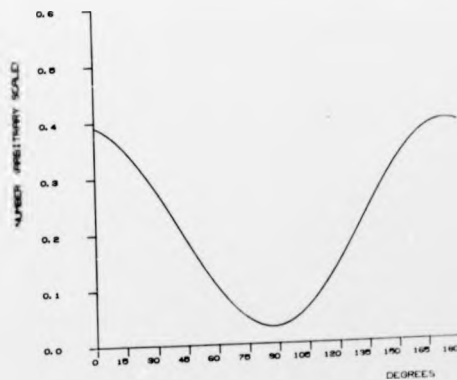


Figure 6.13(c) The angular distribution curve associated with Figure 6.13(a).

The analysis was performed by computer and the output was presented graphically. Figure 6.13 shows part of an SEM micrograph of an extruded glass-ceramic specimen and the number of intersections and angular distribution curves associated with this area.

A similar analysis was carried out on a number of micrographs in which the crystal orientation was expected to be random. In these cases the number of intersections showed no dependence on the orientation of the test grid.

6.4.5 Determination of the Volume Fraction and Inter-Crystal Spacing

The volume fraction of the crystalline phases in the glass-ceramic studied was evaluated by a point counting method (1,2). In this analysis a grid containing P points is superimposed on a plane section of the poly-phase specimen. The number of points P_α , which fall on the α phase are counted. The volume fraction of the α phase V_α , is then given by:

$$V_\alpha = \frac{P_\alpha}{P} \quad \text{Equation 6.5}$$

and the standard deviation in V_α , $\sigma(V_\alpha)$ is given by:

$$\sigma^2(V_\alpha) = \frac{1}{P} [V_\alpha(1 - V_\alpha)] \quad \text{Equation 6.6}$$

A grid consisting of 100 points was drawn onto positive prints of the SEM micrographs and the number of grid points falling on the crystalline phases in the glass-ceramic was counted. The size of the grid was such that the number of points falling on a single crystal did not exceed unity. The volume fraction and the error associated with this value were calculated from Equations 6.5 and 6.6.

The mean free distance λ , was also evaluated (15). This parameter may be considered as the mean edge-to-edge distance along a straight line between particles or second phase regions. It is defined as:

$$\lambda = \frac{1 - V_\alpha}{N_\alpha} \quad \text{Equation 6.7}$$

where V_α is the volume fraction of the α phase and N_α is the number of intersections of the α phase per unit length of test line.

Equation 6.7 is easily derived and follows from the fact that the number of particles intersected by the test line is the same as the number of matrix areas intersected. Therefore the lineal fraction occupied by the matrix is λN_α , which equals the volume fraction occupied by the matrix $(1 - V_\alpha)$. The mean free distance λ , is an extremely useful parameter, because it involves no assumptions as to the size, shape or location of the second phase.

Another particle parameter which possesses great value and generality is the mean intercept length \bar{L}_3 . This parameter may be thought of as a measure of a grain or particle "diameter". For a non-space-filling system of particles:

$$\bar{L}_3 = \frac{V_\alpha}{N_\alpha}$$

Equation 6.8

where V_α and N_α are defined above and \bar{L}_3 may be considered as an average lineal measure of the "size" or "diameter" of a particle in the α phase. A unique value of \bar{L}_3 is obtained for any granular or particulate microstructure regardless of the degree of convexity or concavity. No assumptions as to the size or reference to the sphericity of the particle are required (1,2). The mean free distance λ , and the mean particle "diameter" \bar{L}_3 , were derived using Equations 6.7 and 6.8 from the values of V_α and N_α measured on glass-ceramic surfaces.

References

1. R. T. DeHoff and F. N. Rhines, Quantitative Microscopy (McGraw-Hill Book Co. Inc. 1968)
2. E. E. Underwood, Quantitative Stereology (Addison-Wesley Publishing Co. Inc. 1970)
3. M. Born and E. Wolf, Principles of Optics (Pergamon Press, London 1965)
4. H. Lipson, Optical Transforms (Academic Press, London 1964)
5. P. J. Woods, Phil. Mag. 28 193 (1973)
6. A. Klug and D. J. De Rosier, Nature 212 29 (1966)
7. N. M. Tovey, Proc. 4th Ann. Symp. on SEM (I.I.T. Research Inst. Chicago 1971)
8. F. T. S. Yu and R. J. Bieringer, Applied Optics 10 2269 (1971)
9. R. J. Bieringer, *ibid*, 11, 2714 (1972)
10. R. J. Bieringer, *ibid*, 12, 249 (1973)
11. R. J. Bieringer and R. C. Hedler, *ibid*, 12, 2558 (1973)
12. S. A. Saltykov, Stereometric Metallography (2nd edition: Metallurgizdat, Moscow 1958)
13. J. E. Hilliard, Trans. A.I.M.E. 224 1201 (1962)
14. R. M. Smith and D. I. H. Atkinson, unpublished work.
15. R. L. Fullman, Trans. A.I.M.E. 197 447 (1953)

CHAPTER 7: THE MICROSTRUCTURE AND PHYSICAL PROPERTIES
OF THE GLASS-CERAMICS STUDIED

7.1 Introduction

In this chapter the microstructure and physical properties of the glass-ceramic compositions studied are described. These results are for the control specimens with a randomly oriented microstructure which were used as a comparison with the extruded specimens of the same composition. The variation with heat-treatment of the microstructure, density, coefficient of thermal expansion and electrical and mechanical properties are presented. The results of the physical property measurements of the glass-ceramic are related to the microstructure. The experimental techniques used to measure these properties are described in Chapter 3.

7.2 The Glass Compositions Studied

The microstructure of the glass-ceramics produced by the devitrification of two glass compositions were studied by scanning electron microscopy; Table 7.1 gives the two glass compositions in mol.%. The compositions are based on the $\text{Li}_2\text{O} - \text{SiO}_2$ glass system; in glass A the ratio of SiO_2 to Li_2O is the same as is present in lithium disilicate crystals ($\text{Li}_2\text{O} \cdot 2\text{SiO}_2$). This glass system was chosen as a 'model' glass-ceramic system because despite its simplicity it shows many of the features encountered with more complex glass-ceramics. These include glass-in-glass phase separation, the formation of metastable crystal phases and the ability to form a fine-grained high-strength glass-ceramic when a suitable nucleating agent is included in the glass composition.

	SiO ₂	Li ₂ O	K ₂ O	Al ₂ O ₃	P ₂ O ₅	B ₂ O ₃
Glass A	610	305	15	10	10	50
Glass B	675	240	15	10	10	50

Table 7.1 Glass Compositions in mol. %.

	Exotherm °C	Endotherm °C	T _g °C
Glass A	610 700(?)	~880	460
Glass B	660	~950	450

Table 7.2 Temperatures of exothermic and endothermic transitions of the glasses in Table 7.1.

Chapter 2 contains a review of the investigations which have been made of the $\text{Li}_2\text{O}-\text{SiO}_2$ glass system and the devitrification products when a suitable nucleating agent is present.

In the glasses studied in this work phosphorus pentoxide was added as a nucleation catalyst; this constituent is known to promote the formation of a fine-grained microstructure in glass-ceramics and is particularly effective in compositions based on the lithia silica system (1,2). It has also been shown that P_2O_5 influences the morphology of phase separation in the $\text{Li}_2\text{O}-\text{SiO}_2$ system (1).

In the compositions studied potassium oxide introduces non-bridging oxygen ions into the glass network and prevents the formation of a continuous system. This results in changes in the properties of the glass including a reduction in the viscosity (3); K_2O also reduces cracking in the glass-ceramic by allowing stress relief by viscous deformation, this is probably because it lowers the viscosity of the residual glassy phase during crystallisation. Aluminium oxide helps to prevent two phase separation occurring in a melt or glass which contains phosphorus pentoxide; boric oxide has the property of decreasing the time needed to achieve satisfactory melting and refining and also lowers the viscosity of the melt (3).

The glass-ceramics produced by the devitrification of glass compositions, very similar to those studied in this work, have been studied by Miles and McMillan (4). The major crystalline phase in these glass-ceramics was lithium disilicate which had a needle shaped morphology. In this present investigation a glass-ceramic in which the aspect ratio of the major crystalline phase was non-unity was required for the hot extrusion experiments.

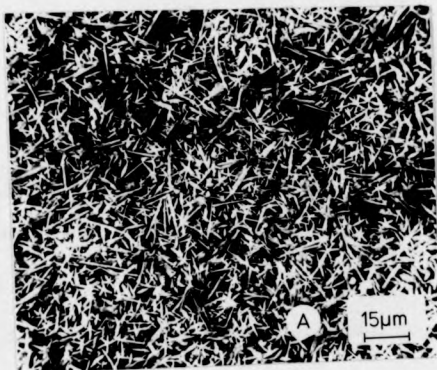


Figure 7.1(a) Glass A; 1 hour, 650°C.



Figure 7.1(b) Glass A; 1 hour 650°C.



Figure 7.1(c) Glass A; 1 hour, 650°C: surface crystallisation.

7.3 Differential Thermal Analysis Results

The temperatures at which exothermic or endothermic phase transitions were detected by the differential thermal analysis of glass A and B are shown in Table 7.2; these values are extrapolated onset transition temperatures (see Chapter 3 for details).

The DTA thermogram of glass A is shown in Figure 3.3; from this graph it can be seen that a second exothermic peak possibly occurs at approximately 700°C. It was found that the two exothermic peaks in glass A could not be clearly resolved with the DTA apparatus.

The results of the differential thermal analysis of glasses A and B were used as a guide to the range of temperature over which the heat treatment experiments were performed.

7.4 Glass-Ceramic Microstructures

7.4.1 The Microstructure of the Glass-Ceramic Devitrified from Glass A

The effect of heat treating samples of glass A at temperatures between 650°C and 950°C was investigated; specimens of the glass were placed in a furnace at the heat-treatment temperature and rapidly cooled to room temperature after periods of one and two hours. The microstructures of the glass-ceramics produced were examined by the scanning electron microscopy of surfaces of the samples etched for 30 secs. in a 3% HF solution.

Figures 7.1-7.2 are a series of representative micrographs of the glass-ceramic microstructure produced by heat treating samples of glass A for a period of one hour at temperatures between 650°C and 900°C.

Devitrification at 650°C (Figure 7.1(a)) produce a single crystalline phase which was identified as lithium disilicate by X-ray powder diffraction. The majority of the crystals are of a needle shape, approximately 10 μm long and 2 μm in width; a second crystal morphology can be seen in which the crystals are "star" shaped with three, four or six "arms" visible in the

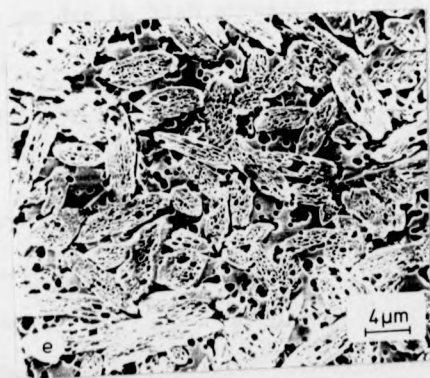
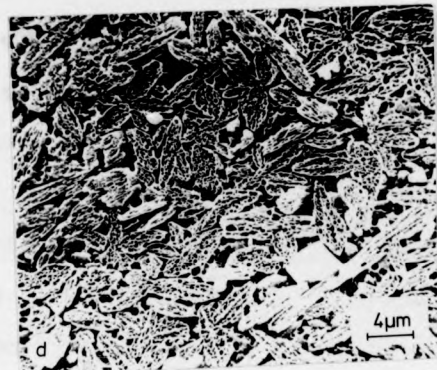
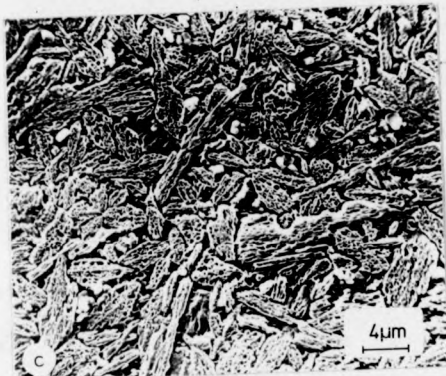
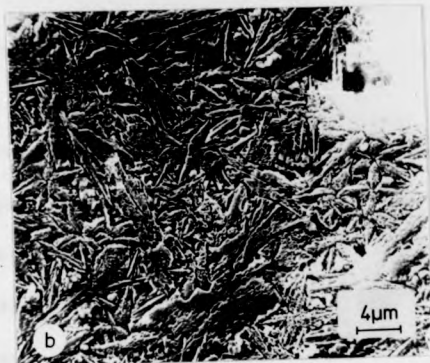


Figure 7.2 The glass-ceramic produced by devitrifying glass A for 1 hour at the following temperatures:

- | | |
|------------|------------|
| (a) 700°C. | (d) 850°C. |
| (b) 750°C. | (e) 900°C. |
| (c) 800°C. | |

micrograph. Figure 7.1(b) shows one of these crystals with three visible "arms"; a volume of material between the crystals has been removed by the etching process to reveal the intersection of the "arms". In the bulk material the crystals are randomly oriented whereas at the surface of the glass-ceramic the crystalline phase is aligned (Figure 7.1(c)). The crystals have grown with the major axis perpendicular to the surface of the specimen to produce a layer of glass-ceramic material one crystal length thick with an aligned microstructure (5). The mechanism of surface crystallisation was not investigated in the present work.

The lithium disilicate crystals in this specimen show no preferential etching on the surface; the crystals have been evenly etched to produce a smooth exterior.

Figure 7.2(a) is a micrograph of a specimen of the glass heat-treated at 700°C for one hour. The crystalline phase of lithium disilicate is almost entirely of a "star" shaped morphology. The boundary between the crystal and glass phases is very heavily etched and this is thought to be due to high stresses in this area. High stresses will be produced in these regions by a mismatch of the thermal expansion coefficients of the two phases.

Heat-treating the glass at 750°C produces a glass-ceramic with two crystalline phases. The microstructure of this sample (Figure 7.2(b)) consists of a major phase of needle-shaped lithium disilicate crystals and a minor phase which was believed to be tridymite (A in Figure 7.2(b)). The appearance of this phase is consistent with the occurrence of the second exotherm in the differential thermal analysis of the glass composition (Figure 3.3). The surface of the lithium disilicate crystals has been preferentially removed by the etching solution.

The microstructures of the glass-ceramics which result from heat-

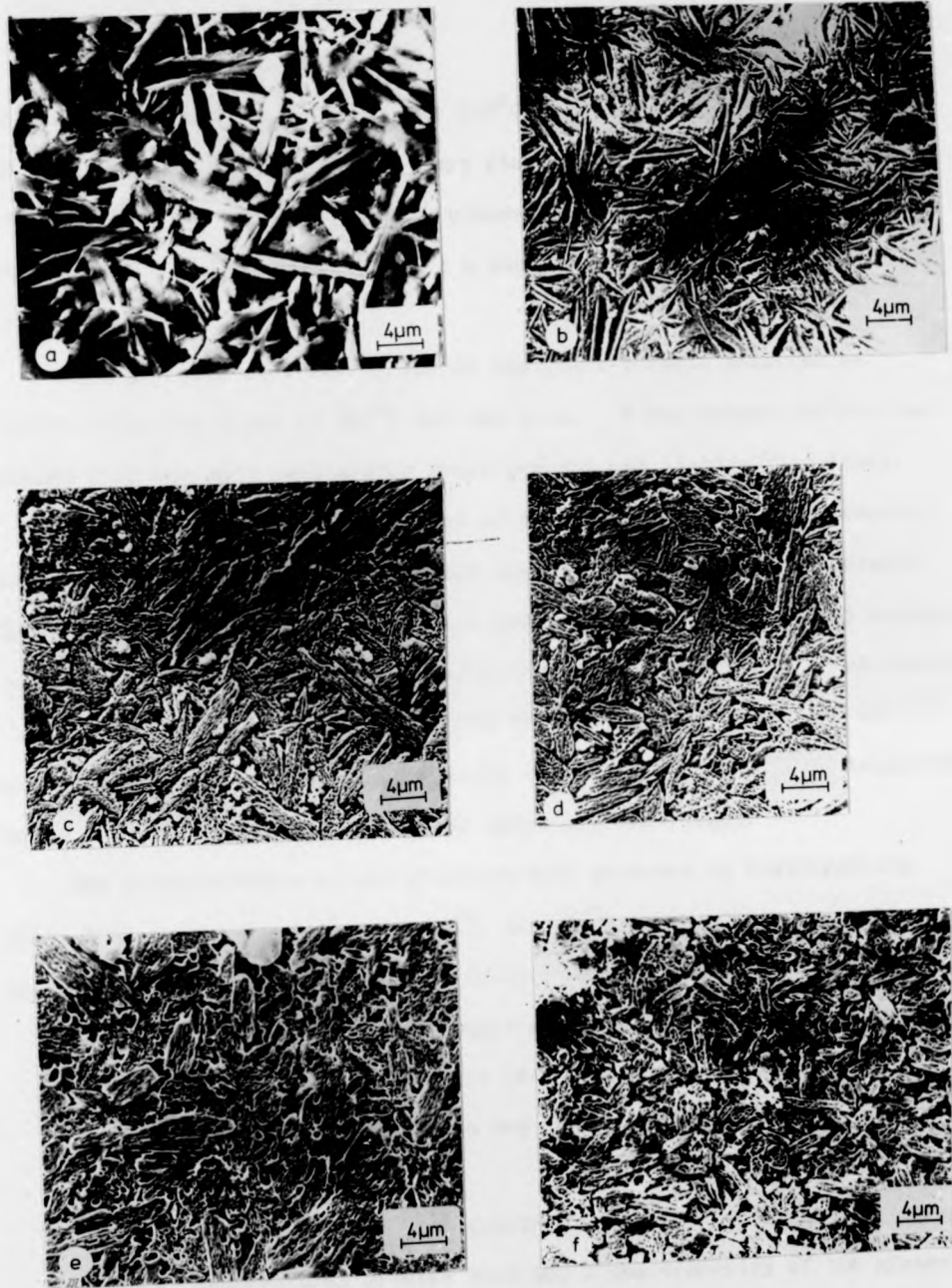


Figure 7.3 The glass-ceramic produced by devitrifying glass A for two hours at the following temperatures:

- | | |
|------------|------------|
| (a) 650°C. | (d) 800°C. |
| (b) 700°C. | (e) 850°C. |
| (c) 750°C. | (f) 900°C. |

treating a specimen of the glass at 800°C (Figure 7.2(c)) and 850°C (Figure 7.2(d)) for one hour are very similar to the microstructure of the 750°C heat treatment. The glass-ceramics contain a needle shaped lithium disilicate phase and a minor phase of tridymite, together with a residual glassy phase.

Figure 7.2(e) is a micrograph of the glass-ceramic produced by devitrifying the glass at 900°C for one hour. X-ray powder diffraction showed that the only crystalline phase present was lithium disilicate.

Figures 7.3 (a - f) are a series of micrographs of the glass-ceramic produced by heat-treating glass A for two hours at temperatures between 650°C and 900°C. The crystal phases and microstructures are very similar to those produced by a one hour heat-treatment of the glass. Heat-treating the glass at temperatures greater than 900°C produced thin sheets of glass-ceramic material. The viscosity of the material at these temperatures was low and the glass-ceramic flowed under its own weight.

The microstructure of the glass-ceramic produced by heat-treating glass A at temperatures between 650°C and 950°C for periods of one hour and two hours can be summarised as follows:

- (i) in all cases the glass-ceramic contained a major crystalline phase of lithium disilicate; in the temperature range 750°C - 850°C a minor crystalline phase which was believed to be tridymite is also present.
- (ii) the lithium disilicate crystals have a needle-shaped morphology.
- (iii) at temperatures greater than 900°C the viscosity of the glass-ceramic is such that the material flows under its own weight.

7.4.2 The Microstructure of the Glass-Ceramic Devitrified from Glass B

Figures 7.4 (a - g) are scanning electron micrographs of the glass-ceramic microstructure produced by heat-treating samples of glass B at temperatures between 650°C and 950°C for a period of one hour.

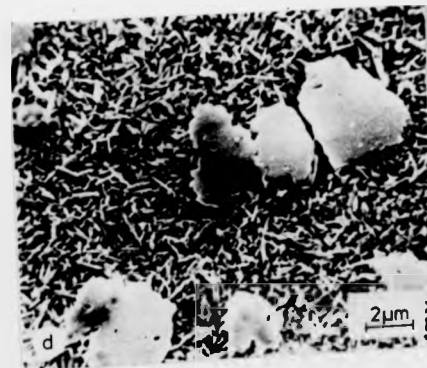
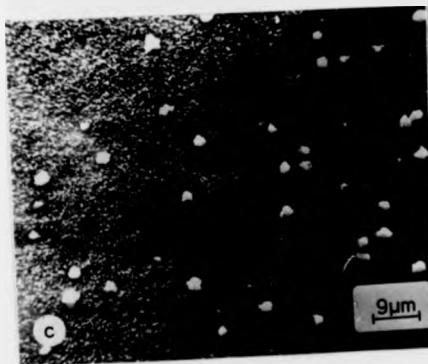
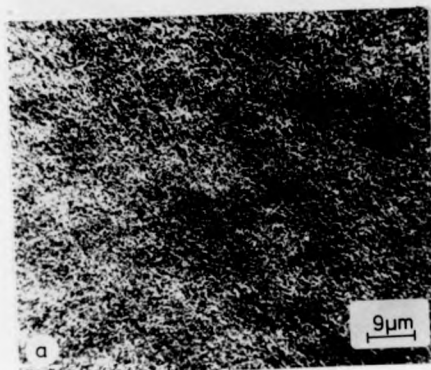


Figure 7.4 The glass-ceramic produced by devitrifying glass B for one hour at the following temperatures:

- | | |
|------------|------------|
| (a) 650°C. | (c) 750°C. |
| (b) 700°C. | (d) 800°C. |

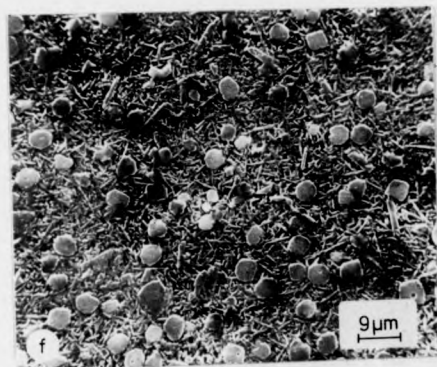
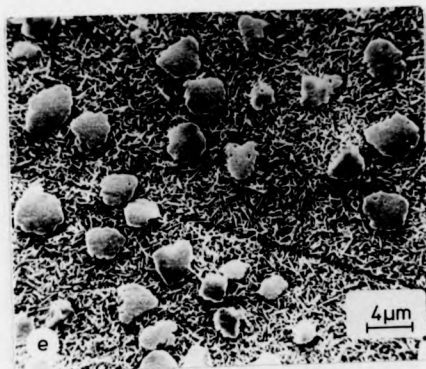


Figure 7.4 The glass-ceramic produced by devitrifying glass B for one hour at the following temperatures:

(e) 850°C. (g) 950°C.

(f) 900°C.

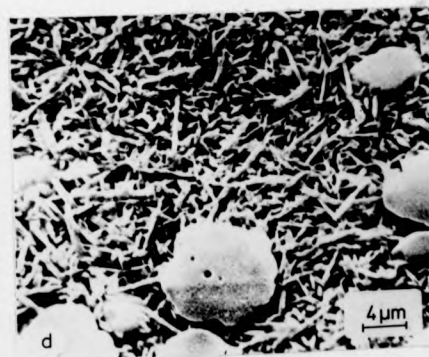
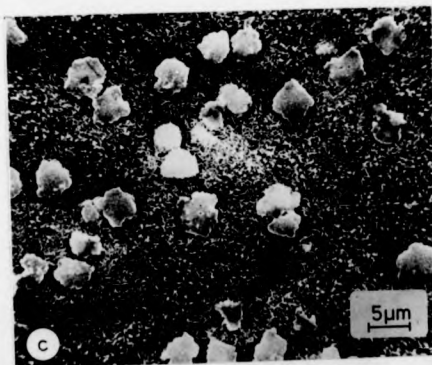
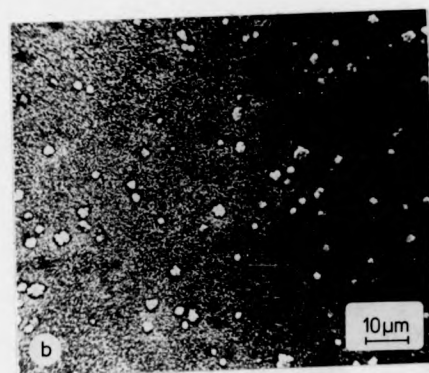
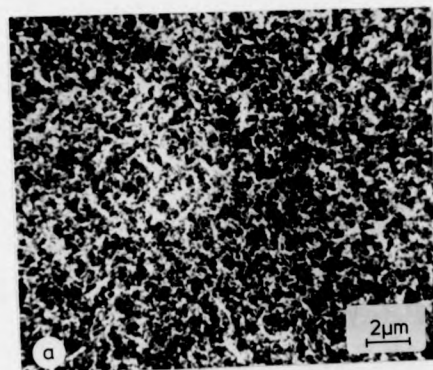


Figure 7.5 The glass-ceramic produced by devitrifying glass B for two hours at the following temperatures:

- | | |
|------------|------------|
| (a) 650°C. | (c) 750°C. |
| (b) 700°C. | (d) 800°C. |

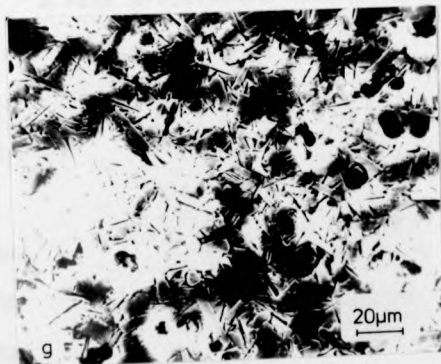
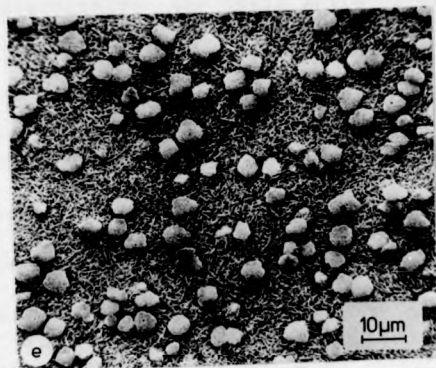


Figure 7.5 The glass-ceramic produced by devitrifying glass B for two hours at the following temperatures:

- (e) 850°C. (g) 950°C.
(f) 900°C.

The microstructure of a specimen heat-treated at 650°C is shown in Figure 7.4(a). The glass-ceramic had a milky white appearance and contained crystalline phases of lithium disilicate and silica; in the electron micrograph no crystalline phases are resolved. Figures 7.4(b) and (c) show the result of heating the glass at 700°C and 750°C respectively; the small white "blobs" on the micrographs are believed to be tridymite crystals.

Heat-treatment of the glass at 800°C (Figure 7.4(d)) and 850°C (Figure 7.4(e)) results in the crystallisation of silica and lithium disilicate in each specimen. The latter phase comprises the fine needle shaped crystals ($\sim 1 \mu\text{m}$ long) in the micrographs; this was confirmed by selected area diffraction using transmission electron microscopy. Figure 7.4(f) shows the glass-ceramic produced by a heat-treatment at 900°C for 1 hour; this microstructure is very similar to that shown in Figure 7.4(e) (1 hour 850°C).

A high temperature form of silica is the only crystalline phase present when the glass is heat-treated for 1 hour at 950°C (Figure 7.4(g)); this glass-ceramic contains a small volume fraction of glass and a crystalline phase of closely packed rectangular blocks.

Figures 7.5 (a - g) show the microstructure of the glass-ceramic when glass B is heat-treated for two hours at temperatures between 650°C and 950°C . The structure of the material is very similar to that produced when the glass is heat-treated for one hour. The two hour heat treatment at 900°C (Figure 7.5(f)) contains lithium disilicate and a silica crystal phase; the latter phase having a rectangular morphology in comparison with a round morphology in the one hour heat treatment (Figure 7.4(f)).

The microstructure of the glass-ceramic devitrified from glass B at temperatures between 650°C and 950°C can be summarised as follows:

Observed Å	Tridymite Å	α Cristobalite Å	β Cristobalite Å	α Quartz Å	β Quartz Å	Keatite Å
4.29	4.27		4.15	4.26	4.34	4.50
4.06	4.08	4.05				3.72
3.87	3.83			3.43	3.40	3.42
3.38	3.37					3.11
3.19	3.16	3.14	2.92			2.52
2.49	2.49	2.49	2.53	2.46	2.50	

Table 7.3 The d-spacings of a specimen of glass B heat-treated for one hour at 950°C.

(i) heat-treatment at temperatures between 650°C and 900°C results in a glass-ceramic with two crystalline phases of lithium disilicate and a high temperature form of silica, together with a residual glass phase.

(ii) a 950°C heat treatment produces one crystalline phase of silica.

(iii) the lithium disilicate crystals have a needle shaped morphology when glass B is crystallised at temperatures between 800°C and 900°C.

7.4.3 Comments on the Glass-Ceramic Microstructures

In the preceding sections the crystalline phases were identified by X-ray diffraction of powdered samples and transmission electron diffraction of fragmentation specimens. The electron diffraction patterns were analysed with the aid of a computer programme written by P.S. Bell (6). The measured d-spacings of a specimen of glass B heat-treated for one hour at 950°C are shown in Table 7.3; in this table the d-spacings of tridymite, keatite and α and β cristobalite and quartz are also included. From this data it can be concluded that the crystal phase in this specimen is tridymite. Figure 7.4(g), which is a micrograph of this specimen, indicates that the volume fraction of the glass phase is very low; difficulties arise from these results in deciding where in this glass-ceramic the high percentage of lithia in the original glass B composition is situated. In the following this crystalline phase is referred to as tridymite.

The crystallisation products detected in this work cannot be easily related to the binary lithia-silica phase diagram (see Chapter 2).

In the following sections glass-ceramic A is understood to mean "a glass-ceramic devitrified from glass A".

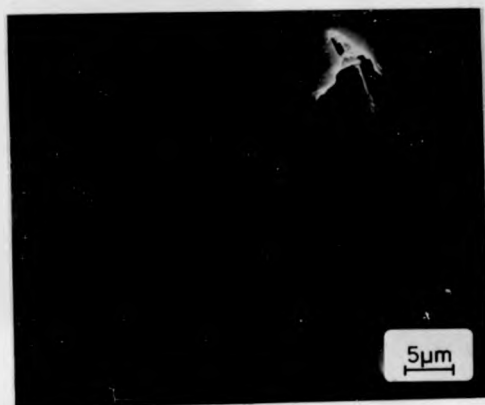


Figure 7.5(A) The polished surface of a specimen of glass-ceramic A heat-treated for two hours at 800°C; the secondary electron mode.

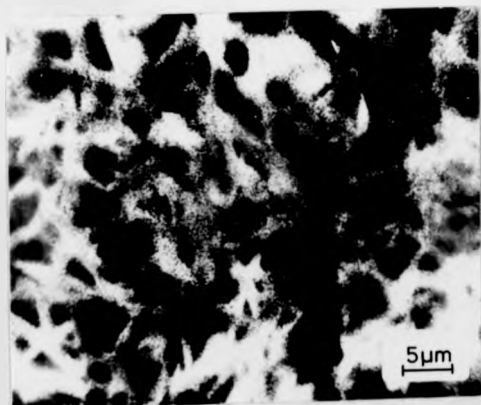


Figure 7.5(B) The area in Figure 7.5(A) observed in the cathodoluminescence mode.

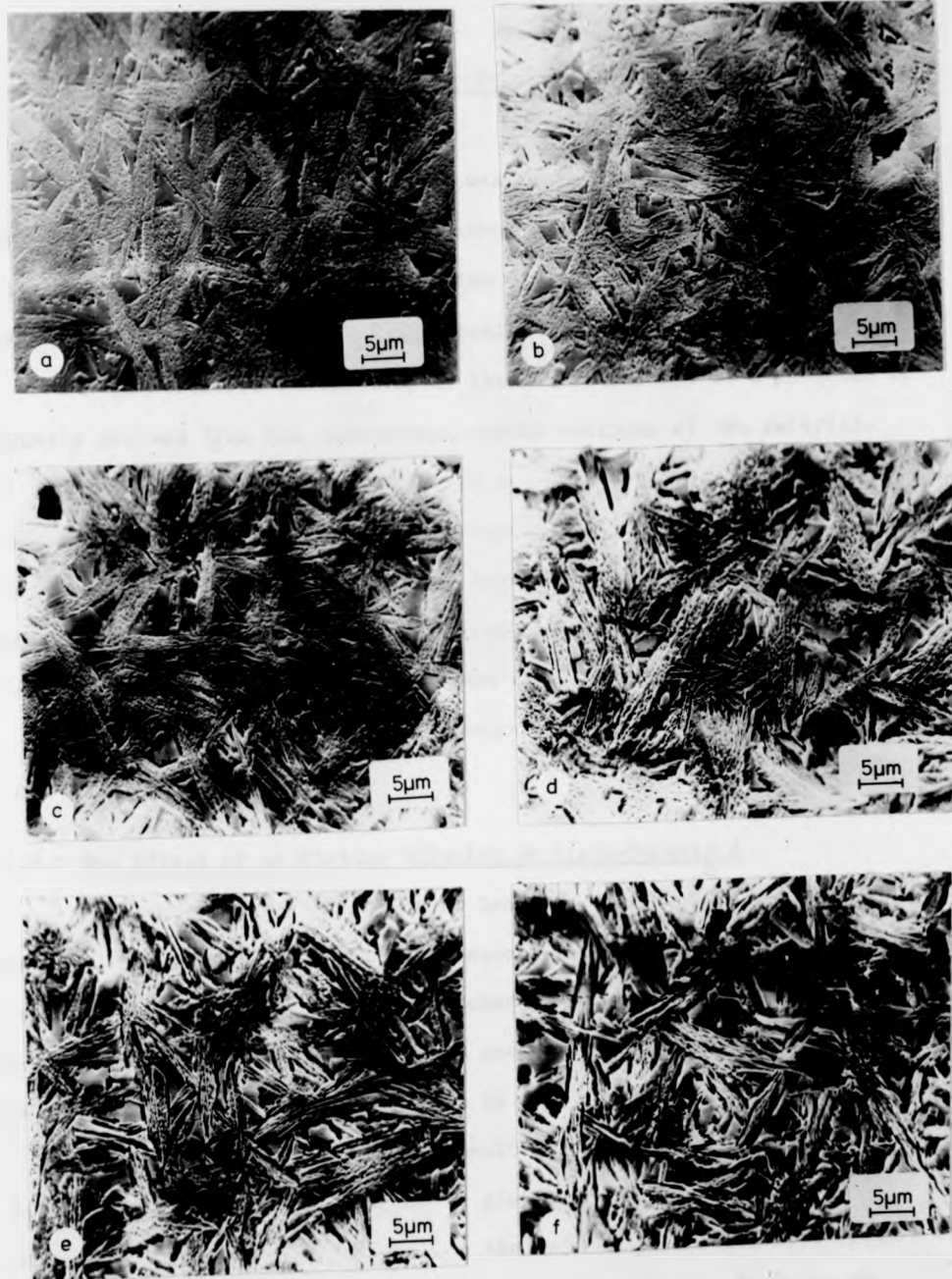


Figure 7.6 The topographical contrast produced by etching a specimen of glass-ceramic A for various times:

- | | |
|-----------------|-----------------|
| (a) 10 seconds. | (d) 40 seconds. |
| (b) 20 seconds. | (e) 50 seconds. |
| (c) 30 seconds. | (f) 60 seconds. |

7.5 The Statistical Analysis of Glass-Ceramic A

7.5.1 Introduction

The major part of this research was performed using glass-ceramics derived from glass A; glass B was extruded to produce a glass-ceramic with an aligned microstructure (Chapter 8) but the properties of this material compared with the control specimens were not investigated.

The quantitative description of the microstructure of a material is usually derived from two dimensional random sections of the material. In the present work the microstructure of the glass-ceramics investigated was examined by scanning electron microscopy; to produce a contrast between the glass matrix and all the crystalline phases present, the surface of the material had to be etched. The microstructure can then be examined by a topographical contrast mechanism.

The effect of different etch times was investigated for glass-ceramics crystallised from glass A.

7.5.2 The Effect of an Etching Solution on Glass-Ceramic A

Seven specimens of glass A were heat-treated for two hours at 800°C and a surface of each glass-ceramic specimen was polished to a 1 μm diamond paste finish. Each specimen was etched in a 3% solution of hydrofluoric acid for a period of time between 10 seconds and 1 minute; the etched surface was prepared for examination by scanning electron microscopy.

Figures 7.5 and 7.6 show the resulting microstructure for different times in the etching solution. The glass-ceramic which has not been etched shows very little contrast in the secondary electron mode (Figure 7.5(A)) and a strong contrast between the lithium disilicate crystals and the glass matrix in the cathodoluminescence mode (Figure 7.5(B)). The effect of a ten second etch can be seen in Figure 7.6(a); Figures 7.6 (b - f) show the topographical contrast produced by increasing the etching time

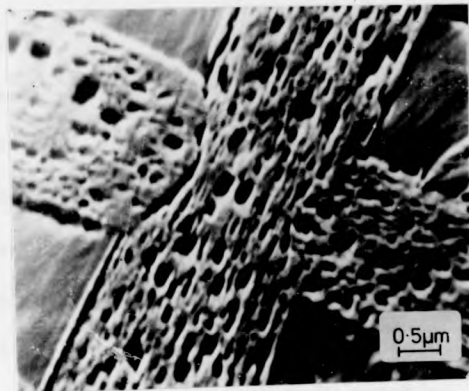


Figure 7.7 The "spotty" surface of etched lithium disilicate crystals.

by increments of ten seconds (Figure 7.6(f) is a 60 second etch). As the etching time is increased the boundary between the crystals and the glass is progressively deepened (compare Figure 7.6(b) with 7.6(f)). The topographical contrast is a consequence of the fact that the glass phase is etched at a faster rate than the crystalline phases in the glass-ceramic.

The lithium disilicate crystals are also etched by the solution to produce a rough surface; Bell (7) has proposed that as the disilicate crystals cool, precipitation of metal oxide particles occurs from the solid solution. These precipitated particles are etched faster than the crystal matrix to produce the "spotty" crystal surface (Figure 7.7).

The micrographs contain approximately the same number density of crystals for increasing etch times and the topographical contrast does not appreciably change for times less than 30 seconds. However, interpretation of the microstructure becomes increasingly difficult for etch times greater than 40 seconds. Similar results were obtained for glass-ceramics devitrified from glass A at temperatures of 700°C and 900°C.

In the present work all scanning electron microscope glass-ceramic specimens were etched for thirty seconds in a 3% hydrofluoric acid solution to produce a topographical contrast. The results of the statistical analysis of the micrographs of these etched surfaces were assumed to be equivalent to results obtained from polished two-dimensional surfaces.

7.5.3 The Volume Fraction and Mean Particle Spacing of Glass-Ceramic A

The variation in the volume fraction of the crystalline phases as a function of the heat treatment of glass A was determined (Chapter 6 contains details of the analysis technique). Figures 7.8(a) and 7.8(b) show this variation for one hour and two hour heat-treatments respectively.

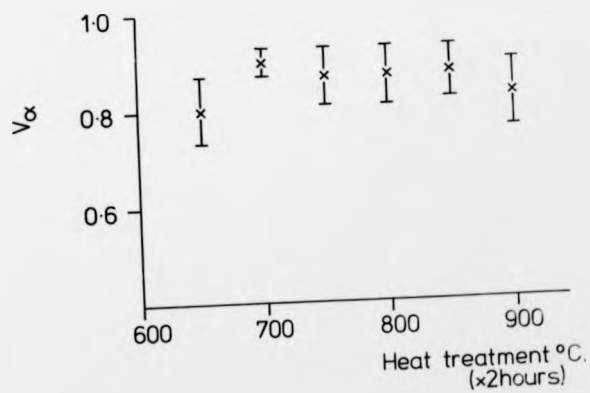
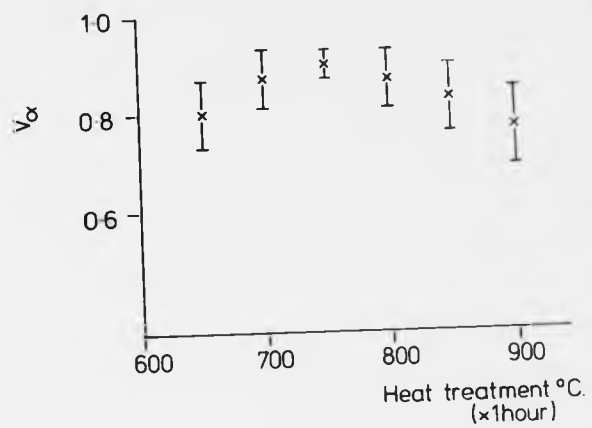


Figure 7.8 The variation in the volume fraction of the crystalline phase of glass-ceramic A as a function of heat-treatment; (a) one hour and (b) two hour heat-treatment.

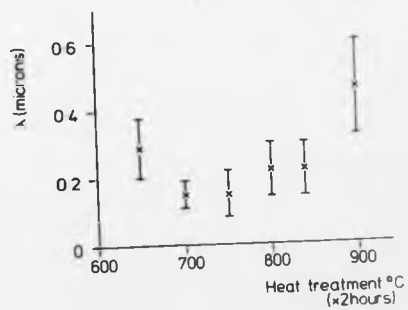
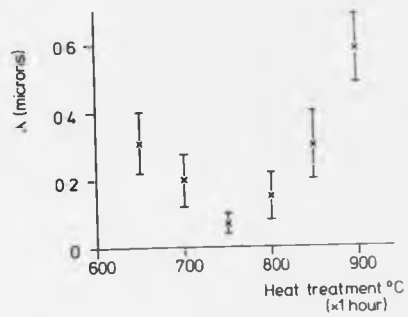


Figure 7.9 The variation in the mean crystal spacing λ , with the temperature of heat-treatment of glass A for (a) one hour and (b) two hours.

For the one hour heat-treatment the volume fraction of the crystalline phases shows a maximum of 90% at a heat-treatment temperature of approximately 750°C. This temperature corresponds to that at which the second crystalline phase of tridymite was first detected. The volume fraction of the crystalline phases for a two hour heat-treatment of glass A is approximately constant at 85%.

The mean crystal - crystal spacing for glass-ceramic A was determined by the method described in Chapter 6. Figures 7.9(a) and 7.9(b) show the variation in the mean crystal spacing λ , with the temperature of the heat-treatment for times of one hour and two hours respectively. Both heat-treatment times show a minimum in the value of λ at approximately 750°C; this corresponds with the first appearance of the second crystalline phase in the glass-ceramic.

7.6 Density of Glass-Ceramic A

The density ρ , of the glass-ceramic devitrified from glass A was independent of the heat-treatment temperature and time and had a value of:

$$\rho = 2.417 \pm 0.003 \text{ gms/cc.}$$

This value is the average of 36 measurements; three measurements of each sample of 12 different heat-treatments.

The density of the original glass ρ_{GLASS} was:

$$\rho_{\text{GLASS}} = 2.363 \pm 0.005 \text{ gms/cc (30 measurements)}$$

A volume change of approximately 3% (1% linear change) has occurred with the crystallisation of the glass. Scanning electron microscopy of polished surfaces of the glass-ceramics showed no voids present after devitrification.

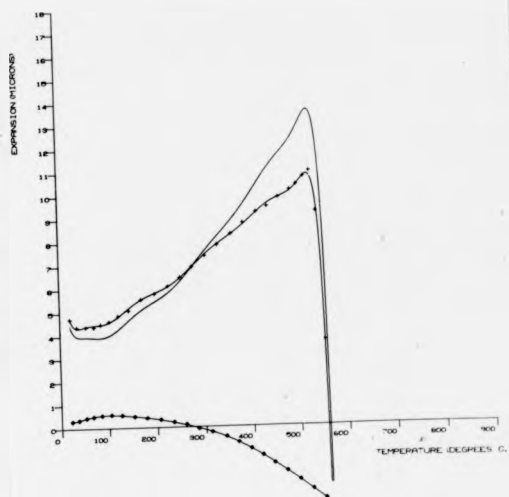


Figure 7.10 The thermal expansion of a specimen of glass A measured as a function of temperature.

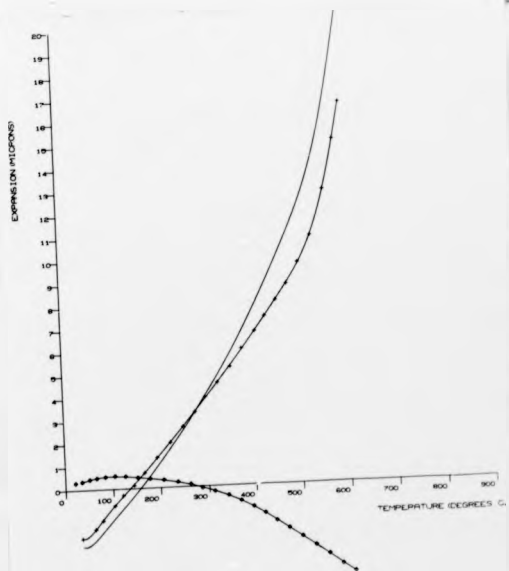


Figure 7.11 A typical expansion curve of a specimen of glass-ceramic A.

7.7 The Coefficient of Thermal Expansion

7.7.1 Results

The thermal expansion of glass A was measured as a function of temperature. Figure 7.10 shows the expansion of a 0.275 cm thick specimen and the expansion curve corrected for the characteristic expansion of the dilatometer. X-ray powder analysis of the specimen after the expansion experiment showed that no crystallisation had taken place.

The coefficient of thermal expansion of glass A α_{GLASS} , calculated from Figure 7.10 is:

$$\alpha_{\text{GLASS}} = 12.72 \cdot 10^{-6} / \text{deg. C.}$$

for the temperature range (100 - 500) $^{\circ}\text{C}$.

The specimen of glass A shows a dilatometric softening temperature M_g , above which the glass softens very rapidly:

$$M_g \approx 500^{\circ}\text{C}.$$

The coefficient of thermal expansion was measured for specimens of glass-ceramic A heat-treated for two hours at temperatures between 600 $^{\circ}\text{C}$ and 900 $^{\circ}\text{C}$. Figure 7.11 shows a typical expansion curve of a specimen of glass-ceramic A; from this graph it can be seen that the expansion of the specimen is composed of two linear regions of differing gradients. The expansion of the specimen can be described by the coefficients of thermal expansion α_1 and α_2 , measured from these linear regions. The temperature range over which α_1 and α_2 were measured is given approximately by:

$$\alpha_1 - (150 - 350)^{\circ}\text{C}$$

$$\alpha_2 - (500 - 650)^{\circ}\text{C}$$

The point of intersection of tangents to the two linear regions of the expansion curve defines an inflexion temperature $T_{\text{inflex}}^{\circ}\text{C}$.

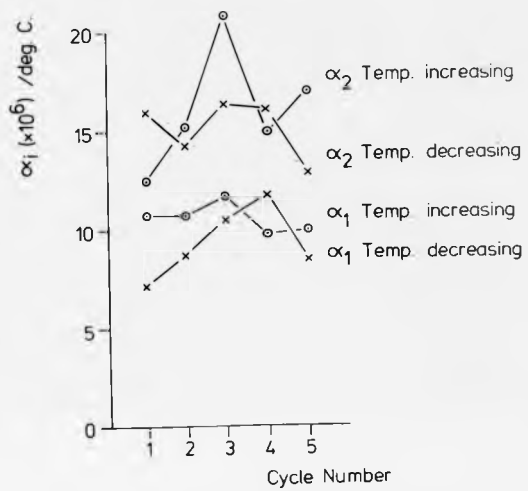


Figure 7.12 The variation of the thermal expansion coefficients α_1 , with cycling of the dilatometer.

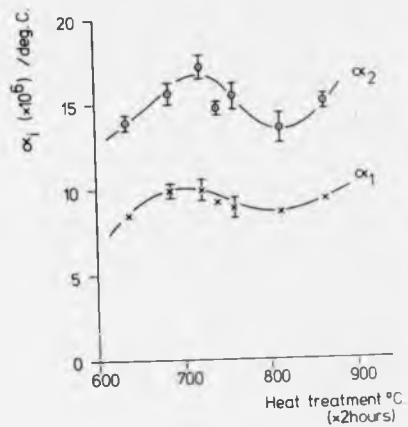


Figure 7.13(a) The variation of the thermal expansion coefficients α_i with the temperature of a two hour heat-treatment for glass-ceramic A.

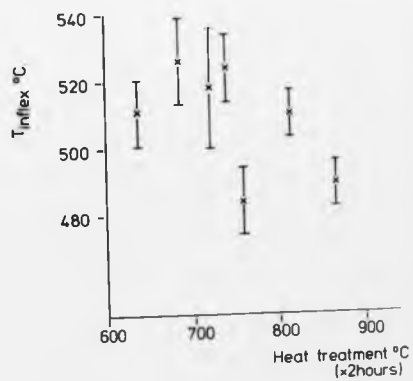


Figure 7.13(b) The variation of the inflexion temperature T_{inflex} with different temperatures of a two hour heat-treatment of glass-ceramic A.

For each dilatometer specimen the values of α_1 , α_2 and T_{inflex} were measured ten times by repeating the temperature cycle of the dilatometer; the α_i values were measured from expansion curves corrected for the characteristic expansion of the dilatometer. A systematic variation in the value of α_i with cycling was not observed for any of the specimens (Figure 7.12). The scatter in the values of α_i is caused by random errors; a systematic variation of α_i with cycling of the dilatometer would indicate that the glass-ceramic specimen was undergoing further devitrification. The maximum temperature of the dilatometer cycle was always less than the temperature at which the glass-ceramic specimen was originally heat-treated.

Figure 7.13(a) shows the variation of α_i with the temperature of a two hour heat-treatment for glass-ceramic A. The two expansion coefficients α_1 and α_2 show the same variation with heat-treatment temperature; both have a maximum value at a temperature of approximately 720°C:

$$\alpha_1(\text{max}) = 10.10^{-6}/\text{deg.C.}$$

$$\alpha_2(\text{max}) = 16.10^{-6}/\text{deg.C.}$$

and a minimum value at approximately 820°C of:

$$\alpha_1(\text{min}) = 9.5.10^{-6}/\text{deg.C.}$$

$$\alpha_2(\text{min}) = 13.7.10^{-6}/\text{deg.C.}$$

The variation of the inflexion temperature T_{inflex} , with different temperatures of a two hour heat-treatment of glass-ceramic A is shown in Figure 7.13(b); this curve shows a maximum value of T_{inflex} of:

$$T_{\text{inflex}}(\text{max}) \approx 520^\circ\text{C.}$$

at a heat treatment temperature of 700°C.

7.7.2 Discussion

There is no obvious correlation between the variation of α_i with the

Temp. range deg. C.	$\alpha_1 (\times 10^6)$ /deg. C.
20-100	4.85
- 200	7.86
- 300	9.07
- 400	9.86
- 500	10.16
- 600	11.0
- 700	11.5
- 800	12.3

Table 7.4 The coefficient of thermal expansion α_1 , for a glass-ceramic crystallised from a glass of the $\text{Li}_2\text{O} \cdot 2\text{SiO}_2$ composition (after Phillips and Partridge (8)).

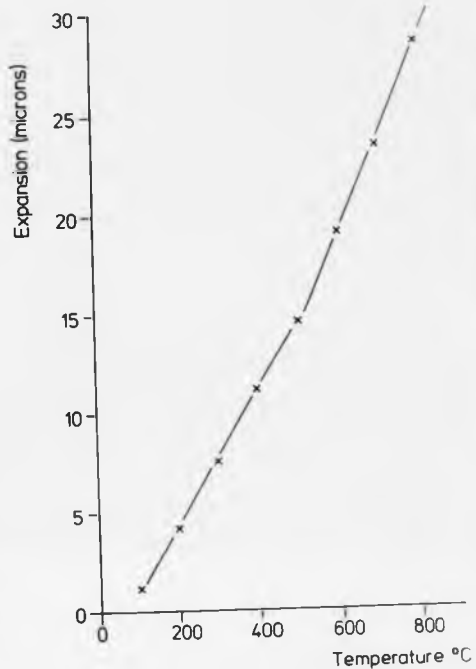


Figure 7.14 The expansion-temperature curve of a 0.3 cm specimen calculated from the data of Table 7.4.

heat-treatment temperature and the volume fraction and mean crystal spacing of the glass-ceramic (Figures 7.8b and 7.9b). The inflexion temperature has a maximum value at approximately the same heat treatment temperature as the minimum in the value of the mean crystal-crystal spacing; no physical explanation can be found for this correspondence.

Phillips and Partridge (8) have measured the coefficient of thermal expansion α_L , for a glass-ceramic crystallised from a glass of the lithium disilicate composition ($\text{Li}_2\text{O} \cdot 2\text{SiO}_2$). The values of α_L measured over various temperature ranges are shown in Table 7.4; these values show a gradual increase as the range of temperature over which they are measured is increased. If the thermal expansion of a 0.3 cm specimen of the Phillips and Partridge composition (loc.cit.) is calculated from the data in Table 7.4, then the expansion-temperature curve of the sample is shown in Figure 7.14. This graph shows the same characteristics of two linear regions that have been observed in the present work (cf. Figure 7.11). Values of α_1 , α_2 and T_{inflex} measured from Figure 7.14 are:

$$\alpha_1 = 9.86 \cdot 10^{-6} / \text{deg.C.} \quad (100 - 500)^\circ\text{C}$$

$$\alpha_2 = 15.67 \cdot 10^{-6} / \text{deg.C.} \quad (500 - 800)^\circ\text{C}$$

$$T_{\text{inflex}} \approx 520^\circ\text{C.}$$

These values of the thermal expansion coefficients and the inflexion temperature are similar to those obtained in this work.

The thermal expansion of tridymite shows an inflexion at approximately 140°C (9) and is linear with temperature above this value.

The thermal behaviour of a composite material has been considered by Kingery (10), who gives the following expression for the expansion coefficient α_c of a composite material:

$$\alpha = \frac{\sum_i \frac{\alpha_i K_i F_i}{\rho_i}}{\sum_i \frac{K_i F_i}{\rho_i}}$$

Equation 7.1

where α_i = expansion coefficient of the i^{th} phase
 K_i = bulk modulus
 ρ_i = density
 F_i = weight fraction

If the Poisson's ratio of the components is similar, then the elastic moduli may be used in place of the bulk moduli K_i . This expression for α assumes an ideal material in which no cracks develop, the contraction of each phase is the same as the over-all contraction, and all microstresses are pure hydrostatic tension and compression. Equation 7.1 is derived with the further assumption that the phases are randomly distributed in the matrix phase.

McMillan et al. (11) have shown that expansion coefficients calculated by Equation 7.1 for a $\text{Li}_2\text{O} - \text{ZnO} - \text{SiO}_2$ glass-ceramic agree well with experimentally determined values. Similarly Freiman and Hench (12) found the relationship to be valid for $\text{Li}_2\text{O} - \text{SiO}_2$ glass-ceramics. In this present work attempts to fit theoretical values predicted by Equation 7.1 with the experimentally determined values were not very successful; difficulties were found in ascribing values to the moduli and expansion coefficients of the individual phases present.

7.8 Mechanical Properties

7.8.1 Introduction

In the present work the modulus of rupture σ_f , and the Young's modulus in bending E_b , were measured for specimens of glass-ceramic A.

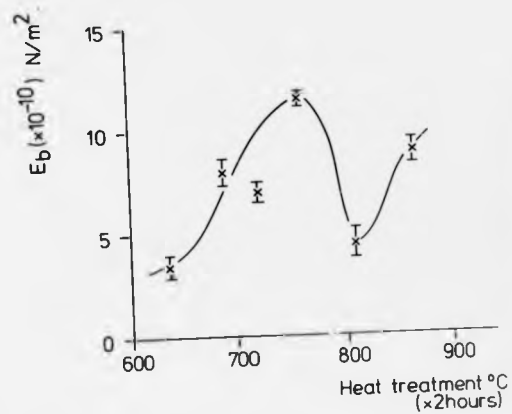


Figure 7.15 The variation of the Young's modulus E_b , of glass-ceramic A with various two hour heat-treatment temperatures.

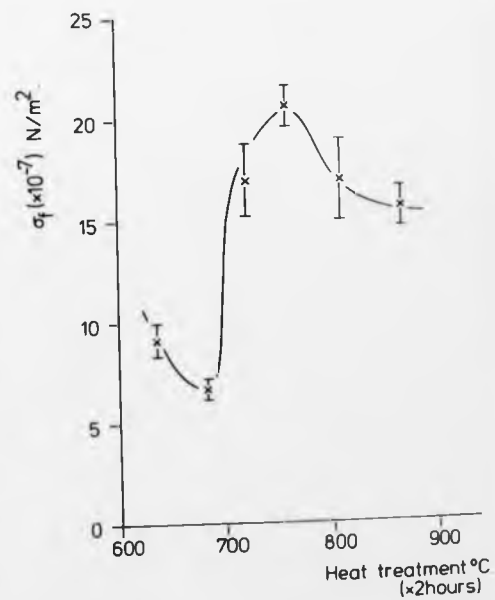


Figure 7.16 The variation of the modulus of rupture σ_f , of glass-ceramic A with various two hour heat-treatment temperatures.

The Knoop and Vickers hardness values were also determined for these samples. The heat-treatments referred to in the following sections were each carried out for a period of two hours unless otherwise stated.

7.8.2 Young's Modulus and Rupture Modulus Results

The moduli of the glass-ceramic specimens were measured using a three-point bending technique. On average ten specimens were used for each modulus determination.

The values of the moduli for the as cast glass A were found to be:

$$E_b = (5.35 \pm 0.62) 10^{10} \text{ N/m}^2$$

$$\sigma_f = (9.67 \pm 0.56) 10^7 \text{ N/m}^2$$

Figure 7.15 shows the variation of the Young's modulus of glass-ceramic A with various heat-treatment temperatures. This graph has the same general shape as the variation of the thermal expansion coefficients with temperature (Figure 7.13(a)).

The Young's modulus has a maximum value of:

$$E_b(\text{max}) \approx 11.5 \cdot 10^{10} \text{ N/m}^2$$

for a two hour heat-treatment at 760°C.

The minimum value of this modulus is given approximately by:

$$E_b(\text{min}) \approx 3.5 \cdot 10^{10} \text{ N/m}^2$$

for a heat treatment at either 640°C or 800°C.

The variation of the modulus of rupture of glass-ceramic A with different heat treatment temperatures is shown in Figure 7.16. The modulus has a maximum value of:

$$\sigma_f(\text{max}) \approx 20.5 \cdot 10^7 \text{ N/m}^2$$

for a two hour heat-treatment at 760°C.

The minimum value of the rupture modulus was found to be for glass-ceramic A heat treated at 680°C:

$$\sigma_f(\text{min}) \approx 6.5 \cdot 10^7 \text{ N/m}^2$$

7.8.3 Discussion of Moduli Results

The maximum values of the moduli of glass-ceramic A are approximately twice the values obtained for the original glass for specimens which have received the same pre-abrasion treatment.

Rossi (13) has considered the elastic behaviour of composite materials with a low concentration of the included phase. In this analysis the Young's modulus of the composite E is assumed to be related to the Young's modulus of the matrix, E_o , by the expression:

$$E = E_o (1 + M_E C_i)$$

where C_i is the volume fraction of the included phase and

$$M_E = \left(\frac{E_i - E_o}{E_o} \right) K_E$$

where E_i is the Young's modulus of the individual phase and K_E is the stress concentration arising in the matrix as a consequence of the stress interaction between the particle and the matrix.

In the present work the volume fraction of the crystalline phases in the glass-ceramic was greater than 75%; consequently this theory is not applicable to the system studied.

In two-phase systems the over-all elastic modulus is intermediate between the high and low modulus components. When the bond between the phases is continuous, the strain in each constituent is the same, to a first approximation, and most of the applied stress is carried by the high modulus component. The resulting elastic modulus E , when two phases having the same value for Poisson's ratio are present is given by a law of mixtures (14):

$$E = E_1 V_1 + E_2 V_2$$

where E_i is the Young's modulus of each individual phase and V_i is the volume fraction of the i^{th} phase such that:

$$V_1 + V_2 = 1$$

The volume fraction of the crystalline phases in glass-ceramic A heat-treated for two hours was approximately 85% and was independent of the heat-treatment temperature (Figure 7.8(b)). The law of mixtures will not therefore predict the observed variation in the value of Young's modulus. It is worth noting, however, that Hasselman and Fulrath (15) have determined the Young's modulus for a composite of a glass containing crushed sapphire as the dispersed phase and shown that the experimental results for this system fall well below the values predicted from the law of mixtures.

The mechanical strengths of glass-ceramics are controlled by the size and distribution of microcracks in the surface and it is postulated that these factors are determined by the microstructure of the glass-ceramics. This suggestion appears to be valid, if the microcracks are propagated with greater difficulty across the crystal/glass boundaries than through the intervening glass. In this case the lengths of the microcracks will be related to the sizes and volume fractions of the crystal phases and there will be an optimum microstructure resulting in a minimum microcrack length and therefore a maximum mechanical strength.

It has been suggested that the mechanical strength of a polycrystalline aggregate σ , is related to the mean grain diameter d , by the relationship (16, 17):

$$\sigma = k_1 d^{-1/2} \quad \text{Equation 7.2}$$

where k_1 is a constant.

The implication in equation 7.2 is that the crack length c , in the Griffith equation:

$$\sigma = \left[\frac{2E\gamma}{\pi c} \right]^{1/2} \quad \text{Equation 7.3}$$

is proportional to the grain diameter d . In Equation 7.3 E is the Young's modulus of the material and γ is the effective surface energy

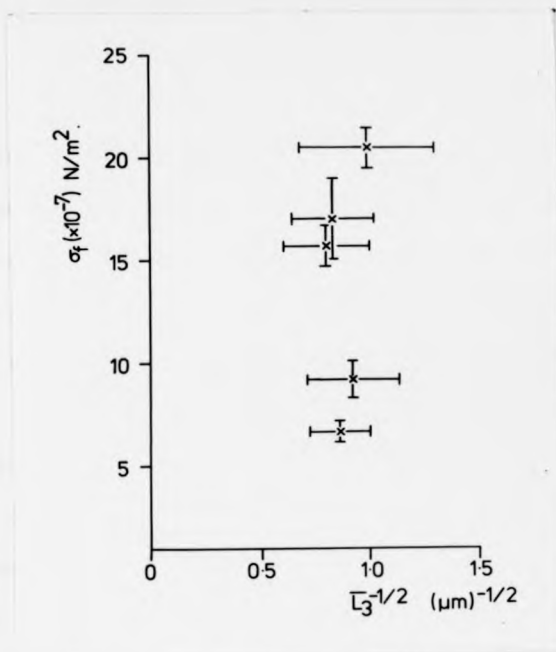


Figure 7.17 The variation of the rupture modulus σ_f , with the square root of the mean crystal size of glass-ceramic A.

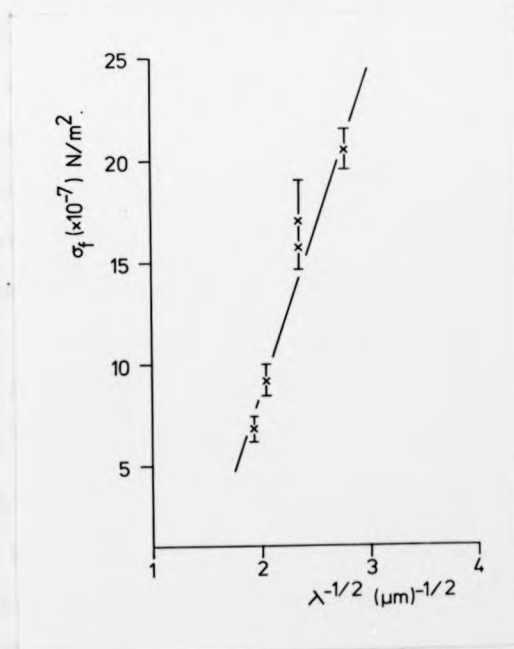


Figure 7.18 The dependence of the rupture modulus with the mean free path λ , for glass-ceramic A.

for crack initiation. Tashiro and Sakka (18) have shown that equation 7.2 holds for a glass-ceramic based on a $\text{Li}_2\text{O} - \text{SiO}_2$ glass composition. This suggests that the critical flaws are present within the crystal grains and do not extend into the glass phase or that they exist at the glass-crystal interface and are therefore proportional to the circumference of the grains.

In the present work the variation of σ_f with the square root of the mean crystal size is shown in Figure 7.17. It can be seen from this graph that this dependence of the strength on the grain size does not explain the difference in the values of the rupture modulus observed.

In a glass-crystal composite such as a glass-ceramic containing a relatively strong crystalline dispersion, fracture could be initiated within the glass matrix. Hasselman and Fulrath (loc.cit.) have suggested that for such composites at a sufficiently high volume fraction of the crystalline phase the maximum flaw size in the glass is restricted by the presence of the dispersion. This implies that the flaws present in the glass are terminated at the crystal-glass boundaries and the spacing between the crystals or the mean free path in the glass phase will, therefore, be a critical parameter in determining the mechanical strength of the composite.

Equation 7.2 can therefore be modified to:

$$\sigma = k_2 \lambda^{-\frac{1}{2}} \quad \text{Equation 7.4}$$

where k_2 is a constant and λ is the mean free path in the glass phase. Hench et al. (12) have reported a similar dependence of strength on the mean free path, in a partially crystallised glass of molecular composition $70\text{SiO}_2 \cdot 30\text{Li}_2\text{O}$. The result as expressed in Equation 7.4 is also consistent with the work of Hing and McMillan (19).

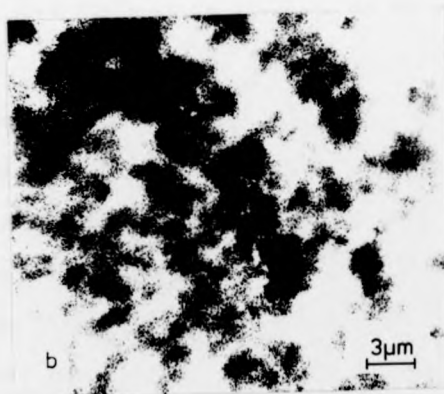
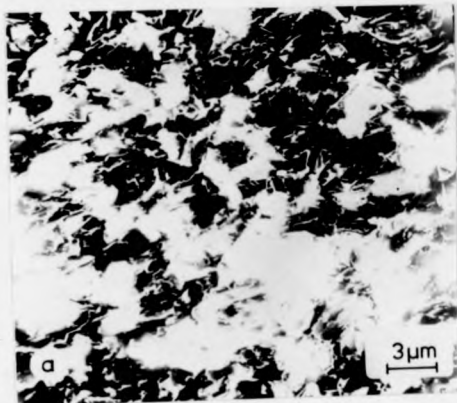


Figure 7.19 A typical fracture surface of glass-ceramic A examined in (a) the secondary electron mode and (b) the cathodoluminescence mode of the SEM.

Figure 7.18 shows the dependence of the rupture modulus with the mean free path λ , for glass-ceramic A studied in the present work. Examination of equation 7.3 reveals that the surface energy for crack initiation in the glass phase γ , can be calculated from the slope k_2 of the graph shown in Figure 7.18 by means of:

$$\gamma \approx \frac{k_2^2}{E}$$

If the maximum value of E_b ($\approx 11.5 \cdot 10^{10} \text{ N/m}^2$) is substituted into this equation then:

$$\gamma \approx 0.2 \text{ J/m}^2$$

This value for the surface energy is low compared with that result quoted by Hing et al. (loc.cit) of

$$\gamma \approx 4 \text{ J/m}^2$$

which is similar to that reported by other workers (15, 20, 21).

It can be concluded from the above discussion that the strength of glass-ceramic A is controlled by microcracks in the glass phase; the strength of the material is dependent on the mean free path in the glass phase. Figure 7.19(a) and (b) shows a typical fracture surface of glass-ceramic A examined in the secondary electron mode and the cathodoluminescence mode respectively of the scanning electron microscope. It is not possible from these micrographs to determine whether or not the crack was propagated only in the glass phase and deflected by the crystal-glass boundaries.

7.8.4 Microhardness Measurements

Figures 7.20(a) and 7.20(b) show respectively the variation of the Vickers and Knoop hardness numbers with the heat-treatment temperature of glass-ceramic A for periods of one and two hours.

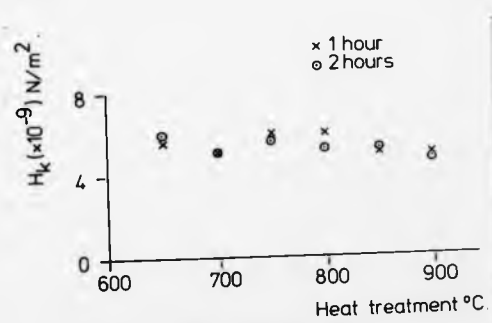
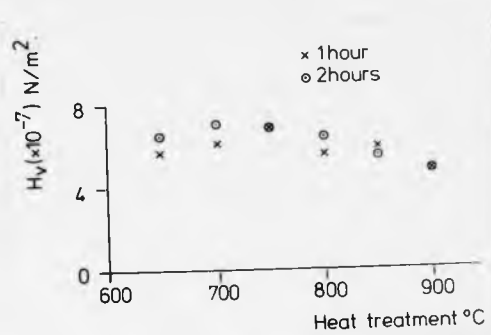


Figure 7.20 The variation with heat-treatment temperature of (a) the Vickers and (b) the Knoop hardness numbers for glass-ceramic A.

The Vickers hardness number H_v , shows little variation with heat-treatment temperature or time and has an average value of approximately:

$$H_v \approx 6 \cdot 10^7 \text{ N/m}^2$$

In general the Vickers hardness of a substance is related to its yield strength, σ_f , by (18):

$$H_v = 2.68 \sigma_f$$

this relationship is approximately valid in the present work. However the variation of the rupture modulus with heat-treatment of glass-ceramic A (Figure 7.16) does not show the same behaviour as the Vickers hardness (Figure 7.20).

The average value of the Knoop hardness H_k , for glass-ceramic A is given approximately by:

$$H_k \approx 5.5 \cdot 10^9 \text{ N/m}^2$$

The two techniques of measuring the hardness of the same material produce results which differ by approximately two orders of magnitude. This differential and the mechanism of the deformation of the material are not understood.

Tashiro and Sakka (18) have shown that for a glass-ceramic based on a $\text{Li}_2\text{O-SiO}_2$ glass composition the Vickers hardness is related to the average diameter d of the constituent grains by:

$$H_v = k_3 d^{-1/2}$$

This equation is of the same form as equation 7.2 and implies that the fracture mechanism for the specimen is transcrystalline.

In the present work the average grain size of the crystals in glass-ceramic A has a constant value of approximately:

$$d \approx 1.5 \mu\text{m}.$$

The validity of the modified version of equation 7.2 for the hardness

of the specimen cannot therefore be completely checked. The constant k_3 in the modified equation can be related to the surface energy γ , of the material in the manner described in section 7.8.3. This results in a value for the surface energy for crack initiation in the crystalline phase of:

$$\gamma \approx 0.03 \text{ J/m}^2$$

which is an order of magnitude less than the value calculated for crack initiation in the glass-ceramic from the rupture modulus data.

This implies that the propagating crack is not affected by the glass-crystal boundaries; with this argument it is difficult to reconcile the fact that the yield strength of glass-ceramic A is approximately twice that of the original glass.

It is believed that the deformation and crack propagation of a glass-ceramic by an indentation method is controlled by different mechanisms to those which exist in bending experiments; consequently it is difficult to justify a comparison of the surface energies calculated from the data of the two experiments.

7.9 The Electrical Properties of Glass-Ceramic A

7.9.1 Introduction

In the present work the electrical volume resistivity ρ , the dielectric constant k , and the loss angle $\tan \delta$, were measured over a range of temperatures for glass-ceramic A devitrified at different temperatures. Each of these electrical properties was measured at 100 Hz and frequencies increasing by a factor of 10 to 1 M Hz.

7.9.2 The Resistivity of Glass-Ceramic A

The ionic conductivity of a glass or crystal increases rapidly as the temperature is raised; the dependence of the resistivity ρ , on the

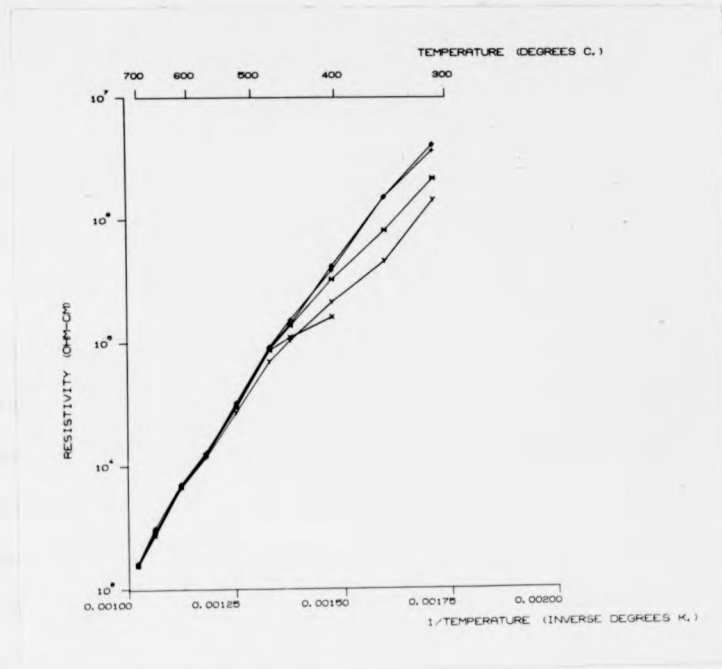


Figure 7.21 The variation in the volume resistivity with the reciprocal of the absolute temperature for a specimen of glass-ceramic A.

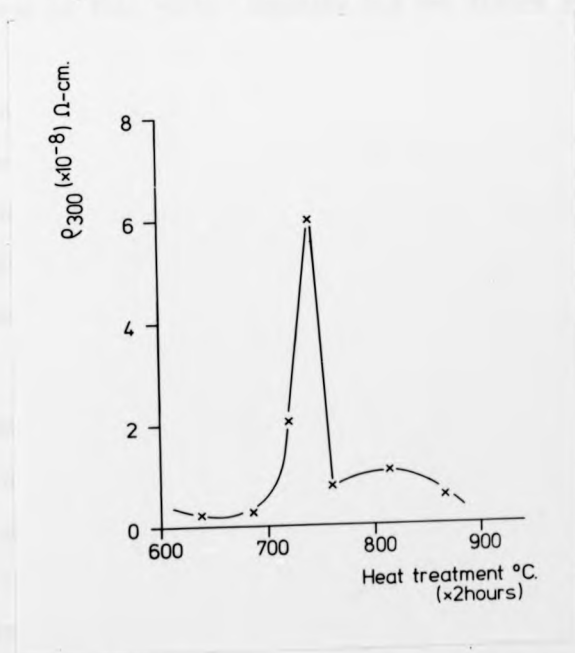


Figure 7.22 The variation of the resistivity at 300°C ρ_{300} with the heat-treatment temperature for glass-ceramic A.

absolute temperature T , can be expressed by the Rasch-Hindrichsen equation (22):

$$\rho = A \exp \left[\frac{E}{RT} \right] \quad \text{Equation 7.5}$$

where E is the activation energy for conduction for the particular glass or crystal and A is a constant. Hence a linear relationship should exist between the logarithm of resistivity and the reciprocal of absolute temperature.

Figure 7.21 shows the variation in the volume resistivity with reciprocal temperature for a specimen of glass-ceramic A. The resistivity measured at the five different frequencies for each temperature of measurement is plotted on this graph. This graph is a typical example of the resistivity - temperature dependence measured for all the glass-ceramic specimens in this work; equation 7.5 was fitted by a least squares method to the resistivity data taken at each frequency and the constants A and E evaluated.

In the present work no dependence on the measurement frequency was observed for the values of the constants A and E evaluated from data taken above 300°C .

The activation energy for a specimen of glass A, E_{GLASS} was found to be:

$$E_{\text{GLASS}} = 15.5 \text{ kcal/mole}$$

$$\text{and } \ln A = -5.6$$

For this glass specimen a sharp increase in the resistivity was observed at a temperature of approximately 600°C ; this increase was associated with the initial devitrification of the sample.

The resistivity at 300°C , ρ_{300} , was calculated from the experimentally determined values of A and E for specimens of glass-ceramic A and is shown in Figure 7.22. The abscissa of this graph is the temperature of a two

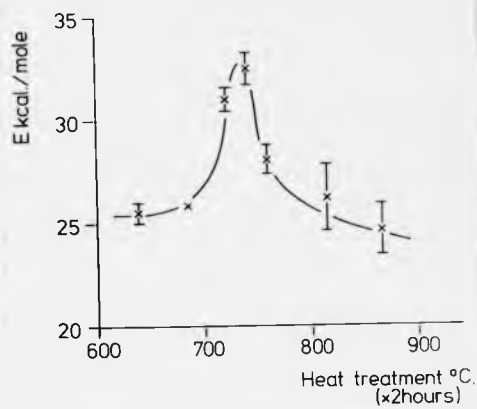


Figure 7.23 (a) The variation of the activation energy E , with heat-treatment temperature of glass-ceramic A.

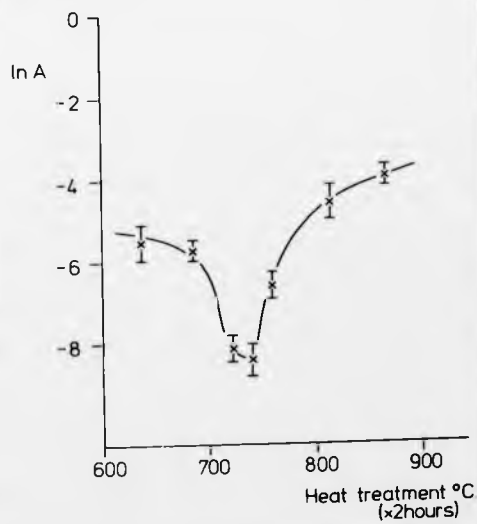


Figure 7.23 (b) The variation of the pre-exponential constant $\ln A$, with the heat-treatment temperature of glass-ceramic A.

hour heat-treatment at which glass A was devitrified. This curve shows a maximum value for the resistivity of $6.10^8 \Omega\text{-cm}$, when glass A is crystallised at approximately 740°C .

Figure 7.23(a) shows the variation of the activation energy E , with the heat-treatment temperature. This curve shows a maximum value of the activation energy E_{max} , of:

$$E_{\text{max}} \approx 33 \text{ kcal/mole}$$

for a specimen heat-treated at approximately 740°C .

Similarly, the variation of the pre-exponential constant in Equation 7.5, $\ln A$, with the heat-treatment temperature (Figure 7.23(b)), shows a minimum value of

$$\ln A_{\text{min}} \approx -8.5$$

for a specimen of glass A devitrified at approximately 740°C .

7.9.3 Discussion of Resistivity Measurements

The ionic conductivity in a glass-ceramic is a complex process because of the presence of both crystalline and glassy phases. Low resistivity is generally associated with the presence of highly mobile cations such as alkali metal ions. The important factors are the concentration and the mobility of the cations. The mobility is strongly affected by the phase through which the ion is moving. For a given temperature a certain fraction of ions have sufficient energy to surmount the energy barrier between adjacent sites. In glasses the energy barrier has no fixed value as it has in crystals, and the average barrier height is lower. Thus the conversion of a glass to a glass-ceramic should increase the resistivity. The boundaries between the phases also hinder ionic migration and increase the resistivity.

In the present work the resistivity of the glass measured at 300°C was found to be:

$$\rho_{\text{GLASS}} (300^\circ\text{C}) \approx 3.10^3 \Omega\text{-cm.}$$

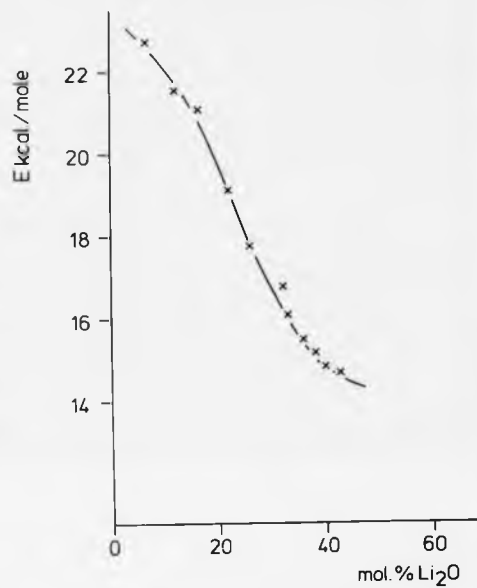


Figure 7.24 The variation of the D.C. activation energy for glasses in the $\text{Li}_2\text{O}-\text{SiO}_2$ system with varying molecular percentages of Lithia (after Kuznetsov (23)).

This value is approximately five orders of magnitude lower than the equivalent measurements on the glass-ceramic.

The resistivity of glass-ceramic A shows a sharp peak, for a glass heat-treated at approximately 740°C for two hours (Figure 7.22); at this temperature the second crystalline phase of tridymite was first observed. The variation of the volume fraction and mean crystal spacing with heat-treatment temperature do not show such a sharp maximum or minimum at this temperature (Figures 7.8(b) and 7.9(b)).

It can be concluded that the observed changes in the resistivity of glass-ceramic A with different heat-treatment temperatures are not only a function of the microstructure of the material but also a function of the type and mobility of the ionic carriers.

Kuznetsov (23) has measured the D.C. activation energy for glasses in the $\text{Li}_2\text{O}-\text{SiO}_2$ system with varying molecular percentages of lithia. This data shows a decrease in the activation energy as the percentage of lithia in the glass is increased (Figure 7.24) and this is presumably associated with an increase in the number of ionic current carriers in the glass and changes in the glass structure. For a 10 mol.% content of lithia, Kuznetsov (loc.cit) obtained an activation energy of 23 kcal/mole; this is approximately the same as the lowest values measured in this work for glass-ceramic A (Figure 7.23(a)). It must be noted however, that the glass-ceramic contained a crystalline phase as well as a glass phase of uncertain composition. The peak observed in the activation energy for glass-ceramic A (Figure 7.23(a)) can be partly attributed to a decrease in the number of ionic current carriers in the glass-ceramic, if the data shown in Figure 7.24 is extrapolated to lower lithia content.

The Rasch-Hindrichsen equation (Equation 7.5) can be derived for the D.C. resistivity of glasses if it is assumed that the glass shows a

behaviour typical of a thermally activated process and that the current carriers are predominately ions. The appropriate model then consists of an ion undergoing thermal vibration in a potential well. The ion will have a finite and equal probability of surmounting the barrier and moving to any of the adjacent potential wells. The effect of an electric field is to lower the potential barrier on one side of the well and raise it on the other by an equal amount thus favouring the motion of the ion in a particular direction. The electric field does not "activate" or pull the ions out of their potential wells; it merely directs a random diffusion of the ions already taking place in its absence.

It can be shown by performing an analysis of this model that the pre-exponential constant in the Rasch-Hindrichsen equation can be interpreted as (24, 25):

$$A = \frac{2kT}{e^2 \lambda^2 n v b}$$

where λ is the distance between two neighbouring potential wells in the structure, n is the number of ions per unit volume of charge e , v is the vibrational frequency of the ion in its well and the number of neighbouring jump sites is given by b . It is possible to perform this derivation using Eyring's rate process theory (26); in this case the constant v is given by kT/h where h is Plank's constant. Then the pre-exponential constant A , is no longer explicitly dependent upon the temperature T .

When alkali ions are thought to be responsible for conductivity in a glass the constant $\ln A$, usually has a value between 1.5 and -4.5 (25).

A variation in the pre-exponential constant A , can therefore be attributed to the following processes (27):

- (i) variation of the concentration of mobile ions n
- (ii) the change of the jump mechanism of the ions in question
- (iii) variations in the jump distance λ

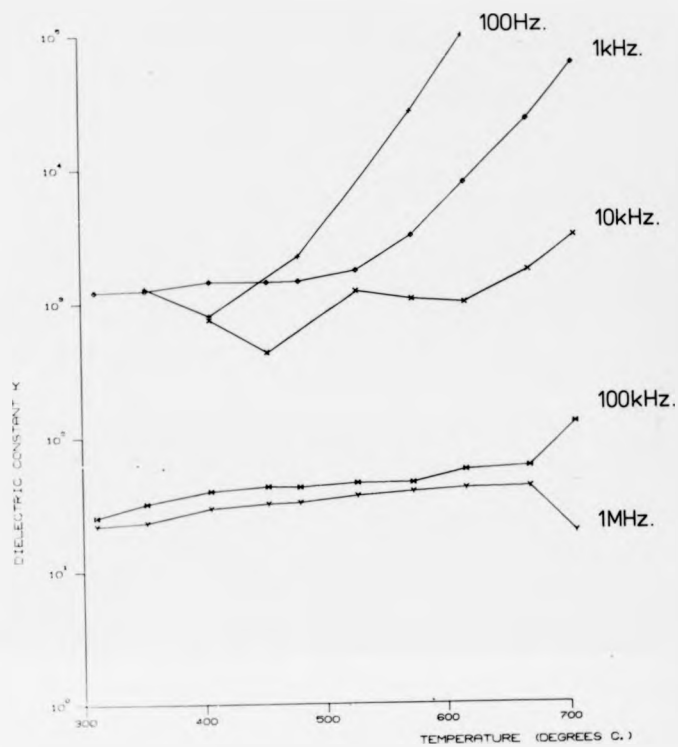


Figure 7.25 The variation of the dielectric constant, k , with measuring temperature.

The minimum observed in the variation of $\ln A$ with temperature (Figure 7.23(b)) coincides with the first detection of a crystal phase of tridymite in the glass-ceramic. This variation in A can be attributed partly to changes in the three parameters discussed above by the appearance of the new crystal phase. It must be noted however, that the constant A shows a similar variation with heat-treatment temperature to the changes in the crystal-crystal spacing in the glass-ceramic (Figure 7.9(b)).

7.9.4. The Dielectric Constant and Loss Tangent of Glass-Ceramic A:

Introduction

The capacitance and resistance were measured for specimens of glass-ceramic A as a function of temperature. The samples were produced by a two hour heat-treatment of glass A at various temperatures between 600°C and 900°C. The measurements were interpreted in terms of the dielectric constant or permittivity k , of the specimens and the loss tangent $\tan \delta$.

For studying the effects of heat-treatments it is convenient to calculate $\tan \delta$ at a particular frequency for each specimen. Here $\tan \delta$ is defined to be equal to:

$$\tan \delta = \frac{1}{\omega CR}$$

where ω is the angular frequency and C and R are the measured capacitance and resistance respectively. The advantage of using this parameter is that it is independent of the electrode configuration and the thickness of the specimen. Frequencies of 100 KHz and 1 MHz were chosen for the analysis of the dielectric constant and loss tangent.

7.9.5. The Dielectric Constant of Glass-Ceramic A

Figure 7.25 shows the variation of the dielectric constant, k , with temperature T , for the five measuring frequencies between 100 Hz and 1 MHz. This is a typical graph and the following comments are valid for all the dielectric constants measured on different glass-ceramic specimens.

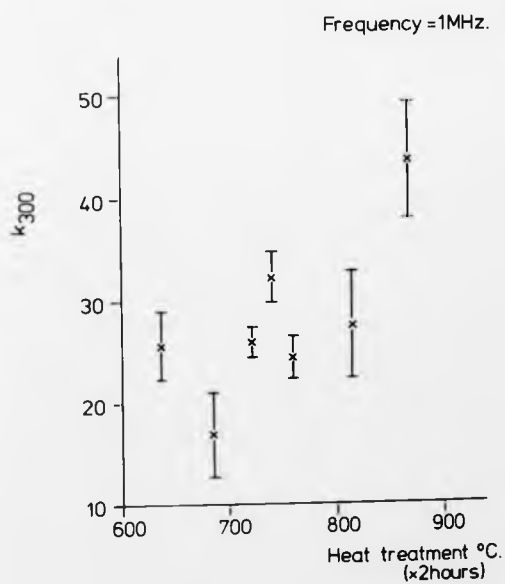
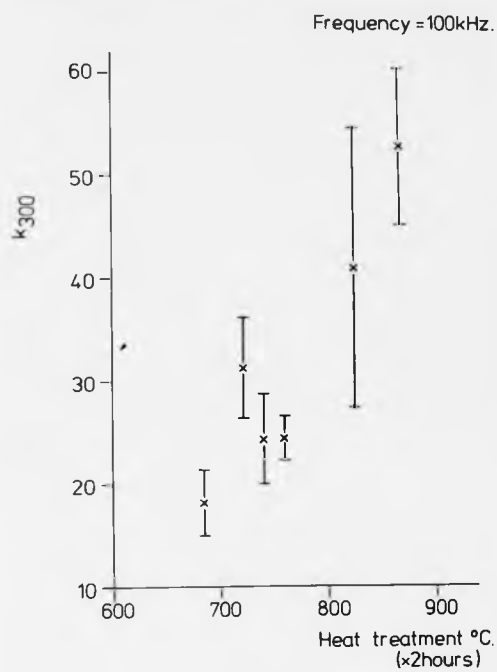


Figure 7.26 The variation of the dielectric constant k_{300} with heat-treatment temperature of glass-ceramic A for frequencies of (a) 100 kHz and (b) 1 MHz.

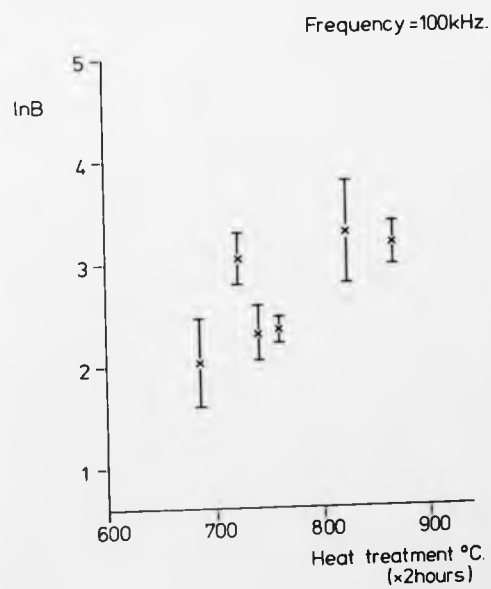
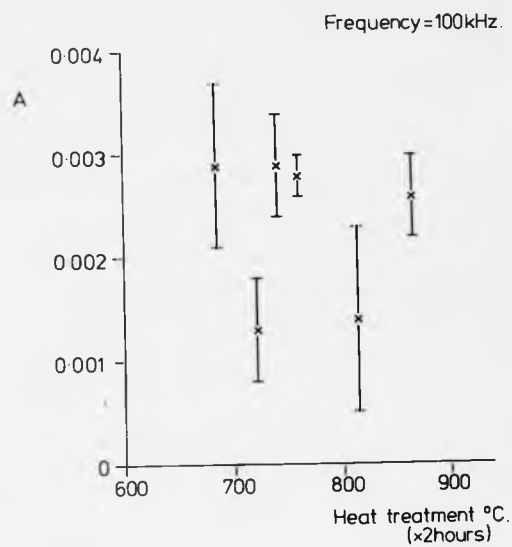


Figure 7.27 The variation of the constants A and B in Equation 7.6 with heat-treatment temperature for a frequency of 100 kHz.

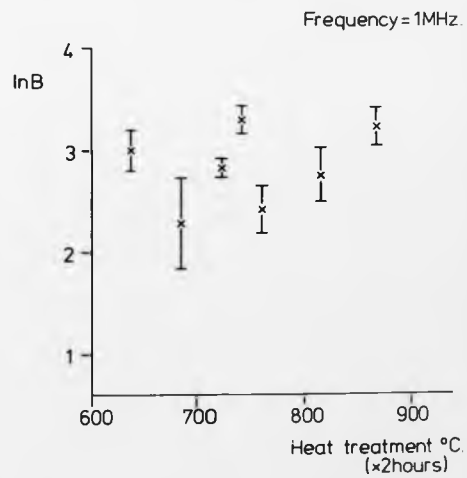
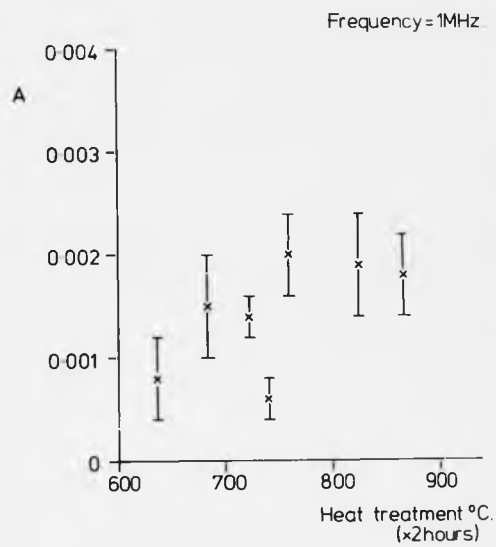


Figure 7.28 The variation of the constants A and B in Equation 7.6 with heat-treatment temperature for a frequency of 1 MHz.

(i) The dielectric constant decreases as the measuring frequency is increased; at low frequencies (< 10 kHz) the dielectric constant increases rapidly with the increasing temperature of the specimen.

(ii) At frequencies of 100 kHz and 1 MHz the dielectric constant varies slowly with increasing temperature.

The dielectric constant at frequencies of 100 kHz and 1 MHz appears to be an exponential function of the temperature T , at which it is measured (Figure 7.25). The data for each glass-ceramic specimen was fitted by a least squares method to a function of the form:

$$k = B \exp (AT) \quad \text{Equation 7.6}$$

and the dielectric constant measured at 300°C k_{300} , calculated from the constants A and B . These constants were evaluated for glass-ceramic specimens heat-treated at different temperatures.

The variation of the dielectric constant k_{300} , with heat-treatment temperature of the glass-ceramic is shown in Figure 7.26(a) and (b) for frequencies of 100 kHz and 1 MHz respectively. These graphs show that k_{300} increases with increasing heat-treatment temperature.

Figures 7.27(a) and (b) respectively show the variation of the constants A and B in Equation 7.6 with heat-treatment temperature for a frequency of 100 kHz. Similar graphs are plotted in Figures 7.28(a) and (b) for a frequency of 1 MHz. No definite conclusions can be drawn from these graphs.

7.9.6. Comments on the Dielectric Constant Measurements

In most glass-ceramics the dielectric constants are not markedly different from those of the parent glass. The effect of temperature on the permittivity of a glass-ceramic is similar to the results obtained on other ionic solids such as ceramics and glasses.

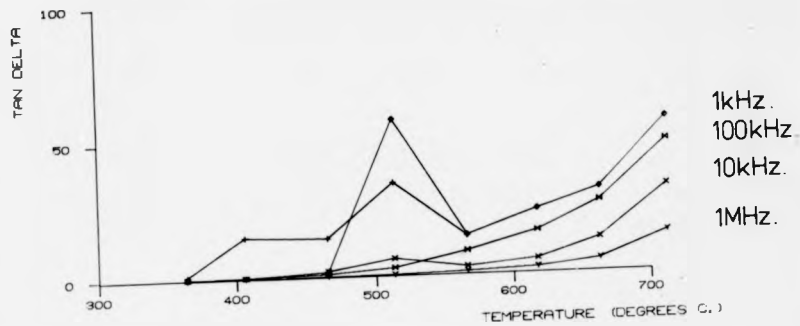


Figure 7.29 The variation of the loss tangent with temperature T, for a typical glass-ceramic specimen studied in this work.

The dependence of the dielectric constant on the frequency and temperature at which it is measured which was observed in this work is similar to that reported by Partridge and McMillan (28) for glass-ceramics.

The increases of permittivity at low frequencies with temperature are related to the increasing contribution from ion mobility and crystal imperfection mobility. The combined effect of these contributions produce an increase in the permittivity.

7.9.7 The Loss Tangent of Glass-Ceramic A

When an electric field is established in a dielectric, electrical energy is stored within the material and on removal of the field the energy may be wholly recoverable. Usually only part of the energy is retrieved; that part of the energy which is lost appears as heat. In an alternating field, therefore, a power loss occurs for insulating materials. The ratio between the irrecoverable and recoverable parts of the electrical energy is expressed as $\tan \delta$, the loss tangent or power factor.

Figure 7.29 shows the variation of the loss tangent with temperature T , for a typical glass-ceramic specimen studied in this work. The loss tangent decreases with increasing frequency.

Strutt (29) has measured the dielectric constant and power factor of several commercial glasses. He obtained the empirical relationship:

$$\tan \delta = \beta \exp(\alpha T) \quad \text{Equation 7.7}$$

in which the constants β and α depend upon the composition of the glass and the frequency of measurement, α decreasing with increasing frequency. Equation 7.7 has been largely substantiated for glasses measured at frequencies in the audio-range and from room temperature to approximately 300°C (30 - 33).

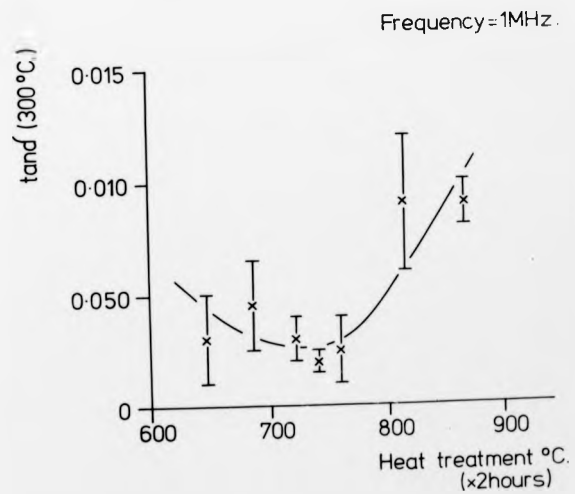
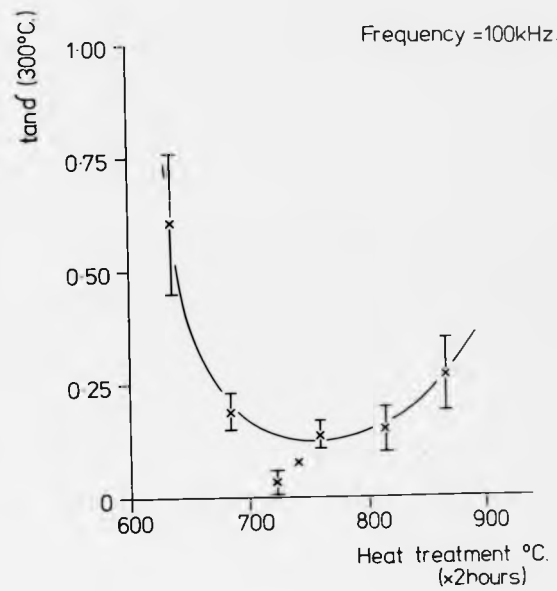


Figure 7.30 The variation of $\tan \delta_{300}$, with the original heat-treatment of glass-ceramic A for frequencies of (a) 100 kHz and (b) 1 MHz.

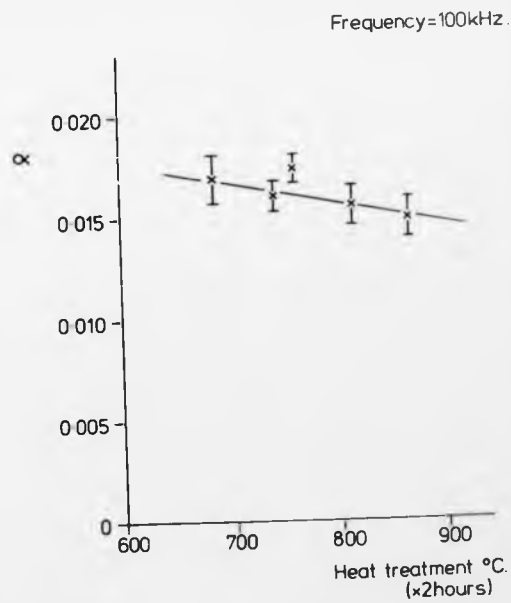
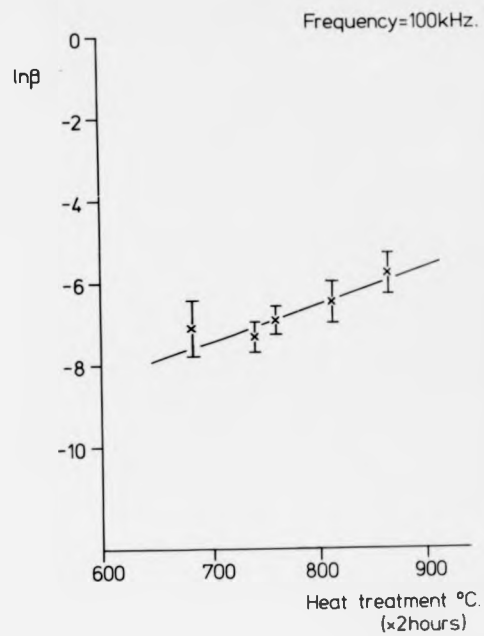


Figure 7.31 The variation of the constants β and α in Equation 7.7 with temperature for a frequency of 100 kHz.

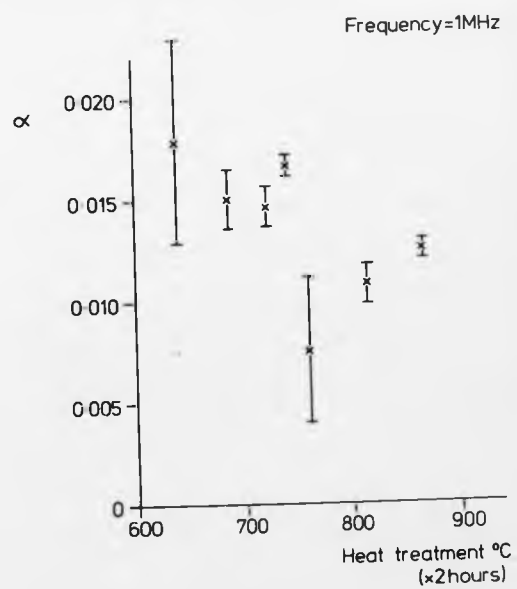
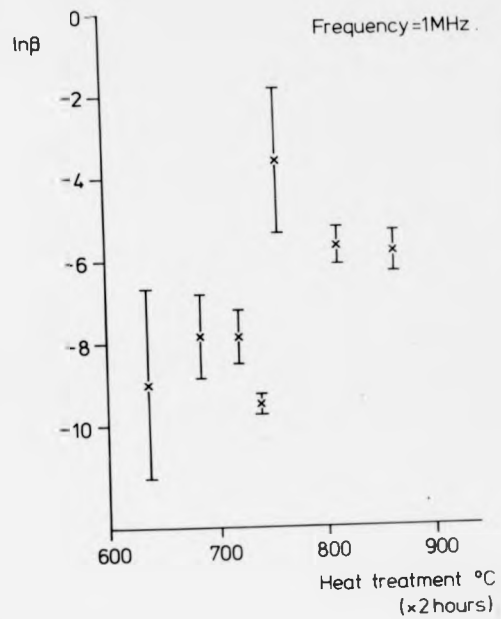


Figure 7.32 The variation of the constants β and α in Equation 7.7 with temperature for a frequency of 1 MHz.

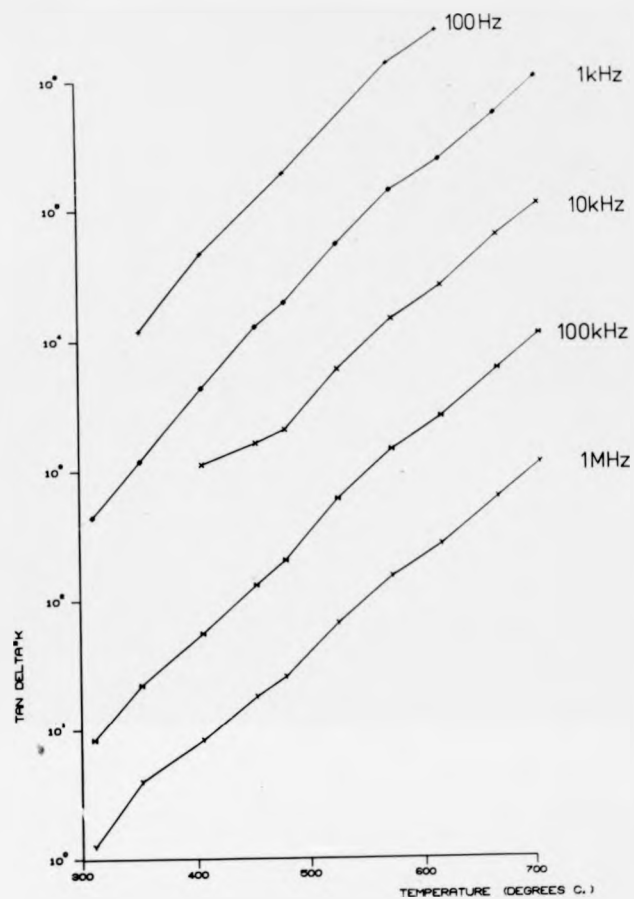


Figure 7.33 The dependence of the product $k \cdot \tan \delta$ on the measuring temperature and frequency for a typical glass-ceramic specimen studied in this work.

In the present work equation 7.7 was fitted by a least squares method to the loss tangent data measured as a function of increasing temperature for specimens of glass-ceramic A and frequencies of 100 kHz and 1 MHz; from the constants α and β the loss tangent at 300°C, $\tan \delta_{300}$, was calculated.

Figures 7.30(a) and (b) show the variation of $\tan \delta_{300}$ with the original heat-treatment of the glass-ceramic for frequencies of 100 kHz and 1 MHz respectively. Both curves show a minima at a heat-treatment temperature of approximately 750°C.

The variation of the constants β and α with the heat treatment temperature for a frequency of 100 kHz is shown in Figures 7.31(a) and (b) respectively. Similar graphs for a frequency of 1 MHz are shown in Figures 7.32(a) and (b).

The dependence of the product of the dielectric constant and the loss tangent, $k \cdot \tan \delta$ on the measuring temperature and frequency is shown for a typical glass-ceramic specimen in Figure 7.33. At each measuring frequency a linear relationship exists and the product $k \tan \delta$, decreases with increasing frequency. This behaviour is to be expected; from a consideration of the equations from which k and $\tan \delta$ were calculated (Chapter 3 contains the details) it can be seen that:

$$k \cdot \tan \delta \propto \frac{1}{\omega R}$$

where ω is the angular frequency and R is the resistance of the specimen; the resistance R is given by:

$$R \propto \exp\left(\frac{A}{T}\right)$$

where A is a constant and T is the temperature. Therefore:

$$k \tan \delta \propto \frac{1}{\omega} \cdot \exp\left(-\frac{A}{T}\right)$$

7.9.8 Comments on the Loss Tangent Results

For a dielectric (such as a glass) there are four processes contributing to the loss tangent (after Stevels (27)):

- (i) conduction losses
- (ii) ionic relaxation losses
- (iii) deformation losses and
- (iv) vibration losses.

Losses in the first of these classes are directly related to the D.C. conductivity of the glass and are due to the migration of ions (principally alkali metal ions) in the applied field.

Ionic relaxation losses arise because in an A.C. field some ions oscillate between potential wells which are separated by a smaller energy barrier than the ion would have to surmount in order to contribute to the D.C. conductivity.

Deformation losses are associated with the deformation of the glass network structure, and vibration losses are due to a resonance phenomenon; all ions in the glass will vibrate about their equilibrium position with a certain natural frequency which, in resonance with an applied field, will lead to the absorption of energy.

Losses due to the first two mechanisms predominate in the low frequency range below approximately 1 MHz and those due to the second two processes at high frequencies above about 10^4 MHz.

For a glass-ceramic the mechanism is more complicated than for a glass, since it is difficult to assess the effect of the various crystal phases and of the residual glass phase, of which the composition is not usually known with any accuracy. It is likely in most cases, however, that the glass phase is the main contributor to dielectric losses.

Harper and McMillan (34) have assumed that $\tan \delta$ for a partially devitrified $\text{Li}_2\text{O} - \text{SiO}_2$ glass is a linear combination of two constant

values, $\tan \delta_{cr}$ and $\tan \delta_g$, for the crystalline and amorphous phases weighted according to their respective volume fractions. Thus:

$$\tan \delta = V_f \tan \delta_{cr} + (1 - V_f) \tan \delta_g$$

where V_f is the volume fraction of crystalline phase present in the composite material.

In the present work the variation of $\tan \delta$ with the microstructure of the glass-ceramic (Figures 7.30(a) and (b)) shows no similarity with the volume fraction variation (Figure 7.8b) which is approximately constant. However, there is a marked correlation between the $\tan \delta$ values and the mean crystal - crystal spacing (Figure 7.9(b)).

The empirical equation relating the loss tangent of glasses to the measuring temperature (Equation 7.7) appears from the present work to be true for glass-ceramics; it must be also noted that in the case of glass-ceramics the equation was used outside the range of temperature and frequency for which it has been verified for glass.

Tomozawa and Doremus (35) have shown that for measurements of the dielectric properties of glasses with silver paste or gold sputtered film electrodes, anomalously high dielectric losses and high capacitances can result. They show that the use of stainless steel electrodes can reduce these losses and capacitances substantially. In the present work it is not known whether or not the dielectric properties measured are absolute values; this is not considered to be important because the results obtained can be interpreted in terms of relative values.

7.10 A Summary of the Properties of Glass-Ceramic A

In the following the main features of the microstructure and physical properties of the glass-ceramic devitrified from glass A at various temperatures are briefly summarised.

(i) Microstructure

In all the heat-treatments between 650°C and 900°C the glass-ceramic contained a major crystalline phase of lithium disilicate; in the heat-treatment temperature range of 750°C - 850°C a minor crystalline phase of tridymite was also present.

(ii) Statistical Description of the Microstructure

The volume fraction was approximately independent of the heat-treatment temperature and the mean crystal - crystal spacing showed a minimum for the glass-ceramic devitrified at approximately 750°C.

(iii) Thermal Expansion Coefficient

Two thermal expansion coefficients were measured for each specimen. The variation of these coefficients with heat-treatment temperature was measured; both showed maxima at a temperature of approximately 700°C.

(iv) Young's Modulus and Rupture Modulus

These moduli were measured for each heat treatment temperature and the Rupture modulus was correlated with the mean crystal - crystal spacing in the material. Both moduli showed a maximum value at approximately 750°C.

(v) Microhardness Values

The Knoop and Vickers hardness numbers were measured for the glass-ceramic specimens. Both hardness measurements were approximately independent of the heat-treatment temperature and the Vickers hardness was correlated with the invariance of the mean crystal size.

(vi) Resistivity

The resistivity showed a maximum value for specimens heat-treated at approximately 750°C; this maximum value was reflected in the variation with heat treatment temperature of the activation energy for conduction and the pre-exponential constant of an Arrhenius equation.

(vii) Dielectric Constant and Loss Tangent

The dielectric constant of the glass-ceramics was found to be a steadily increasing function of the heat-treatment temperature. The loss tangent showed a minimum value for a glass-ceramic heat treated at approximately 750°C.

References

1. S. V. Phillips & P. W. McMillan, *Glass Tech.* 6 46 (1965)
2. P. W. McMillan and G. Partridge, British Patent No. 924,996 (1963)
3. P. W. McMillan, *Glass-Ceramics* (Academic Press, London & New York 1964)
4. J. Miles and P. W. McMillan, unpublished work.
5. C. L. Booth and G. E. Rindore, *J. Am. Ceram. Soc.* 47 25 (1964)
6. P. S. Bell, unpublished work.
7. P. S. Bell, private communication.
8. S. V. Phillips & G. Partridge, private communication.
9. W. Eitel, *Silicate Science*, Vol. III (Academic Press, New York & London 1965)
10. W. D. Kingery, *Introduction to Ceramics* (John Wiley & Sons, Inc., New York 1960)
11. P. W. McMillan, S.V. Phillips & G. Partridge, *J. Mat. Sci.* 1 269 (1966)
12. S. W. Freiman and L. L. Hench, *J. Am. Ceram. Soc.* 55 86 (1972)
13. R. C. Rossi, *J. Am. Ceram. Soc.* 51 433 (1968)
14. Zvi Hashin, p. 313 in *Ceramic Microstructures*: edited by R. M. Fulrath and J. A. Pask (John Wiley & Sons, Inc., New York 1968)
15. D. P. H. Hasselman & R. M. Fulrath, p. 343 *ibid.*
16. E. Orowan, *Repts. Prog. Phys.* 12 185 (1949)
17. Y. Utsami & S. Sakka, *J. Am. Ceram. Soc.* 53 286 (1970)
18. M. Tashiro & S. Sakka, *Kyoto Univ. Inst. for Chem. Res. Bull.* 42 351 (1964)
19. P. Hing and P. W. McMillan, *J. Mat. Sci.* 8 1041 (1973)
20. R. C. Roesler, *Proc. Phys. Soc. (London) Ser.B.* 69 981 (1956)
21. E. B. Shand, *J. Am. Ceram. Soc.* 44 21 (1961)
22. E. Rasch & F. Hindrichsen, *Z. Elektrochem.* 14 41 (1908)
23. A. Ya Kuznetsov, *J. Phys. Chem. Moscow* 33 20 (1959)
24. J. M. Stevels, *Progress in the Theory of the Physical Properties of Glass* (Elsevier, Amsterdam, 1948)

25. A. E. Owen in Progress in Ceramic Science, Vol. 3 editor J. R. Burke
(Pergamon Press Ltd., Oxford 1963)
26. S. Glasstone, K. J. Laidler, H. Eyring, The Theory of Rate Processes
(McGraw-Hill, New York 1941)
27. J. M. Stevels, Handbuch der Physik Vol XX; Electrical Conductivity II
28. G. Partridge and F. W. McMillan, Glass Technology 4 173 (1963)
29. M. J. Strutt, Arch. Elektrotech, 25 715 (1931)
30. L. S. McDowell and H. L. Begeman, Phys. Rev. 33 55 (1929)
31. J. M. Stevels, J. Soc. Glass Technol. 30 31T (1946)
32. J. M. Stevels, ibid 34 80 T (1950)
33. H. Moore and R. C. De Silva, ibid 36 5 T (1952)
34. H. Harper and F. W. McMillan, Phys. Chem. Glasses 13 97 (1972)
35. M. Tomozawa and R. H. Doremus, J. Non-Cryst. Solids 14 54 (1974)

CHAPTER 8: THE PROPERTIES OF A HOT EXTRUDED GLASS-CERAMIC

8.1 Introduction

This chapter contains details of the microstructure and properties of a glass-ceramic which has been hot extruded. The results of measuring the physical properties of the extruded material in directions perpendicular and parallel to the preferred crystal orientation are presented. These measurements include the electrical and mechanical properties of the material, the coefficient of thermal expansion and the determination of the crystallographic orientation using an X-ray diffractometer technique.

8.2 The Hot Extrusion of Glass A and Glass B

8.2.1 General Considerations

The hot extrusion apparatus and method of operation have been described in Chapter 5; glass-ceramics devitrified from glasses A and B (the compositions are given in Table 7.1) were extruded using this apparatus in the constant pressure mode of operation.

The crystal morphologies of these two glass-ceramics have been described in Chapter 7.

8.2.2 Extrusion of Glass-Ceramic A

Initially a glass-ceramic devitrified from glass A was extruded. In all cases a glass billet was placed in the die and heat-treated for approximately thirty minutes at a predetermined extrusion temperature which was held constant at $\pm 1\%$ and was measured by a thermocouple situated in the die near the aperture. The constant pressure mode of operation was used and the total time for an extrusion experiment was approximately two hours including the preliminary heat-treatment period.

Eight extrusion experiments were carried out with this composition;

Run	Extrusion Temp °C.	Load Kg.	Time mins.
1	840	900	120
2	820	900	120
3	800	2500	150
4	880	130	180
5	880	80	90
6	850	800	120

Table 8.1 The total experimental time, the temperature and the load at which samples of glass-ceramic A were extruded.

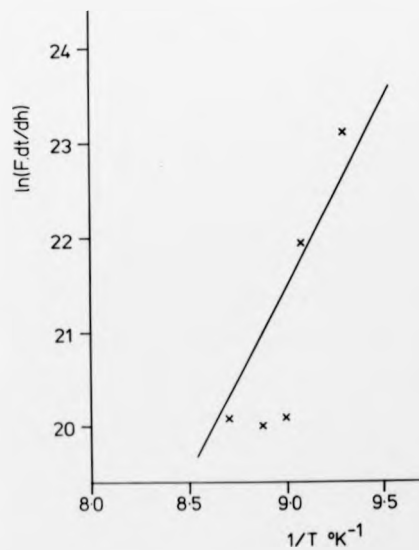


Figure 8.1 The variation of $\ln \left(F \cdot \frac{dt}{dh} \right)$ with the inverse of the absolute temperature for the extrusion of glass-ceramic A.

of these, six were considered to be successful. An experiment was considered unsatisfactory when less than 2 cm. of material was extruded or the extruded material was too fluid and necking occurred.

Table 8.1 shows the total experimental time, the temperature and the load at which samples of glass-ceramic A were extruded. The microstructure and physical properties of the extruded material of this composition were studied in detail.

During an extrusion experiment, the rate of descent of the plunger and the temperature of the die were monitored every two minutes. From a consideration of Equation 5.1 it can be seen that the rate of descent of the plunger (dh/dt), is related to the applied load on the plunger F , by:

$$\frac{dh}{dt} \propto \frac{F}{\eta}$$

where η is the viscosity of the extruding material. If this equation is combined with Equation 5.3 then:

$$\exp\left(\frac{E_{\eta}}{RT}\right) \propto F \cdot \frac{dt}{dh}$$

where T = absolute temperature of the material

E_{η} = activation energy for viscous flow.

Figure 8.1 is a plot of $\ln\left(F \cdot \frac{dt}{dh}\right)$ versus the inverse of the absolute temperature for the extrusion of glass-ceramic A; the gradient of the line evaluated by a least squares fit of the data provides a measure of the activation energy:

$$E_{\eta} (\text{glass-ceramic A}) = (79 \pm 28) \text{ kcal/mole.}$$

In the extrusion of this glass-ceramic through the die, the diameter of the product was the same as that of the die aperture; the surface of the extruded rod was smooth and no evidence was found of the die material diffusing into the glass-ceramic.

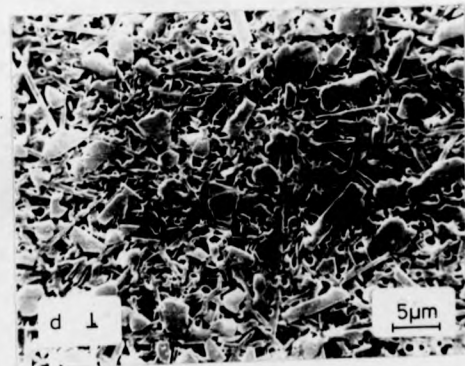
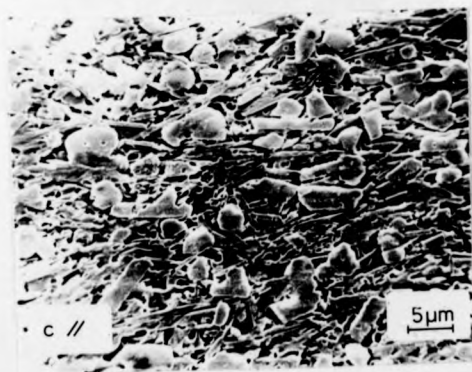
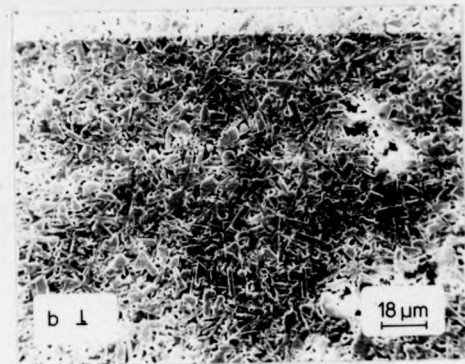
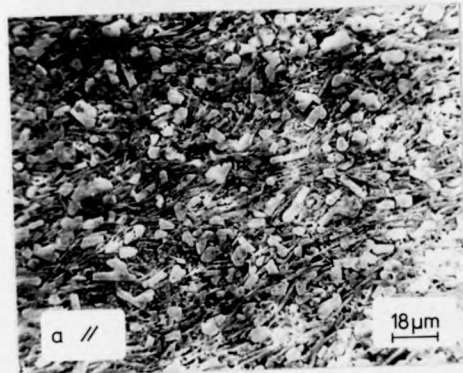


Figure 8.2 A series of SEM micrographs of sections parallel and perpendicular to the extrusion axis of various specimens of glass-ceramic B.

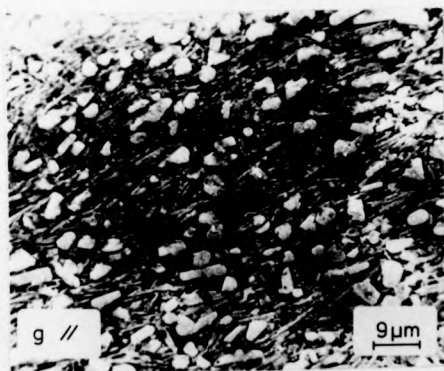
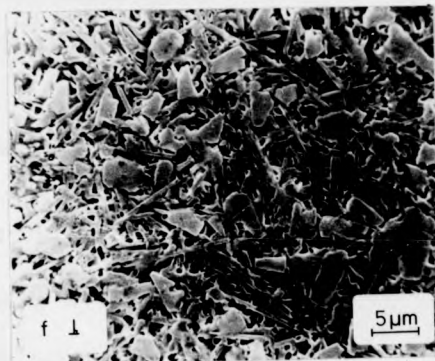
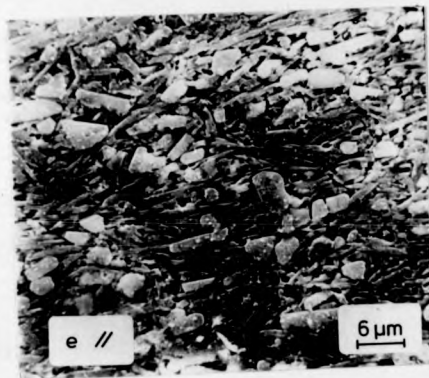


Figure 8.2 A series of SEM micrographs of sections parallel and perpendicular to the extrusion axis of various specimens of glass-ceramic B.

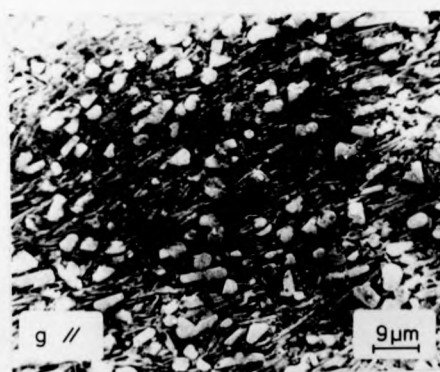
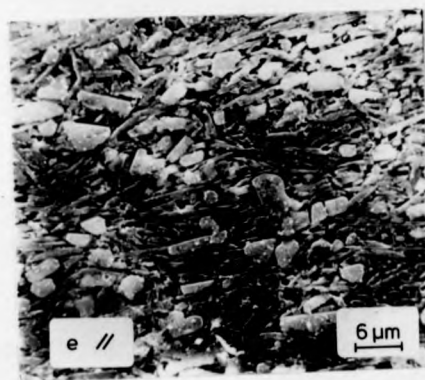


Figure 8.2 A series of SEM micrographs of sections parallel and perpendicular to the extrusion axis of various specimens of glass-ceramic B.

8.2.3 Extrusion of Glass-Ceramic B

Glass-ceramics devitrified from glass B were also extruded. In this case approximately 7 cm of extruded material was produced in 90 minutes; the total time for these experiments, including the initial heat-treatment stage was approximately 2 hours.

It was found that this composition could be extruded with the present apparatus in the approximate temperature range 840°C - 900°C where the viscosity of the material was between 10^{11} poise and $5 \cdot 10^9$ poise.

Figure 8.2 is a series of scanning electron micrographs of sections parallel and perpendicular to the extrusion axis of various specimens of glass-ceramic B. From these micrographs it can be seen that there is a preferred orientation of the crystalline phases parallel to the extrusion axis (Figures 8.2(a) and (c)). Preliminary analysis of the microstructure showed that this morphological orientation was a maximum at the surface of the extruded rod and that the degree of orientation of the crystals was independent of the quantity of material extruded. Sections perpendicular to the extrusion axis showed no preferred crystal orientation (for example Figures 8.2(b) and (d)).

The second crystalline phase of tridymite has produced localised disturbances in the flow of the material which has resulted in an inferior alignment of the lithium disilicate phases in these regions. (Figures 8.2(g) and (h)). This effect is a consequence of the different dimensions of the two crystal phases and is analogous to the flow of different size logs down a river.

In all the samples of glass-ceramic B extruded, a cylindrical shaped region concentric with the extrusion axis, of a single crystal phase was observed surrounded by a glass-ceramic of two crystalline phases. The former region consisted of a block-like crystal structure of the same

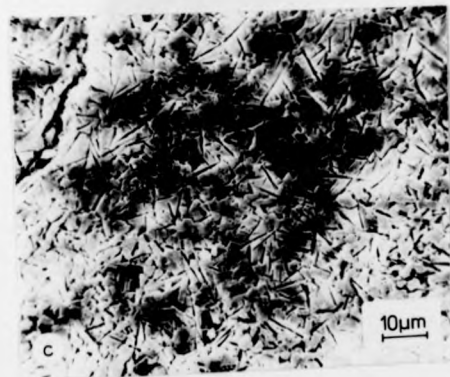
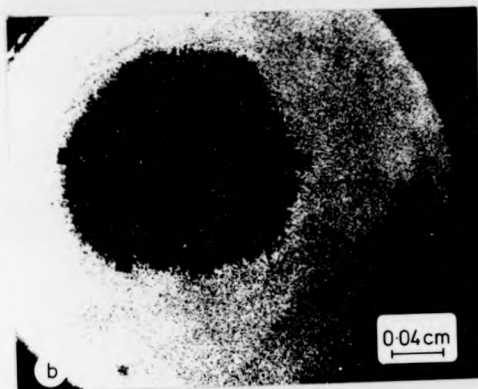
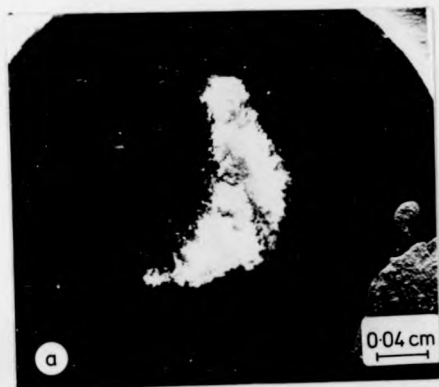


Figure 8.3 SEM micrographs of an extruded specimen of glass-ceramic B perpendicular to the axis: (a) secondary electron mode; (b) cathodoluminescence mode of (a); (c) the microstructure of the central region in (a) and (b).



Figure 8.4 Sections parallel to the extrusion axis of glass-ceramic B:
(a) secondary electron mode and (b) the cathodoluminescence
mode of the area in (a).

morphology as that which was formed by heat-treating samples of glass B at 950°C. The material cladding this cylindrical region had the same crystal morphology as control specimens heat-treated at the extrusion temperature. This phenomenon can be clearly seen in low magnification micrographs of sections perpendicular (Figure 8.3) and parallel (Figure 8.4) to the extrusion axis. Figure 8.3(a) shows this second crystalline phase in the secondary electron mode of the scanning electron microscope; the region can be clearly distinguished using the cathodoluminescence mode (Figure 8.3(b)). The small dark regions in this micrograph are areas that had been previously irradiated during examination at higher magnification (Chapter 4 contains details of the decay with time of the cathodoluminescence intensity). The microstructure of the central region in Figure 8.3(a) and (b) is shown in Figure 8.3(c) and that of the outer "cladding" material in Figure 8.2(d). A similar contrast can be seen in sections parallel to the extrusion axis (Figure 8.4(a) and (b)).

The boundary between these two glass-ceramic phases is very sharp and an analysis of SEM micrographs of sections cut parallel and perpendicular to the axis showed that this boundary was defined approximately by rotating a parabola about the extrusion axis. The apex of this paraboloid of revolution points in the direction of extrusion; it should be noted that a similar parabolic boundary was observed when a billet consisting of alternate layers of glass-ceramic and cupric oxide was extruded. (cf. Figure 5.9).

The extruded rods of glass-ceramic B which are composed of an inner and outer region of different crystal morphologies are believed to be a consequence of the temperature gradient in the extrusion die. This temperature gradient is caused by convection currents and asymmetries introduced into the system by the non-uniform RF heating of the die.

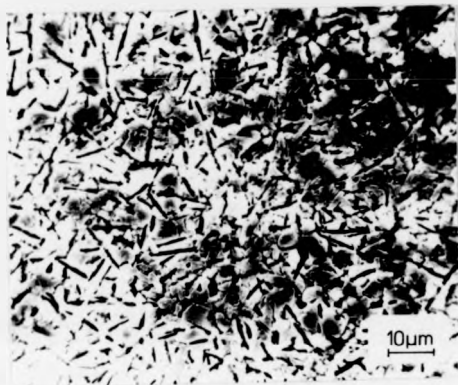


Figure 8.5 The morphology parallel to the extrusion axis in the "core" of an extruded specimen of glass-ceramic B.

When the initial glass billet is heat-treated prior to extrusion a glass-ceramic with layers of different crystalline phases will result; the uppermost layer will contain a high temperature crystalline phase and the bottom layer, the crystalline phases corresponding to the heat-treatment temperature. Between these two layers there will exist a transition region. The glass-ceramic which is then extruded consists of layers of different crystal morphologies and extruding this, results in an effect which is identical to that observed in determining the flow of material in the die (Chapter 5).

The crystals in the "core" of the extruded rod have a non-unitary aspect ratio but no morphological orientation was detected; it is believed that this is caused by the small volume fraction of glass phase present in this glass-ceramic material. The resulting morphology parallel to the extrusion axis (Figure 8.5) indicates that the structure is "locked tight" similar to a log-jam in the river and logs analogy. In the outer cylindrical region of the extruded rods where the crystal phases of lithium disilicate and tridymite are present, the former phase is aligned parallel to the extrusion axis.

In all the specimens examined in the scanning electron microscope no crystals were observed which were broken or could have been broken by the extrusion process. This implies that the crystals which are aligned can move in the glass matrix and that any stress concentrations resulting from crystal-crystal interactions are relieved by the relatively fluid glass matrix.

8.2.4 General Conclusions on the Extrusion of Glass B

The hot extrusion of glass B did not produce a glass-ceramic with an aligned crystal microstructure throughout the material. At all the temperatures at which the material was extruded, a high temperature

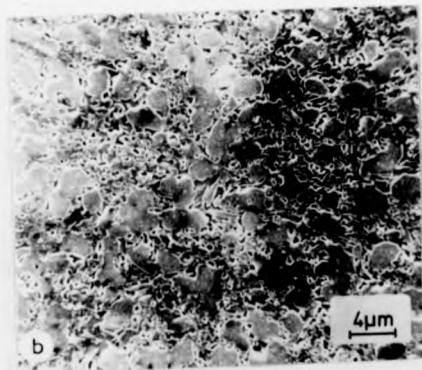
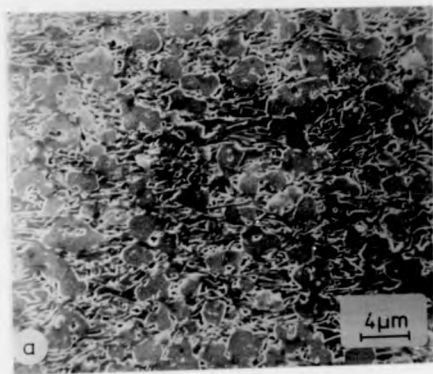


Figure 8.6 Typical SEM micrographs of Extrusion Run 7: (a) parallel and
(b) perpendicular to the extrusion axis.

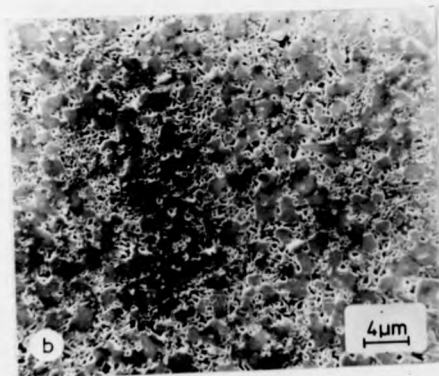


Figure 8.7 Typical SEM micrographs of Extrusion Run 2: (a) parallel and
(b) perpendicular to the extrusion axis.

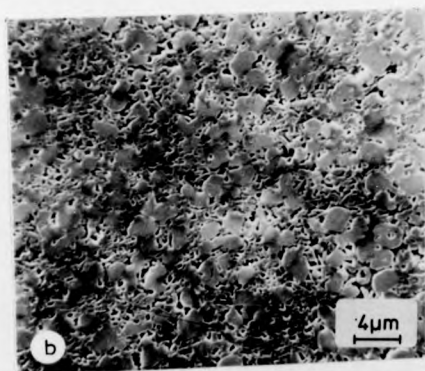
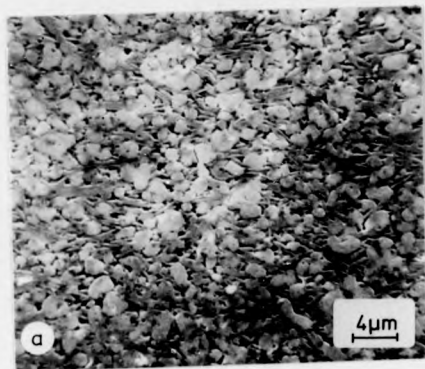


Figure 8.8 Typical SEM micrographs of Extrusion Run 3: (a) parallel and (b) perpendicular to the extrusion axis.

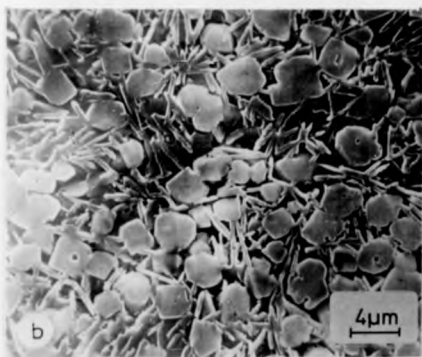
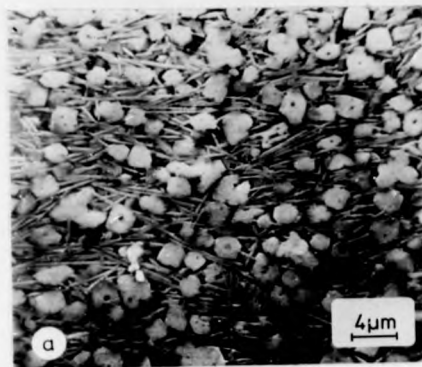


Figure 8.9 Typical SEM micrographs of Extrusion Run 4: (a) parallel and (b) perpendicular to the extrusion axis.

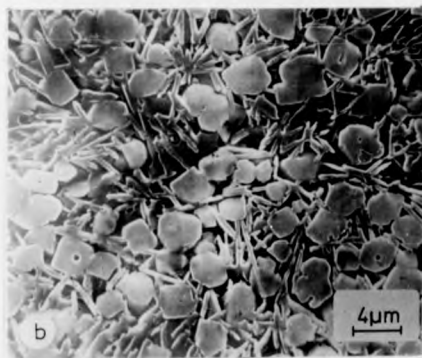
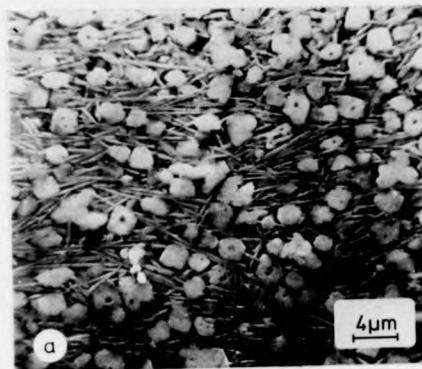


Figure 8.9 Typical SEM micrographs of Extrusion Run 4: (a) parallel and (b) perpendicular to the extrusion axis.

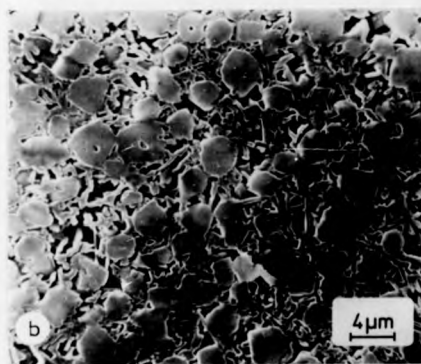
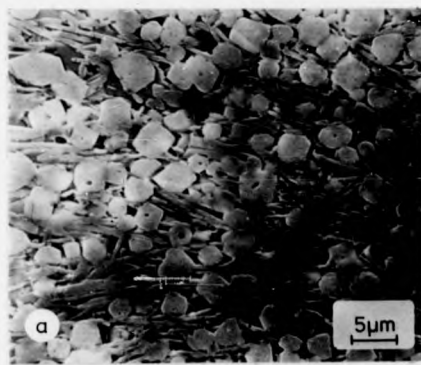


Figure 8.10 Typical SEM micrographs of Extrusion Run 5: (a) parallel and (b) perpendicular to the extrusion axis.

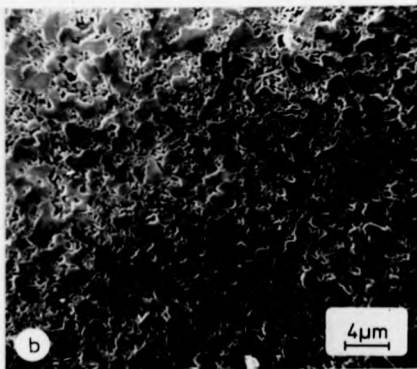
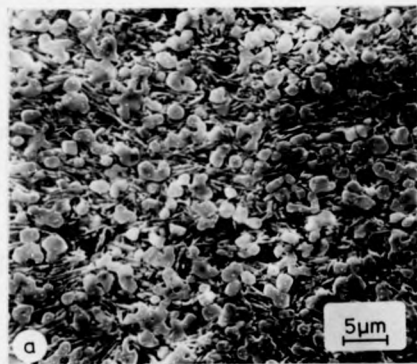


Figure 8.11 Typical SEM micrographs of Extrusion Run 6: (a) parallel and (b) perpendicular to the extrusion axis.

crystalline phase was present in the centre of the extruded rod. This cylinder of material was surrounded by a tube of glass-ceramic material with an aligned microstructure.

The physical properties of the resulting material were not investigated because of the presence of this high temperature crystal phase which would complicate the interpretation of these results. The extrusion of glass B was discontinued because of the above considerations.

8.3 The Microstructure of Extruded Specimens of Glass-Ceramic A

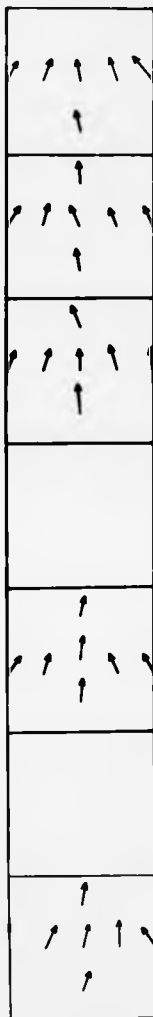
8.3.1 Introduction

Figures 8.6-8.11 are typical micrographs of the structure produced by extruding glass-ceramic A; Figure 8.6(a) and (b) are of sections respectively parallel and perpendicular to the extrusion axis of Extrusion Run 1. The notation of the figures is such that Figure 8.11 corresponds to Extrusion Run 6 in Table 8.1

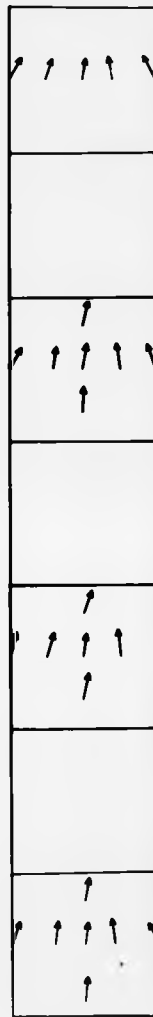
From these micrographs it can be seen that ~~at~~ all the temperatures at which extrusion was carried out, the resulting glass-ceramic contained two different crystal morphologies. X-ray diffraction of powdered specimens of each sample showed that lithium disilicate and tridymite crystalline phases were present. The needle-shaped disilicate phase is morphologically oriented parallel to the extrusion axis and in the cases where the tridymite crystals have a non-unitary aspect ratio, these show a similar orientation. The shape and volume fraction of the tridymite crystals varies with the length of time of the extrusion experiment and the extrusion temperature and pressure.

In all the areas of the extruded specimens examined at high magnification a marked difference was evident between the parallel and perpendicular sections of the material. The micrographs indicate that the tridymite crystal phase, which in some cases occupies a greater volume fraction than the disilicate phase, produces an inferior alignment.

Run 1



Run 2



Run 3

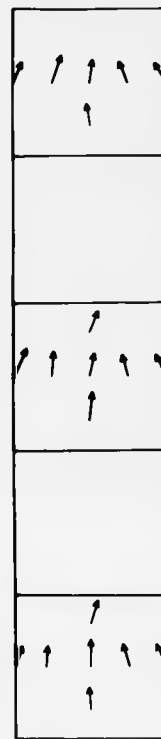


Figure 8.42 The angular distribution function determined in a number of places on sections parallel to the extrusion axis of specimens of glass-ceramic A.

Run 4

Run 5

Run 6

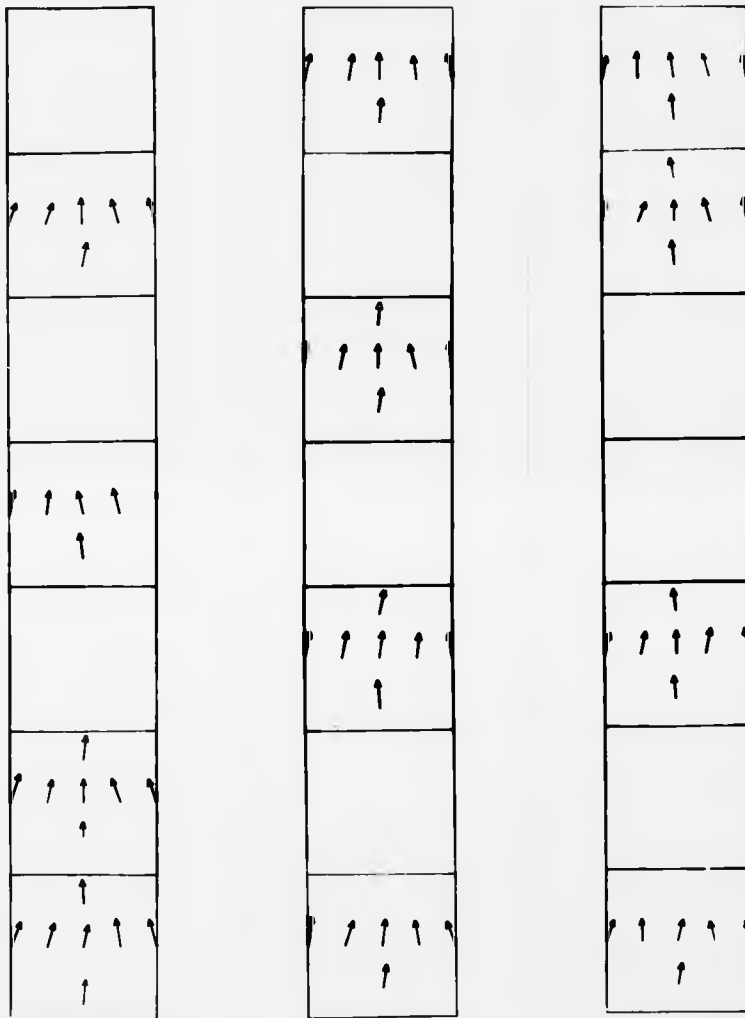


Figure 8.12 The angular distribution function determined in a number of places on sections parallel to the extrusion axis of specimens of glass-ceramic A.

8.3.2 Statistical Analysis of the Morphological Orientation

The variation of the microstructure with position in the extruded rod was analysed statistically in terms of the volume fraction of the crystalline phases, the mean crystal-crystal spacing and the degree of orientation of the crystals. Chapter 6 contains the details of the methods used to determine these parameters. No distinction was made in this analysis between the two different crystal phases present in the material and the numbers describing the microstructure were evaluated on sections parallel and perpendicular to the extrusion axis.

The angular distribution function was determined in a number of places on sections through and parallel to the extrusion axis; these data are represented in Figure 8.12 by vectors drawn on a schematic diagram of these sections. The end-point of each of these vectors is at the approximate position of the area which was analysed and it points in the direction of the maximum value of the angular distribution curve. The magnitude of the vector is inversely proportional to the width of the distribution function.

It is evident from these diagrams that the extruded glass-ceramic contains an aligned crystal microstructure, the magnitude of which is independent of the quantity of material which is extruded. This orientation is symmetric about the axis of the rod and the direction of the vectors in Figure 8.12 suggests that the maxima in the distribution curves are tangents to parabolas drawn on the sections. This concept of parabolas is consistent with the Hagen-Poiseuille flow of a Newtonian fluid down a tube (Chapter 5 contains details of this). The minimum value of the angular spread of the long axes of the crystals with the extrusion axis in the material was found to be 40° and the maximum was 60° . In the present work a randomly oriented specimen is defined as one which has an angular spread of 180° . The largest degree of orientation (which corresponds to the minimum angular spread) was found to be at the surface of the material where the greatest flow velocity

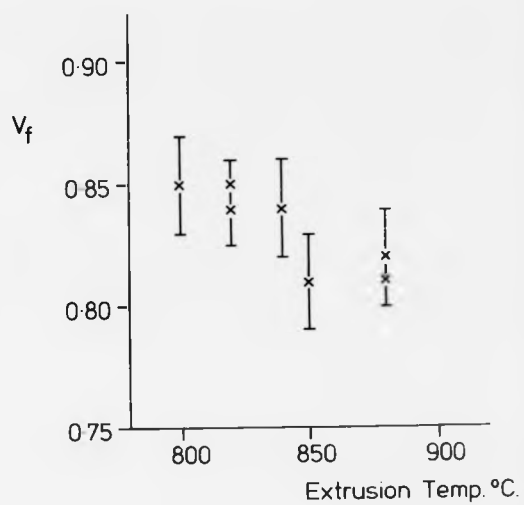


Figure 8.13(a) The variation of the volume fraction V_f , with the extrusion temperature.

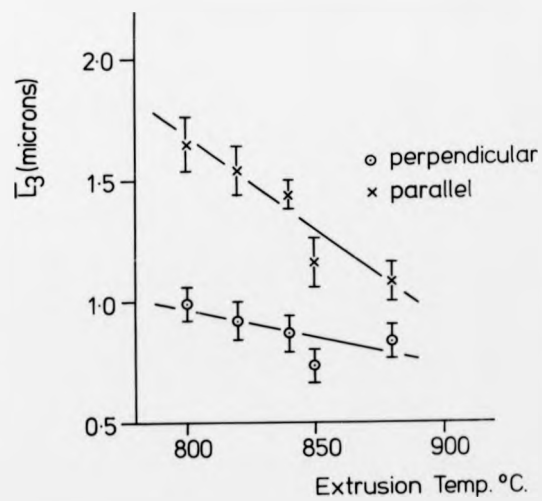


Figure 8.13(b) The variation of the mean crystal size \bar{L}_3 , with the extrusion temperature.

gradient exists; the smallest degree existed in the centre of the extruded rod. Sections perpendicular to the extrusion axis had a randomly oriented microstructure.

It can be tentatively concluded from this analysis that the crystals in the material are aligned in directions which correspond with tangents drawn to the velocity flow profile of the extruded material.

In the six extrusion experiments which were analysed statistically the volume fraction V_f , of both crystal phases was determined from the micrographs analysed in the evaluation of each angular distribution curve. The variation of this parameter with the extrusion temperature is shown in Figure 8.13(a); it can be seen from this curve that the volume fraction slowly decreases with the increasing extrusion temperature. The mean crystal-crystal spacing in this material was measured in directions parallel and perpendicular to the extrusion axis and was found to be constant for the six samples analysed. In the radial direction it had a value of:

$$\lambda_R = 0.17 \pm 0.03 \mu\text{m}$$

and parallel to the extrusion axis:

$$\lambda_p = 0.28 \pm 0.04 \mu\text{m}.$$

The difference between these values is a reflection of the different pressure gradients which exist in the material whilst it is being extruded.

No radial or axial length dependence of the volume fraction or mean crystal spacing was detected in the six samples which were extruded at different temperatures and applied punch pressures. It can be deduced from this that little or no further crystal growth occurs in the glass-ceramic material during the extrusion process. The variation in the mean crystal size \bar{L}_z , with the extrusion temperature is shown in Figure 8.13(b); in this graph the lengths of the crystals were evaluated in directions parallel and perpendicular to the extrusion axis. At a given extrusion

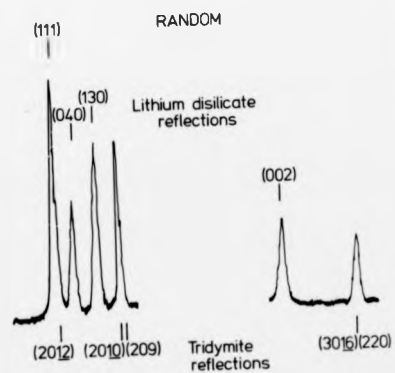
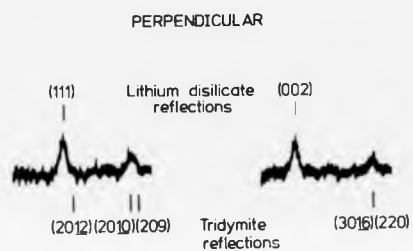
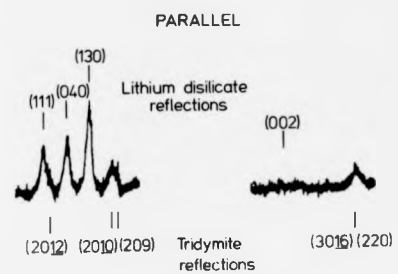


Figure 8.14 Part of the reflected X-ray intensity of specimens cut
 (a) parallel and (b) perpendicular to the extrusion axis;
 (c) is the intensity from a specimen with a random
 arrangement of crystals.

temperature the ratio of these two lengths is the mean aspect ratio of the crystals present in the glass-ceramic; if this ratio has a value of one then the crystals are isometric. It should be noted from this graph that this ratio is a decreasing function of the extrusion temperature.

8.3.3 Determination of the Crystallographic Orientation

Rindone (1) has measured a preferred crystallographic orientation of lithium disilicate crystals in the surface of a glass-ceramic specimen using an X-ray technique. The crystals formed with their (002) planes parallel to the surface. In the bulk of the material the crystals were randomly oriented.

Donnay and Donnay (2) have studied the crystal geometry of lithium disilicate and found it to be orthorhombic; the crystals consist of {010} plates, elongated along the $[001]$ direction.

In the present work the crystallographic orientation of the lithium disilicate crystals in the extruded specimens was determined by an X-ray diffraction technique.

Polished and lightly etched specimens cut parallel and perpendicular to the extrusion axis were irradiated with a Cobalt K_{α} beam of X-rays and the reflected intensity was recorded. A standard two circle diffractometer was used for these experiments and the samples were mounted in an amorphous cold mounting resin ("Specifix" was found to be suitable).

The intensity of the (hkl) reflections was measured relative to that from the (111) planes of the lithium disilicate phase in each sample; this procedure was adopted so that specimens of different size areas could be compared.

Figures 8.14(a) and (b) are part of the reflected X-ray intensity from specimens cut parallel and perpendicular to the extrusion axis.

(hkl)	Random $I_{(hkl)}/I_{(111)}$	Parallel $I_{(hkl)}/I_{(111)}$	Perpendicular $I_{(hkl)}/I_{(111)}$
(111)	100	100	100
(130)	~ 60	~ 200	v.weak
(040)	~ 50	~ 150	v.weak
(002)	~ 30	v.weak	~ 80

Table 8.2 The intensity of the (hkl) reflections measured relative to that of the (111) reflection for the lithium disilicate crystal phase in the extruded specimens.

The diffracted intensity from a specimen with a random arrangement of crystals is shown in Figure 8.14(c); the Bragg reflections from this specimen are more intense because a larger area of the sample was irradiated compared with the extrusion samples.

A comparison of these three figures shows that the (040) and (130) reflections from the lithium disilicate phase are missing from the specimen cut perpendicular to the axis. In the case of the parallel samples the (002) reflection is very weak or non-existent. The (002) plane is referred to rather than the (001) since the latter reflection did not appear in the X-ray pattern. It must also be noted that for this crystal phase the values of the reflected intensity from the (hkl) planes relative to that from the (111) planes are different for the random and extruded samples; in particular this ratio for the (130) reflection from the parallel extruded sample is approximately three times the value obtained for the random specimens.

The reflected intensities associated with the tridymite crystal phase are independent of the orientation of the section from the extruded specimens; the relative values of these intensities show little difference to those obtained for the random specimens.

Two samples from each extruded glass-ceramic A specimen were analysed using this technique; the diffraction patterns obtained showed no dependence upon the position the section was cut from the length of the extruded rod.

The intensity of the (hkl) reflections measured relative to that of the (111) reflection for the lithium disilicate crystal phase are summarised in Table 8.2. From a consideration of these data it can be deduced that the disilicate crystals are crystallographically aligned with the [001] direction parallel to the extrusion axis; the tridymite crystal phase shows no crystallographic orientation.

8.3.4 Comments on the Microstructure of the Extruded Glass-Ceramic

The results obtained from the statistical analysis of the microstructure of the extruded specimen indicate that the crystal phases in the material are morphologically aligned with their major axes parallel to the extrusion axis.

The X-ray diffraction experiments showed that the lithium disilicate phase was also oriented with its c crystallographic axis parallel to the extrusion axis; however, the material has no bulk preferred orientation with respect to the a or b directions in this crystal.

A study of the surface crystallisation in the control specimens of glass-ceramic A showed that the lithium disilicate crystals were formed with their (002) planes parallel to the surface; the long axis of the crystal being the [001] direction. This data correlates with the determination of the major axis of the disilicate phase in the extruded specimens using X-ray and scanning electron microscopy techniques.

It must be noted that the statistical analysis was carried out on micrographs of small areas of the material whereas in the X-ray diffraction experiments all of the section of the extruded specimen was used. It can be concluded from this that the extruded material exhibits a bulk orientation of the lithium disilicate crystal phase.

8.4 The Density of the Extruded Material

The density of the extruded specimens was measured and found to be a constant within experimental error for the six extruded samples; it had an average value of:

$$\rho = 2.65 \pm 0.01 \text{ gms/cc.}$$

This is approximately 10% higher than the density measured for the control specimens of this glass-ceramic ($\rho = 2.417 \pm 0.003 \text{ gms/cc}$).

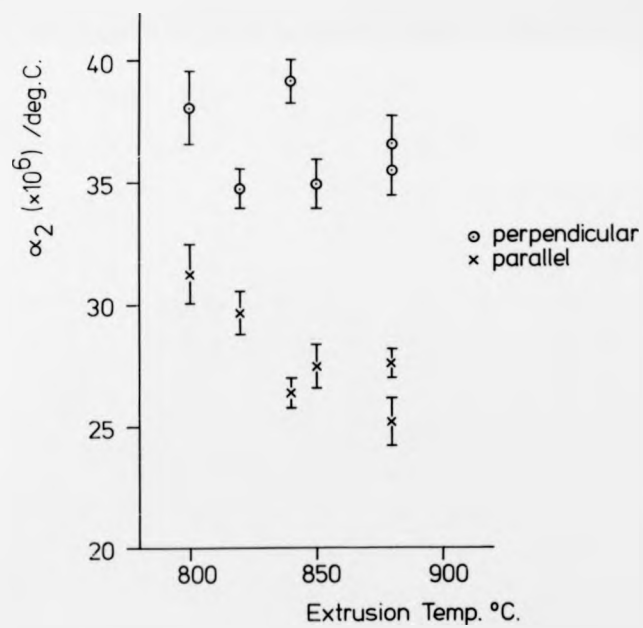
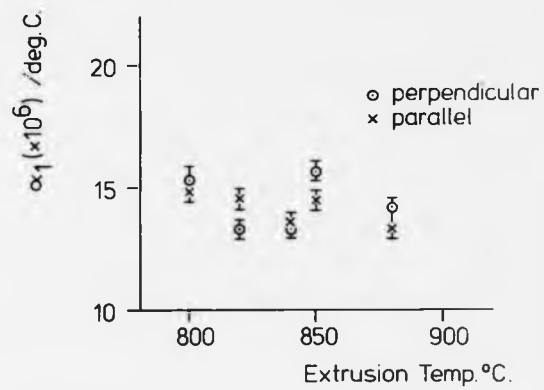


Figure 8.15 The variation with the extrusion temperature of (a) the low temperature expansion coefficient α_1 , and (b) the high temperature coefficient α_2 .

In both the extruded and control materials the volume fraction of the crystalline phases was approximately 85% and the observed increase in the density is believed to be associated with a densification of the glass phase during the extrusion process. It must be noted however, that the density showed no variation with the extrusion pressure.

8.5 The Coefficient of Thermal Expansion of the Extruded Material

8.5.1 Results

The coefficients of thermal expansion were evaluated for specimens of the extruded glass-ceramic in directions parallel and perpendicular to the extrusion axis. The expansion of each specimen was measured as a function of temperature and these data were corrected for the characteristic expansion of the dilatometer in the manner described in Chapter 3.

Each expansion curve for these samples showed two linear regions and an inflexion similar to that shown in Figure 7.11. In a technique analogous to the one used for the control specimens of glass-ceramic A (Chapter 7), the dilatometer was cycled and the expansion coefficients α_1 and α_2 were calculated from the linear parts of the corrected expansion-temperature curves. The temperature of the inflexion on this curve, T_{inflex} , was also measured. No systematic variation of α_1 , α_2 or T_{inflex} were noted with the dilatometer cycle; the average of the values obtained from cycling the dilatometer are quoted in this work.

The low temperature expansion coefficient α_1 , measured over the approximate temperature range (150 - 350)^oC is shown in Figure 8.15(a) as a function of the extrusion temperature. The values measured perpendicular and parallel to the extrusion axis are both shown in this graph and no differences exist between them.

The average value of α_1 measured for all the extruded samples in the two directions was found to be:

$$\alpha_1 \approx 14.0 \cdot 10^{-6} / \text{deg.C.}$$

The high temperature expansion coefficient α_2 , which was measured over the approximate temperature range (500-650) $^{\circ}$ C is shown as a function of the extrusion temperature in Figure 8.15(b). It can be seen from this graph that the extruded material expands more in a direction perpendicular to the extrusion axis than in the parallel direction for the same extrusion temperature. In the former case the expansion coefficient has a value:

$$\alpha_2 \text{ (perpendicular to axis)} \approx (35 - 40)10^{-6}/\text{deg.C.}$$

and measured parallel to the extrusion axis:

$$\alpha_1 \text{ (parallel to axis)} \approx (25 - 31)10^{-6}/\text{deg.C.}$$

The extruded material clearly has an anisotropic coefficient of thermal expansion measured in the temperature range (500-650) $^{\circ}$ C.

A measure of the degree of anisotropy D.A., can be evaluated by considering the ratio of the expansion coefficient in two perpendicular directions; for an isotropic system this ratio would be unity. The average value of D.A. for the extruded specimen of glass-ceramic A is:

$$\text{D.A.} = 1.32 \pm 0.05$$

The inflexion temperature T_{inflex} was found to be independent of the extrusion temperature and orientation of the dilatometer specimen:

$$T_{\text{inflex}} = (500 \pm 15)^{\circ}\text{C.}$$

This temperature is approximately the same as the inflexion temperature measured for the control specimens of glass-ceramic A (Figure 7.13(b)).

8.5.2 Comments on the Expansion Coefficient Results

The low temperature expansion coefficient α_1 , measured for the extruded specimens shows no anisotropy and is approximately a factor of three greater than the equivalent measurements on the control samples (Figure 7.13(a)). The high temperature expansion coefficient α_2 in the case of the control samples heat-treated in the range 800 $^{\circ}$ C - 900 $^{\circ}$ C had a value of:

$$\alpha_2 \text{ (random)} \approx 15.10^{-6}/^{\circ}\text{C.}$$

This is a factor of approximately two smaller than the equivalent measurements parallel to the extrusion axis and in the case of measurements perpendicular to this axis a factor of approximately $\frac{1}{2}$.

It is believed that the observed anisotropy is a consequence of the crystallographic orientation of the lithium disilicate crystals in the extruded material.

Glasser (3) has studied the coefficient of thermal expansion of sodium disilicate using a high temperature X-ray camera technique. Sodium disilicate is not isostructural with lithium disilicate but the two structures are very similar and might be expected to show similar thermal expansion values.

For $\alpha_{III} Na_2 Si_2O_5$ which is a phase stable up to approximately $700^\circ C$, the coefficients of thermal expansion show a marked thermal anisotropy. The a and c directions expand with rising temperature whilst the b direction contracts.

In the present work the extruded glass-ceramic which consisted of lithium disilicate crystals oriented parallel to their c-axis and a randomly oriented tridymite phase had a greater coefficient of expansion perpendicular to the c-axis than parallel to it. This material had no preferred orientation with respect of the a or b directions in the crystal and therefore independent expansion measurements of these two directions could not be made.

The glass phase in the extruded glass-ceramic could contain structural elements which exhibit a preferred orientation (4,5). This alignment would contribute to the anisotropy observed in the expansion coefficient α_2 ; however, it is thought that this effect is negligible because the temperature range over which α_2 was measured is greater than the dilatometric softening temperature of the parent glass (Chapter 7).

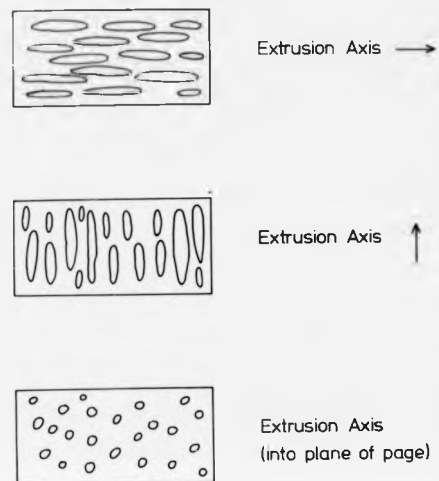


Figure 8.16 A schematic diagram of the orientation of the crystals in the three types of specimen prepared for the three point bend experiments.

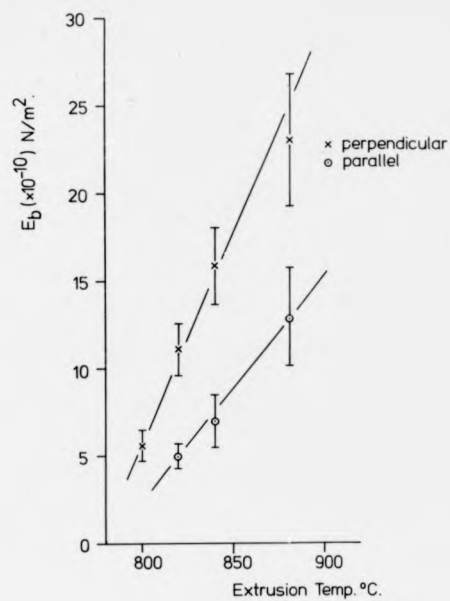


Figure 8.17(a) The variation of the Young's modulus E_b , with the extrusion temperature.

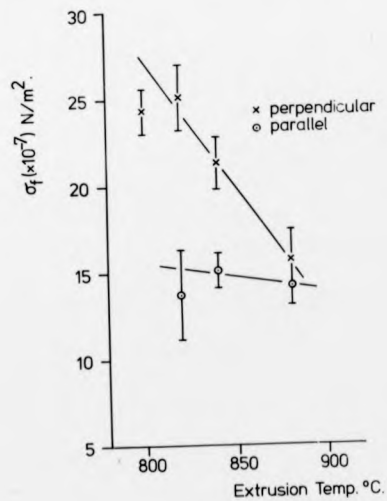


Figure 8.17(b) The variation of the rupture modulus σ_f , with the extrusion temperature.

8.6 Mechanical Properties of the Extruded Material

8.6.1 The Young's Modulus and Rupture Modulus

The Young's modulus in bending and the rupture strength were measured on samples of the extruded glass-ceramic prepared so that these moduli could be evaluated for three orthogonal orientations of specimens cut from the extruded rod. These three orientations correspond to three-point bend specimens prepared with their major axis parallel and perpendicular to the extrusion axis; in the latter case there are two possible orientations for the crystals. Figure 8.16 schematically shows the orientation of crystals in these three types of specimen.

The moduli measured on specimens prepared from the two orthogonal sections perpendicular to the extrusion axis were identical and in the following no distinction is made between these measurements.

Figure 8.17(a) shows the variation of the Young's modulus E_b , with the extrusion temperature for the two orientations of the specimens. From this graph it can be seen that the modulus is greater for specimens loaded perpendicular to the extrusion axis compared with parallel to this axis. The maximum value of the Young's moduli measured for the two loading directions relative to the extrusion axis were found to be:

$$\begin{aligned} E_b \text{ (max; perpendicular)} &= 23.10^{10} \text{ N/m}^2 \\ E_b \text{ (max; parallel)} &= 13.10^{10} \text{ N/m}^2 \end{aligned}$$

In this case the extrusion temperature was 880°C. Both of these values are greater than the maximum value observed for the control samples of glass-ceramic A which was:

$$E_b \text{ (max; control)} = 11.5.10^{10} \text{ N/m}^2$$

for a two hour heat-treatment at 760°C.

The variation in this modulus determined for the control specimens heat-treated between 800°C and 900°C (Figure 7.15) is similar to that of the extruded samples.

The degree of anisotropy D.A., for this property of the material has an average value of:

$$\text{D.A.} = 2.1 \pm 0.2$$

The variation of the rupture modulus σ_f , with the extrusion temperature for the two orientations of the applied load is shown in Figure 8.17(b). In this case also the modulus shows anisotropic properties having a greater rupture strength when loaded perpendicular to the extrusion axis. The maximum value of this modulus for the two loading conditions was found to be for an extrusion temperature of 820°C:

$$\begin{aligned}\sigma_f (\text{max; perpendicular}) &= 25 \cdot 10^7 \text{N/m}^2 \\ \sigma_f (\text{max; parallel}) &= 14 \cdot 10^7 \text{N/m}^2\end{aligned}$$

The rupture strength of a control specimen of this glass-ceramic heat-treated at a similar temperature for two hours was:

$$\sigma_f (\text{control}) \approx 16 \cdot 10^7 \text{N/m}^2$$

Control specimens of glass-ceramic A showed a similar variation of the rupture modulus with heat-treatment to that observed for the extruded samples (Figure 7.16).

The degree of anisotropy for the rupture modulus has a maximum value for an extrusion temperature of 820°C:

$$\text{D.A. (max)} = 1.8$$

8.6.2 Comments on the Moduli Measurements

The Young's Modulus and the rupture strength of the material were both found to be a function of the loading direction of the specimens relative to the extrusion axis. The material has a greater value for each of these moduli when loaded in a direction perpendicular to this axis.

This difference can be partly attributed to the different crystal-crystal spacings in the two directions in the extruded material.

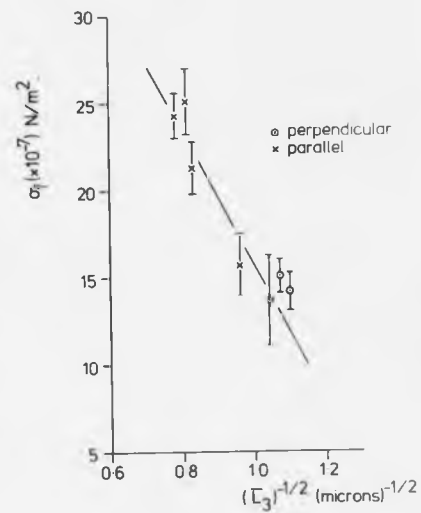


Figure 8.18(a) The variation of the rupture modulus with the inverse of the square root of the mean crystal size for the extruded material.

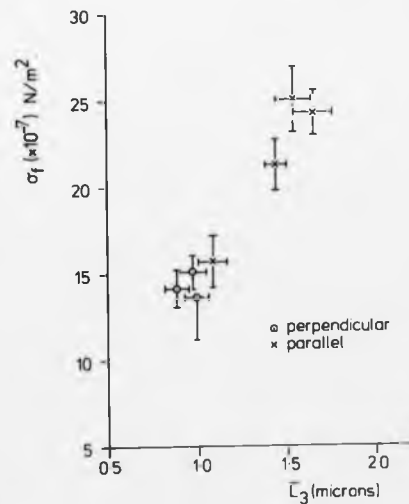


Figure 8.18(b) The variation of the rupture modulus with the mean crystal size for the extruded material.

However a statistical analysis of the microstructure showed that the mean spacing was approximately independent of the extrusion temperature whereas the measured moduli are a function of this temperature.

The elastic modulus E , of a two phase composite can be interpreted in terms of a law of mixtures where the modulus of each phase is weighted by a number proportional to the volume fraction of that phase (Chapter 7). In the case of the extruded specimens, the anisotropy observed in the Young's modulus cannot be understood in terms of this concept because the volume fraction is not a vector quantity, i.e. it is not associated with a direction in the material.

The variation in the rupture modulus with the extrusion temperature is very similar to the variation in the mean crystal size (Figure 8.13(b)). The mechanical strength of a polycrystalline material σ , can be related to the mean grain diameter d , by:

$$\sigma = k_1 d^{-\frac{1}{2}} \quad \text{Equation 7.2}$$

where k_1 is a constant (section 7.8.3).

Figure 8.18(a) is a graph of the rupture modulus against the inverse of the square root of the mean crystal size for the extruded material; in this graph the strengths measured in the two directions are shown. It can be seen from this that the rupture strength is related to the mean crystal size in the material; the gradient of this curve which is negative implies that as the grain size increases, the rupture strength increases.

Equation 7.2 is based on Griffith's flaw theory of fracture and also on the following assumption: when a tensile force is applied, a microcrack having a length nearly equal to the diameter of the crystal grain is first produced along a cleavage plane of the crystal and this crack penetrates into the neighbouring grains crossing the phase boundaries as a result of the stress concentrations at the crack tip; the crack finally propagates to produce entire fracture.

In a manner analogous to that used in Chapter 7, the surface energy for crack initiation, γ , can be calculated from the slope of k_1 of the graph shown in Figure 8.18(a) by means of:

$$\gamma \approx \frac{k_1^2}{E_b}$$

If the average value of the Young's modulus E_b ($\approx 15 \cdot 10^{10} \text{ N/m}^2$) is substituted into this equation then:

$$\gamma \approx 1 \text{ J/m}^2$$

It should be noted however, that a plot of the rupture strength against the mean crystal size in the extruded material indicates that a linear relationship exists between these two variables (Figure 8.18(b)). This dependence of the rupture modulus is probably a consequence of the stress concentrations between the phases and it is believed to be more fundamental than the rupture strength variation with the inverse of the square root of the mean particle size.

A further factor which controls the strength of a glass-ceramic is the mismatch of the thermal expansion coefficients of the phases present. The importance of these coefficients arises from the fact that the glass-ceramics were extruded at high temperature. As the extruded material cools, it reaches a temperature T_c , below which stress relaxation processes in the glass matrix are halted and on further cooling, stresses are built up in the matrix and crystals due to thermal expansion mismatch.

The stress in the matrix σ_T , due to a mismatch in the expansion coefficients is primarily a function of the parameter (6,7):

$$\sigma_T \approx (\bar{\alpha}_m - \bar{\alpha}_p) \Delta T E_m \quad \text{Equation 8.1}$$

where ΔT is the temperature decrease below T_c , $\bar{\alpha}_m$ and $\bar{\alpha}_p$ are the mean expansion coefficients of the matrix and crystalline phase respectively over that temperature range and E_m is the Young's modulus of the matrix at the final temperature. If this stress parameter is positive the

matrix is in compression and if it is negative the matrix is in tension; this assumes that the moduli of the crystal phase are greater than those of the glass matrix and that a strong bond exists between the two phases. It is possible that the local tensile stress in the matrix due to thermal mismatch can be greater than the matrix tensile strength; in this case the matrix will crack.

The exact functional dependence of the stress due to the mismatch in the expansion coefficients depends upon the interaction of stresses from all the crystals in the matrix and will therefore depend upon the geometry of the crystal arrangement, the elasticity of the crystals and the matrix, the glass-crystal bonding and on local stress concentrations. In the absence of an exact evaluation of this relationship only qualitative observations can be made using the calculated thermal stress parameters.

Equation 8.1 can be used to calculate the stress in the matrix in directions parallel and perpendicular to the extrusion axis if the following assumptions are made:

(i) The Young's modulus of the matrix E_m , is equal to the modulus of the parent glass:

$$E_m \approx E_{\text{GLASS}} \approx 5.10^{10} \text{N/m}^2$$

(ii) The expansion coefficient of the matrix $\bar{\alpha}_m$, is the same as that of the parent glass:

$$\alpha_m \approx \alpha_{\text{GLASS}} \approx 13.10^{-6} / \text{deg.C.}$$

(iii) The temperature T_C is equal to the dilatometric softening temperature M_g , of the parent glass:

$$T_C \approx M_g \approx 500^\circ\text{C.}$$

(iv) The expansion coefficient of the crystal in the extruded glass-ceramic $\bar{\alpha}_p$, is equal to the measured coefficients parallel and

perpendicular to the extrusion axis:

$$\bar{\alpha}_p \text{ (parallel to axis)} \approx (25-31) 10^{-6}/\text{deg.C.}$$

$$\bar{\alpha}_p \text{ (perpendicular to axis)} \approx (35-40) 10^{-6}/\text{deg.C.}$$

The third of these assumptions is doubtful since the dilatometric softening point corresponds to a viscosity of $10^{11} - 10^{12}$ poise (8). In the case of the extruded glass-ceramic this would correspond to a temperature of the same order as the extrusion temperature. If the above values are substituted into equation 8.1 then the stresses due to thermal mismatch in directions parallel and perpendicular to the extrusion axis are:

$$\sigma_T \text{ (parallel to axis)} \approx -4.10^8 \text{ N/m}^2$$

$$\sigma_T \text{ (perpendicular to axis)} \approx -6.10^8 \text{ N/m}^2$$

The rupture modulus of the parent glass σ_{GLASS} , was found to be (Chapter 7):

$$\sigma_{\text{GLASS}} \approx 10^8 \text{ N/m}^2$$

From these calculations it can be seen that in the two directions the matrix is in tension; furthermore this stress is anisotropic. However, it must be noted that these semi-quantitative calculations only take into account stresses arising from the mismatch in expansion coefficients. The presence of adjoining needle-shaped crystals with a greater thermal expansion coefficient than the glass matrix would also modify the stresses in the vicinity of a crystal. The net effect could be a compressive stress in a direction parallel to the extrusion axis whilst in a radial direction the stresses will be tensile. Therefore the stresses will be even more anisotropic than the above calculations indicate. In addition the pressure applied during the extrusion process will also impart to the material compressive stresses which will be anisotropic because of the nature of the deformation; if this is not the case then a comparison of the thermal stresses in the extruded material with the rupture modulus of

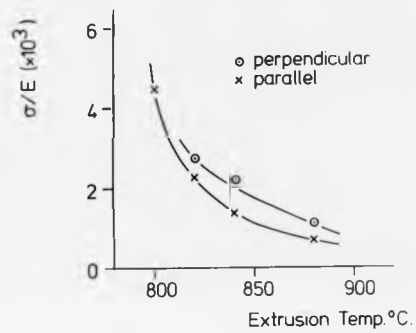


Figure 8.19 The strain at failure (σ/E_b), as a function of the extrusion temperature.

the parent glass suggests that the former would have cracked on cooling. No cracks were observed in the extruded rods.

It is proposed that the anisotropy in the rupture modulus is a reflection of the anisotropy in the internal stresses in the glass-ceramic. The dependence of the rupture modulus on the mean crystal size suggests however, that the Griffith flaws are located in the crystals or in the boundary between the glass and the matrix. The latter supposition is supported by the above calculations which suggest that anisotropic tensile stresses are located in the matrix of the bulk material. The net internal stresses in the extruded material will also be a function of the extrusion temperature and pressure.

Rossi (section 7.8.3) has shown that the Young's modulus of a composite containing a low concentration of dispersed phase is a function of the stress concentrations in the matrix. This theory is not directly applicable to the glass-ceramics studied in this work because of the high volume fraction of crystalline phases ($\sim 85\%$); however it is reasonable to assume that for a high concentration of crystalline phase the Young's modulus will be a function of the stress concentrations between the individual phases. This hypothesis would then explain the observed anisotropy in the Young's modulus in terms of the anisotropic nature of the internal stresses in the extruded material.

The strain at failure (σ/E_b), is shown as a function of the extrusion temperature in Figure 8.19 for the two directions in the extruded material. It can be seen from these curves that this parameter shows little dependence on the direction in which the specimen is loaded and that the strain decreases with increasing extrusion temperature. This behaviour is a consequence of the dependence on the extrusion temperature of the Young's modulus and rupture strength.

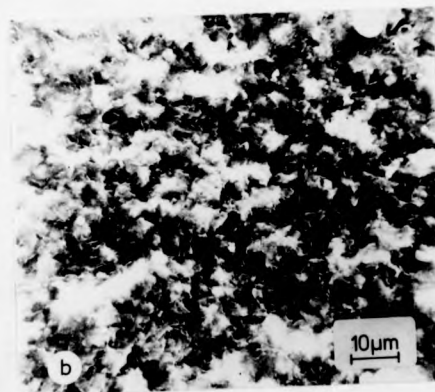
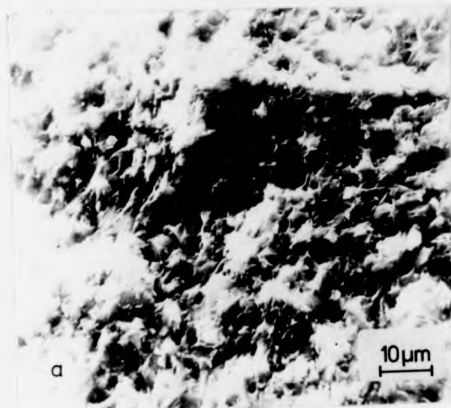


Figure 8.20 SEM micrographs of fracture surfaces (a) parallel and (b) perpendicular to the extrusion axis.

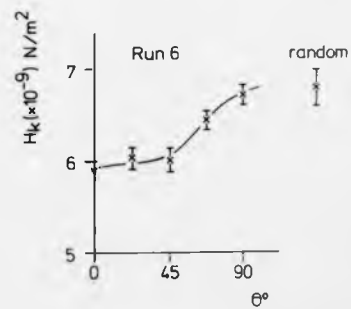
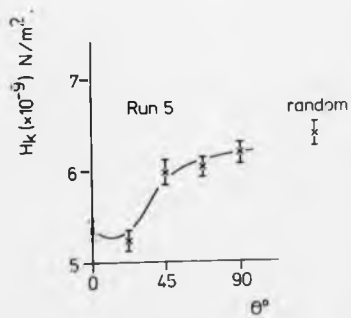
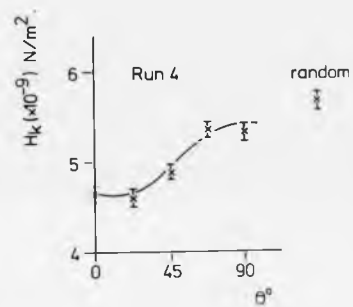
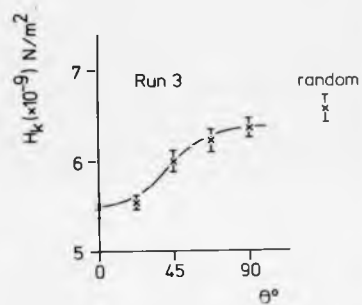
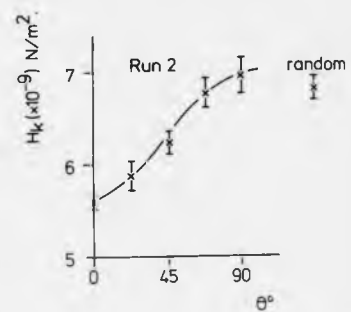
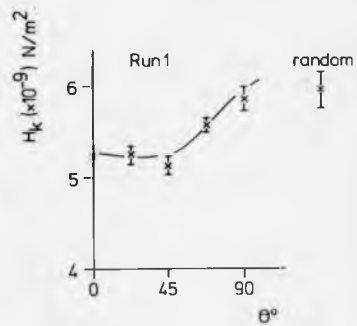


Figure 8.2: The variation of the Knoop hardness number H_k , with the indenter angle θ .

It is probable that fractures are propagated with greater difficulty in the extruded rod perpendicular to the axis, since a crack travelling through the material can be diverted or slowed down as it crosses the boundaries between the crystalline and vitreous phases. In a direction parallel to the extrusion axis the number of these interfaces is less.

Figures 8.20(a) and (b) are scanning electron micrographs of fracture surfaces parallel and perpendicular to the extrusion axis respectively. It is not possible to determine from these micrographs whether the crack front is transgranular or if it has been deflected by the glass-crystal boundaries.

It is interesting to note that the lowest values at the moduli measured for the extruded material are approximately the same as those of the control specimens. However, in a loading direction perpendicular to the extrusion axis the rupture modulus in one case is approximately 60% greater than that measured for the control sample.

8.6.3 The Knoop Microhardness

The Knoop hardness number H_K , was measured on polished sections of the extruded rod prepared parallel and perpendicular to the axis. On sections parallel to this axis the hardness was measured as a function of the angle θ , between the long axis of the indenter and the extrusion axis. When $\theta = 0^\circ$, the indenter was parallel to this axis and $\theta = 90^\circ$ perpendicular. Thirty indentations, evenly spaced across the specimen were made for each hardness evaluation.

The variation of the hardness with the indenter angle θ , for Extrusion Runs 1-6 is shown in Figure 8.21 (a-f). The value of the hardness measured on planes perpendicular to the extrusion axis is also shown.

The average value of the Knoop hardness for the six extrusion samples measured with the indenter parallel to and in the plane of the extrusion

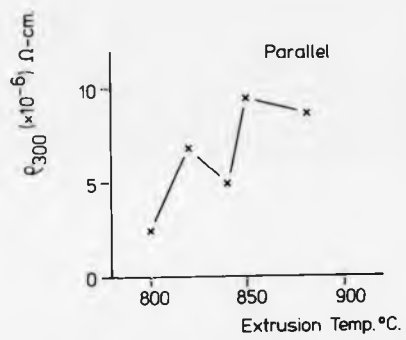
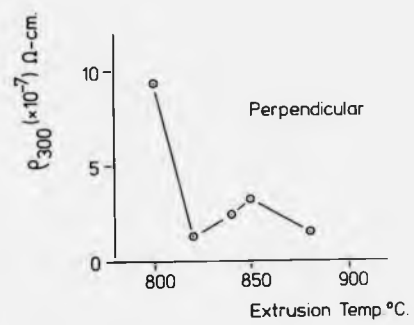


Figure 8.22 The variation of the resistivity at 300°C ρ_{300} , with the extrusion temperature.

axis was:

$$H_K (\theta = 90) = (6.3 \pm 0.3) 10^9 \text{N/m}^2$$

with the indenter perpendicular to the extrusion axis and in a plane parallel with this axis:

$$H_K (\theta = 0) = (5.4 \pm 0.2) 10^9 \text{N/m}^2$$

The hardness measured on planes perpendicular to the extrusion axis had an average value of:

$$H_K (\text{perpendicular to axis}) = (6.4 \pm 0.2) 10^9 \text{N/m}^2$$

and for the control specimens the average value of the Knoop hardness was:

$$H_K (\text{control}) \approx 5.5 10^9 \text{N/m}^2$$

In a manner similar to that described above a degree of anisotropy can be evaluated from the hardness numbers; in this case it has an average value for the six extruded samples of:

$$\text{D.A.} = 1.17 \pm 0.02$$

8.7 Electrical Properties of the Extruded Glass-Ceramic

8.7.1 Resistivity

The variation of the volume resistivity of the extruded samples with temperature was measured in directions parallel and perpendicular to the extrusion axis. For each extruded sample this data was fitted by a least squares method to an Arrhenius equation which was interpreted in terms of a pre-exponential constant $\ln A$, and an activation energy E . These two constants were found to be independent of the frequency of measurement and the average values are quoted in this work.

The resistivity at 300°C ρ_{300} , was calculated from the constants E and $\ln A$ and the variation of this quantity with the extrusion temperature is shown in Figure 8.22 for the two directions in the material. From this graph it can be seen that for all the extruded samples the resistivity measured perpendicular to the extrusion axis is greater than that measured

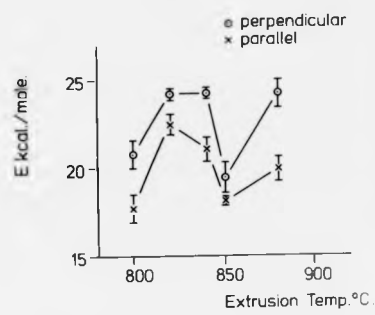


Figure 8.23(a) The variation of the activation energy E , with the extrusion temperature.

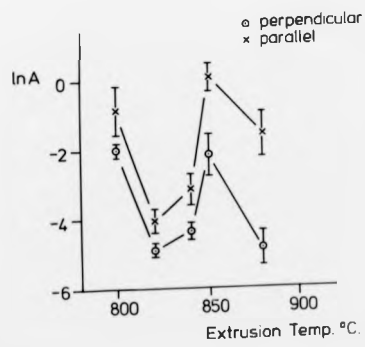


Figure 8.23(b) The variation of the pre-exponential constant $\ln A$ with the extrusion temperature.

parallel to it. A comparison of Figure 8.22 with Figure 7.22 which is the equivalent graph for the control specimens shows that the resistivity of the extruded material is generally lower than that of the control specimens over the same temperature range.

The degree of anisotropy calculated from the resistivity measurements varies between 1.8 for an extrusion temperature of 820°C and 38 (T = 800°C).

This anisotropy in the resistivity measurements is reflected in the variation of the activation energy E and the pre-exponential constant lnA with the extrusion temperature which is shown in Figures 8.23(a) and (b) respectively. The equivalent graphs for the control specimens are shown in Figures 7.23(a) and (b).

The activation energy measured for the extruded specimens is greater in a direction parallel to the extrusion axis than perpendicular; the position is reversed in the case of the pre-exponential constant lnA.

In a direction parallel to the extrusion axis the range of values of the resistivity (calculated for a temperature of 300°C) ρ_{300} , the activation energy E, and the pre-exponential constant lnA are:

$$\rho_{300} \text{ (parallel)} = (2 \text{ to } 10) 10^6 \Omega\text{-cm.}$$

$$E \text{ (parallel)} = (17.5 \text{ to } 22.5) \text{ kcal/mole.}$$

$$\ln A \text{ (parallel)} = - (0 \text{ to } 4)$$

and in a direction perpendicular to this axis:

$$\rho_{300} \text{ (perpendicular to axis)} = (1 \text{ to } 9.5) 10^7 \Omega\text{-cm.}$$

$$E \text{ (perpendicular to axis)} = (19.5 \text{ to } 24.2) \text{ kcal/mole.}$$

$$\ln A \text{ (perpendicular to axis)} = - (2 \text{ to } 5)$$

In the case of the control specimens heat-treated over the same temperature range these parameters had values of:

$$\rho_{300} \text{ (control)} = (5 \text{ to } 10) 10^7 \Omega\text{-cm.}$$

$$E \text{ (control)} = (24.5 \text{ to } 26.5) \text{ kcal/mole.}$$

$$\ln A \text{ (control)} = - (4 \text{ to } 4.5)$$

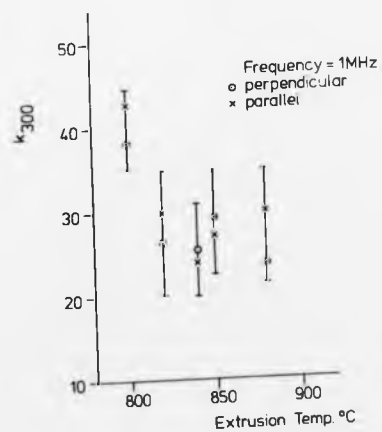
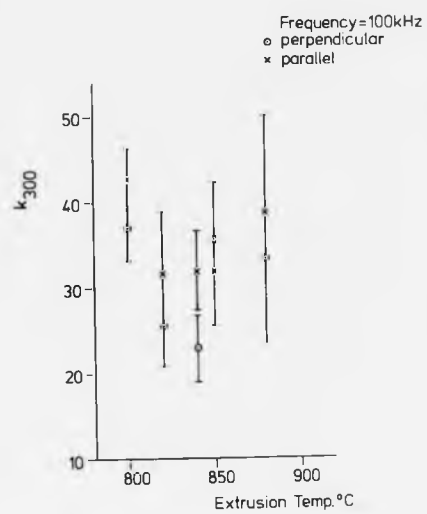


Figure 8.24 The variation of the dielectric constant at 300°C, k_{300} , with the extrusion temperature for frequencies of (a) 100 kHz and (b) 1 MHz.

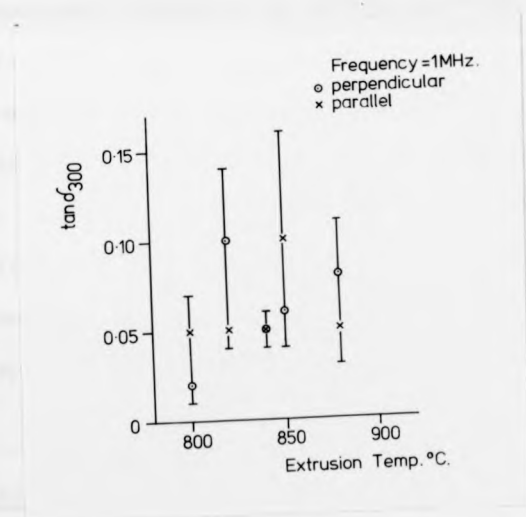
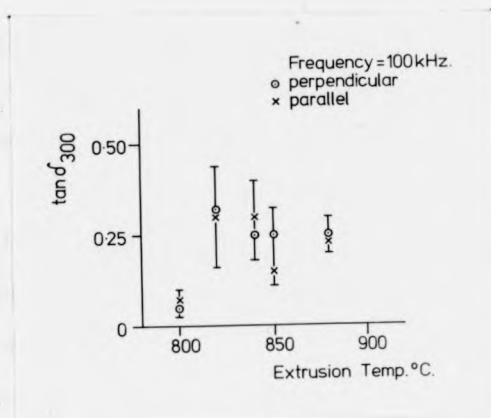


Figure 8.25 The variation of the loss tangent at 300°C, $\tan \delta_{300}$, with the extrusion temperature for frequencies of (a) 100 kHz and (b) 1 MHz.

8.7.2 The Dielectric Constant and Loss Tangent

The dielectric constant k , and the loss tangent $\tan \delta$, were measured as a function of temperature and this data was fitted to two equations of the form:

$$X = \alpha \exp (\beta T)$$

where X is the dielectric constant or loss tangent and T is the temperature. This procedure is identical to the one described in Chapter 7 for the treatment of these results. From the constants α and β in this equation the dielectric constant at 300°C , k_{300} , and the loss tangent at this temperature $\tan \delta_{300}$, were evaluated.

Figures 8.24(a) and (b) show the variation of k_{300} with the extrusion temperature for measurement frequencies of 100 kHz and 1M Hz respectively; similar graphs for $\tan \delta_{300}$ are shown in Figures 8.25(a) and (b).

The results obtained for these electrical properties in directions parallel and perpendicular to the extrusion axis show no anisotropy. A comparison between these data and the equivalent results for the control specimens (Figures 7.26 and 7.30) indicates that the magnitude of the dielectric constant k_{300} , and the loss tangent $\tan \delta_{300}$ are for the two materials approximately the same over the temperature range $(800 - 900)^{\circ}\text{C}$.

8.7.3 Comments on the Electrical Properties

The magnitude of the resistivity of the extruded materials is a function of the direction, relative to the extrusion axis, in which it is measured; it has a greater value perpendicular to this axis than parallel. The variation of the resistivity with the extrusion temperature (Figure 8.22) cannot be correlated with any similar variation in the mean crystal-crystal spacing in the material; however a comparison of Figures 8.22 and 8.13 shows that the resistivity has the same dependence as the mean crystal size on the extrusion temperature.

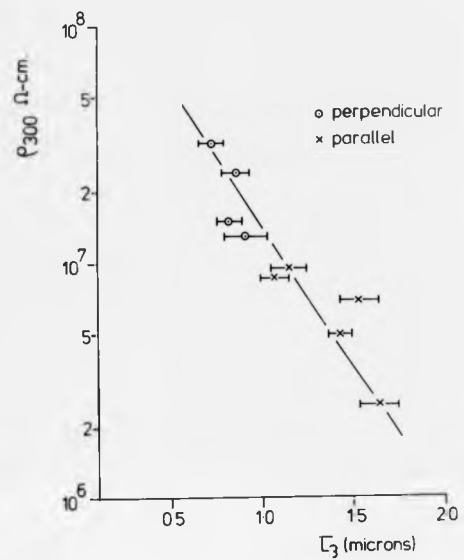


Figure 8.26 The variation of the resistivity with the mean crystal size of the extruded material in directions parallel and perpendicular to the axis.

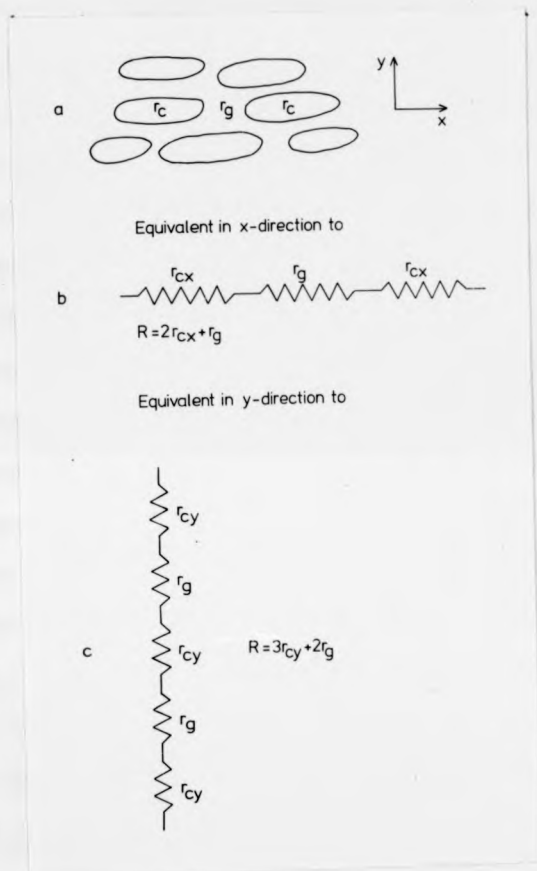


Figure 8.27 A schematic diagram of a two phase system in which the dispersed phase is aligned in a preferred direction.

Figure 8.26 shows the variation of the resistivity with the mean crystal size for directions perpendicular and parallel to the extrusion axis (n.b. the resistivity axis is a log. scale). From this graph it can be seen that there is a correlation between these two parameters. If the curve in Figure 8.26 is extrapolated to zero crystal size (i.e. no crystals in the glass-ceramic) then the resistivity at 300°C is greater than $10^8 \Omega\text{-cm}$. This is difficult to understand when it is noted that the resistivity at this temperature of the parent glass was five orders of magnitude less than that of the equivalent measurement on the control glass-ceramic (Chapter 7).

The resistivity of a single phase material is independent of the length of sample; however if the material is polyphase the net resistivity will be dependent upon the contributions from each phase. This can be seen from a consideration of Figure 8.27(a) which is a schematic diagram of a two phase system in which the dispersed phase is aligned in a preferred direction. The resistance of a length l of this material measured in the x -direction R_x , will be the sum of the contributions from the individual phases (Figure 8.27(b)); in this case:

$$R_x = 2r_{cx} + r_g$$

where r_{cx} = resistance of a single crystal in the x -direction
 r_g = resistance of the glass

Similarly the resistance of a length l , of this material measured in the y -direction R_y will be (Figure 8.27(c)):

$$R_y = 3r_{cy} + 2r_g$$

where r_{cy} = resistance of a single crystal in the y -direction

It is probable that for a real crystal:

$$r_{cy} \neq r_{cx}$$

Hence the resistance of the same length of material measured in the two directions is different.

If this model is applied to a glass-ceramic with an aligned crystal microstructure, the resistivity will be a function of the direction in which it is measured; in the case of a material with a random microstructure this effect will not exist.

It is believed that the ionic conduction in the extruded glass-ceramic depends not only on the size of the crystal grains but also upon the length of the conduction path in the glass phase. The mean crystal-crystal spacings for all the extruded samples were independent of the extrusion temperature and consequently any variation due to this effect is difficult to detect. However it should be noted that the resistivity measurements parallel and perpendicular to the extrusion axis (Figure 8.26) fall into two distinct groups which is believed to be caused not only by the crystal grain size but also by the different crystal-crystal spacings in the two directions.

Charles (9) has shown that the alteration in the structure of glass by hydrostatic pressure has an effect on the electrical properties analagous to the effect of the alteration of structure by heat-treatment. In a study of the electrical properties of a lime glass, Charles found that the resistivity increased with increasing applied pressure.

In the extruded glass-ceramic the stress concentrations arising from mis-matches in the thermal expansion coefficient of the individual phases have been shown to be anisotropic. It is probable that these stress concentrations will have produced structural changes in the glass phase; this would result in the resistivity of this phase being anisotropic.

The interpretation of the pre-exponential constant $\ln A$, has been discussed in Chapter 7; the anisotropy observed in this parameter is a reflection of the variation of the following parameters in the two

directions in the extruded material:

- (i) the concentration of mobile ions
- (ii) the jump mechanism of the ions
- (iii) the jump distance

These three factors will be different in the glass and crystalline phases and the total path length in each of these phases will be a function of direction in the extruded material. It is also very probable that each of these factors will be vector quantities in this material.

In order to relate the observed anisotropy in the values of the pre-exponential constant $\ln A$, and the activation energy E , with the structure of the extruded material it is necessary to have a clear physical understanding of what these constants represent. There has, however, been much theoretical discussion of this and the inter-relation and temperature dependence of these parameters (10-13). Such considerations are considered to be outside the scope of the present work in which these two parameters are used in a comparative type analysis. It should also be noted that there is no systematic variation of $\ln A$ and E with the extrusion temperature (Figure 8.23), which can be related to the results of the statistical analysis of the microstructure.

For a dielectric material consisting of a system of ellipsoids aligned parallel to their major axis and dispersed in a matrix of differing dielectric constant, the dielectric constant of the material will exhibit different values according as the electric field is parallel or at right angles to the major axis of the ellipsoids (14).

In the present work no anisotropy was measured in the dielectric constant for different directions in the extruded material. This is probably a consequence of the phases in the glass-ceramic having

approximately equal dielectric constants. However, it must be noted that the anisotropy in the dielectric constant of an oriented two phase material is not a very large effect and in the glass-ceramics studied the errors are very large for these measurements. A similar anisotropy can exist in the loss tangent $\tan \delta$, however, the errors in these measurements prevent any conclusions being made.

8.8 A Summary of the Properties of the Extruded Material

The main results of the property measurements of the extruded samples of glass-ceramic A are summarised in the following:

(i) Microstructure:

The extruded glass-ceramic consists of two crystalline phases of tridymite and lithium disilicate; the latter phase which is needle shaped is morphologically and crystallographically oriented parallel to the extrusion axis. The degree of orientation is independent of the quantity of material extruded and decreases in a radial direction from the surface to the axis of the extruded rod.

(ii) Thermal Expansion Coefficients:

The low temperature thermal expansion coefficient shows no anisotropy; the magnitude of the high temperature coefficient is greater when measured in a direction perpendicular to the extrusion axis; it is believed that this is a reflection of the anisotropy in the expansion coefficients of the lithium disilicate crystals in the material. The degree of anisotropy for this coefficient is 1.3.

(iii) Young's Modulus and Rupture Modulus:

Both these moduli are greater when the specimen is loaded perpendicular to the extrusion axis; the degree of anisotropy is approximately 2. The rupture modulus of the material is apparently

a function of the mean crystal size and the anisotropy in the Young's modulus is believed to be caused by stress concentrations in the extruded material.

(iv) Knoop Hardness Number:

The hardness number of the extruded material is greater when measured perpendicular to the extrusion axis; the degree of anisotropy is approximately 2. The maximum hardness value measured on a plane parallel to the axis is approximately equal to that measured on a perpendicular section.

(v) Electrical Properties:

The volume resistivity of the material is anisotropic; it is greater measured perpendicular to the extrusion axis. The degree of anisotropy varies between 1.8 and 38 for this property. The resistivity is apparently a function of the mean crystal size in the extruded specimens. The dielectric properties of the material show no anisotropy.

It would appear from these results that the electrical, mechanical and thermal expansion properties of the extruded material are functions of the stress concentrations in the glass-ceramic. The internal stresses in the control samples of this material will be locally anisotropic but when considered over a volume containing many glass-crystal interfaces, the stresses will be isotropic.

McMillan (15) has proposed that during the extrusion process a hydrostatic compression is applied to the glass-ceramic. The extent to which this is "frozen in" depends on the extrusion temperature and the magnitude of the compression applied. The lower the temperature the less is the possible relief of stress when the material emerges from the die; this stress will probably be anisotropic because of the nature of the process.

Furthermore this stress will be modified by a mismatch in the thermal expansion coefficients. The net effect is probably that there are axial compressive stresses and radial stresses that are either tensile or are compressive stresses of much lower magnitude. It seems likely that the net stresses are compressive in both directions but lower in a radial direction and lower for higher extrusion temperatures.

The strain at failure is higher for lower extrusion temperatures because these compressive stresses have first to be neutralised before tension can be applied to the system.

It is believed that the variation of the crystal size with the extrusion temperature leading to an apparent relationship of the form:

$$\sigma_f = k(d)^n$$

where k and n are constants, is coincidental and not of fundamental importance.

These considerations also affect the discussion of the variation of the resistivity ρ_{300} , with the mean particle size. This leads to the nonsensical result that at zero crystal size the resistivity ρ_{300} is greater than $10^8 \Omega\text{-cm}$, which casts doubt on the validity of the resistivity versus mean crystal size relationship. It seems more likely that the observed anisotropy is due to anisotropic stresses in the system.

References

1. G. E. Rindone in Symposium on Nucleation and Crystallization in Glasses and Melts. Edited by M. K. Roser, G. Smith and H. Insley. (Am. Ceram. Soc., Inc., Columbus, Ohio 1962)
2. G. Donnay and J. D. H. Donnay, *Am. Mineralogist* 38 163 (1953)
3. F. P. Glasser, private communication.
4. H. A. Ananich and O. K. Botvin, *Steklo Keram.*, 19 10 (1962)
5. H. A. Ananich and O. K. Botvin *ibid* 22 7 (1965)
6. D. Weyl, *Ber. deut. keram. Ges.* 36 319 (1959)
7. J. Selsing, *J. Am. Ceram. Soc.* 44 419 (1961)
8. P. W. McMillan, *Glass-Ceramics* (Academic Press, London & New York 1964)
9. R. J. Charles, *J. Am. Ceram. Soc.* 45 105 (1962)
10. S. Glasstone, K. J. Laidler and H. Eyring, *The Theory of Rate Processes* (McGraw-Hill, New York 1941)
11. C. Zener in *Imperfections in Nearly Perfect Crystals* edited by W. Shockley (John Wiley, New York 1952).
12. P. W. M. Jacobs and F. C. Tompkins, *Quart. Rev. Chem. Soc. (Lond)* 6 238 (1952)
13. P. Rletschi, *Z. Phys. Chem.* 14 (5) 19 (1958)
14. J. Jeans, *The Mathematical Theory of Electricity and Magnetism* (University Press, Cambridge 1948)
15. P. W. McMillan, private communication.

CHAPTER 9: CONCLUSIONS

9.1 Introduction

This final chapter contains a comparison of the physical properties of the control and extruded glass-ceramics which are described in Chapters 7 and 8 respectively.

9.2 General Considerations

The technique of hot extruding a glass-ceramic has been shown to produce a material in which a crystalline phase is aligned parallel to the extrusion axis; a necessary requirement of this method of orientation is that the crystalline phases have an asymmetric morphology.

Control specimens have also been prepared of the same chemical composition and having the same nominal thermal treatment as the extruded specimens and the physical properties and microstructure of these materials have been investigated.

The control and extruded glass-ceramic specimens both contained crystalline phases of lithium disilicate and tridymite together with a glass matrix. In the case of the extruded material the lithium disilicate phase which was needle-shaped was aligned morphologically and crystallographically parallel to the extrusion axis; no preferred orientation of the tridymite phase was detected. The degree of orientation of the crystalline phases was found to be independent of the quantity of material extruded and decreased in a radial direction from the surface to the axis of the extruded material.

In the control specimens the crystalline phases were randomly oriented in the bulk material; surface crystallisation however produced a layer approximately one crystal length thick in which the crystals were aligned perpendicular to the surface.

If the only difference between the control and extruded specimens is considered to be the degree of orientation of the crystalline phases, then, an average of the anisotropic property measurements should produce a result which is equivalent to that measured on the control samples. This was not found to be the case for any of the property measurements. A direct comparison of the properties of these two materials should therefore be made with care; the two glass-ceramics contained approximately the same volume fractions of crystalline phases but in the case of the extruded samples it is believed that the properties are determined by the internal stress concentrations in the glass matrix and crystalline phases. Therefore the properties of the extruded material are not only a function of the thermal treatment but are also dependent upon the extrusion pressure.

9.3 A Comparison of the Properties of the Control and Extruded Glass-Ceramics

In the following, the main features of the property measurements for the control and extruded glass-ceramic samples are briefly summarised and compared.

The mechanical properties of the extruded material were anisotropic; the maximum value of the Young's modulus and rupture strength of this material was attained when the samples were loaded perpendicular to the extrusion axis. The minimum values of these moduli were approximately the same as the equivalent results for the control samples.

In the case of the control specimens the variation of the rupture modulus with the heat-treatment temperature was correlated with the mean crystal - crystal spacing in the material; however a similar correlation for the extruded specimen was not found. For the latter samples the rupture strength was found to be a function of the mean crystal size in the glass-ceramic but it is believed that this apparent relationship is

probably not of fundamental importance. Furthermore, a consideration of the mismatches in the expansion coefficients of the different phases in the anisotropic specimens showed that internal stresses in this material could be anisotropic. In the case of the control glass-ceramics the stresses would be isotropic when averaged over a volume the size of the mechanical test samples. It is therefore probable that the internal stresses in the specimens produced by mismatches in the expansion coefficients of the phases control the mechanical properties of the bulk material; the extruded samples are also subjected to compressive forces during the extrusion process and the extent to which these are "frozen" into the material will be dependent on the extrusion temperature. The exact derivation of the magnitude of the resultant stresses is extremely complicated.

Two coefficients of thermal expansion were measured for each glass-ceramic; the low temperature coefficient was isotropic for the oriented material and had a value approximately three times that measured for the control samples. The high temperature coefficient was found to be anisotropic for the extruded material and greater in a direction perpendicular to the extrusion axis than parallel to it. The average value of this coefficient for the extruded samples was approximately twice that measured for the randomly oriented material. It is believed that the anisotropy in this coefficient is partly due to differences in the expansion coefficients of the lithium disilicate crystalline phase with crystallographic direction.

It should also be noted that the variation in the expansion coefficients with the heat-treated temperature of the control specimens is similar to that observed for the moduli results; no such similarity was observed for the extruded samples.

The electrical properties of the control and extruded glass-ceramics were also measured; the volume resistivity of the latter material was found to be anisotropic, being greater when measured perpendicular to the extrusion axis. For the extruded specimens the resistivity appeared to be a function of the mean crystal size in the relevant direction in the material; however no such correlation was found between these parameters for the control samples. The resistivity of the control specimens was found to be generally higher than that of the extruded samples. The anisotropy relative to the extrusion axis of the resistivity measurements was reflected in the variation of the activation energy for conduction and the pre-exponential constant of an Arrhenius equation.

It is believed that the ionic conductivity of a glass-ceramic is not only a function of the phases through which the ions are travelling but also of the local stress concentrations in these phases. In the case of the control samples any stress concentrations will be averaged over the path length of the ions and the material will be isotropic; however, this will not be true for the extruded material.

The density of the extruded glass-ceramic was approximately 10% higher than that measured for the control specimens; this increase was believed to be associated with a densification of the glass phase during the extrusion process.

9.4 Other Conclusions

The properties of the control glass-ceramic were measured for specimens heat-treated in the range 650°C to 950°C. The resistivity, Young's modulus rupture strength and thermal expansion coefficients all showed maxima for a heat-treatment temperature of approximately 750°C. The loss tangent was a minimum at this heat-treatment. This temperature corresponded with the first appearance of a second crystalline phase which was believed to be tridymite.

The cathodoluminescence emission from a $\text{Li}_2\text{O-SiO}_2$ glass-ceramic surface when irradiated with an electron beam has also been investigated. A strong mechanism was found to exist which permitted the lithium disilicate crystalline phase to be easily distinguished from the glassy matrix. This technique allows scanning electron micrographs to be recorded without the prior necessity of etching the glass-ceramic surface to produce a topographical contrast.

9.5 Suggestions for Future Work

The suggestions for future work fall into the following main categories:

(i) Other methods of mechanically deforming a glass-ceramic with the object of producing an aligned crystal microstructure should be investigated; for example, rolling the hot material by a method similar to the cold rolling of metals. If this is feasible then sheets of glass-ceramic material would be produced in which the asymmetric crystalline phase was aligned in planes parallel to the rolling direction. However within each plane the crystals will be randomly oriented.

(ii) The hot extrusion of a glass-ceramic should be investigated further; ideally the material should contain only one crystalline phase with an asymmetric morphology. Different die materials and design parameters (e.g. the aperture angle and the length of the die channel) would enable the determination of the controlling factors in the extrusion process.

(iii) An investigation into the variation of the physical properties of the extruded material with direction relative to the extrusion axis and the degree of orientation would help to clarify the effect the microstructure of the material has on these properties. The effect of thermal history and

the presence of internal stresses in the glass-ceramic should be studied. A preliminary study of the latter could be performed by devitrifying glasses subjected to different applied loads and measuring the properties of the resultant glass-ceramic.

(iv) The phenomenon of cathodoluminescence should be studied further; in particular, different glass-ceramic compositions should be investigated and the wavelength of the emitted radiation measured. The dependence of the intensity of the emitted radiation upon the incident angle of the electron beam could also be investigated with a more sophisticated apparatus.

(v) Two areas of theoretical work in particular might give useful information. Firstly a calculation of the physical properties of a two phase system consisting of a continuous matrix with a dispersed discontinuous phase. Secondly, a greater understanding of the cathodoluminescence emitted from crystalline materials will be required if this is to prove a useful technique.

Some observations of glass-ceramic microstructures by cathodoluminescence

The effects of variations of thermal treatment on the microstructures of glass-ceramics prepared by the controlled crystallization of glasses are of interest and, therefore, rapid and convenient methods of characterizing the microstructures are required. The scanning electron microscope (SEM) has become an important tool in the investigation of the surfaces of materials; there are three basic modes in which the SEM can be operated to observe the interactions of an electron beam with the surface of a specimen. These are the electron emission, the X-ray emission and the photon emission from the specimen surface [1].

In this letter we describe some results obtained from observing the cathodoluminescence (CL) or photon emission from a glass-ceramic. The system used to detect the CL consisted of an EMI Type 6255B photomultiplier tube and a 1 in. diameter lens of focal length equal to 1 in. to give a collection angle in excess of 0.75 steradians; a Cambridge Scientific Instruments Ltd, Mk IIA Stereoscan was used.

Two glasses were prepared from compositions shown in Table I; glass A was heat-treated for 2 h at 800°C [2] and glass B was extruded at 825°C. Both glass-ceramics contained needle-shaped crystals of lithium disilicate as their major crystalline phase and a crystalline form of silica as a minor crystalline phase, together with a residual glass phase. Specimens approximately 3 mm thick of each material were polished to 1 μm and coated with a layer approximately 10 nm thick of gold/palladium to prevent charging in the SEM. The polished surfaces were examined in the SEM by the secondary emission mode and the CL mode. The accelerating

potential was 30 kV, the beam current approximately 150 μA and the specimen was positioned normal to the incident electron beam.

TABLE I Glass compositions in mol%.

	SiO ₂	Li ₂ O	K ₂ O	Al ₂ O ₃	P ₂ O ₅	B ₂ O ₃
Glass A	61.0	30.5	1.5	1.0	1.0	5.0
Glass B	67.5	24.0	1.5	1.0	1.0	5.0

Figs. 1 and 2 show a comparison of the same area of glass A observed in the two modes; Fig. 3 shows a sample prepared in the same fashion but etched for 30 sec in a 3% HF solution and observed in the secondary/reflected mode. There is obviously a marked contrast mechanism in the CL mode which enables the lithium disilicate crystalline phase to be easily distinguished from the glassy matrix; the CL micrograph has a speckled appearance because of noise associated with the photomultiplier.

Figs. 4 and 5 show a similar comparison in glass B. A weak contrast mechanism can be observed in the secondary/reflected emission micrograph which is caused by the back-scattered electrons [3]; the darker crystalline regions in Fig. 4 show little electron emission but a strong photon emission in Fig. 5. Prior etching of the glass-ceramic, in the manner described above, enabled the micrograph shown in Fig. 6 to be obtained by the secondary/reflected mode.

CL has been observed in quartz [4] but in the present studies no CL was observed from the silica crystalline phase; one of the emission bands in quartz [5] is positioned outside the range of the photomultiplier tube used and the strong emission from the disilicate phase together with the small volume fraction of the silica crystals makes detection of the CL of the latter difficult.



Figure 1 Secondary/reflective emission from a polished sample of glass A.

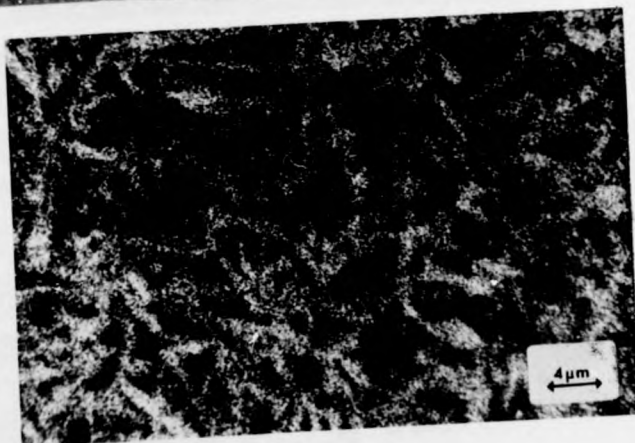


Figure 2 CL from the same area as in Fig. 1.

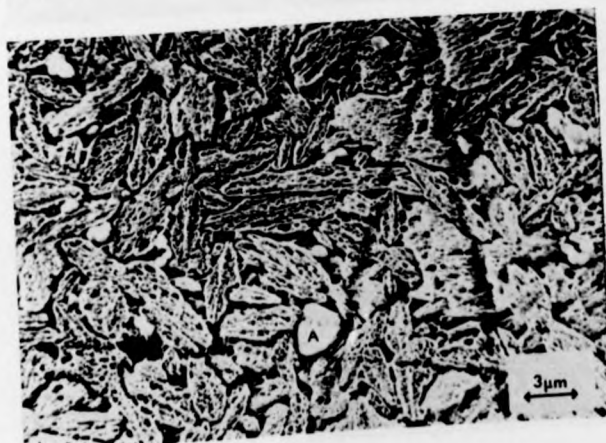


Figure 3 Secondary/reflective emission from etched sample of glass A; A is the silica crystalline phase.

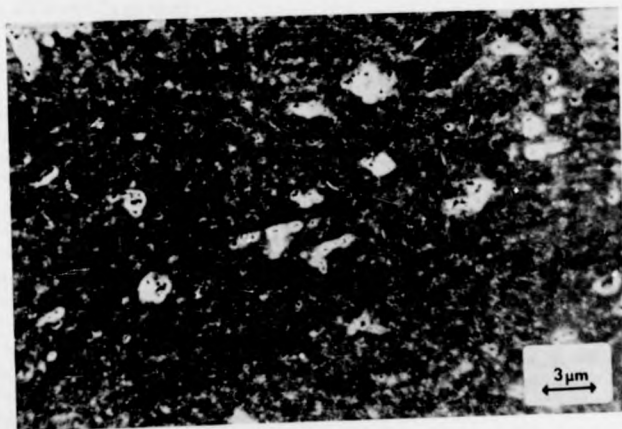


Figure 4 Secondary/reflected emission from a polished sample of glass B.

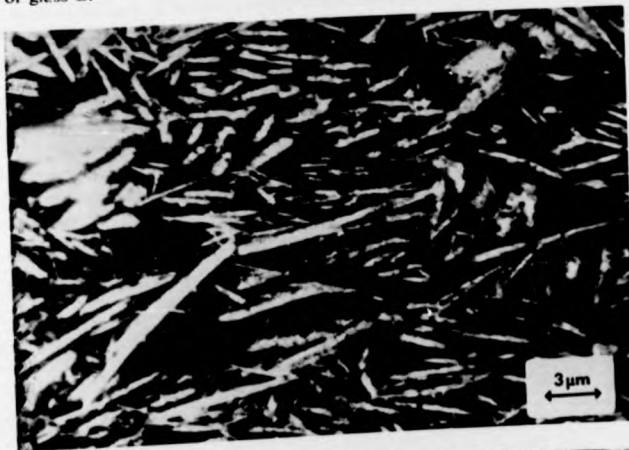


Figure 5 CL from the same area as in Fig. 4.

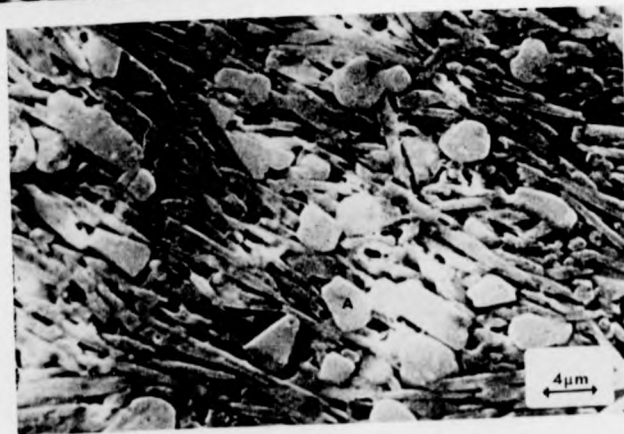


Figure 6 Secondary/reflected emission from an etched sample of glass B: A is the silica crystalline phase and B is the disilicate phase.

It is clear from the present work that observation of CL can provide an additional and valuable technique for the investigation of glass-ceramic microstructures. In this study the CL observed was confined to lithium disilicate crystals. However, this had the advantage of enabling these crystals to be readily distinguished from the crystalline silica phase. With an improved system for detection and analysis of the radiation emitted, it may be possible to extend the technique to selectively reveal the morphology of the silica crystals and of other crystal types in different glass-ceramic compositions. As the micrographs indicate, CL enables micrographs showing good contrast to be obtained without the necessity for etching of the glass-ceramic surface. The latter could cause modifications of the microstructure and clearly this is undesirable.

We conclude that the technique of using CL gives additional valuable information in the investigation of polished glass-ceramic surfaces and also has a considerable potential for characterizing the fracture surfaces of multiphase materials based on elements of low atomic number.

Acknowledgements

The authors would like to thank Mr G. Smith for invaluable assistance with the electron microscope. Gratitude is also expressed to the SRC for financial support.

References

1. P. R. THORNTON, "Scanning Electron Microscopy" (Chapman and Hall, London, 1968).
2. P. W. MCMILLAN, "Glass Ceramics" (Academic Press, 1964).
3. C. W. PRICE and D. W. JOHNSON, 4th Annual Scanning Electron Microscope Symposium, IIT Research Institute, Chicago (1971) p. 145.
4. D. H. KRINSLEY and P. J. W. HYDE, *ibid.*, p. 409.
5. R. F. SIPPEL and A. B. SPENCER, *Proc. Apollo 11 Lunar Science Cong.* 3 (1970) 2413.

Received 26 November
and accepted 27 November 1973

D. I. H. ATKINSON
P. W. MCMILLAN
*Department of Physics,
University of Warwick,
Coventry, Warwickshire, UK*

PATENTS FORM NO. 2

PATENTS ACT 1949

PROVISIONAL SPECIFICATION

43700/74

9 OCT 1974

GLASS CERAMIC BODIES

We, PETER WILLIAM McMILLAN of 1 Hughes Hill, Shrewley, Warwick
and DAVID IAN HEATON ATKINSON of 7 The Larches, Headington, Oxford
both British subjects, do hereby declare this invention to be
described in the following statement:-

This invention relates to glass ceramic bodies and processes for the production thereof.

At present glass ceramic bodies are produced by first forming a glass into a shape, e.g. by rolling, casting or pressing, and
5 subsequently subjecting the glass shape to a heat treatment to induce crystallization therein. Glass ceramic bodies produced in this manner have useful mechanical properties but it has now been found that bodies may be formed with a microstructure which gives rise to a significant increase in the bending strength thereof.

10 According to the present invention a glass ceramic body comprises elongate crystals, the interior of which body at least in the region adjacent the exterior surface thereof having a microstructure in which there is an observable orientation of the crystals in or towards a direction parallel to said surface.

15 According to a further aspect of the present invention, a glass ceramic body comprises elongate crystals the major axes of which are oriented in the same general direction to a sufficient degree that the bending strength of the body perpendicular to said direction is at least 50% greater than the bending strength in said direction.

20 Glass ceramic bodies according to the present invention may be formed by a process in which a bulk of predominantly crystalline material is forced to flow through an aperture.

In practice, the predominantly crystalline material from which the glass ceramic body is formed is produced by heating a bulk of glass to induce crystallization therein. Whilst various glass

compositions may be employed, those which yield elongate crystals as a major phase are preferred and compositions which yield lithium disilicate crystals, which are needle shape, have given good results.

In order to promote crystallization throughout the bulk of the material a nucleating agent is preferably incorporated in the composition. The bulk of material is at least 50% crystalline and may be as much as 90% crystalline when forced through the aperture. It is generally desirable however, for sufficient non-crystalline material to remain to enable flow through the aperture to be readily effected.

The glass ceramic body may be formed for example by extruding the bulk material through a die to yield shaped products such as sheets, rods and fibres or for example by forcing the bulk material through an aperture at least one boundary of which is provided by a roller which rotates to force the material through the aperture, the latter method generally being used for the production of sheet. It is believed that the crystal alignment which results is due to the application of non-uniform stress to the material across the aperture through which it is forced. Particularly in the case of extrusion, frictional forces between the wall of the die and the material which result in a relatively greater resistance to flow through the aperture at the boundaries than at the centre thereof may contribute to producing the resultant and alignment which is particularly pronounced in general in the regions of the glass ceramic body adjacent the surface shaped by the aperture.

In order to produce optimum alignment in the glass ceramic body it is generally desirable for the conditions under which the bulk

material is forced through the aperture to be such that substantially laminar flow results. Good results have been obtained with a Reynolds number many orders of magnitude e.g. 17 or more below the critical lower limit for turbulent flow.

5 The temperature at which the bulk material is maintained whilst forced through the aperture lies within limits above which the crystal begin to redissolve and below which the viscosity is so great that undue pressure is required which at least in an extrusion process is liable to damage the die.

10 The walls of the aperture are preferably heated during the passage of the material therethrough and a temperature gradient may be maintained between the container wall adjacent the rearward portion of the bulk material and the aperture wall adjacent the advancing shaped material e.g. a gradient of 10°C or so, when the
15 aperture communicates with a cooled zone in which the body solidifies.

 The bulk material may be forced through the aperture either at a constant pressure or a constant rate. It is generally more convenient however, to operate at constant pressure, especially when the bulk material is extruded through a die.

20 The glass ceramic body usually has a microstructure in which there is present at least one crystalline phase and the latter is provided by elongate crystals. The degree of crystallinity in the body may be identical to that in the bulk material from which it is formed or may be somewhat greater in cases where crystallization
25 continues whilst the material is forced through the aperture.

Although in the region of the body adjacent the exterior surface thereof the microstructure has an observable orientation of the elongate crystals in or towards the direction parallel to said surface, as hereinbefore indicated, it is not essential for all the
5 elongate crystals in the latter region to be so disposed, provided that the majority have the required orientation. Nor of course is it essential for any of the elongate crystals to be orientated with the major axes strictly parallel to the surface, provided that the microstructure has an observable degree of orientation towards a
10 direction parallel to the surface. Preferably, however, all of the elongate crystals have a required orientation and the latter orientation is strictly parallel to the surface so that optimum strength properties result. In general however, such a desirable microstructure is achieved only in the region of the glass ceramic
15 body immediately adjacent the surface and orientation decreases towards the interior thereof. It will be appreciated that the orientation of the elongate crystals in the microstructure can be observed by techniques such as electron-microscopy.

Generally, in glass ceramic bodies formed by forcing a bulk
20 material through an aperture the elongate crystals in the interior of the bodies at least in the region of the adjacent exterior surface thereof are predominantly oriented in or towards the direction of flow therethrough. Preferably the major axes of the elongate crystals at or near the surface lie within 20° of the direction of flow (in
25 the case of extrusion, the extrusion axis) and at the centre of the body within 60° .

Randomly orientated crystals would of course lie within 90° of the direction of flow.

Glass ceramic bodies of the present invention can have three point bending strengths which are increased by at least 50%, e.g. 5 66% or more relative to bodies in which the elongate crystals are randomly orientated but are otherwise identical. Such properties enable the bodies or articles fabricated therefrom to find application in demanding conditions e.g. as turbine blades. The bodies are also of interest where electrical anisotropy is required, the degree of 10 insulation offered by the bodies in the direction of crystal alignment being substantially different from the degree of insulation in the direction perpendicular thereto.

Apparatus suitable for carrying the present invention into effect will now be described by way of example only with reference 15 to the accompanying drawing.

Referring now to the drawing, a die (1) made in one piece from a high strength, heat resisting nickel based alloy composition (weight percent).. 0.15 C; 1.0 Mn; 8 Fe; 0.015 S; 0.5 Si; 0.5 Cu; 17.0 Cr; balance nickel and cobalt; and capable of withstanding a 20 pressure of 10^7 N/m² at a temperature of 950°C has a cavity (2) for containing a bulk of glass material which communicates with the die aperture (3) by way of a wall portion (4) which makes an angle of 45° with the aperture wall (5). The die (1) is surrounded by R.F. heating coils (6) and is supported on a stainless steel tube (7) 25 which is provided along the length thereof with circumferential coils (8) for through flow of cooling water, connected to an inlet and

outlet (9,10) therefor. The tube (7) is in turn supported as a loose fit on the load cell(11) of an Instron Universal testing machine. The aperture wall (5) of the die (1) is provided with a temperature sensing probe (12) (thermocouple or optical pyrometer) for monitoring the extrusion temperature. The die cavity (2) is dimensioned so as to accommodate a stainless steel plunger (13) cooled by a water jacket (14) and connected to the crosshead (15) of the Instron Universal testing machine.

The apparatus is employed in the following manner. A glass billet is cast placed in the die cavity (2) and then heat treated in situ for a predetermined time at a set temperature to produce a predominantly crystalline material. The plunger (13) is then lowered and extrusion effected through the aperture (3) the temperature being monitored by means of the probe (12). A temperature gradient of approximately 10°C exists between the top of the cavity (2) and the bottom of the die aperture (3) at extrusion temperatures within the range $800-900^{\circ}\text{C}$. A certain amount of material flows in the reverse direction to that of the plunger (13) between the plunger and the cavity (2) and this assists in lubricating the plunger (13) and prevents seizing. When the extruded material clears the die (1) it enters the cooled tube (7) from which it is recoverable by removal of the die (1) from the tube (7).

The present invention is illustrated by the following Example.

Example 1

A glass of composition (mol. percent):-

SiO_2 61.0; Li_2O 30.5; K_2O 1.5; Al_2O_3 1.0; P_2O_5 1.0; B_2O_3 5.0.

is prepared from Brazilian quartz (ground to pass through a 60 mesh sieve), high purity lithium carbonate and AR lithium orthophosphate, potassium carbonate, aluminium oxide and boric oxide. The materials are thoroughly dried, weighed and mixed by milling in a rotary ball mill for three hours. The glass is melted and refined in a platinum crucible at 1400°C until bubble free, quenched into a melting mixture of ice then crushed and dried; this process is repeated in order to achieve good homogeneity. The glass is remelted at 1400°C for 3 hours and then cast into a billet. The billet is placed in the die cavity of the apparatus hereinbefore described and heat treated for 30 minutes at 875°C. The billet is then extruded at 800-900°C with a plunger load 85 kg, the viscosity being 2×10^7 poiseuille, at a volume rate $5 \times 10^{-10} \text{ m}^3/\text{sec}$.

The rod so extruded has the following values for the bending strength (3 point loading):-

a) measured perpendicular to the direction of orientation:

$$2.4 \times 10^8 \text{ Nm}^{-2}.$$

b) measured parallel to the direction of orientation:

$$1.5 \times 10^8 \text{ Nm}^{-2}.$$

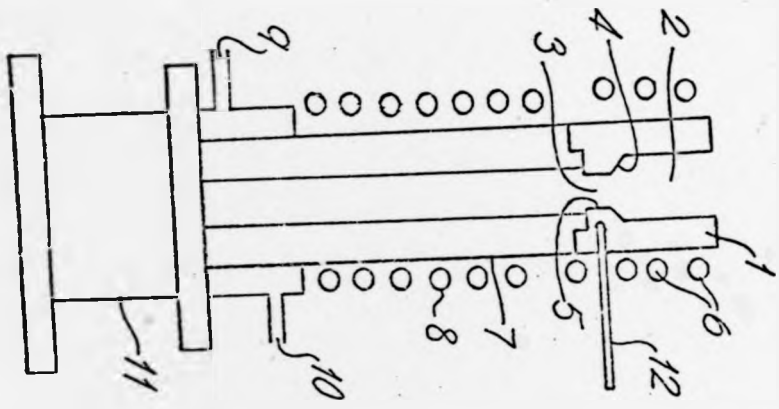
20 Example 2

A glass of composition (mol. percent):-

SiO_2 67.5; Li_2O 30.5; K_2O 1.5; Al_2O_3 1.0; P_2O_5 1.0; B_2O_3 5.0.

is prepared as in Example 1 and cast into a billet. Extrusion is performed similarly. Strength values are similar to those given in Example 1.

R.S. CRESPI
Chartered Patent Agent
Agent for the Applicants



A3700/74

